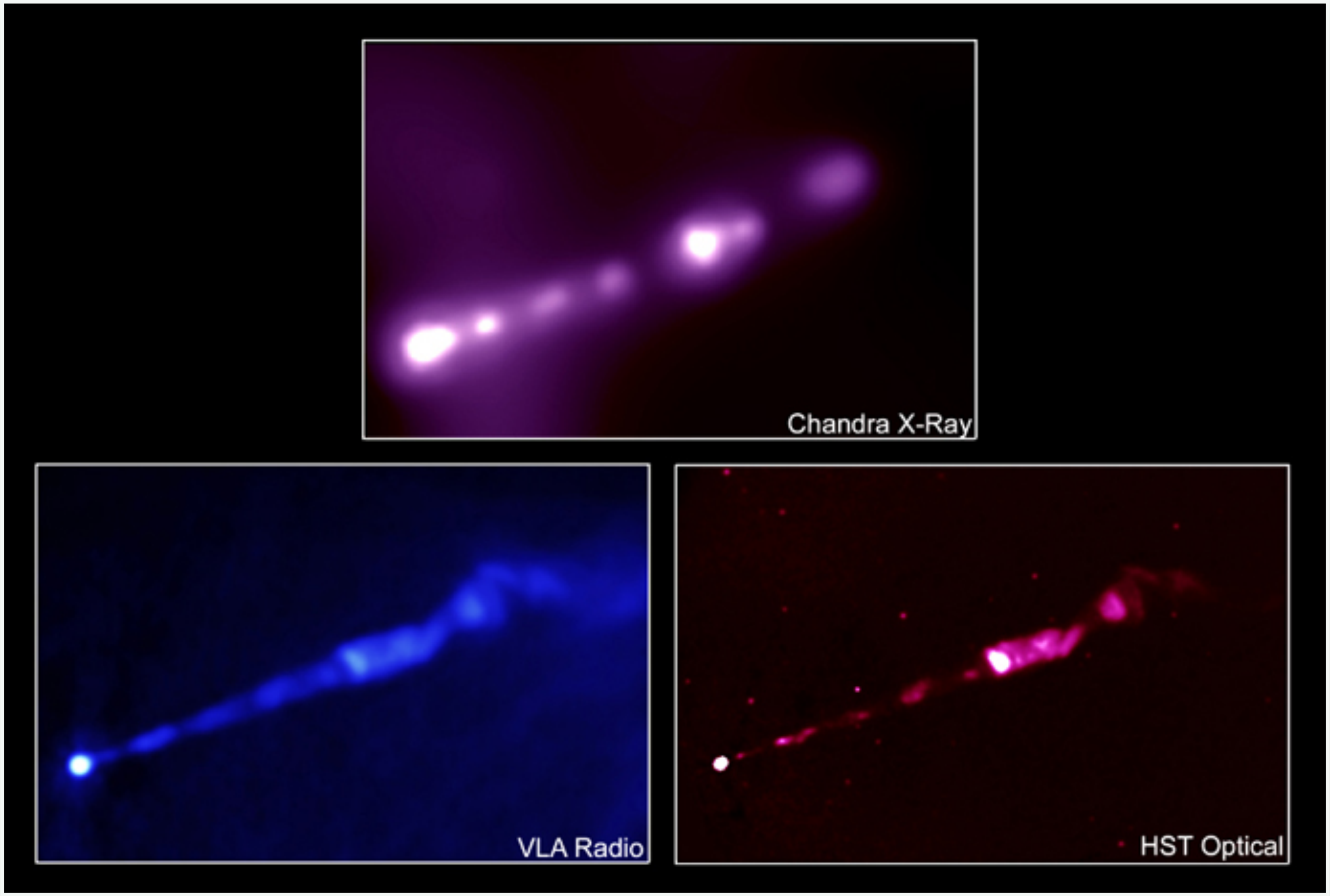

INTRODUCCIÓN A LA ASTROFÍSICA RELATIVISTA

Gustavo E. Romero
Cursada 2020, FCAyG/UNLP

FUENTES DE RAYOS GAMMA

Llamamos fuente de rayos gamma a un sistema astrofísico que emite una fracción significativa de su *luminosidad electromagnética* a energías mayores que 0.5 MeV.

Las fuentes de rayos pueden clasificarse en 2 grandes grupos:

FUENTES γ → **PASIVAS**

FUENTES γ → **ACTIVAS**

❖ Las fuentes pasivas son simplemente “blancos” para flujos de partículas relativistas originadas en una región diferente.

❖ Las fuentes activas, por el contrario, aceleran partículas hasta velocidades relativistas y la interacción de estas partículas con los diferentes campos (de materia o electromagnéticos) locales da lugar a la radiación gamma.

FUENTES PASIVAS

FUENTES PASIVAS → **Difusas**

FUENTES PASIVAS → **Discretas**

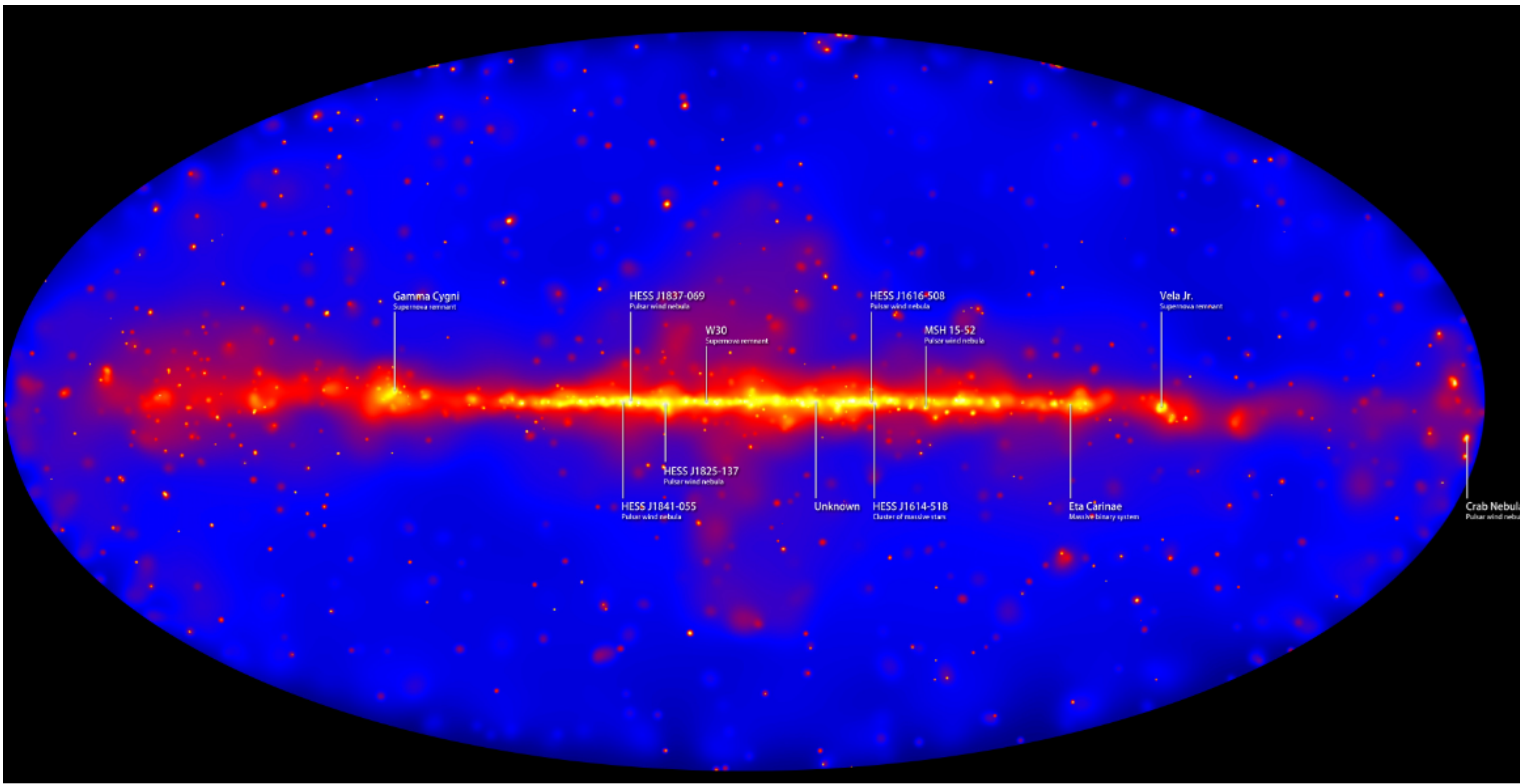

Definamos una emisividad específica

$$\epsilon_\gamma(\vec{r}) = \frac{q_\gamma(\vec{r})}{n(\vec{r})},$$

donde n es la densidad del medio y $q_\gamma(\vec{r})$ la emisividad por decaimientos de π^0 en la dirección $\vec{r}$, el flujo total recibido a una distancia d será:

$$F_\gamma = \frac{1}{4\pi d^2} \int n(\vec{r})\epsilon_\gamma(\vec{r}) d^3r,$$

donde la integral se extiende sobre toda la región donde se distribuye el gas. Si llamamos $\epsilon_{\gamma,0}$ a la emisividad local (en la vecindad del Sol), podemos escribir:

$$\frac{\epsilon_\gamma}{\epsilon_{\gamma,0}} \sim \frac{\omega_{\rm cr}}{\omega_{\rm cr,0}} = \kappa_{\rm S}$$

donde $\omega_{\rm cr}$ es la densidad de energía de los rayos cósmicos, que localmente vale

$$\omega_{\rm cr,0} \sim 1 \text{ eV cm}^{-3}.$$

Luego

$$F_\gamma \sim \frac{1}{4\pi d^2} \int \kappa_{\rm S}\epsilon_{\gamma,0} n(\vec{r}) d^3r.$$

Las fuentes pasivas discretas están formadas por medio interestelar altamente estructurado. En particular, pueden ser fuentes discretas nubes moleculares masivas, nubes de polvo, o incluso nubes más pequeñas ubicadas localmente o próximas a aceleradores de rayos cósmicos.

Si la densidad de una de tales nubes es aproximadamente constante:

$$F_\gamma \sim \frac{M_{\rm cl}}{m_p}\frac{\epsilon_\gamma}{4\pi d^2},$$

donde hemos asumido que la nube esta formada principalmente por H y $M_{\rm cl}$ es la masa total que es irradiada por los rayos cósmicos. Si $\epsilon_\gamma \sim \kappa_{\rm S}\epsilon_{\gamma,0}$,

$$F_\gamma \sim \frac{1}{4\pi d^2}\kappa_{\rm S}\;\epsilon_{\gamma,0}\frac{M_{\rm cl}}{m_p}.$$

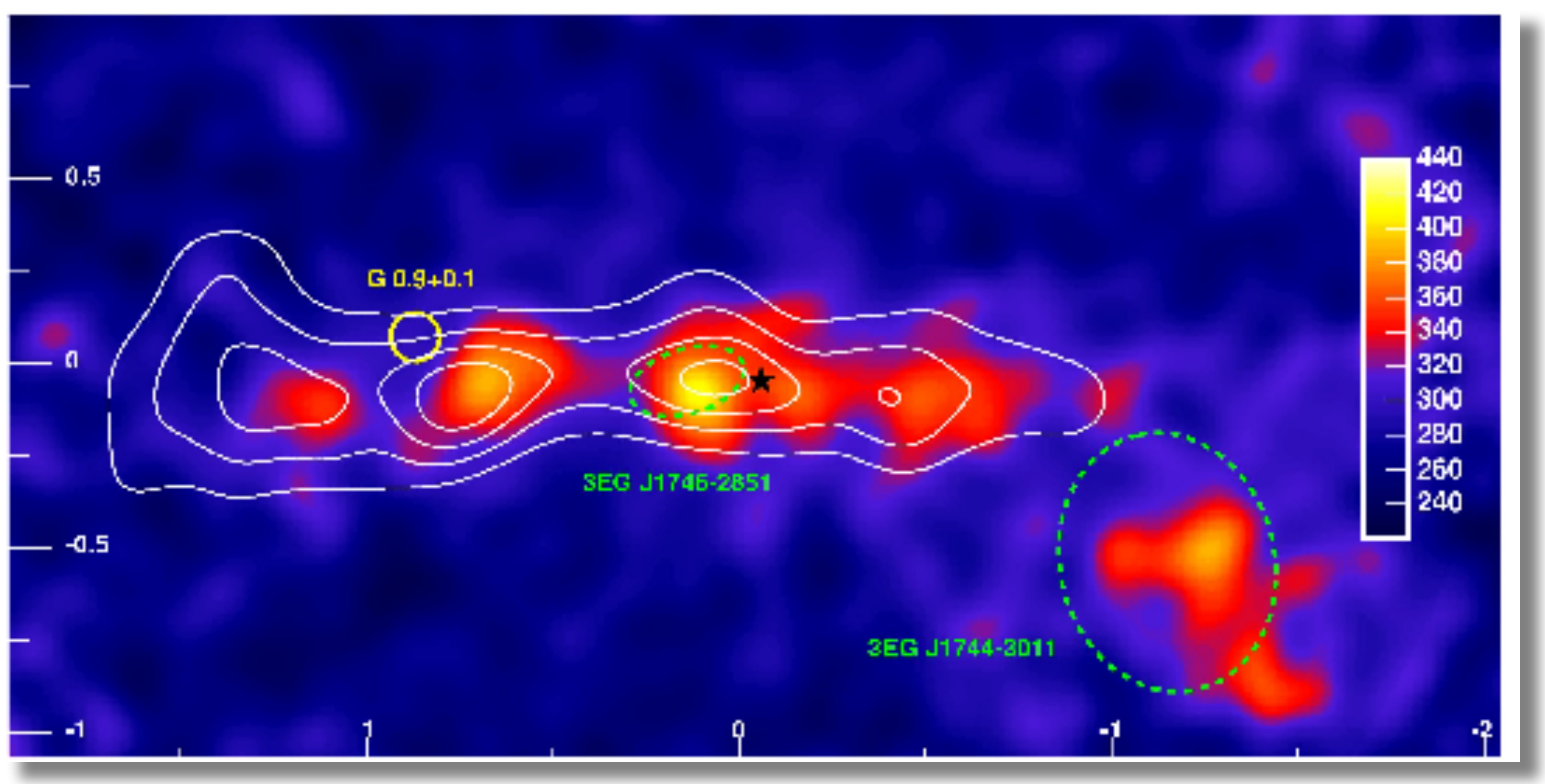

Aharonian et al. 2006

Luego, podemos escribir:

$$\frac{F_\gamma}{\mathrm{cm}^{-2}\ \mathrm{s}^{-1}} \sim 10^{-9} \left(\frac{M_{\mathrm{cl}}}{1000\ M_\odot}\right) \left(\frac{d}{\mathrm{kpc}}\right)^{-2} \kappa_{\mathrm{S}} \left(\frac{\omega_{\mathrm{cr},0}}{\mathrm{eV\ cm}^{-3}}\right) \eta_A,$$

donde η_A es un factor que tiene en cuenta la presencia en el medio de elementos más pesados que el H.

Astron. Astrophys. 303, 872–880 (1995)

ASTRONOMY AND ASTROPHYSICS

On the origin of the γ-ray fields in the Ara region

J.A. Combi* and G.E. Romero*

Instituto Argentino de Radioastronomía, C.C. 5, (1894) Villa Elisa, Prov. de Bs. As., Argentina

Received 16 January 1995 / Accepted 17 March 1995

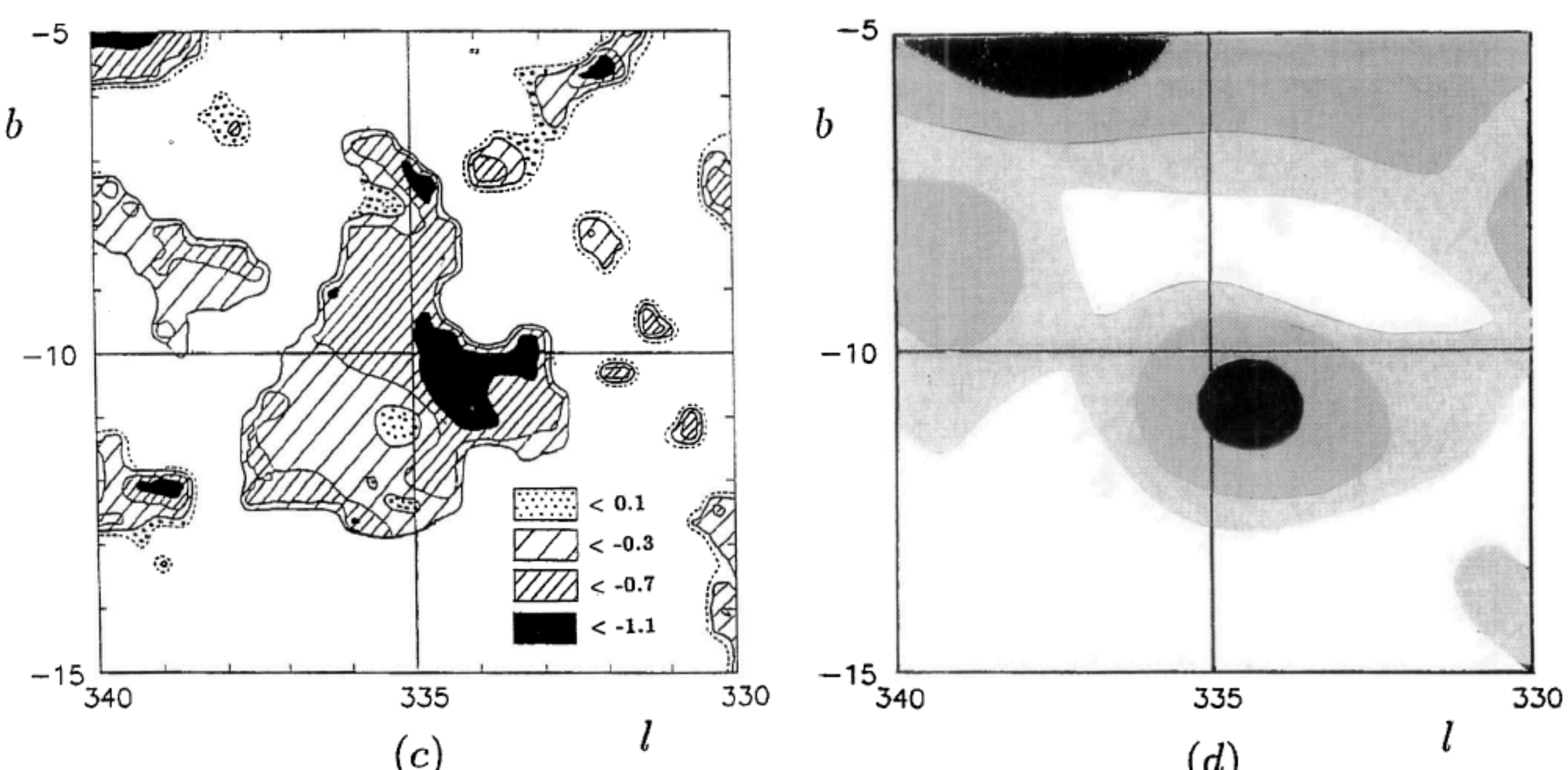

FUENTES ACTIVAS

Fuentes activas no acretantes galácticas
- Pulsares
- Remanentes de supernovas
- Binarias con colisión de vientos

Proto-estrellas, bowshocks, novas, PWNs, estrellas normales, etc

Fuentes activas no acretantes extragalácticas
- Galaxias eruptivas (*starbursts*)
- Cúmulos de galaxias
- Galaxias normales

Binarias con vientos en colisión

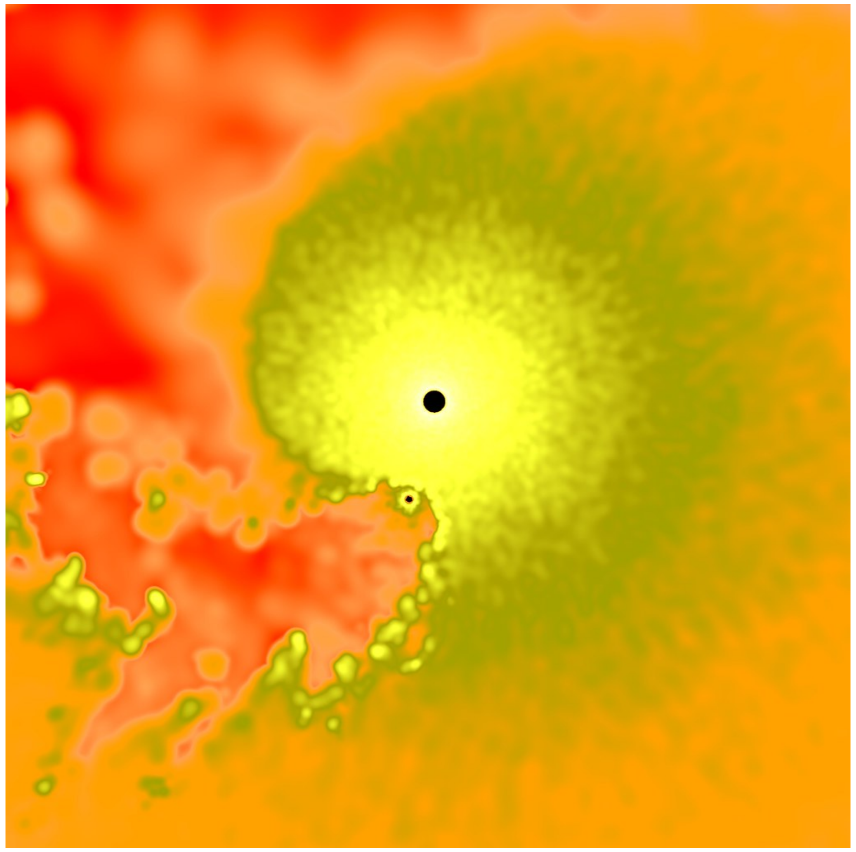

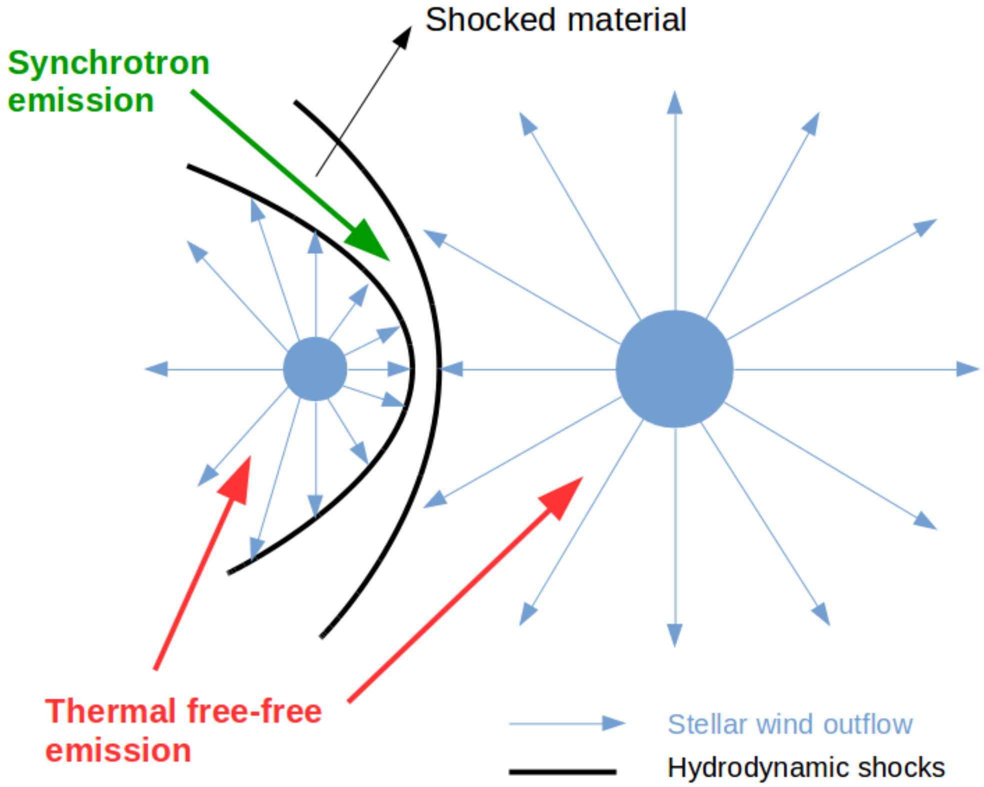

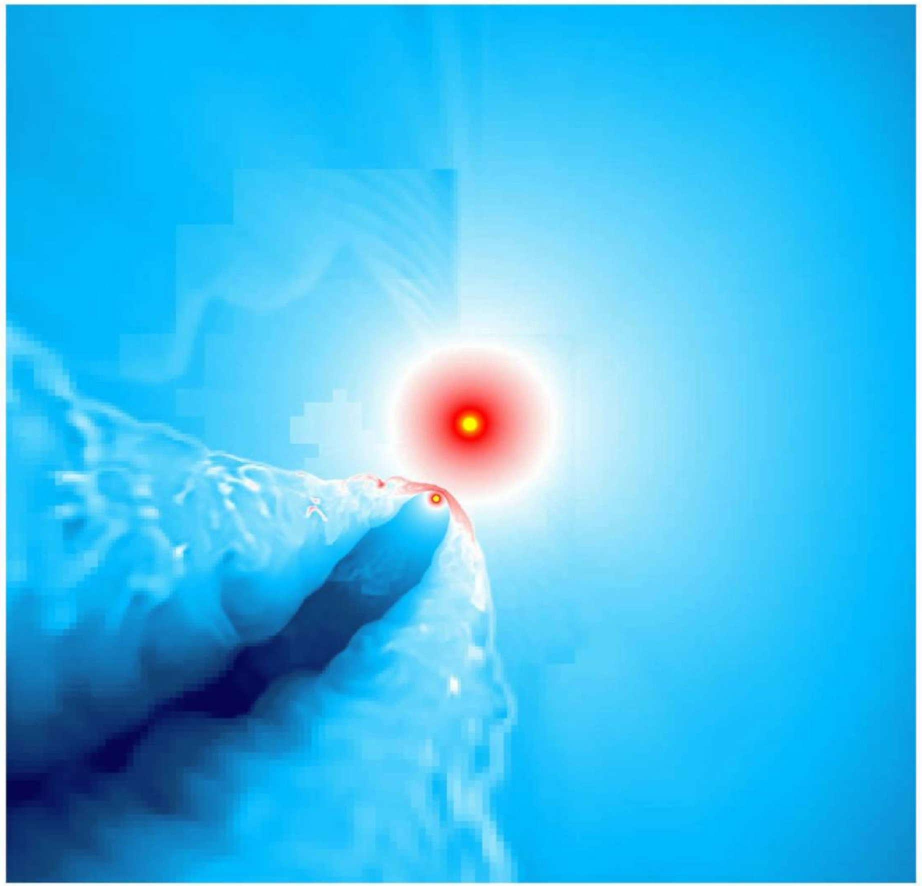

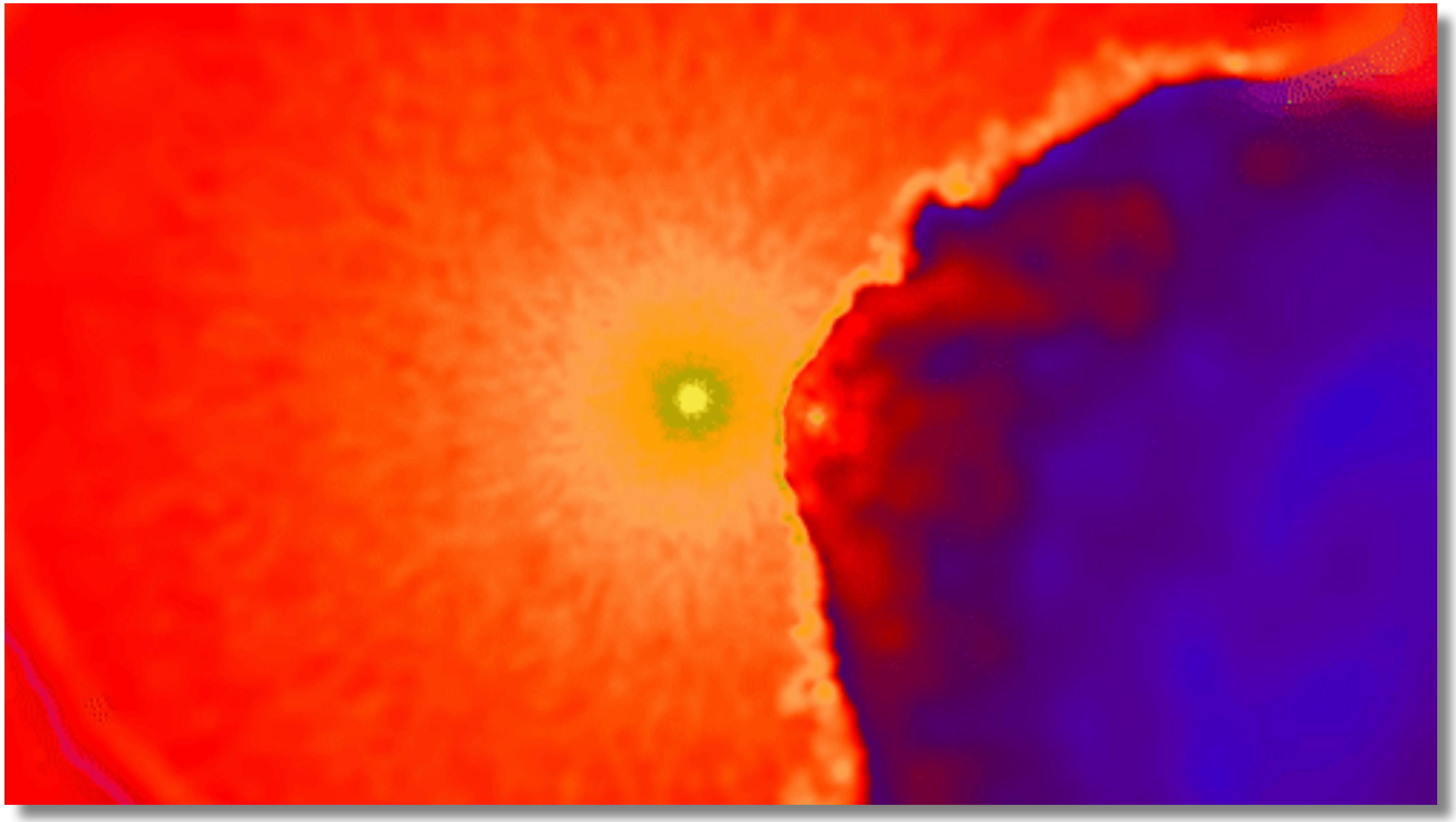

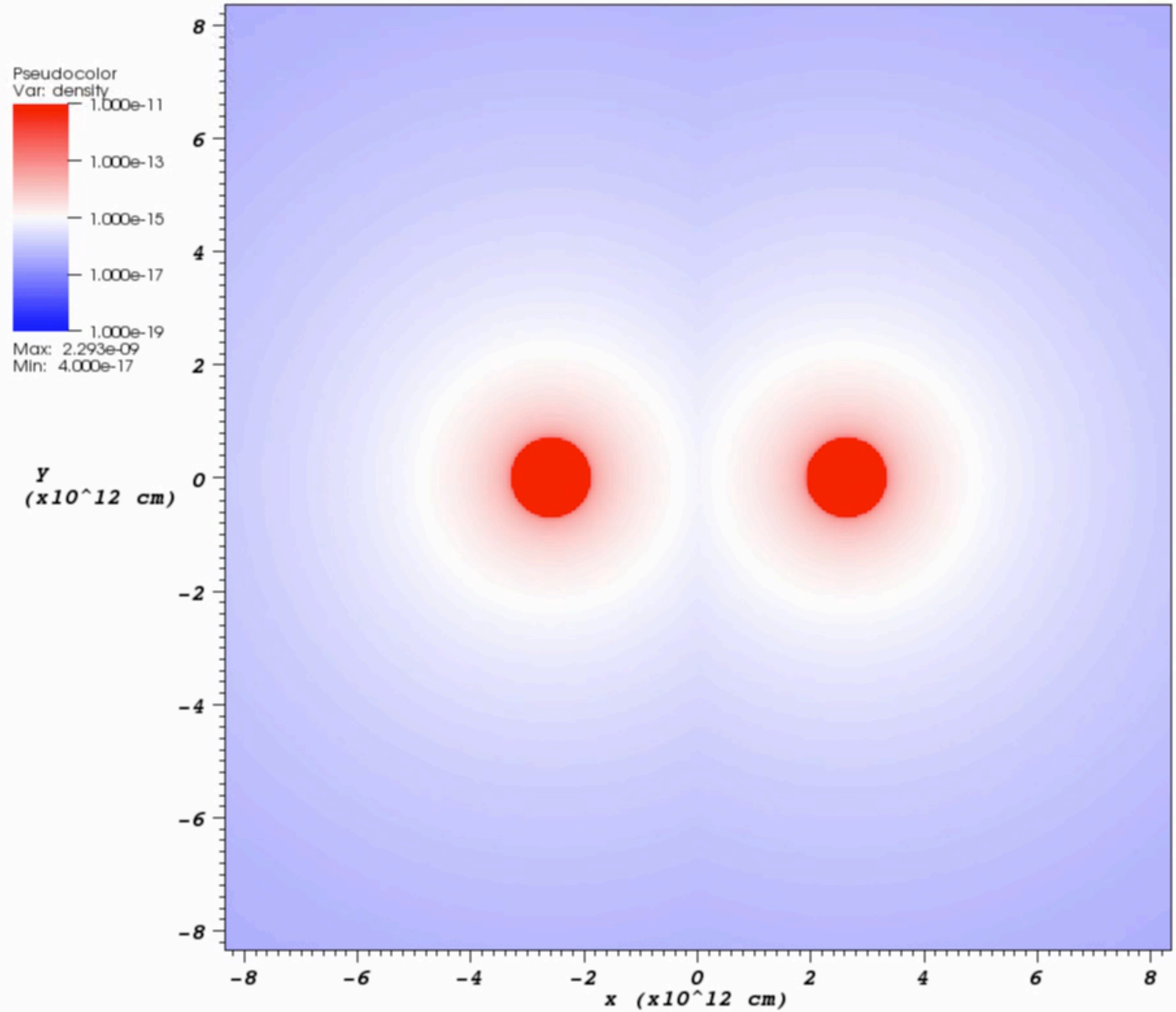
Pseudocolor
Var: density
1.000e-11
1.000e-13
1.000e-15
1.000e-17
1.000e-19
Max: 2.293e-09
Min: 4.000e-17
Y
(x10^12 cm)
x (x10^12 cm)
8
6
4
2
0
-2
-4
-6
-8

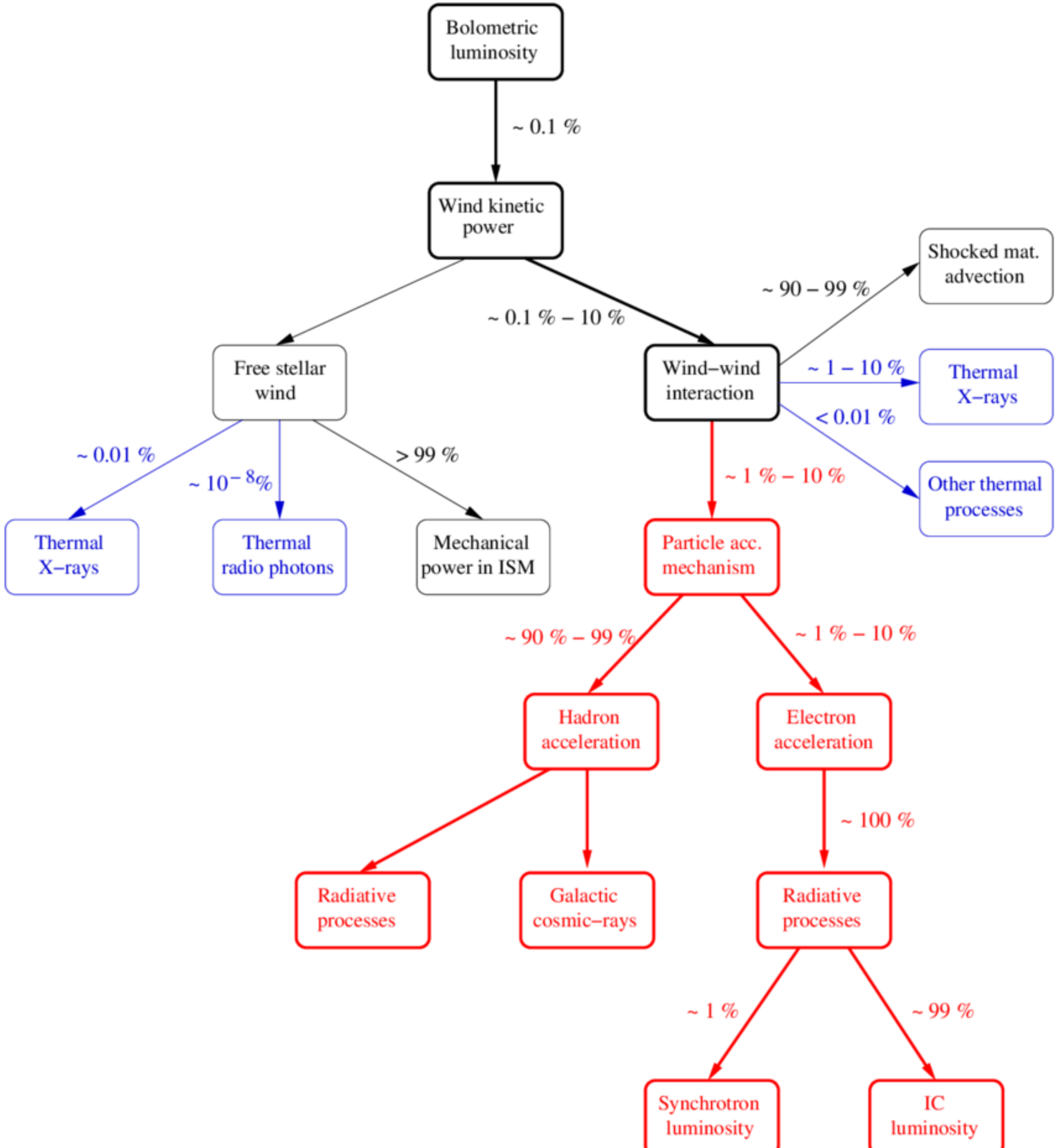

Bolometric luminosity
~ 0.1 %
Wind kinetic power
~ 0.1 % – 10 %
Free stellar wind
Wind–wind interaction
~ 90 – 99 %
Shocked mat. advection
~ 1 – 10 %
Thermal X–rays
< 0.01 %
Other thermal processes
~ 0.01 %
~ 10^−8 %
> 99 %
Thermal X–rays
Thermal radio photons
Mechanical power in ISM
~ 1 % – 10 %
Particle acc. mechanism
~ 90 % – 99 %
~ 1 % – 10 %
Hadron acceleration
Electron acceleration
~ 100 %
Radiative processes
Galactic cosmic–rays
Radiative processes
~ 1 %
~ 99 %
Synchrotron luminosity
IC luminosity

Eta Car is a heavily obscured and peculiar source source (includes a luminous blue variable - LBV - star of 90 solar masses and 5 10^6 L_{sun})

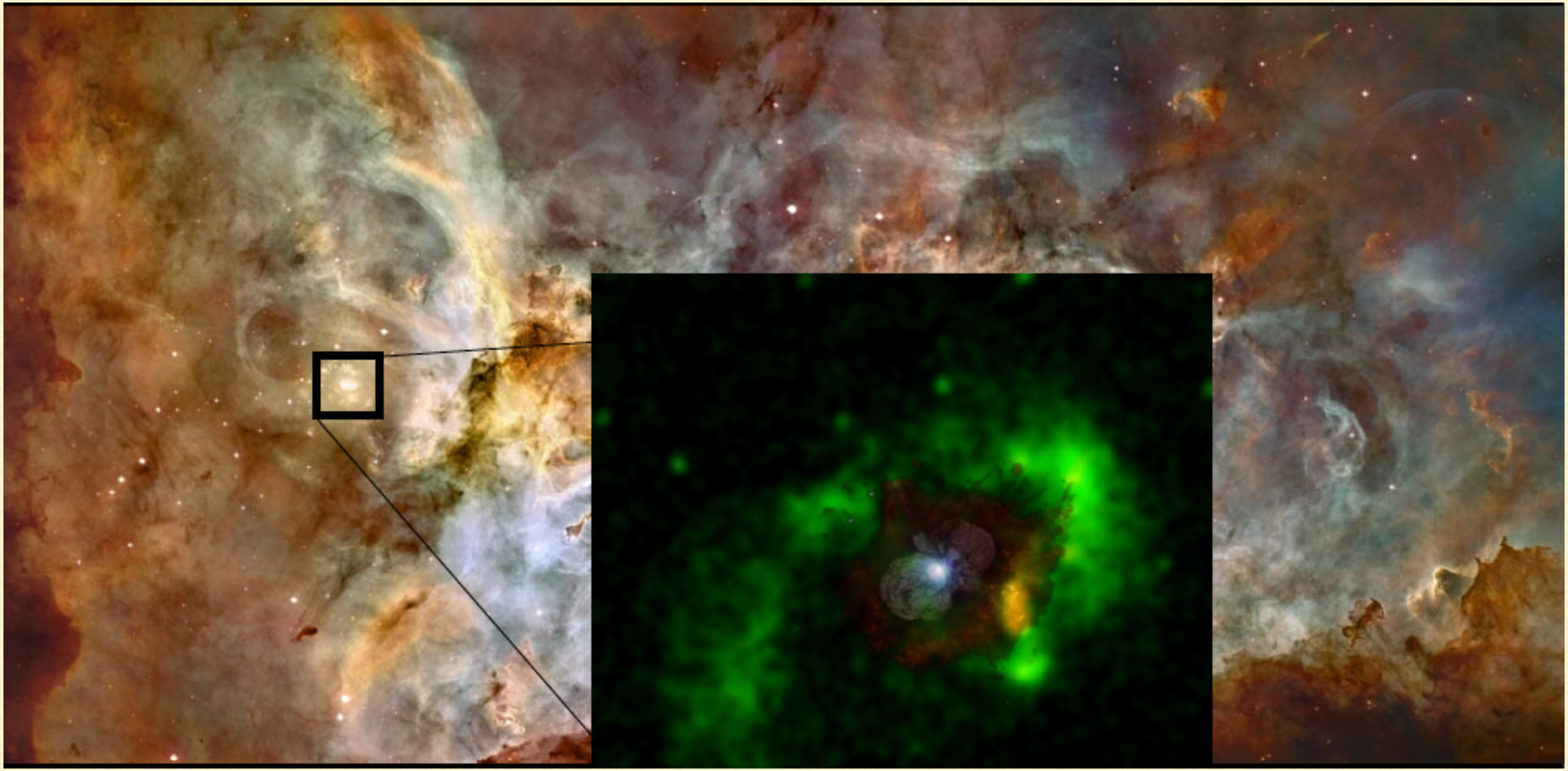

η Carinae: a very Large Hadron Collider

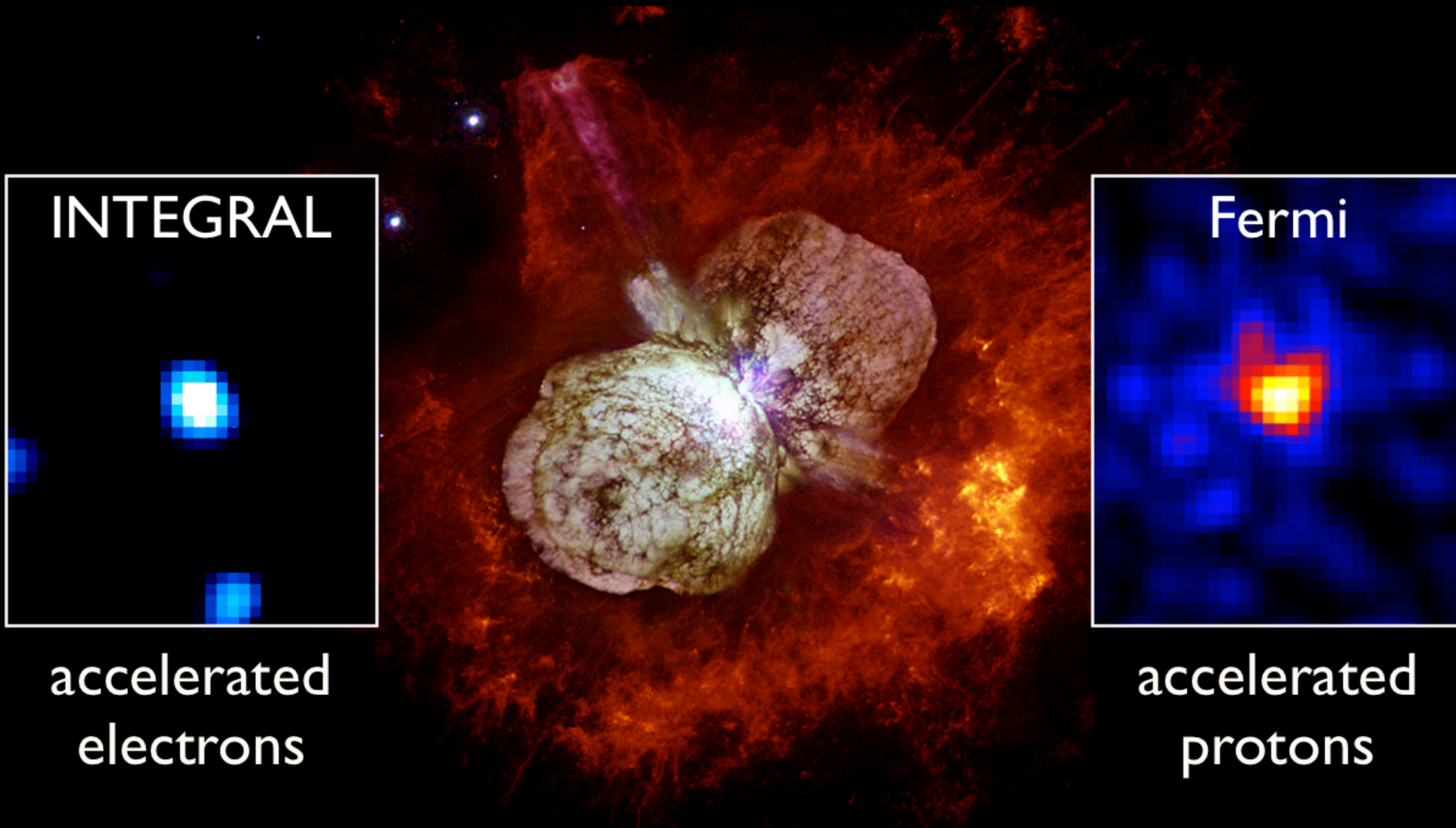

Hubble Space Telescope
stellar wind

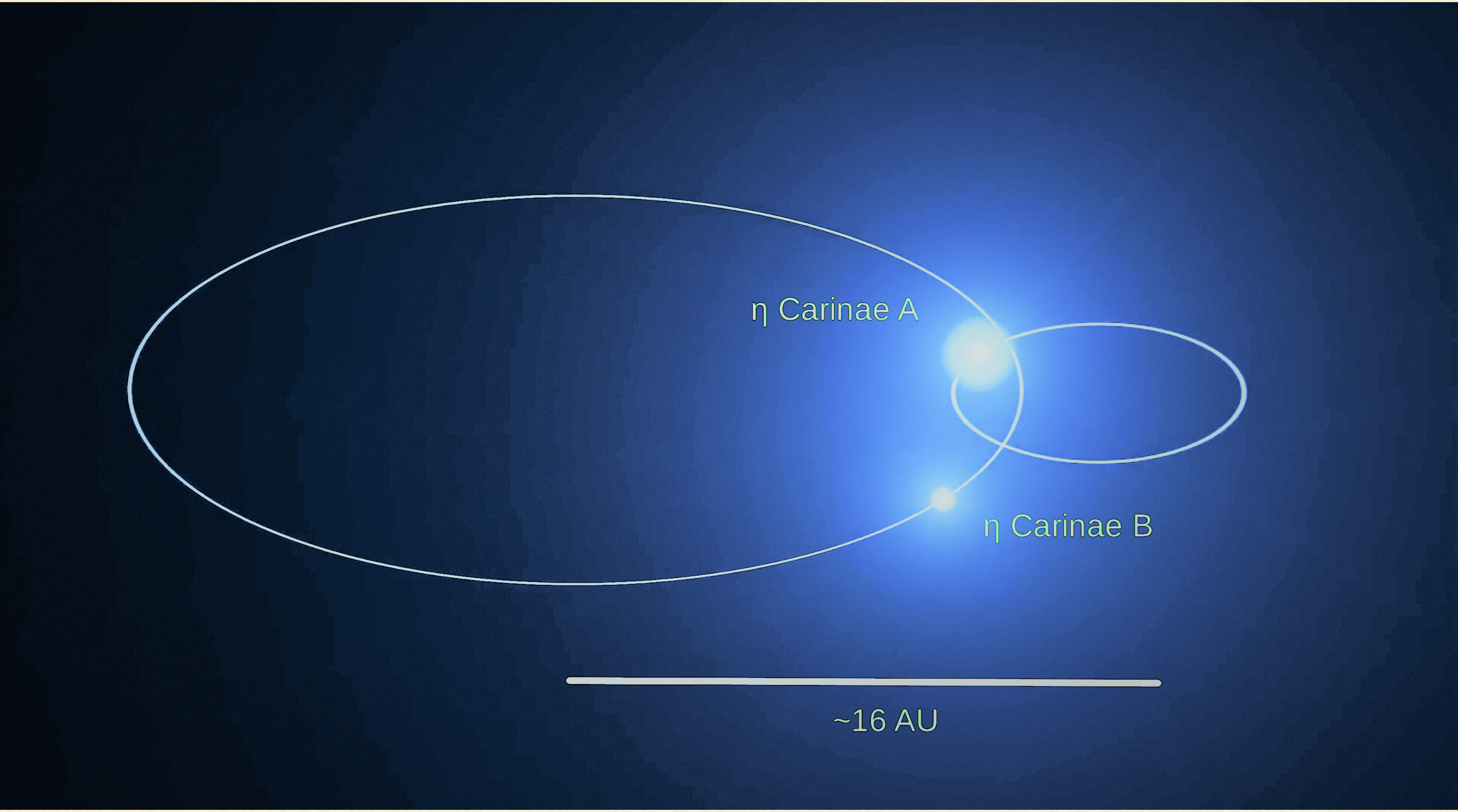
η Carinae A
η Carinae B
~16 AU

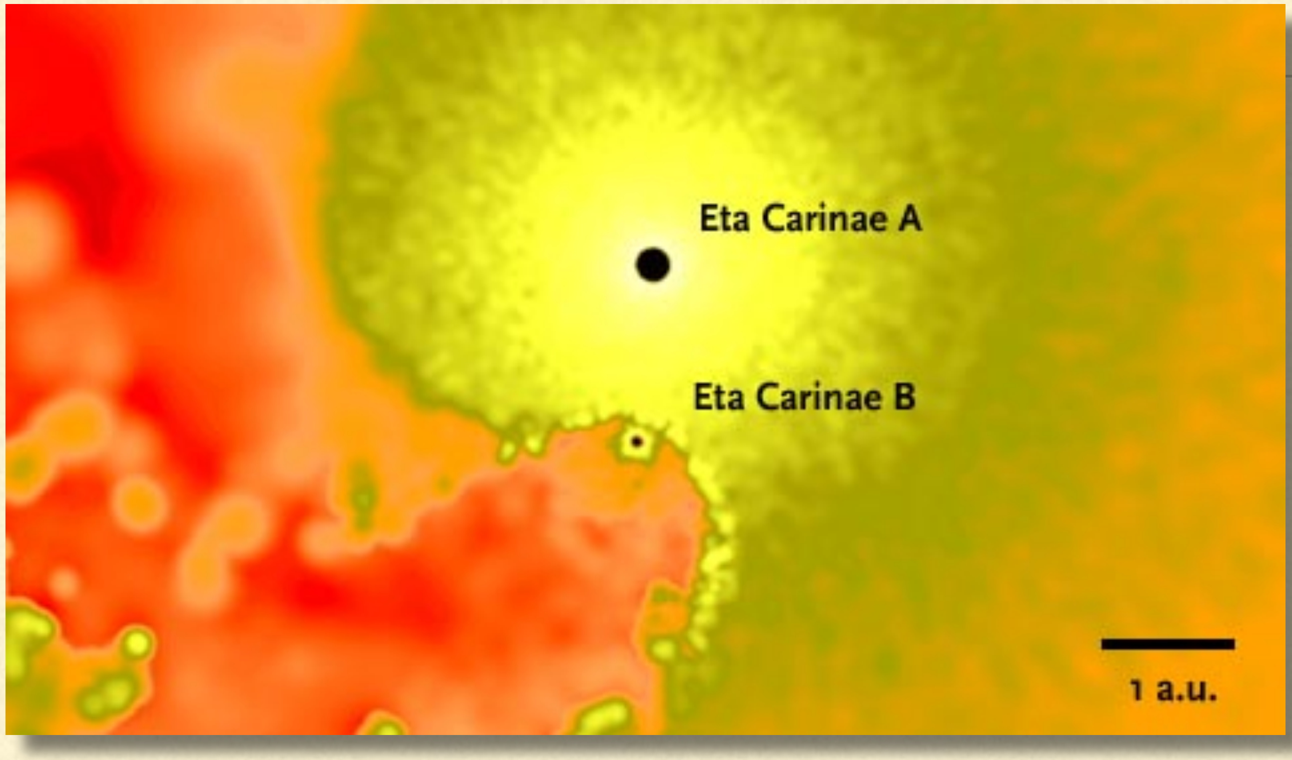

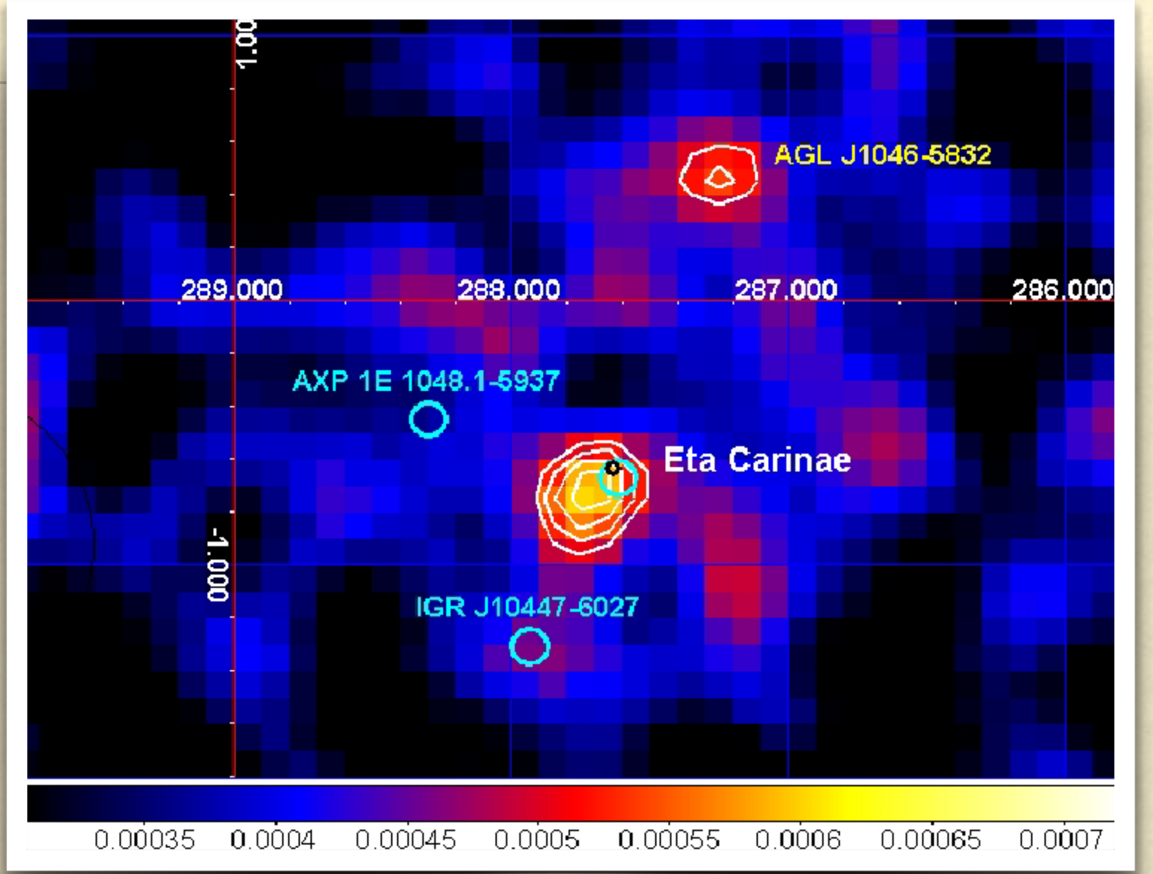

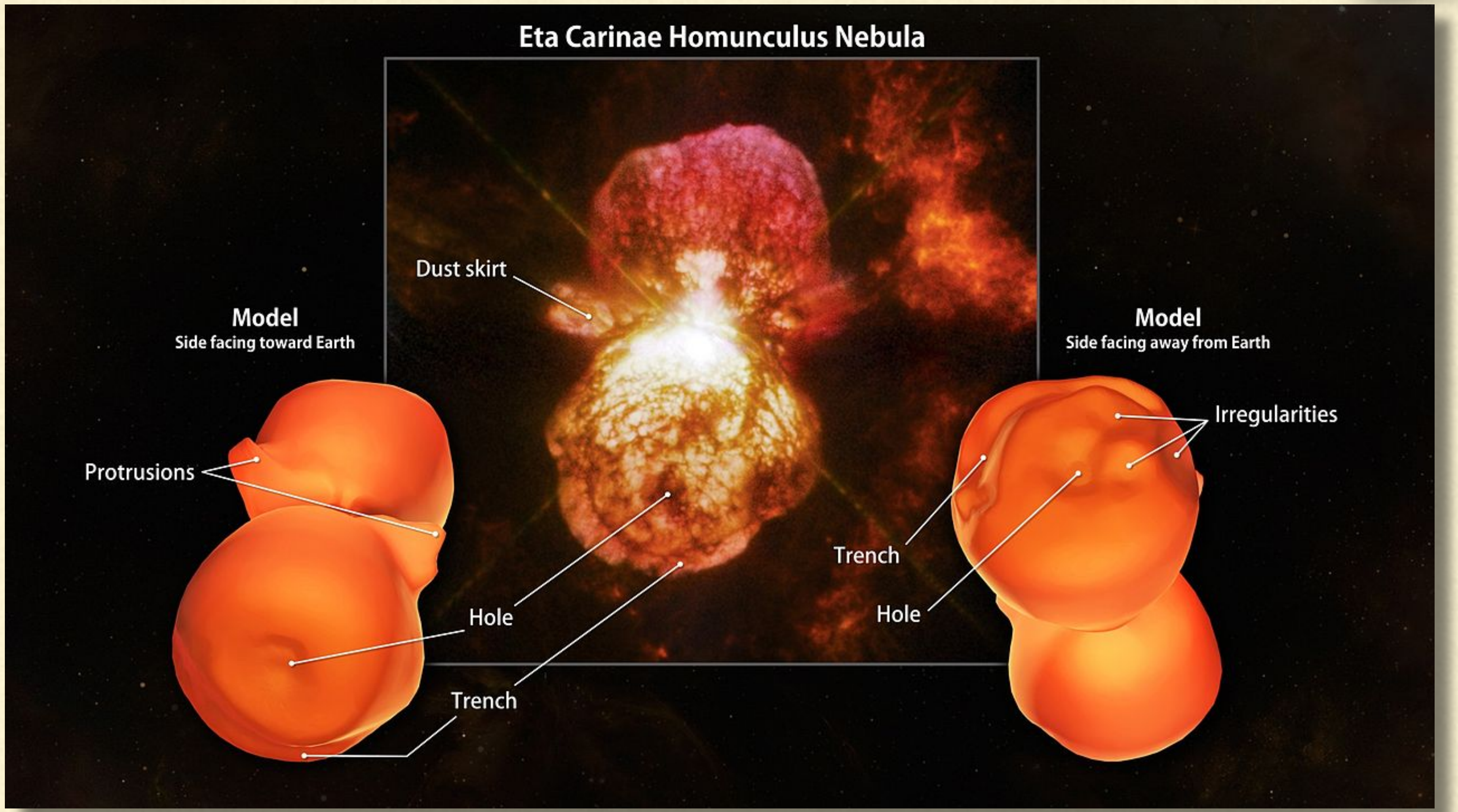

AGILE gamma-ray intensity map in Galactic coordinates of the Car region above 100 MeV (Tavani et al. 2009)

Eta Carinae

Parameter	Value	Reference
d	2.3 ± 0.1 kpc	Davidson & Humphreys (1997)
P	2024 ± 2 d	Corcoran et al. (2005)
i	$45°$	Okazaki et al. (2008)
e	0.9	Smith et al. (2004)
Φ	$27°$	Okazaki et al. (2008)
	$0\text{–}30°$	Parkin et al. (2009)
a	15.4 AU	Corcoran (2001)
M_A	$90\ M_\odot$	Hillier et al. (2001)
M_B	$30\ M_\odot$	Verner et al. (2005)
$\dot{M}_A$	$10^{-3}\ M_\odot\ \mathrm{yr}^{-1}$	Hillier et al. (2001)
	$2.5 \times 10^{-4}\ M_\odot\ \mathrm{yr}^{-1}$	Pittard & Corcoran (2002)
$\dot{M}_B$	$10^{-5}\ M_\odot\ \mathrm{yr}^{-1}$	Pittard & Corcoran (2002)
	$1.5 \times 10^{-5}\ M_\odot\ \mathrm{yr}^{-1}$	Parkin et al. (2009)
$V_{\infty,A}$	$500\ \mathrm{km\ s}^{-1}$	Hillier et al. (2001)
$V_{\infty,B}$	$3000\ \mathrm{km\ s}^{-1}$	Pittard & Corcoran (2002)

Reitberger et al. 2012

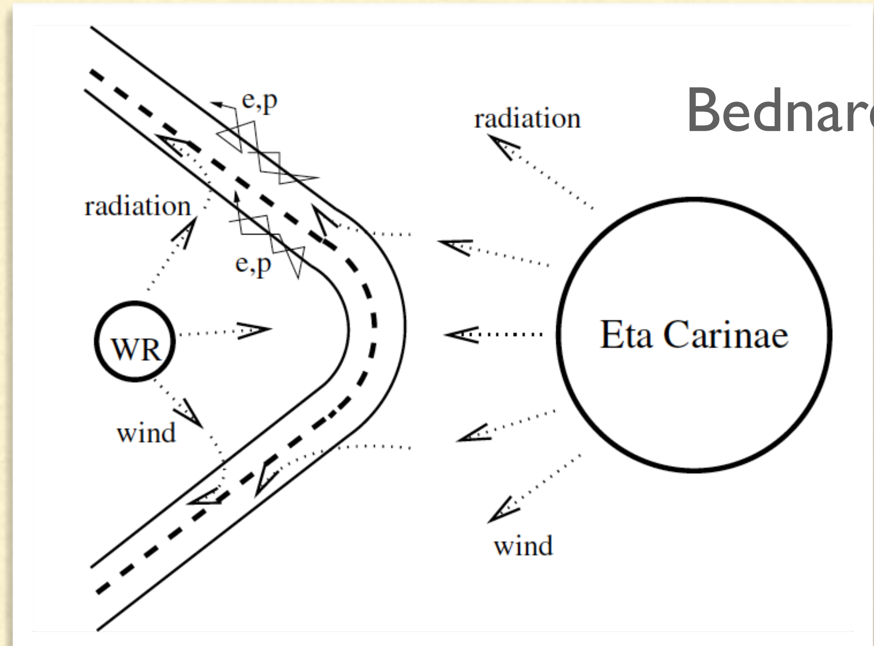

Bednarek & Pabich 2011

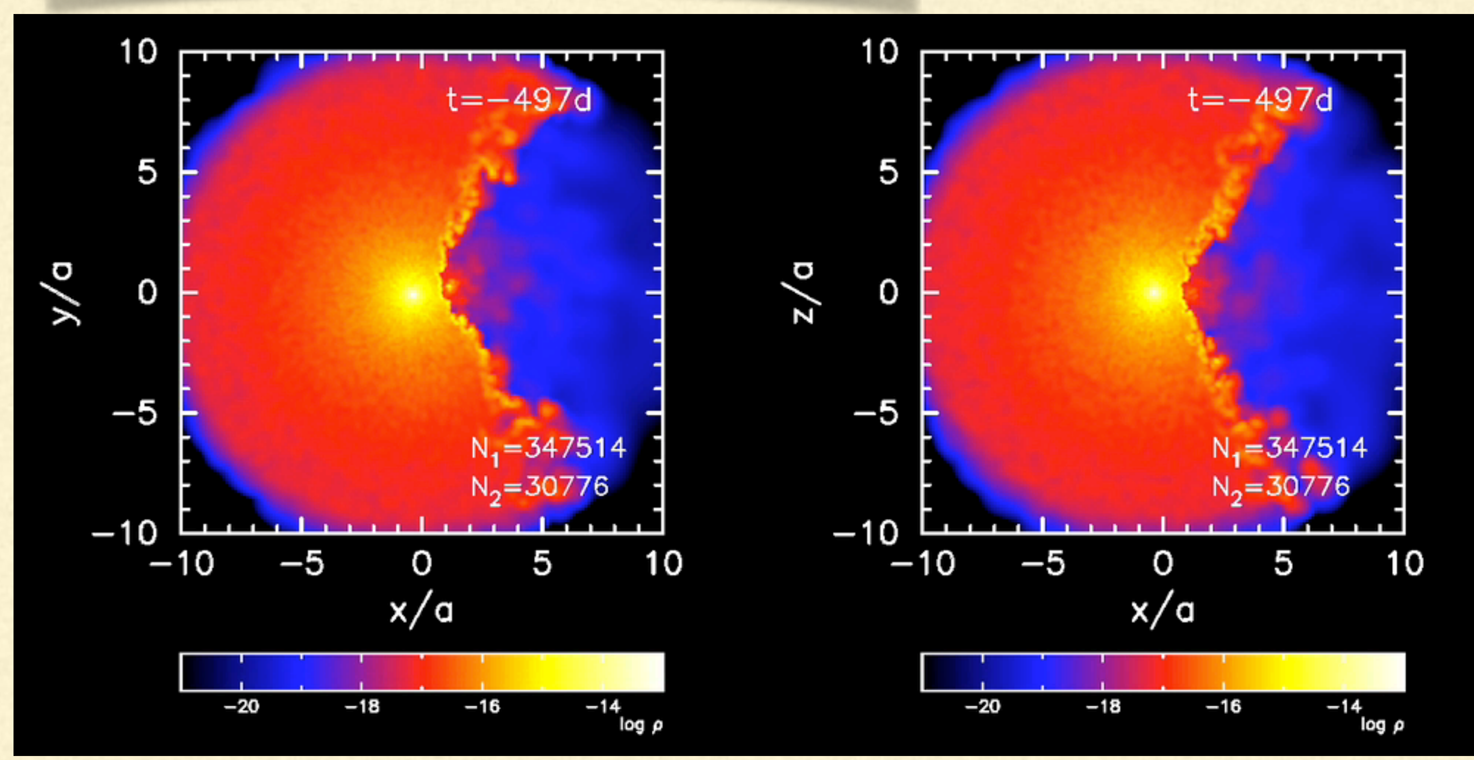

A. Okazaki

Conditions are different in the two shocks and change along the orbit (e.g. Ohm et al. 2015).

Theoretical SED during the periastron passage (Gupta & Razzaque 2017)

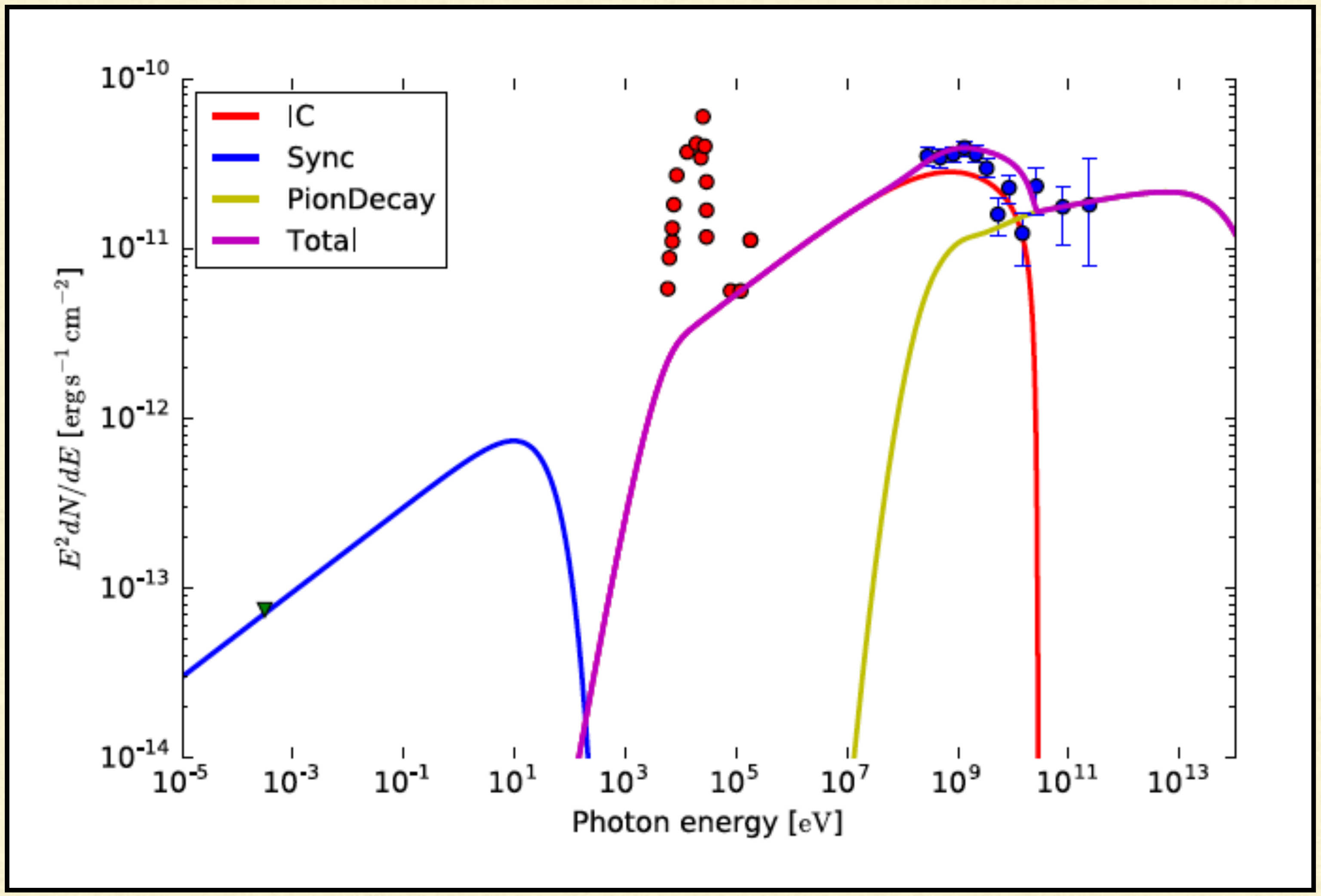

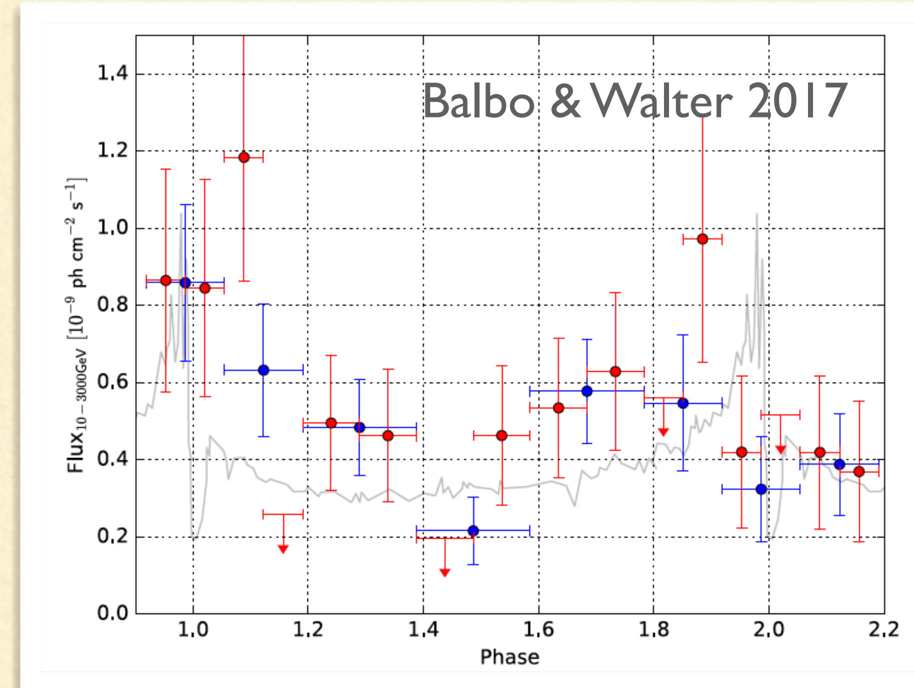

Variability with the orbital phase. Different behavior at low (0.3-10 GeV) and high (>10 GeV) gamma-ray energies.

What are the best candidates for gamma-ray emission?

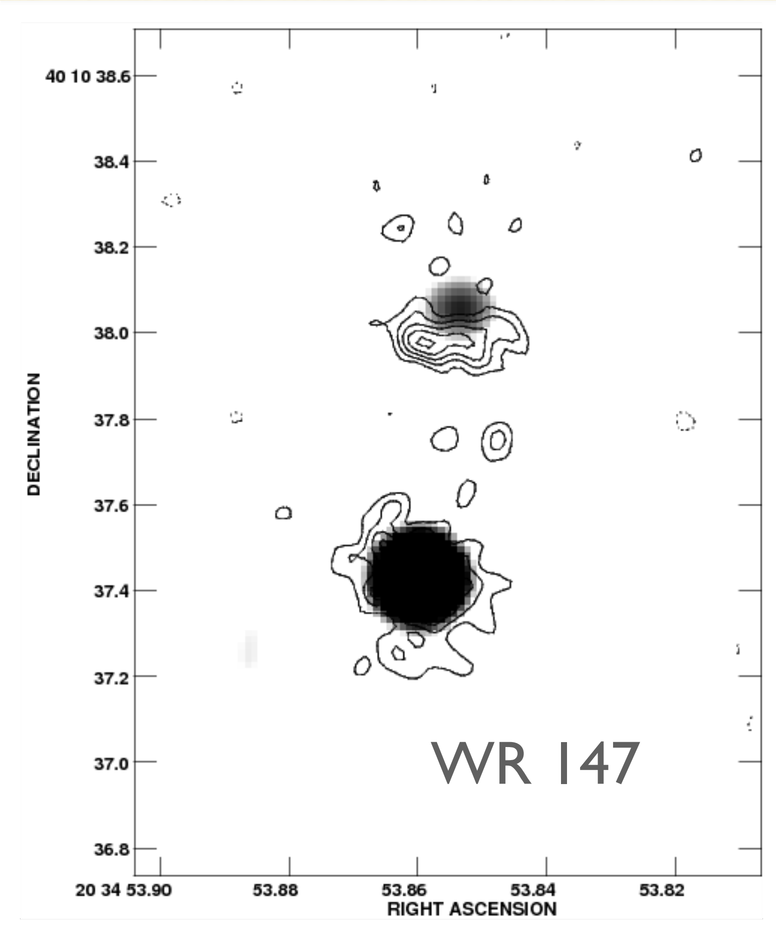

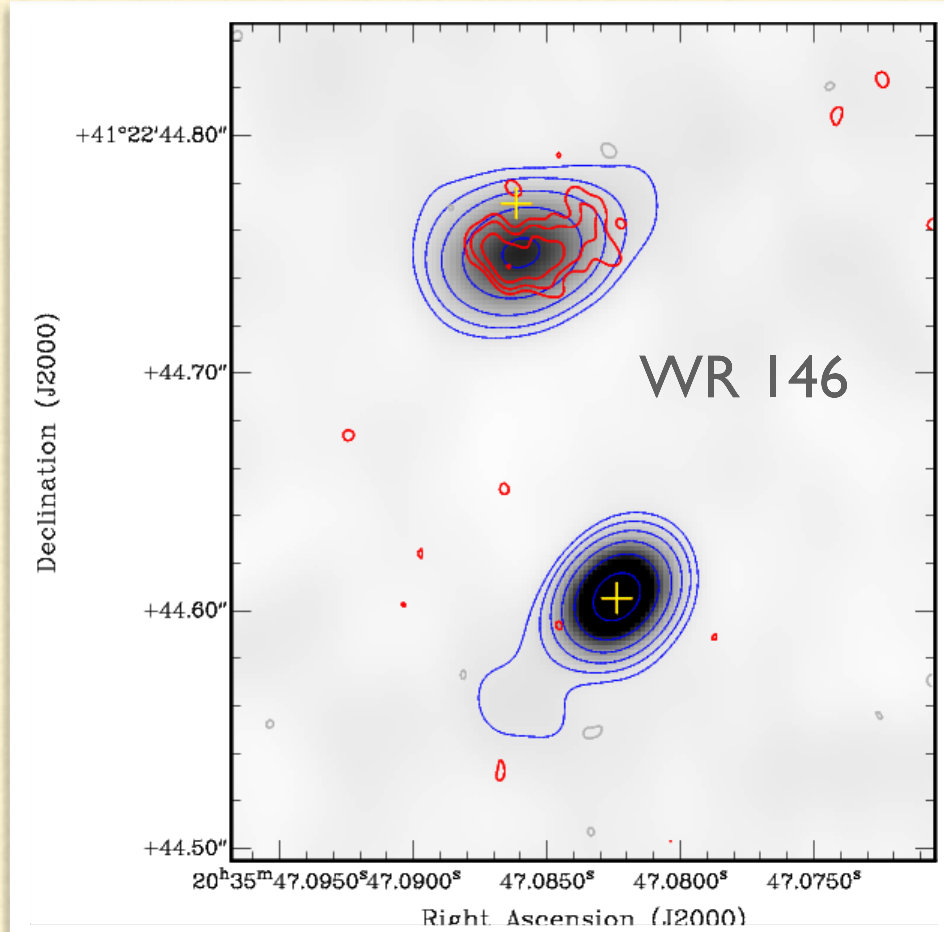

The usual suspects.
See, e.g. Benaglia & Romero 2003

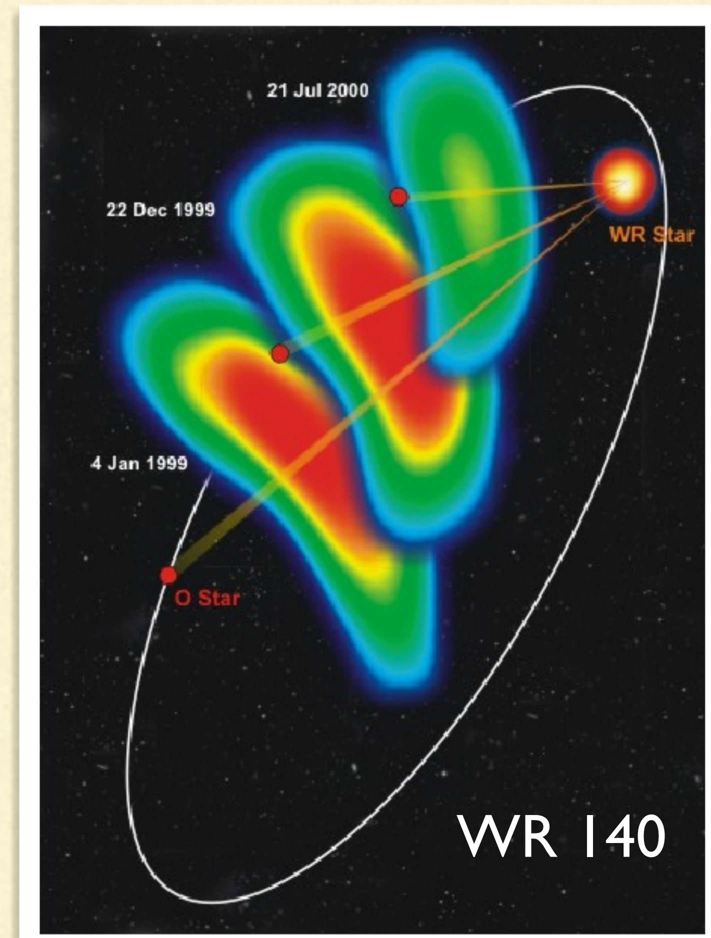

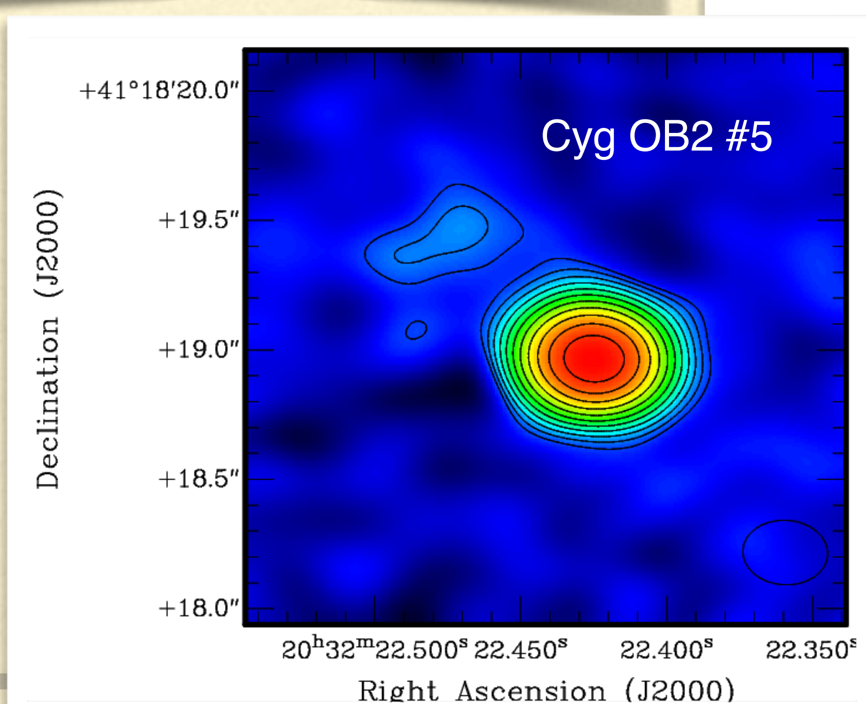

Strong non-thermal radio emitters

However, at the current separation between the components of the system, radio might be favoured over gamma-ray emission

Benaglia + A&A 2015

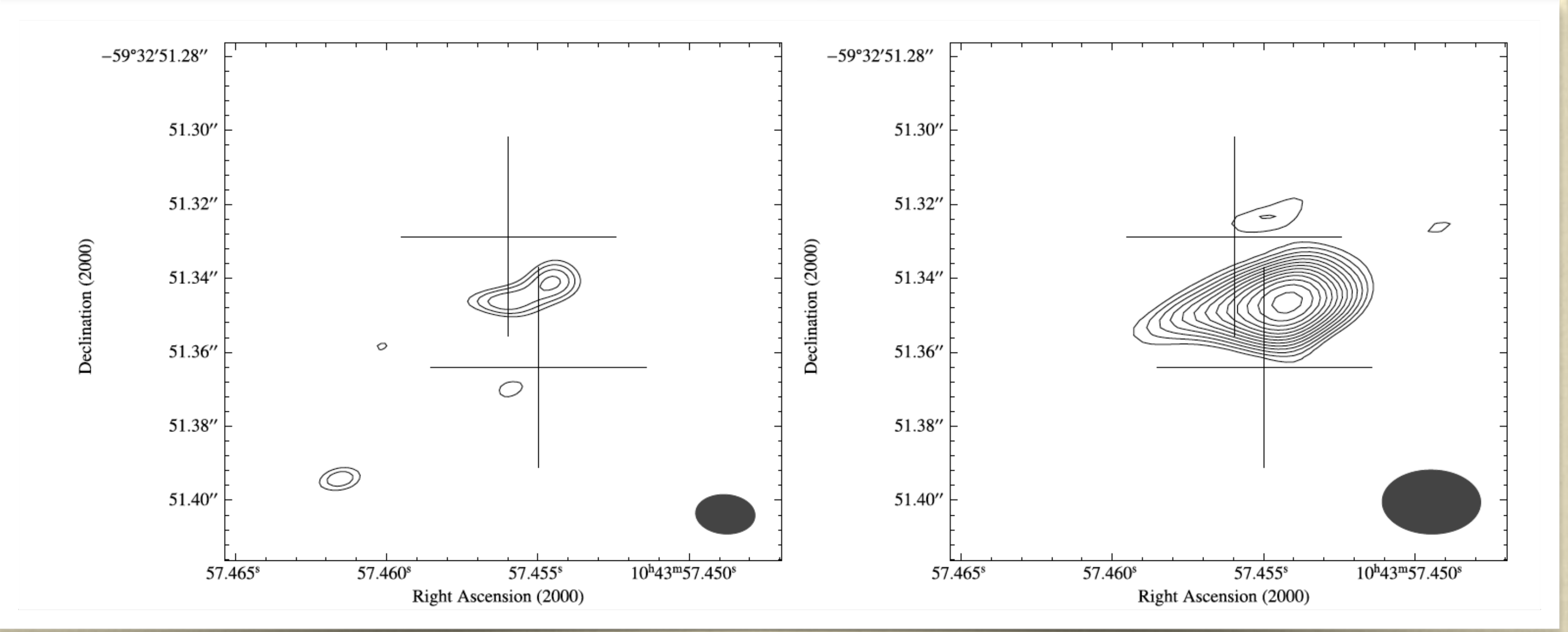

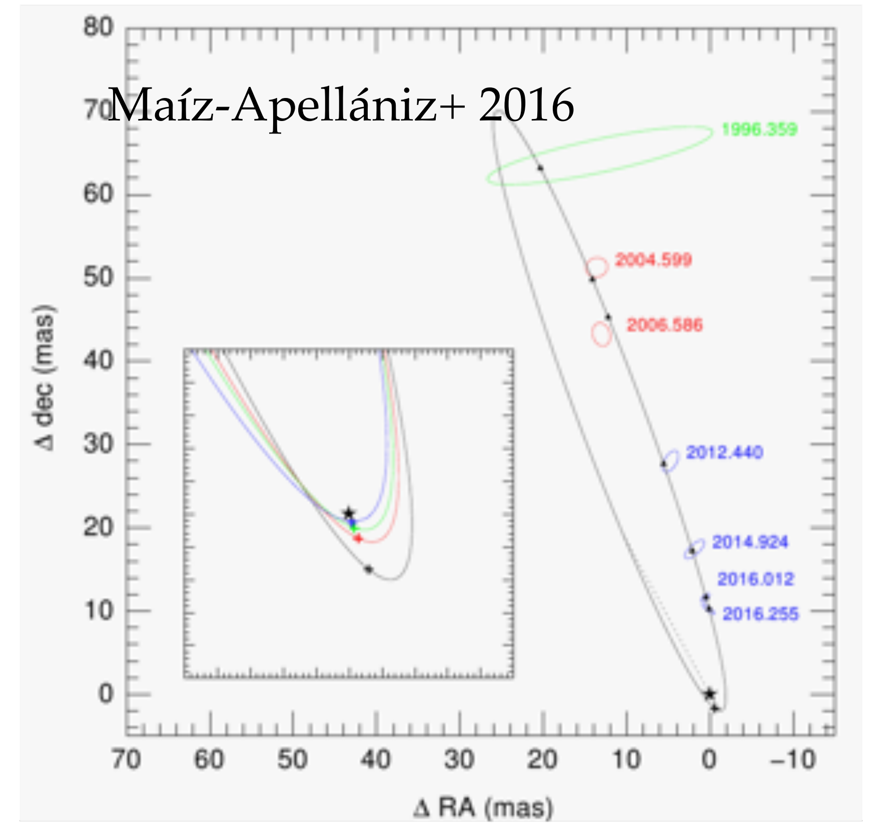

Array/project and date	ν [GHz]	S_ν [mJy]
ATCA/C678		
2003-01-28	4.8	4.1 ± 0.4[a]
2003-01-28	8.6	2.0 ± 0.2[a]
2003-12-20	1.4	9.4 ± 0.9[a]
2003-12-20	2.4	7.8 ± 0.4[a]
2004-05-05	17.8	1.8 ± 0.15[a]
2004-05-05	24.5	1.5 ± 0.35[a]
ATCA/V191B		
2008-08-06	2.3	7.5 ± 0.11
ATCA/C1726		
2009-01-18	4.8	5.6 ± 0.3
2009-01-18	8.6	2.9 ± 0.3
LBA/V191B		
2008-08-06	2.3	2.9 ± 0.51[b]

→ Spectral index ~ -1

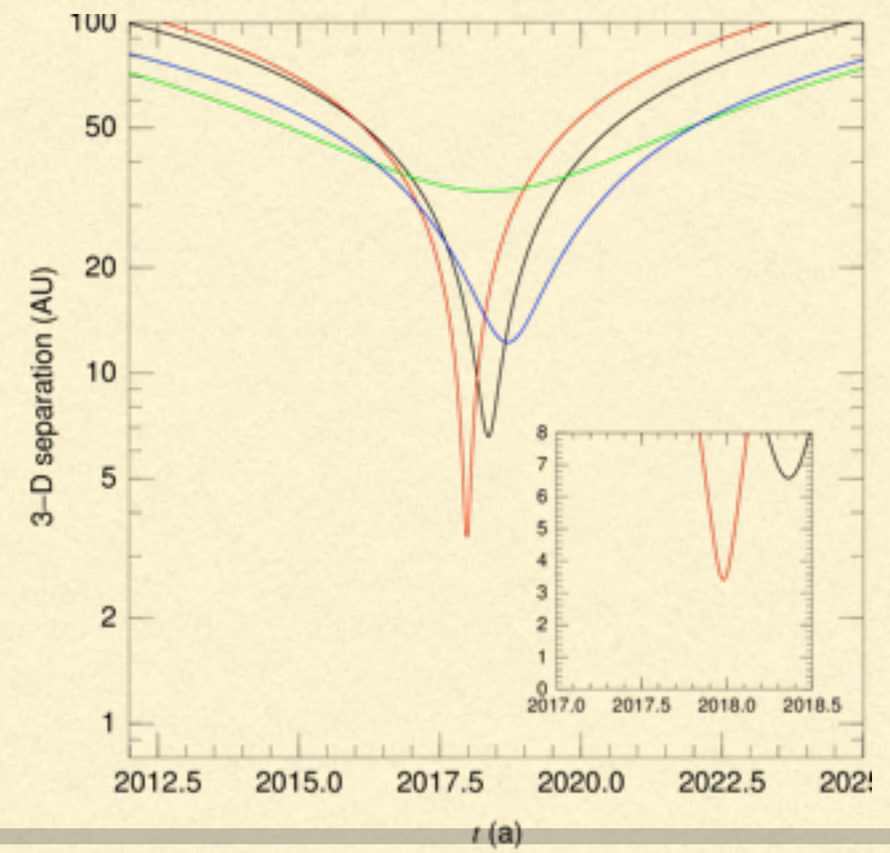

Model (del Palacio et al 2016)

General considerations:

- Wind collision region with axial symmetry.
- Structure with 2 adiabatic and narrow shocks.
- *Q (E)* α E^{-q}, *q* according to the observations in radio.
- Electronic non-thermal emission by synchr, relativistic Bremss, and IC, and hadronic emission from *pp*.
- Free-free absorption in the stellar wind (SSA, R-T effect and γ-γ absorption are all negligible).

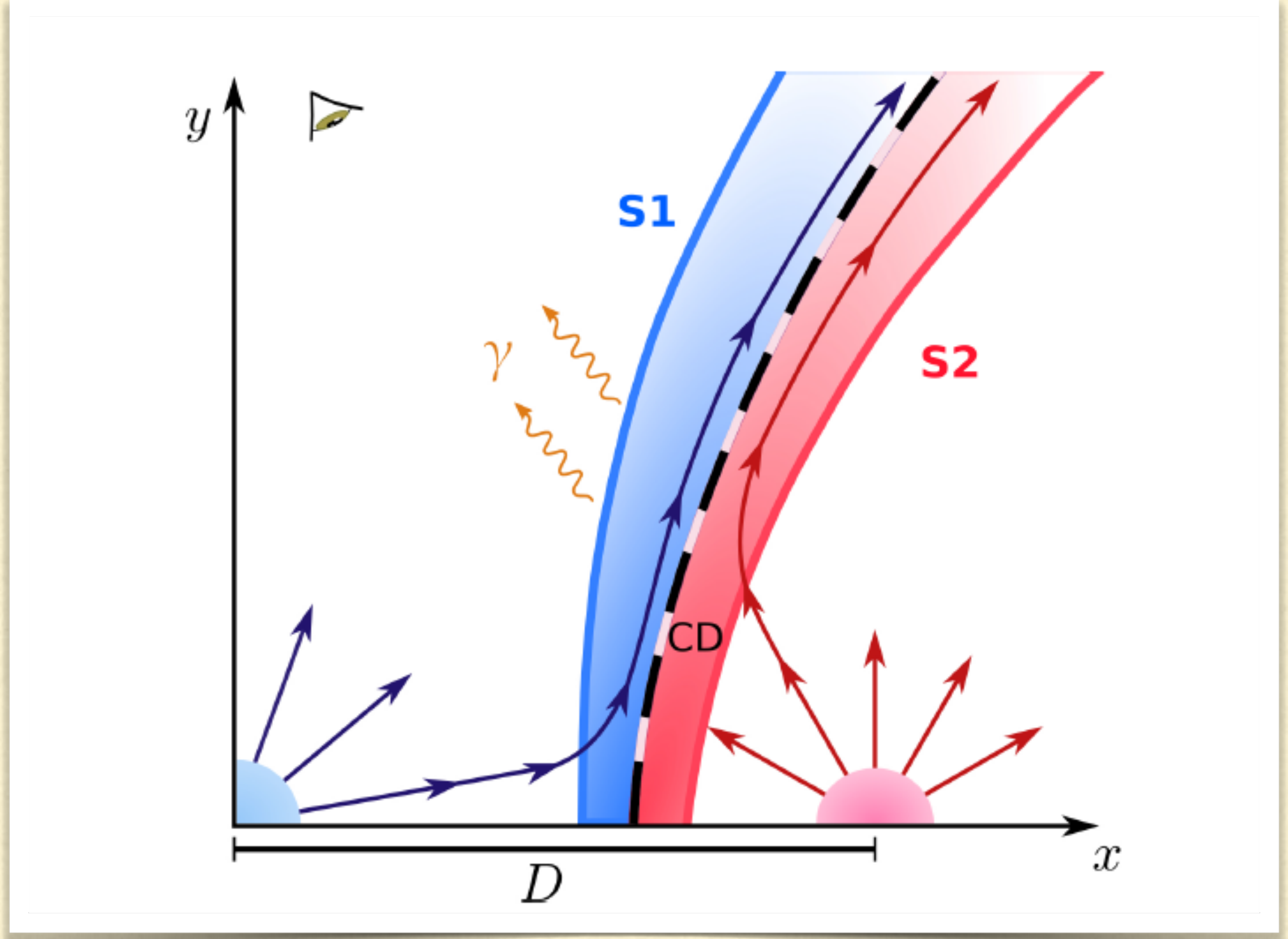

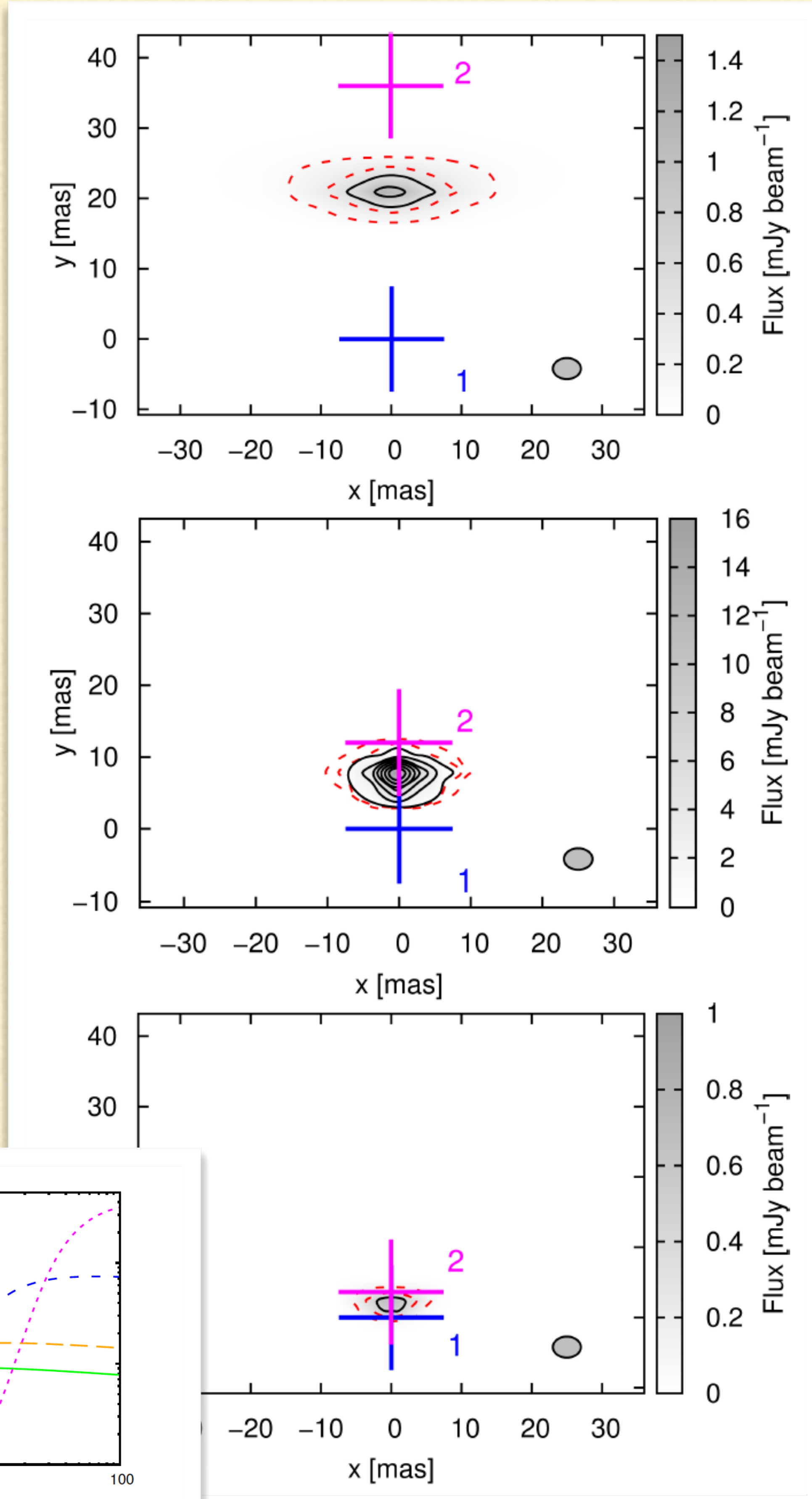

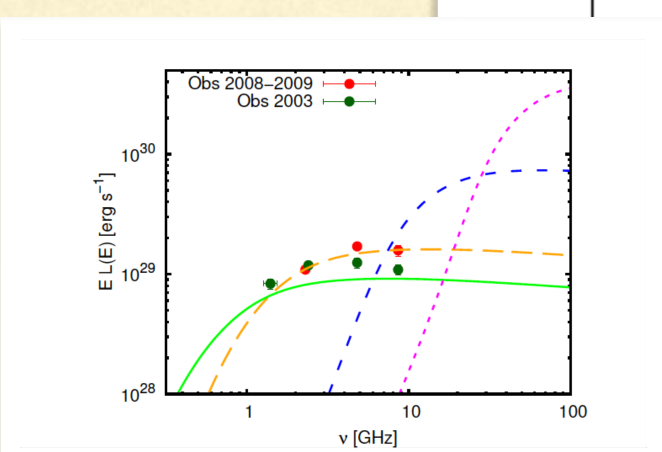

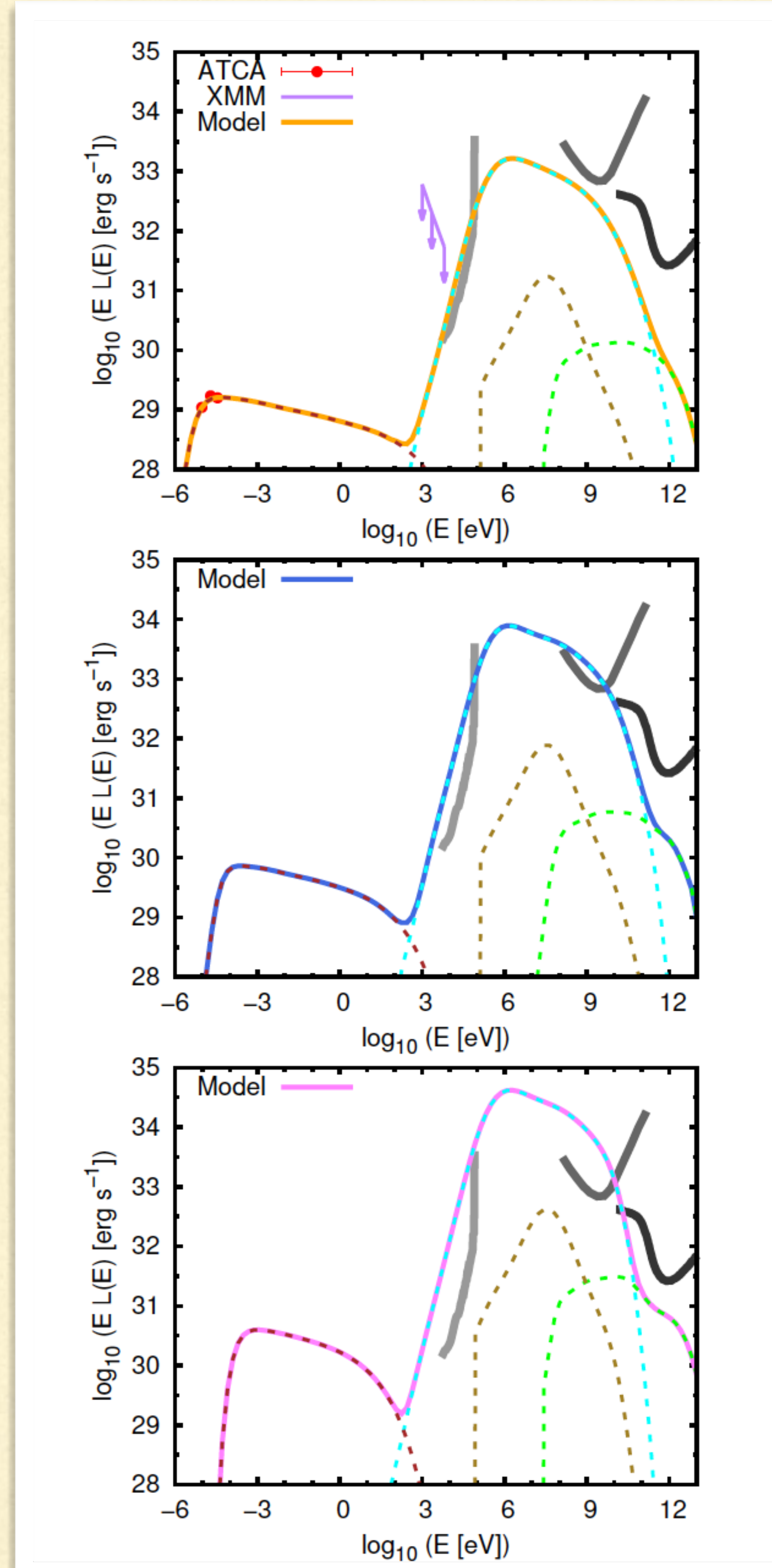

del Palacio et al. A&A, 591, A139, 2016

Binaria: pulsar + estrella O (LS5035)

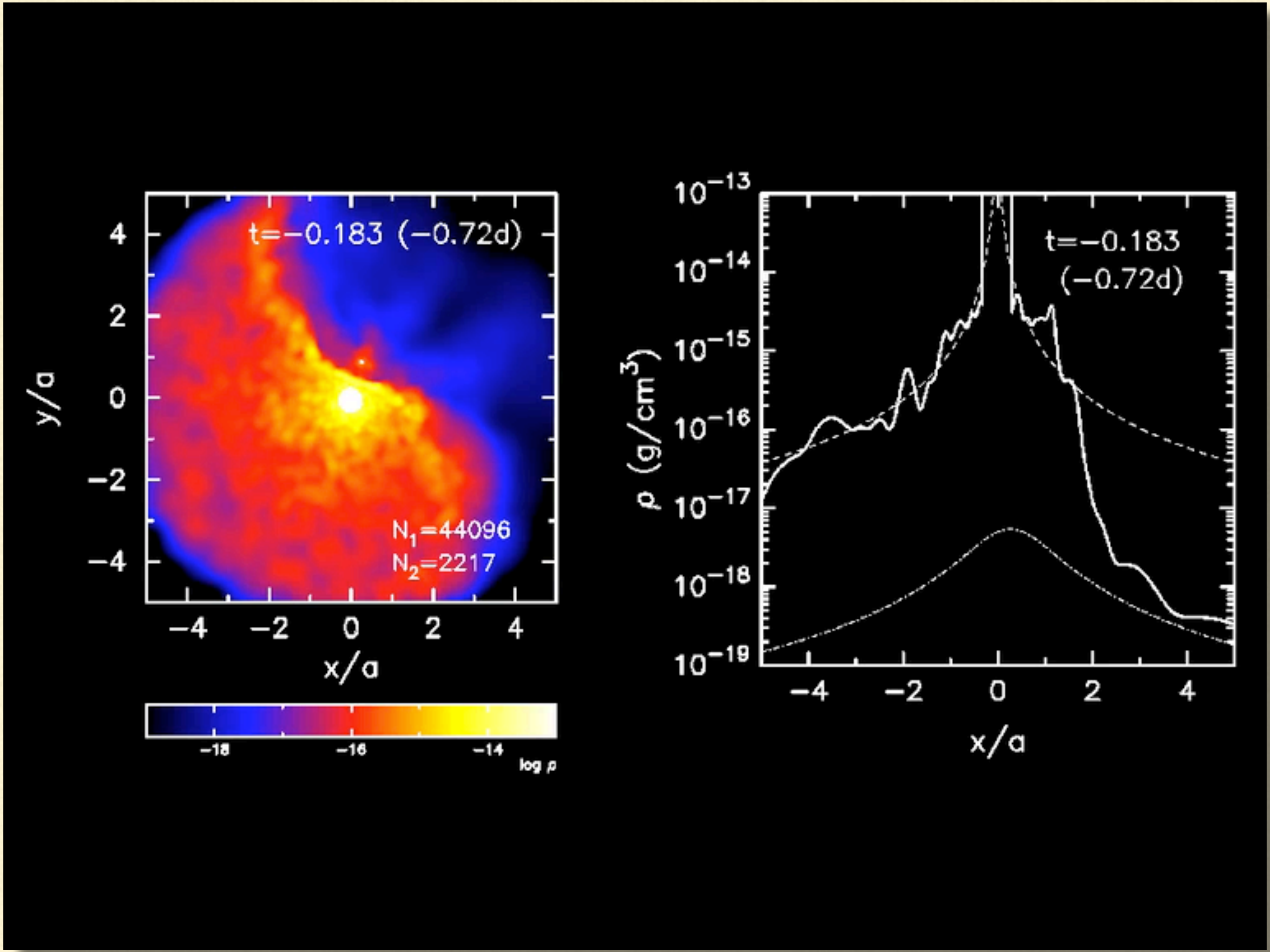

A. Okazaki

Bowshocks

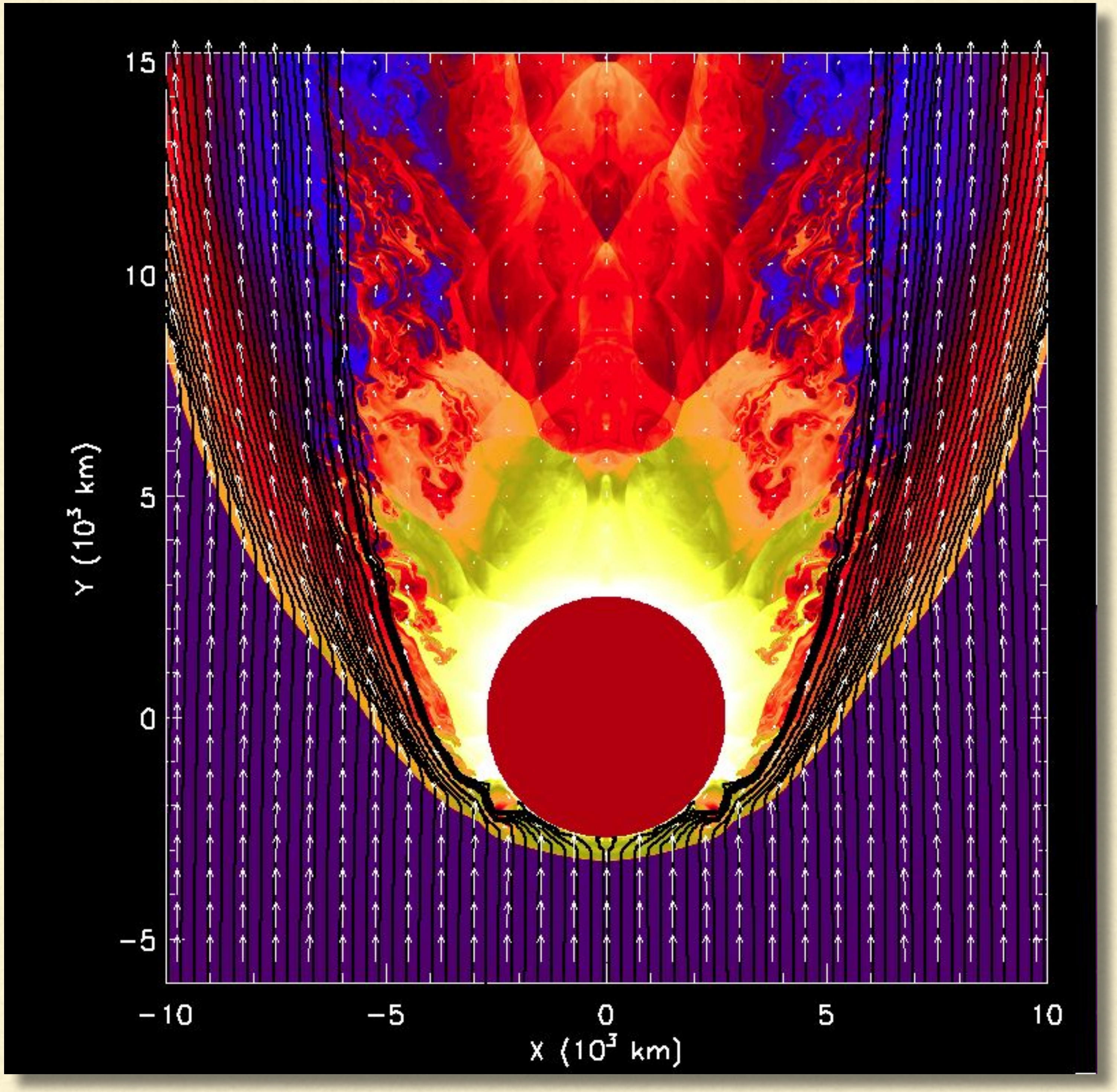
Y (10^3 km)
X (10^3 km)
15
10
5
0
−5
−10
−5
0
5
10

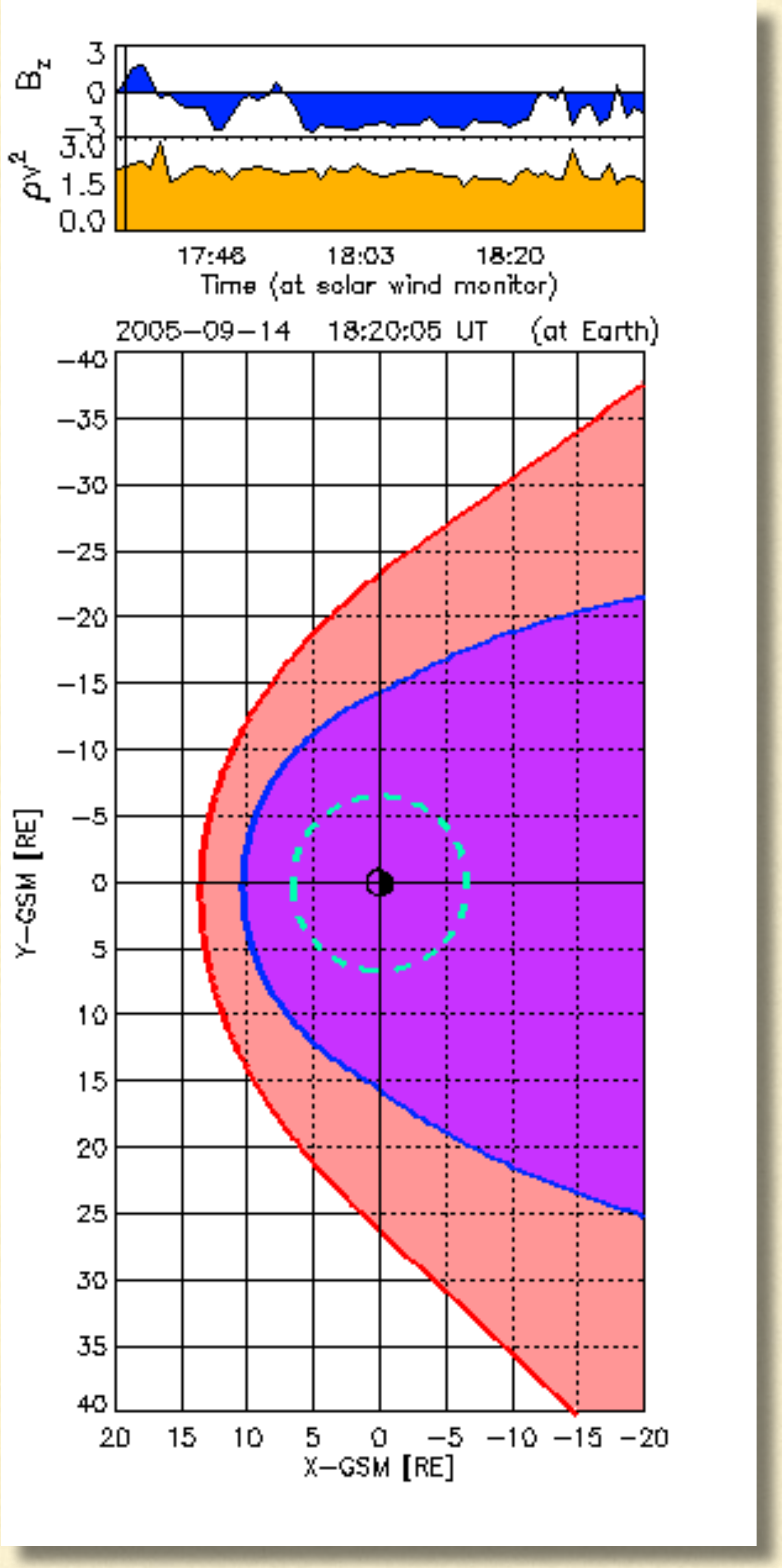
B_z
ρv^2
17:46
18:03
18:20
Time (at solar wind monitor)
2005−09−14 18:20:05 UT (at Earth)
Y−GSM [RE]
X−GSM [RE]

Modeling bowshocks and their emission

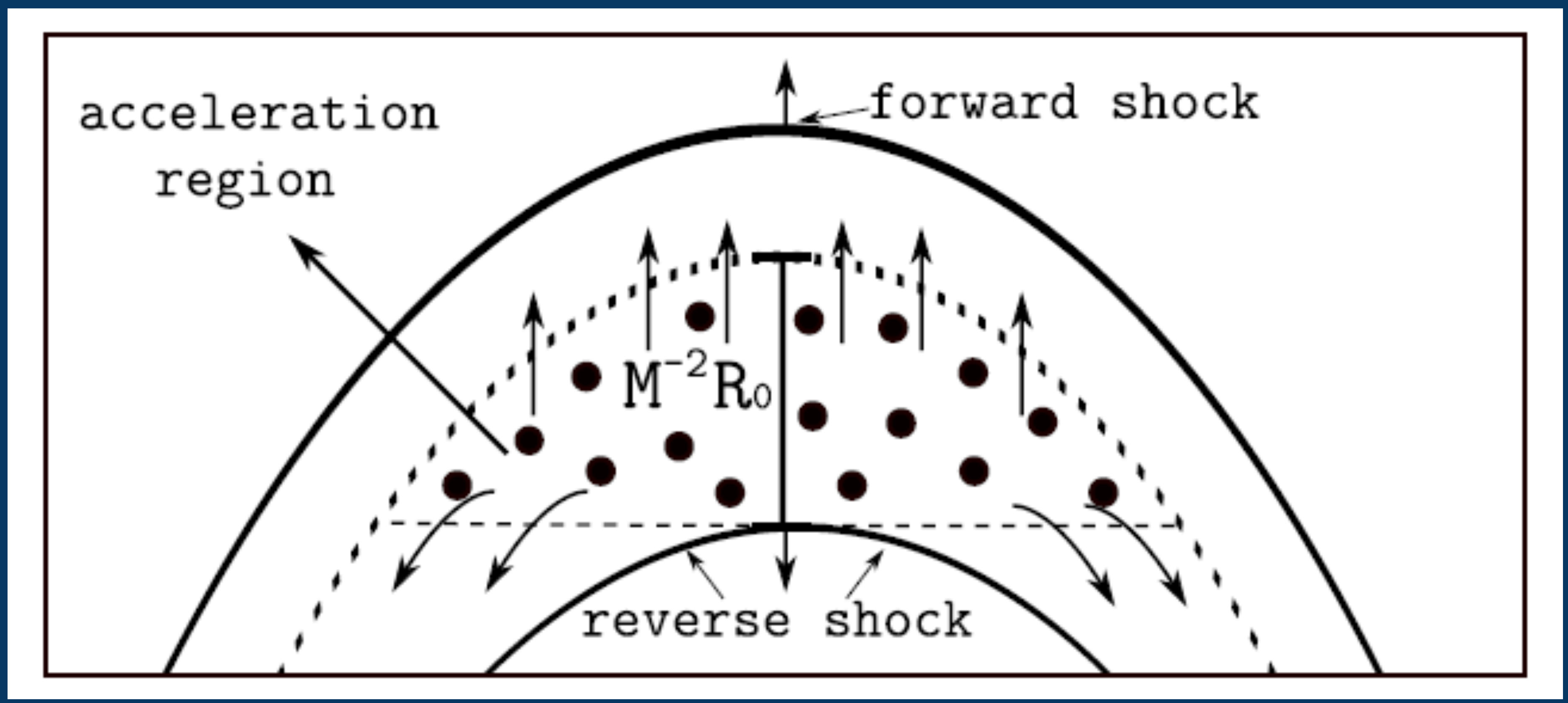

$$R_0 = \sqrt{\frac{\dot{M}_{\rm w} V_{\rm w}}{4\pi \rho_{\rm a} V_\star^2}}.$$

Relativistic particles are accelerated at the reverse adiabatic shock in the stellar wind

Modeling bow-schocks and their emission

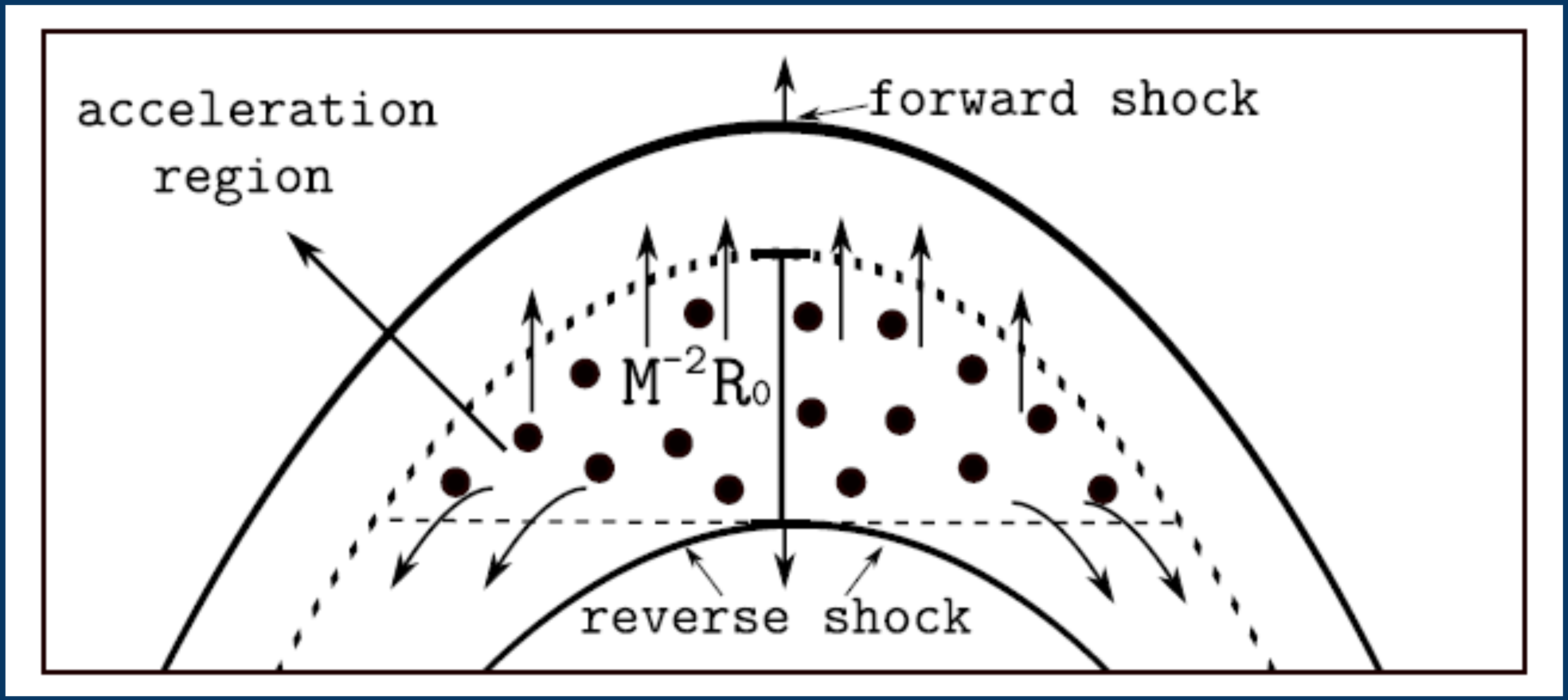

$$\frac{\partial}{\partial E}\left[\frac{\mathrm{d}E}{\mathrm{d}t}\bigg|_{\mathrm{loss}} N(E)\right] + \frac{N(E)}{t_{\mathrm{esc}}} = Q(E),$$

Spectral energy distributions for O4I and O9I stars

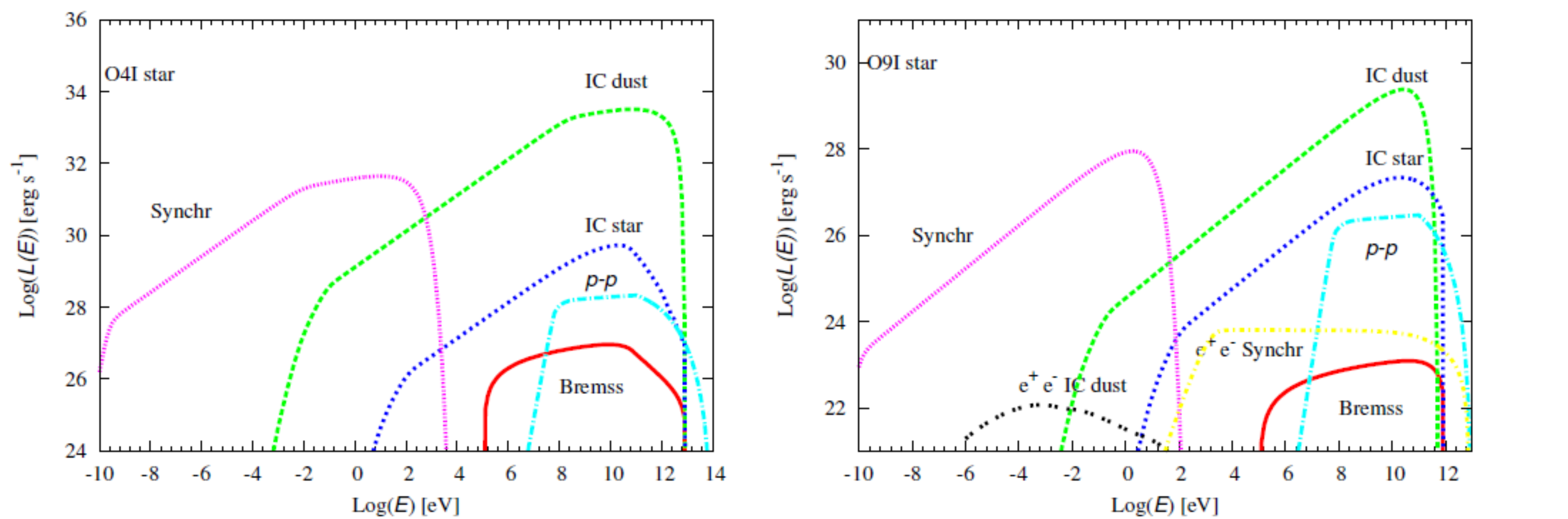

del Valle & Romero 2012, A&A

MSX emission toward BD+43^0 3654

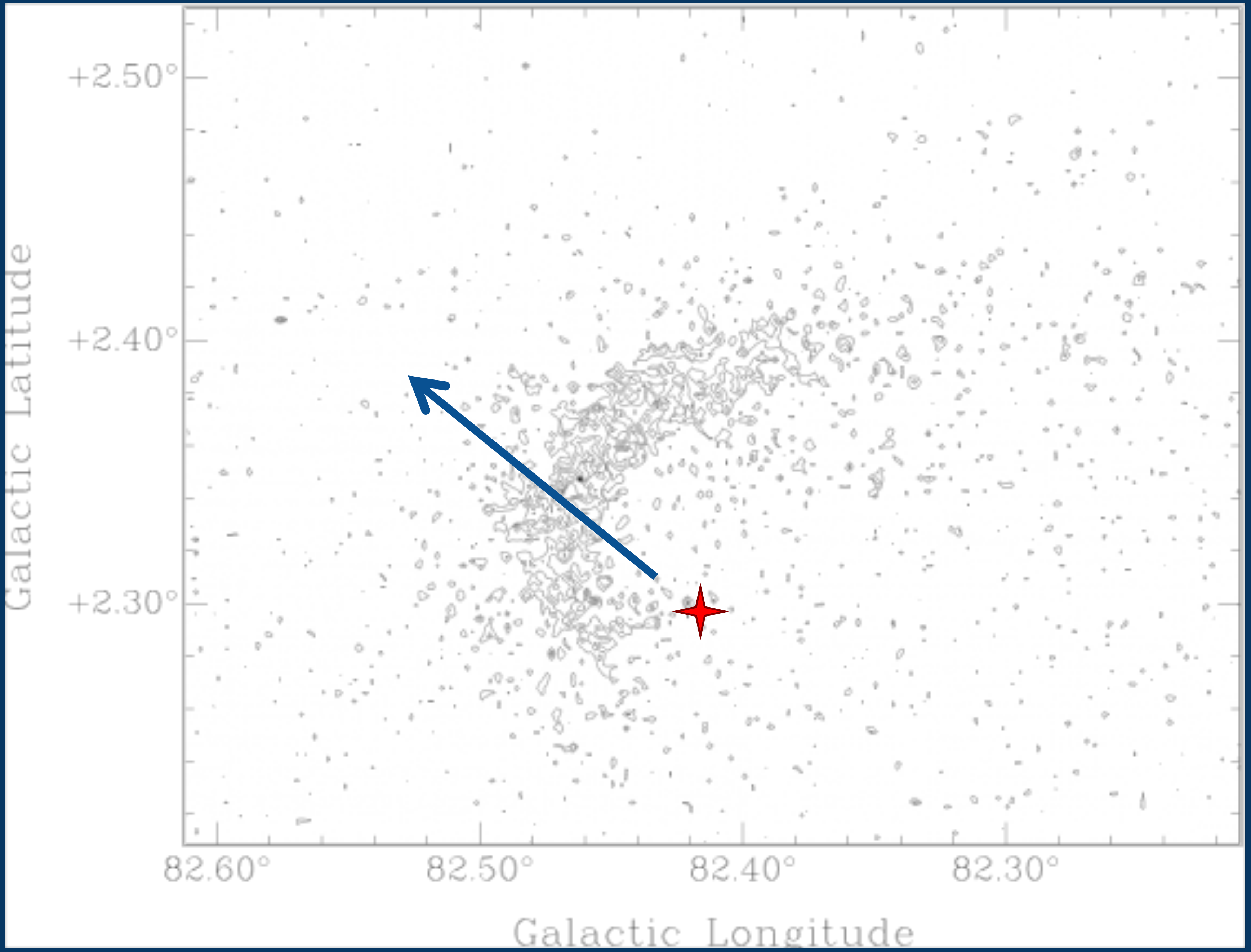

D-band image (14.65 μm)

VLA + MSX images

- s/n (α) $\geq$ 10
- -0.8 $\leq \alpha \leq$ 0.3.
- <α> -0.4

$S(\nu) \sim k\ \nu^{\alpha}$

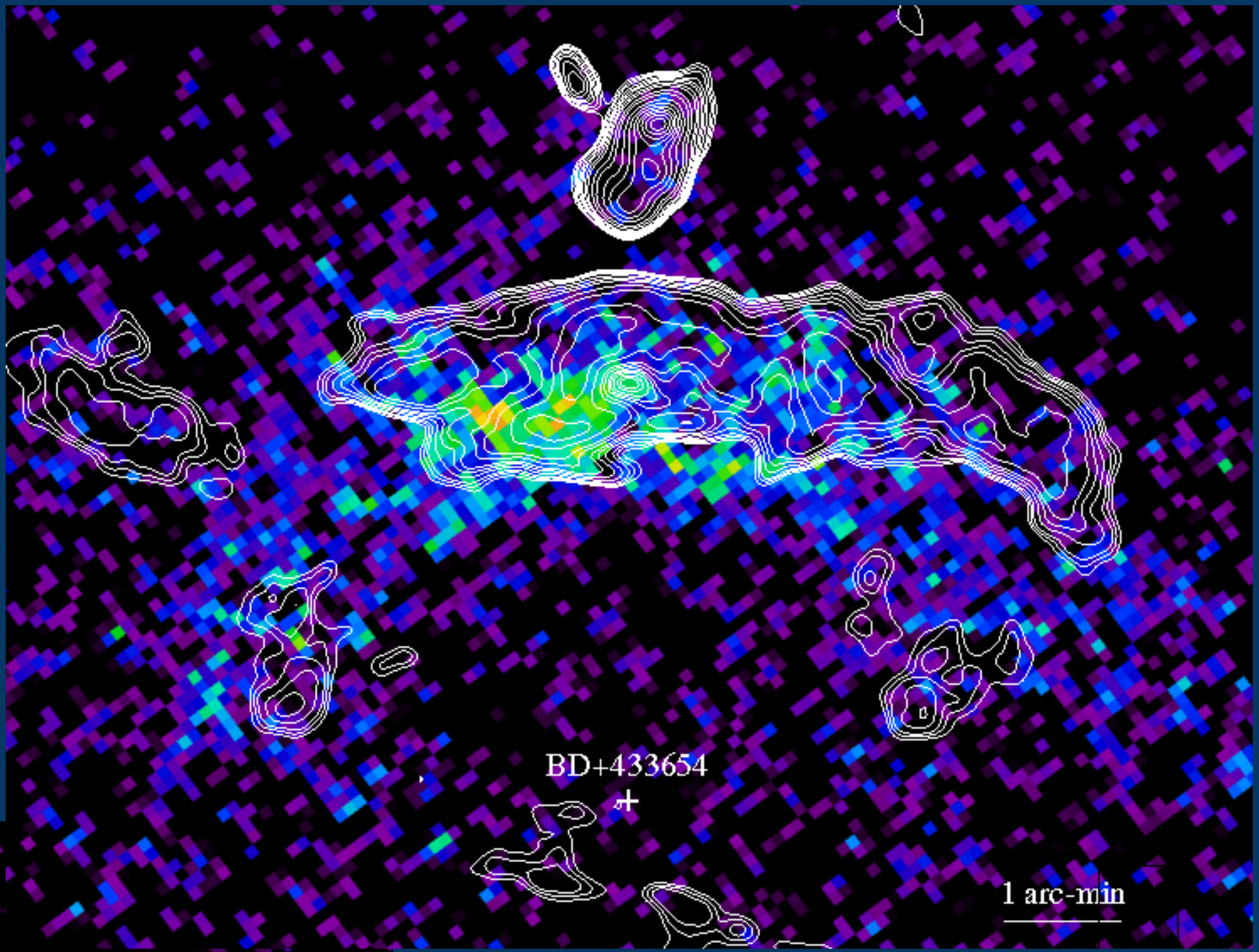

C band (4.86 GHz)

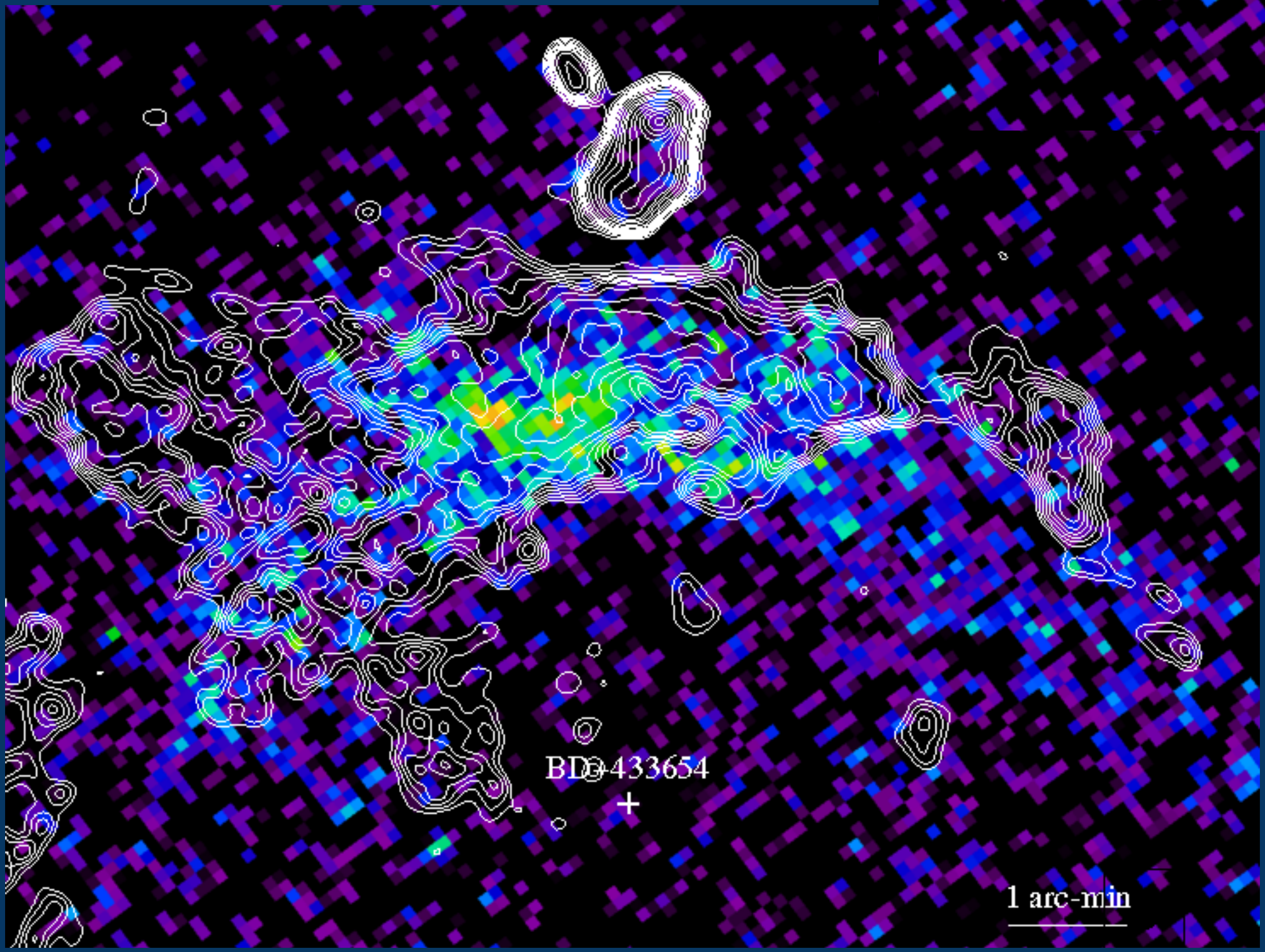

L band (1.42 GHz)

Benaglia, Romero, et al 2010, A&A

SED

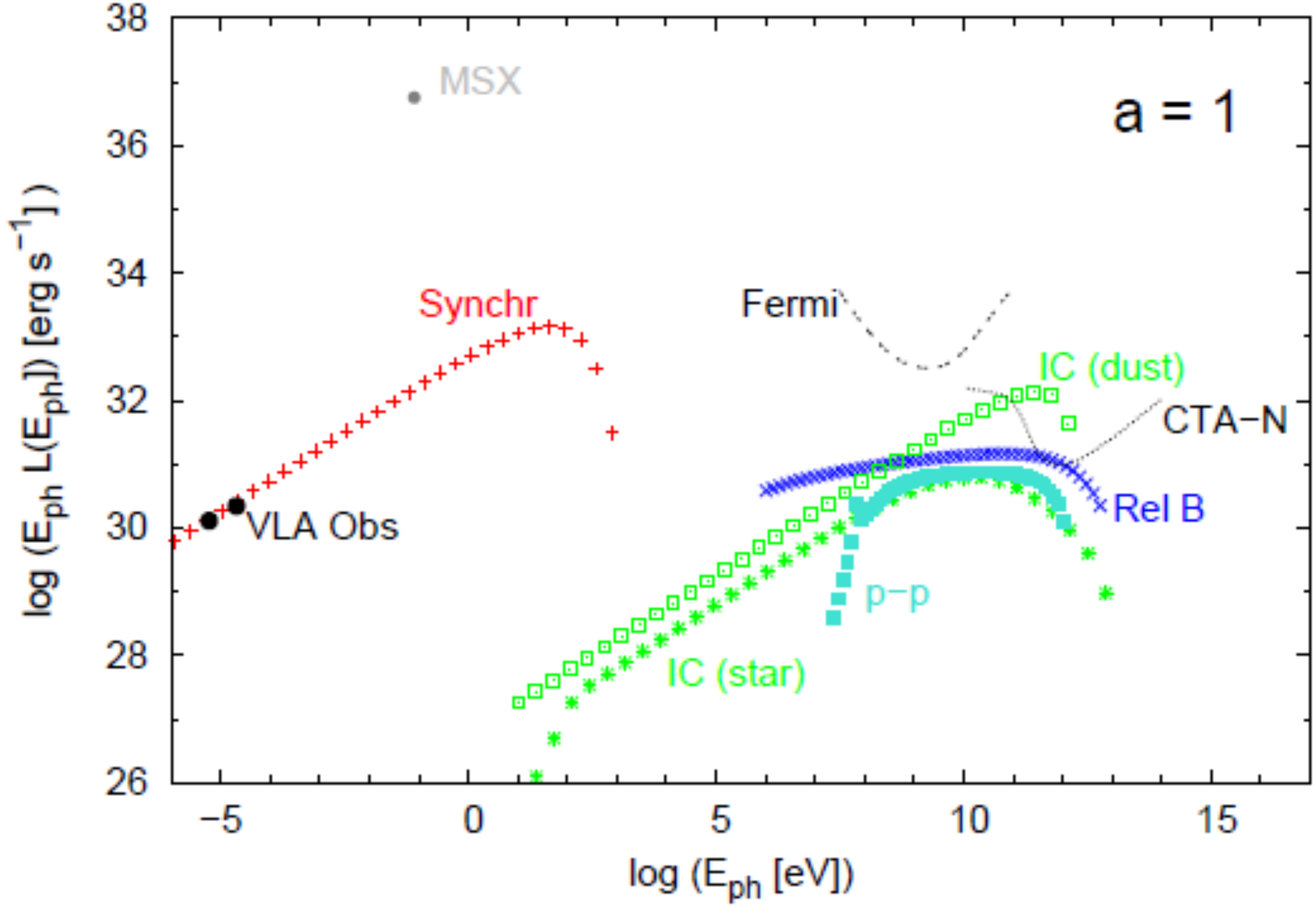

Benaglia, Romero, et al 2010, A&A

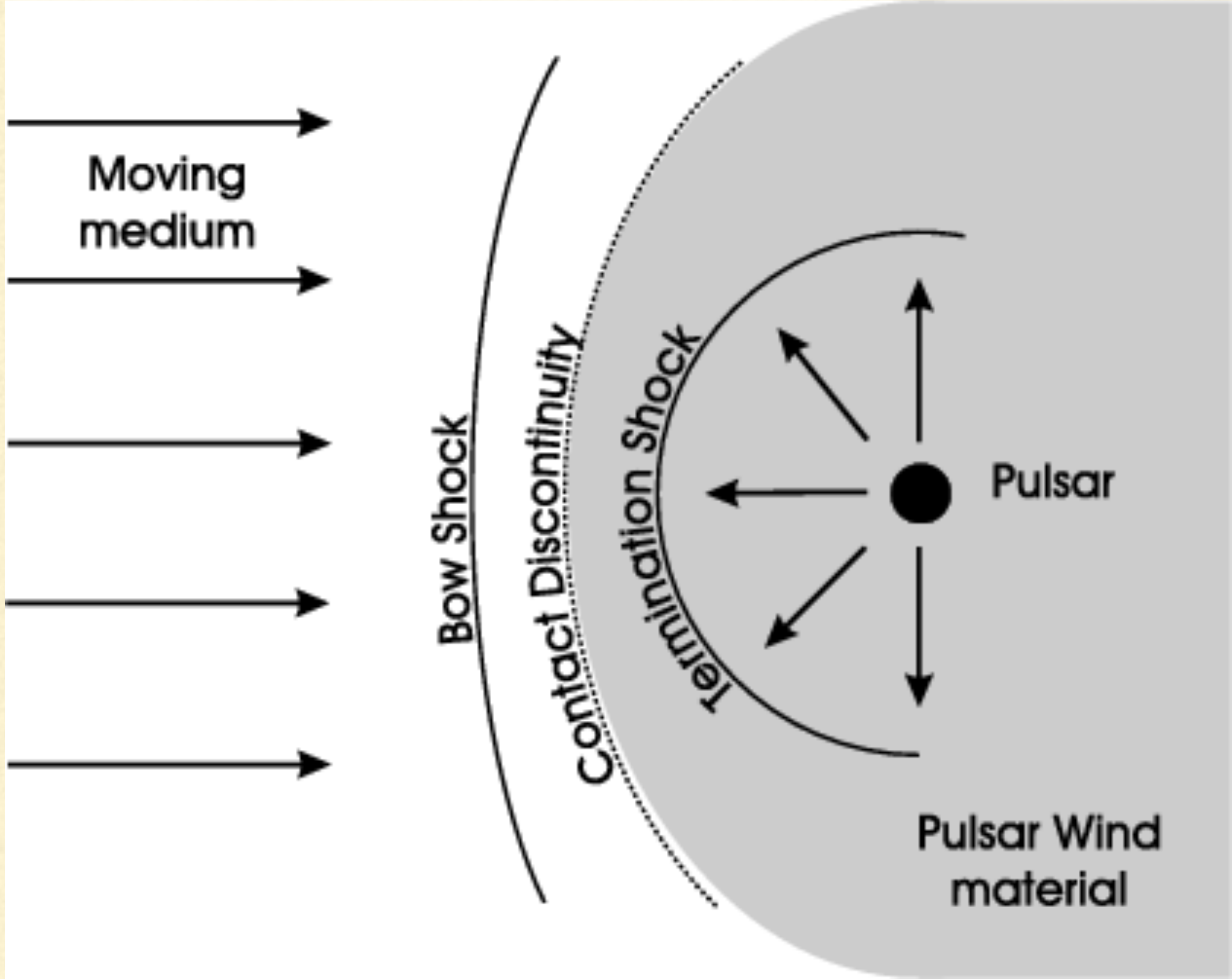
Moving medium
Bow Shock
Contact Discontinuity
Termination Shock
Pulsar
Pulsar Wind material

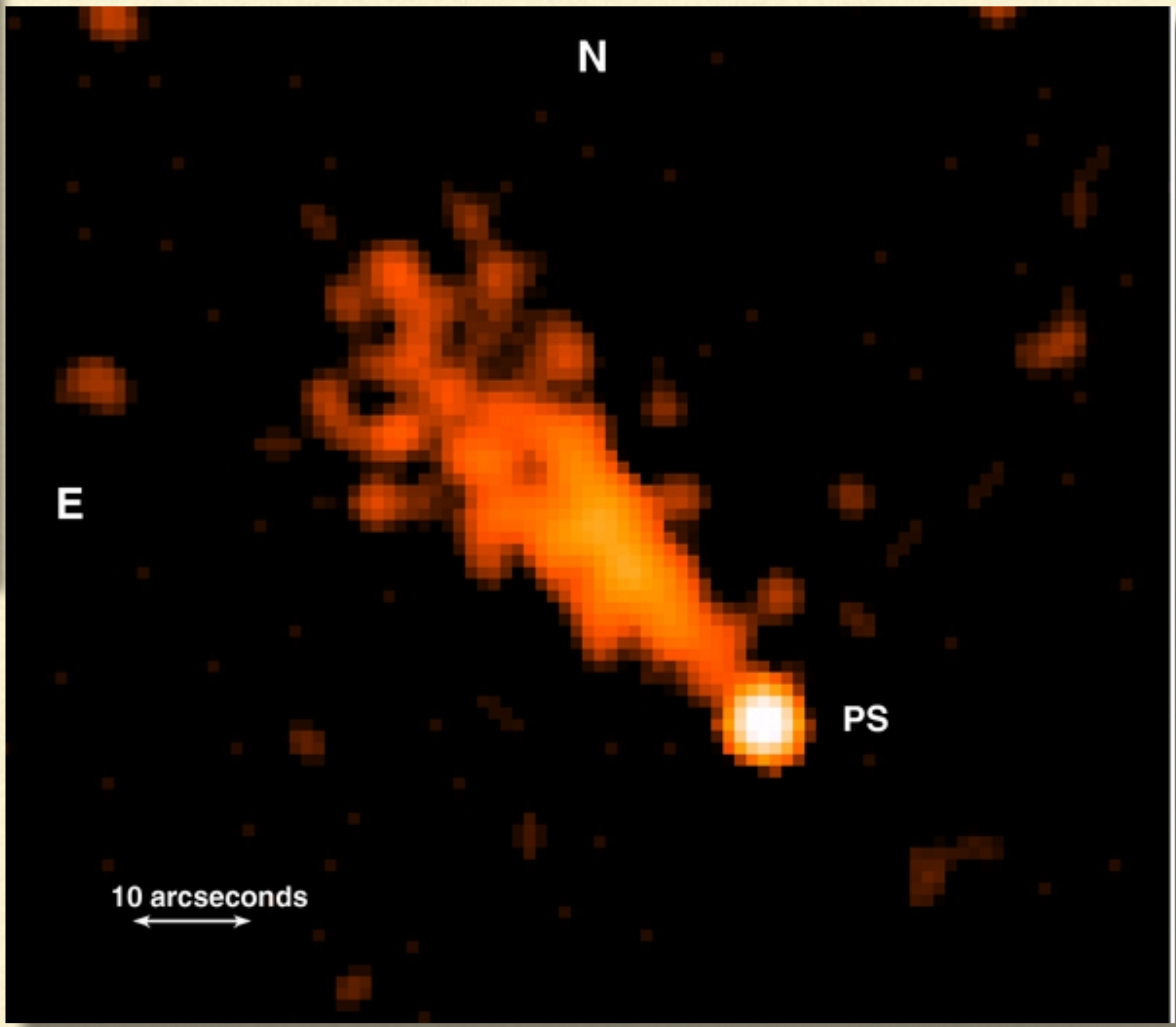
N
E
PS
10 arcseconds

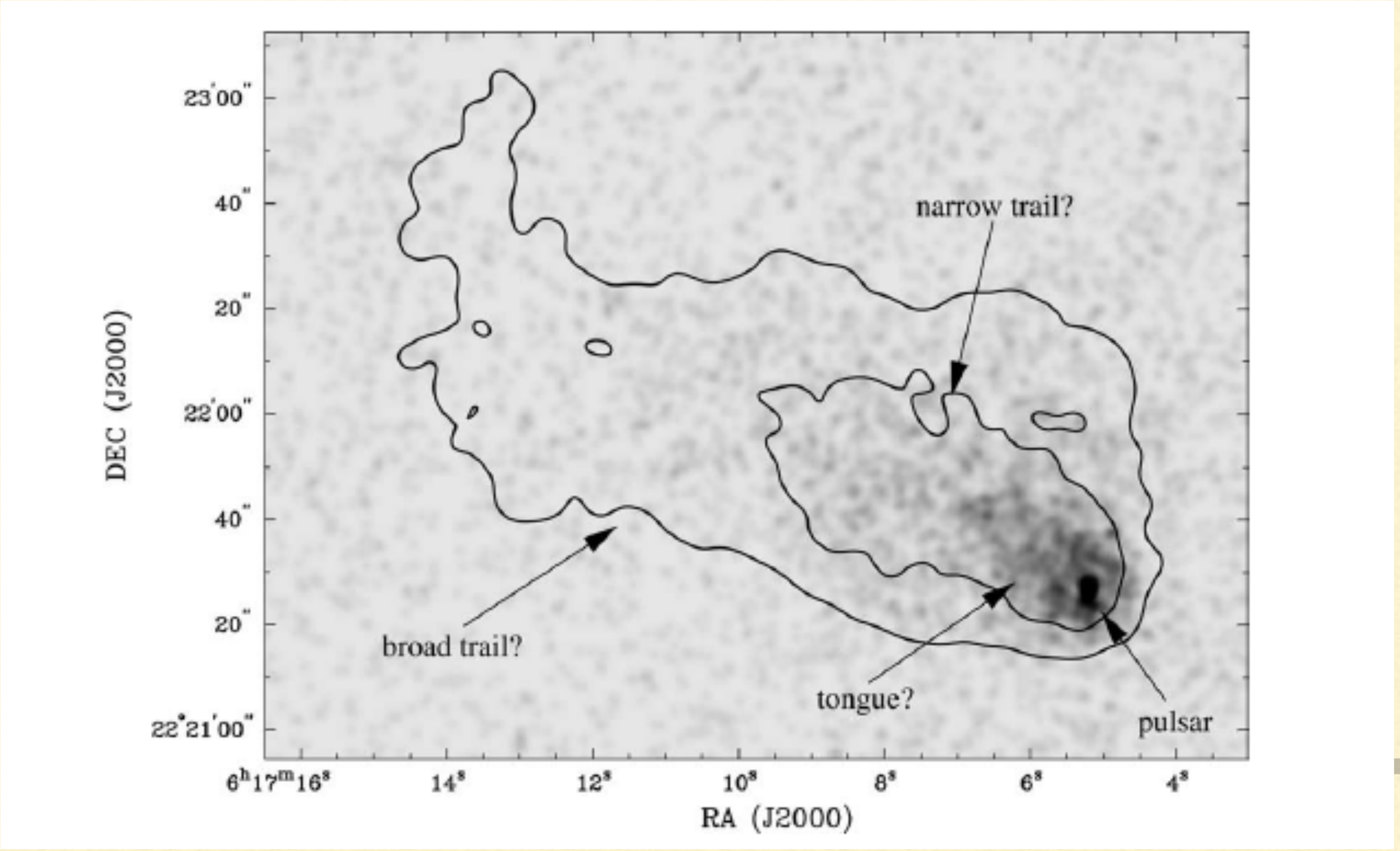
DEC (J2000)
RA (J2000)
narrow trail?
broad trail?
tongue?
pulsar

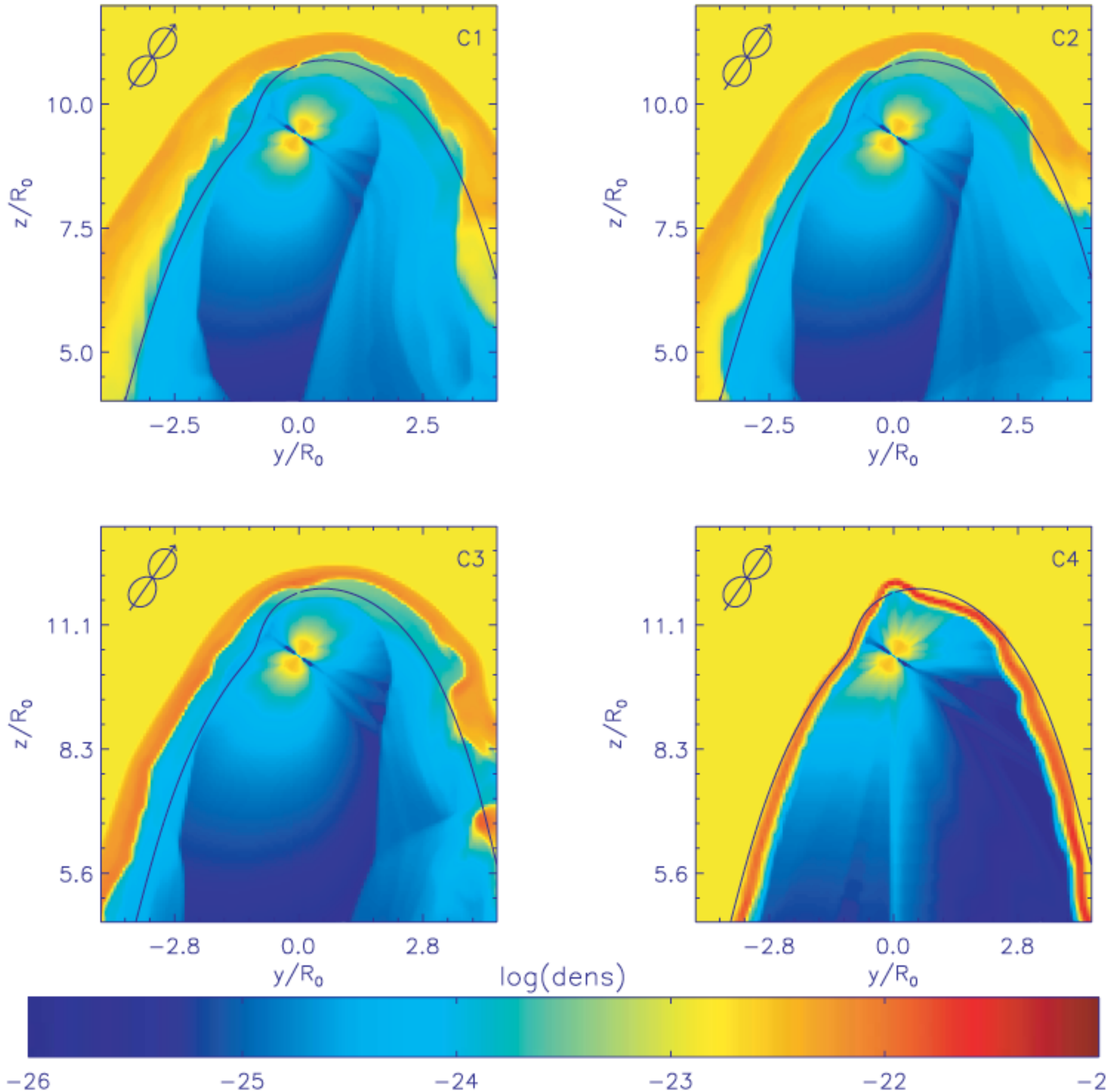
C1
C2
C3
C4
z/R$_0$
y/R$_0$
10.0
7.5
5.0
−2.5
0.0
2.5
11.1
8.3
5.6
−2.8
2.8
log(dens)
−26
−25
−24
−23
−22
−21

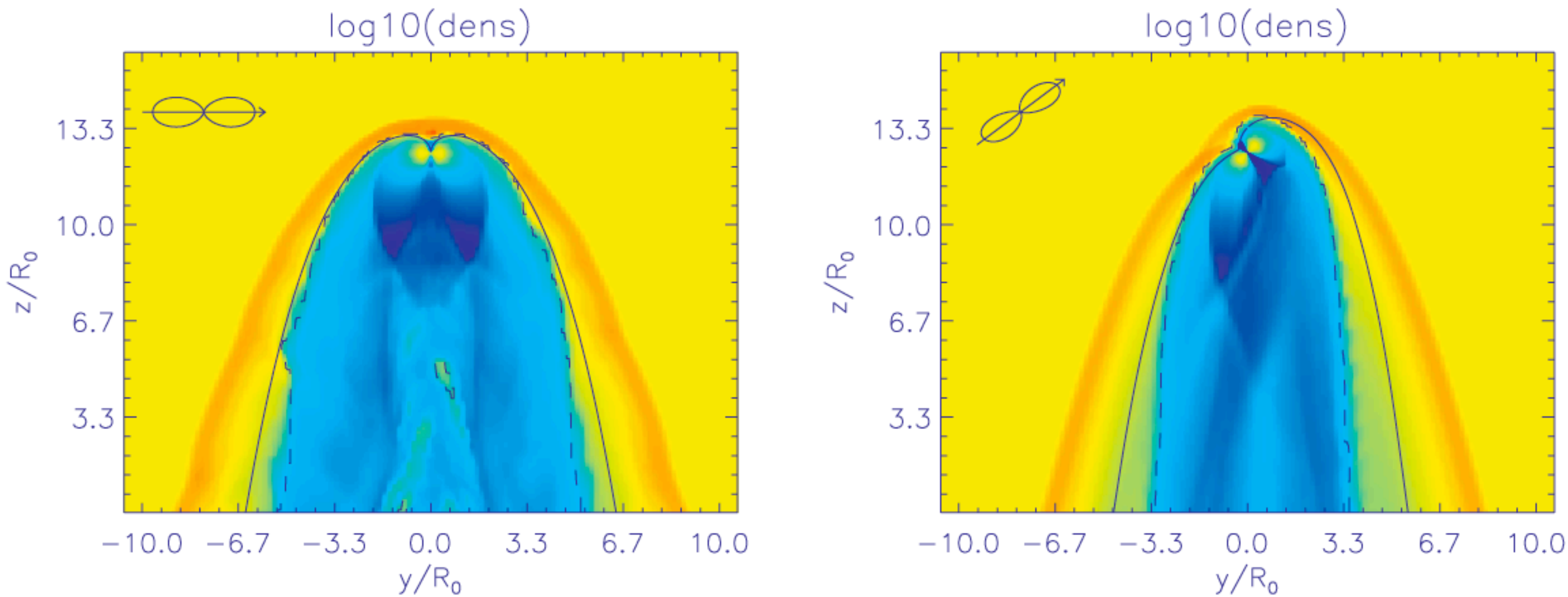

log10(dens)
z/R0
y/R0
13.3
10.0
6.7
3.3
−10.0
−6.7
−3.3
0.0
3.3
6.7
10.0
log10(dens)
z/R0
y/R0

Starburst galaxies

Galaxy M82. Hubble image using different wavelengths. Red: Hydrogen and infrared emission. Yellow-blue: visible light.

- Extremely **high star formation rate**
- Large number of **massive stars**
- **High rate of supernovae** and density of **cosmic rays**
- Large amount of **heavy nuclei**
- **High-infrared** luminosity (from heated gas and dust)
- Non-thermal **radio** and **gamma emission**
- **4.5σ correlation** observed by the Pierre Auger Observatory

Superwind

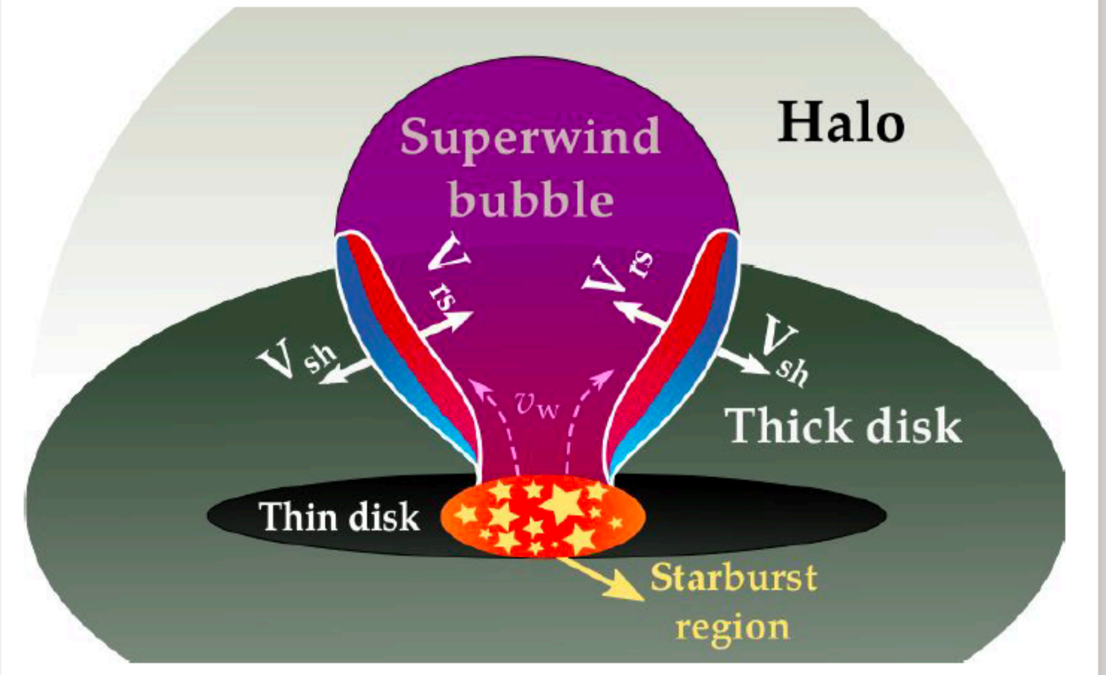

NGC 253

- Very **nearby galaxy** (~ 2.6 Mpc)
- High **star formation rate** ~ 3 $M_\odot$ yr^{-1}
- **Superwind detected** in X-ray, Hα, CO
- Asymmetric superwind (north-west bubble stronger)
- **Non-thermal** radiation from the **central source**
- **Non-thermal** radio **halo**

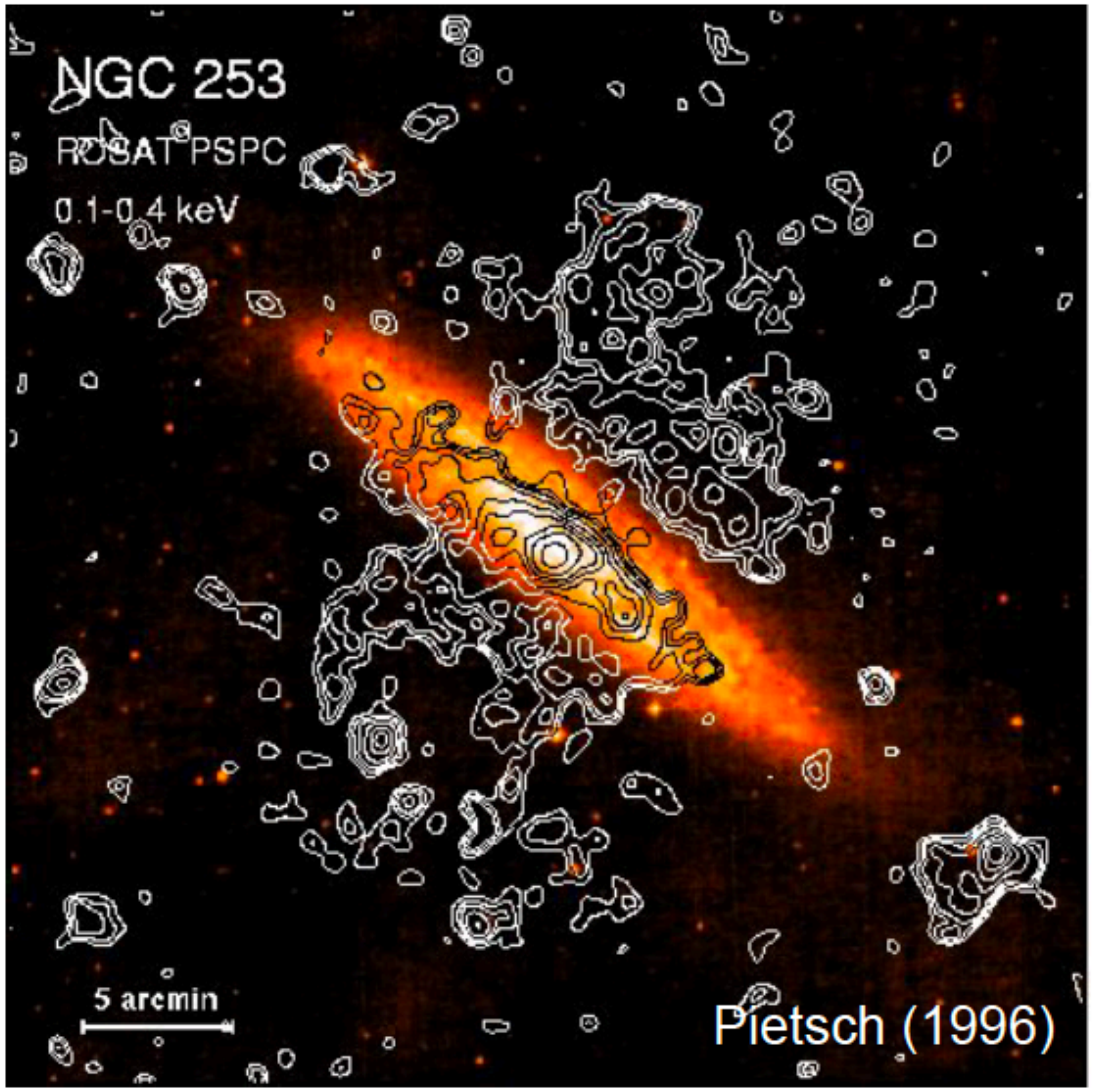

Galaxy NGC 253. X-ray emission contours 0.1 to 2.4 keV (white) on top of an optical image.

Results

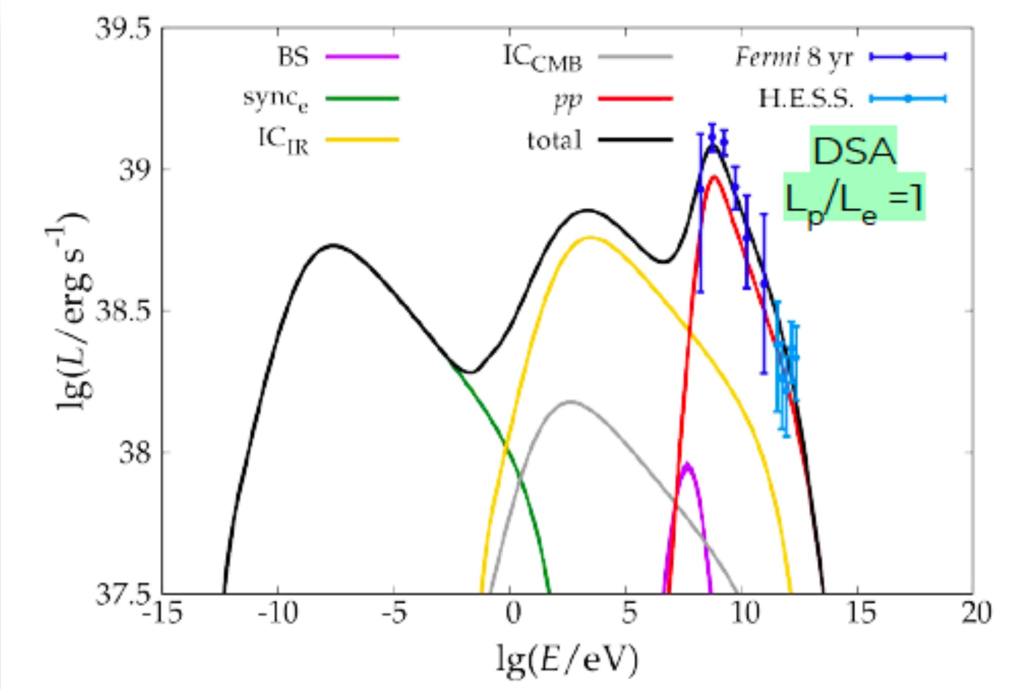

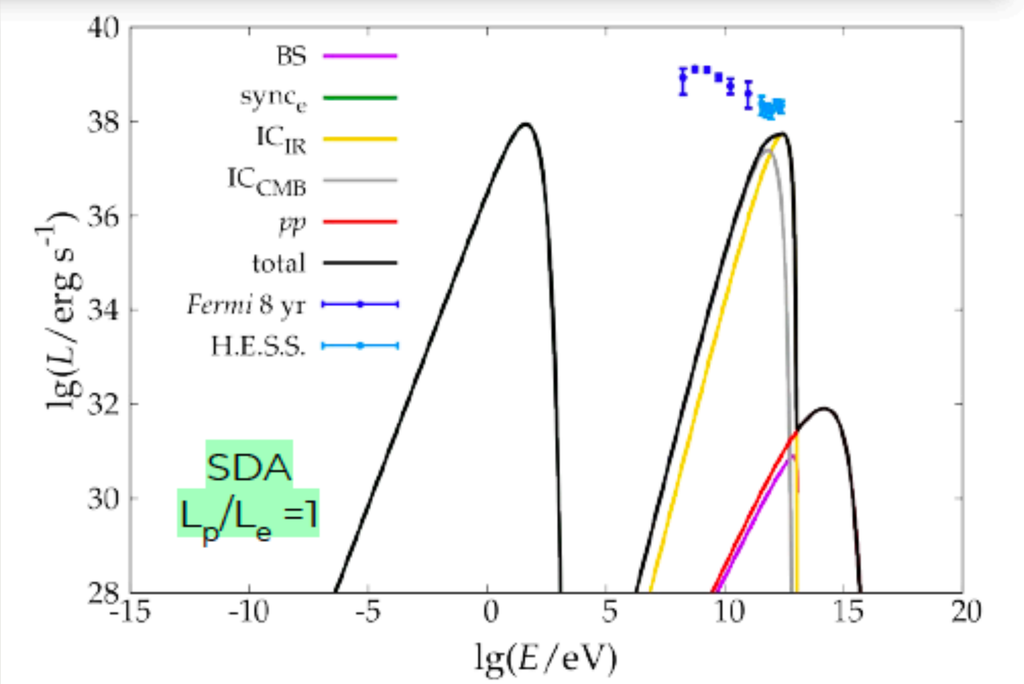

- The superwind of NGC 253 and other **starbursts can produce cosmic rays up to 10^{18} eV**
- Possible to reach the energies by diffusive shock acceleration and stochastic diffusive acceleration.
- **Higher energies impossible** even taking into account the uncertainties of the observational parameters
- The observed **mass loading** and **magnetic field mainly limits**
- Possible to **explain the gamma-radiation of starburst galaxies** with the cosmic rays accelerated in the superwind reverse shock
- Acceleration of **iron up to 100 EeV extremely difficult** in normal circumstances

A. Müller, et al.

Clumps inside the superwind

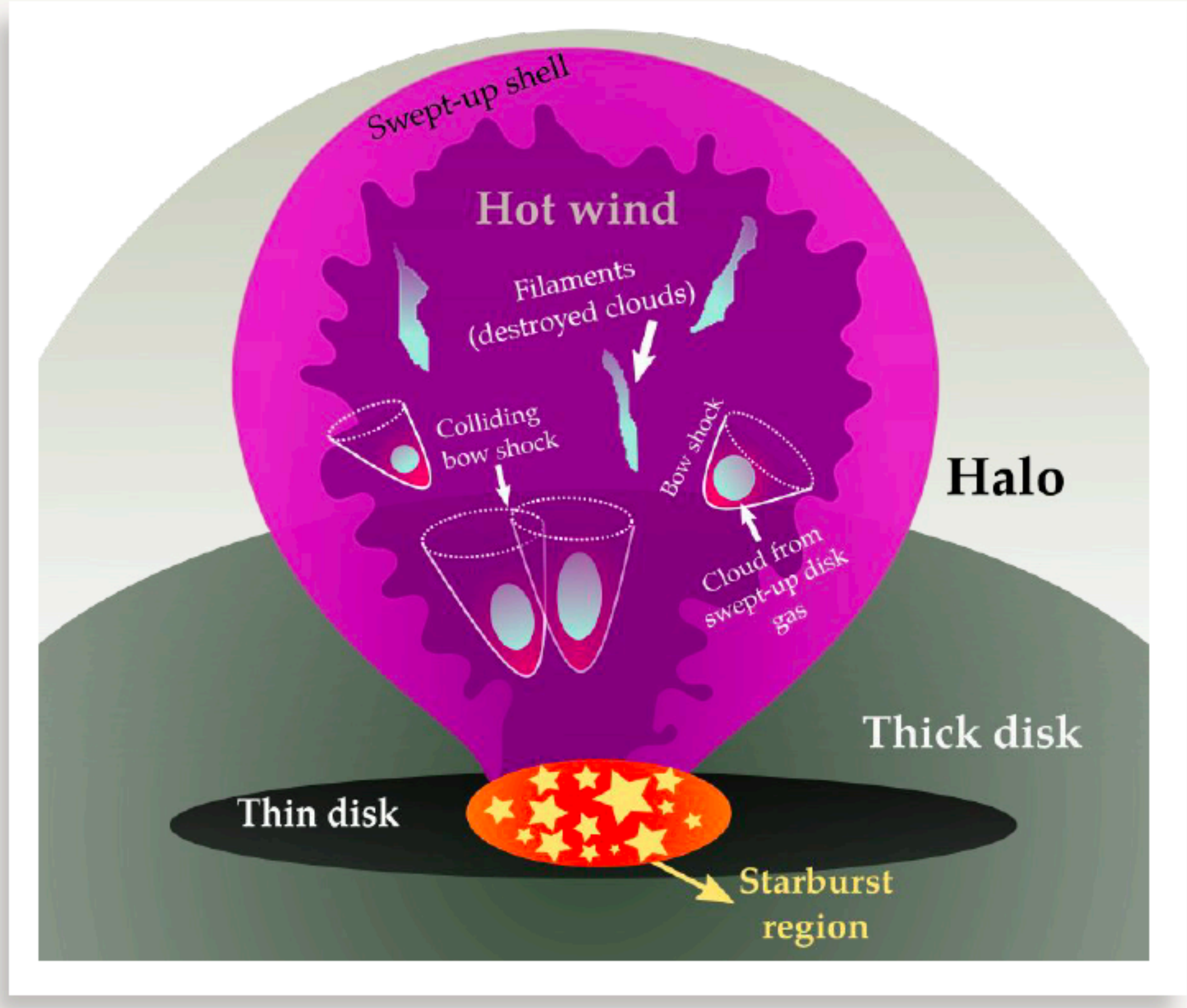

Figure adapted from **Cooper et al. 2009**

- The **superwind** sweeps up **fragments of the galactic disk**, which are denser and colder than the wind plasma
- The **interaction** of the warm **wind** with the dense cold **clouds** produces shock waves (bow shocks)
- Bow shocks studied by other authors to explain absorption and emission lines in the ultraviolet spectra of the superwinds

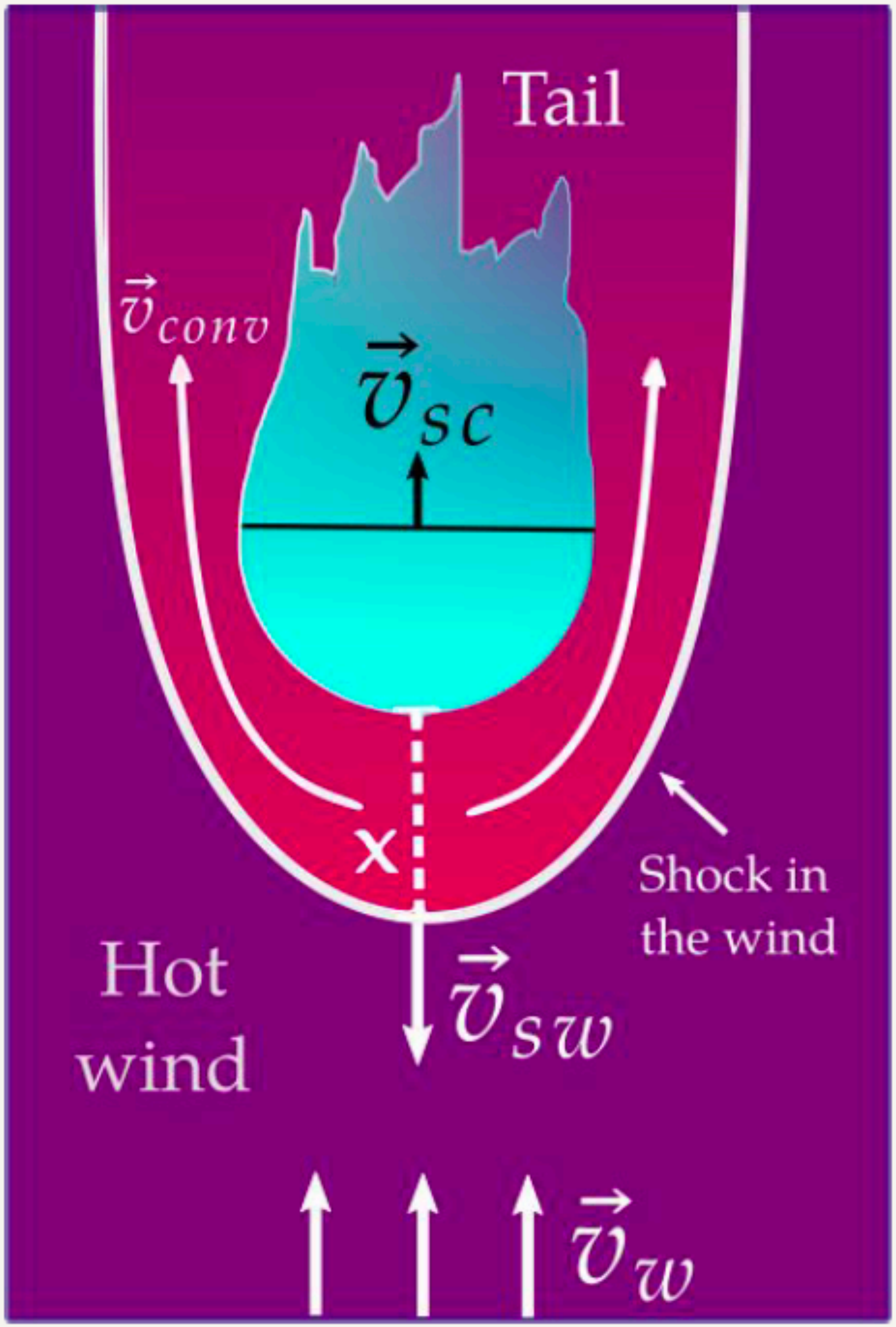
Tail
$\vec{v}_{conv}$
$\vec{v}_{sc}$
x
Shock in the wind
Hot wind
$\vec{v}_{sw}$
$\vec{v}_{w}$

Results

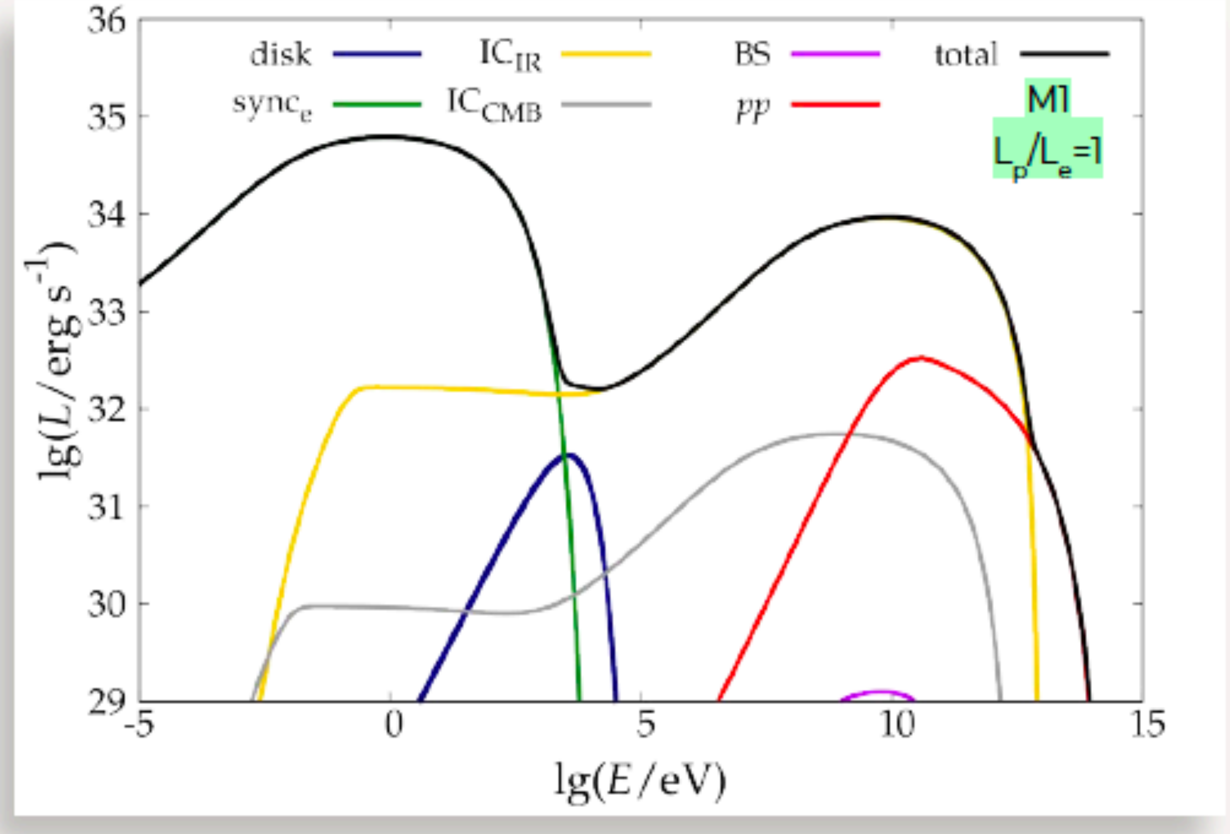
disk
sync$_e$
IC$_{IR}$
IC$_{CMB}$
BS
pp
total
M1
L_p/L_e=1
lg(L/erg s^{-1})
lg(E/eV)

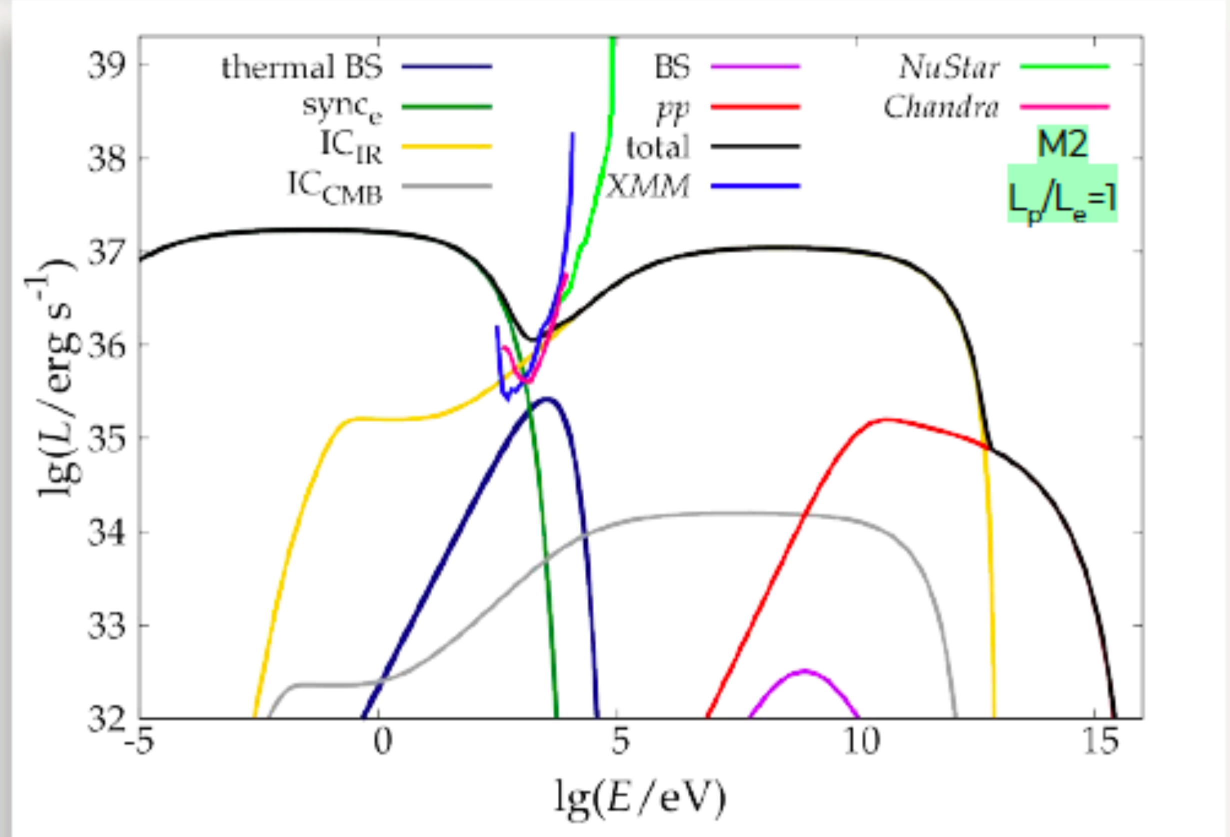
thermal BS
sync$_e$
IC$_{IR}$
IC$_{CMB}$
BS
pp
total
XMM
NuStar
Chandra
M2
L_p/L_e=1
lg(L/erg s^{-1})
lg(E/eV)

Cúmulos de galaxias

- Los cúmulos de galaxias son las mayores estructuras conocidas en el Universo. Están formados por miles de galaxias. El medio intracúmulo está lleno de gas caliente, contaminado químicamente por explosiones de supernova, vientos galácticos, etc.

- Ondas de choque pueden acelerar electrones y protones hasta velocidades ultra-relativistas.

- Los leptones se enfrían por radiación sincrotrón (algunos cúmulos como el de Virgo son detectados en radio como fuentes no-térmicas) y, en principio, por interacciones Compton inverso con fotones del fondo cósmico.

- De aquí que se haya propuesto que ciertos cúmulos de galaxias podrían ser fuentes gamma.

Cúmulos de galaxias

RELEVAMIENTOS ÓPTICOS DE CÚMULOS DE GALAXIAS

Cúmulo de Coma

Cúmulo de Virgo

Inicialmente identificados como grandes concentraciones de galaxias (Abell 1958; Zwicky et al. 1966; Abell et al. 1989):

❖ cientos de galaxias en una región de ~1 Mpc,

❖ detectadas hasta profundidades de varios cientos de Mpc.

Cúmulos de galaxias

Cúmulo de Coma

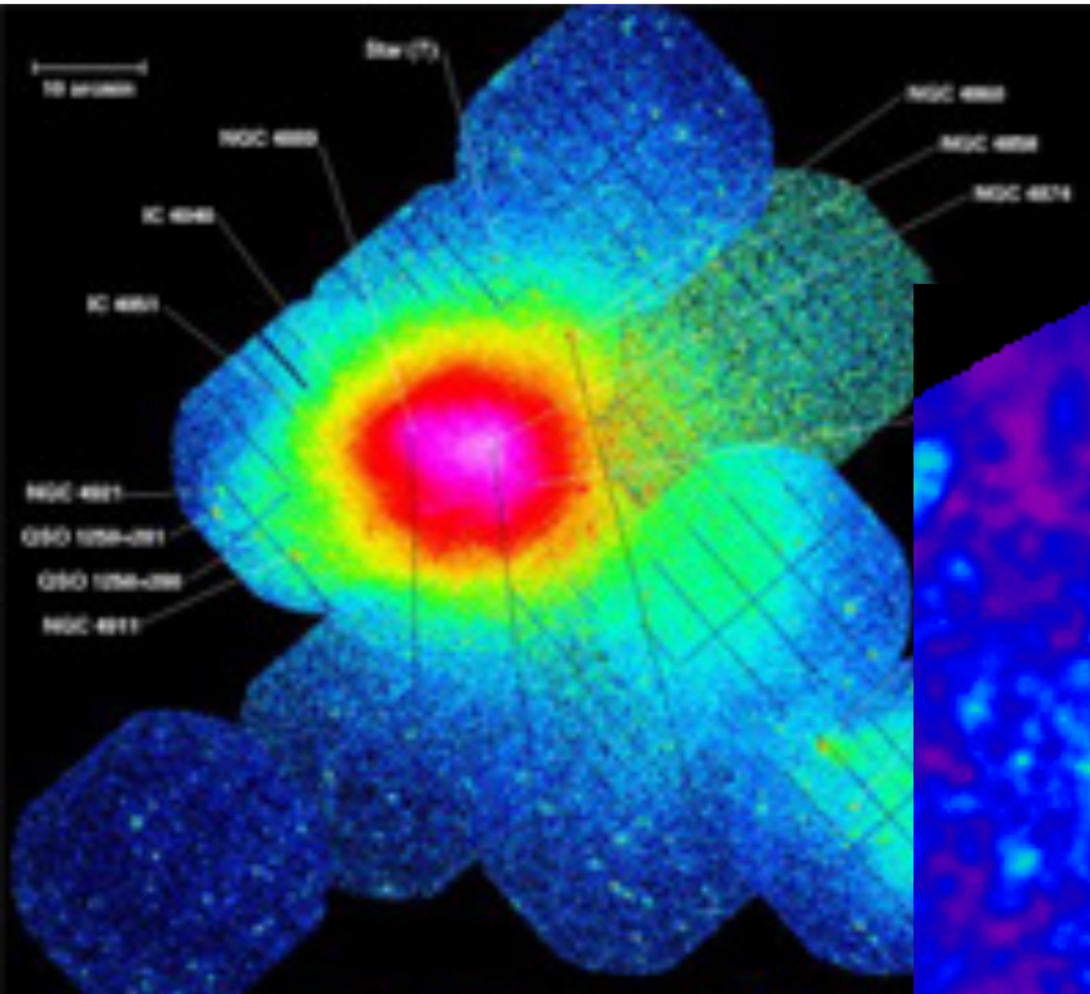

XMM-Newton

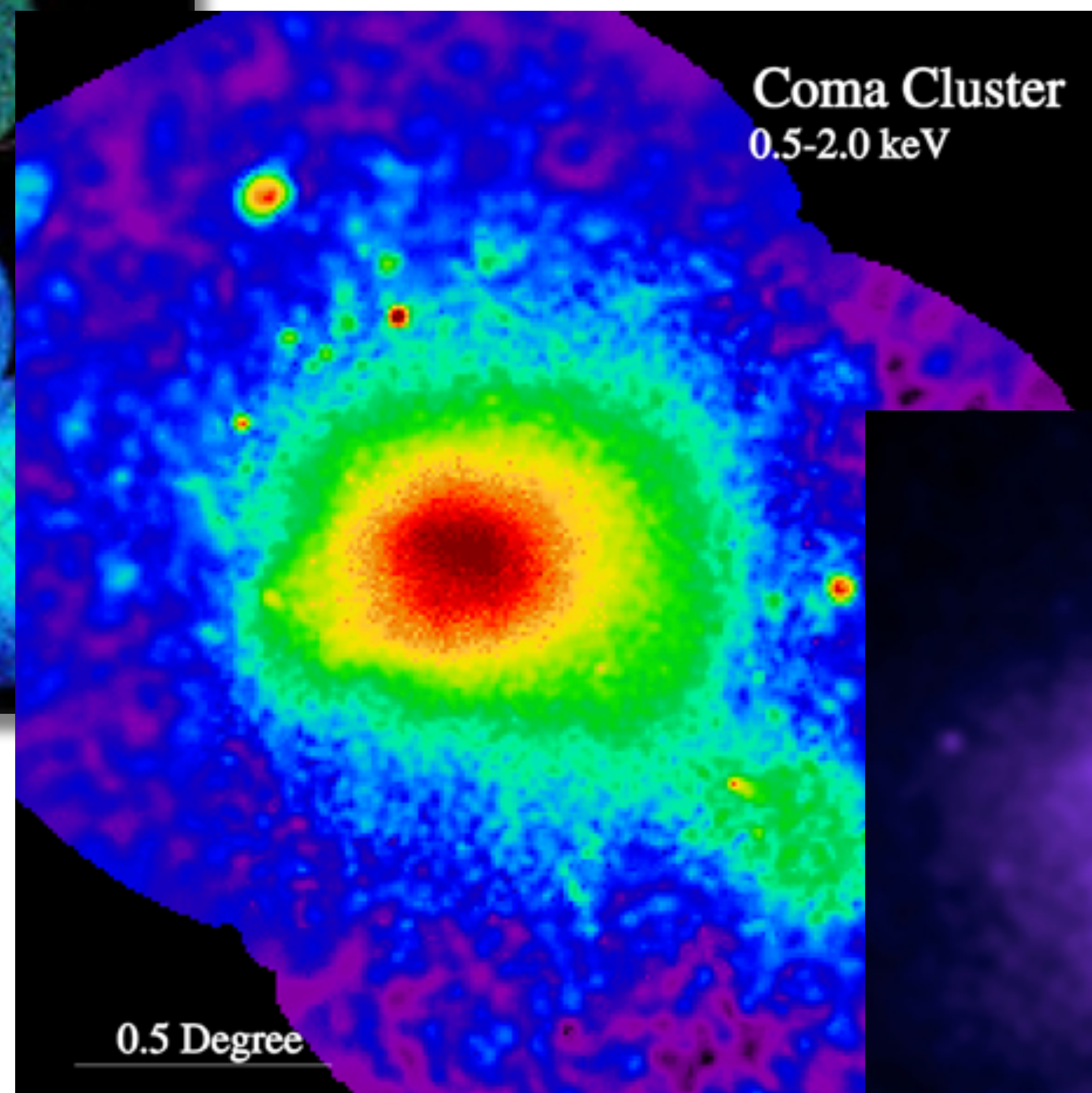

ROSAT

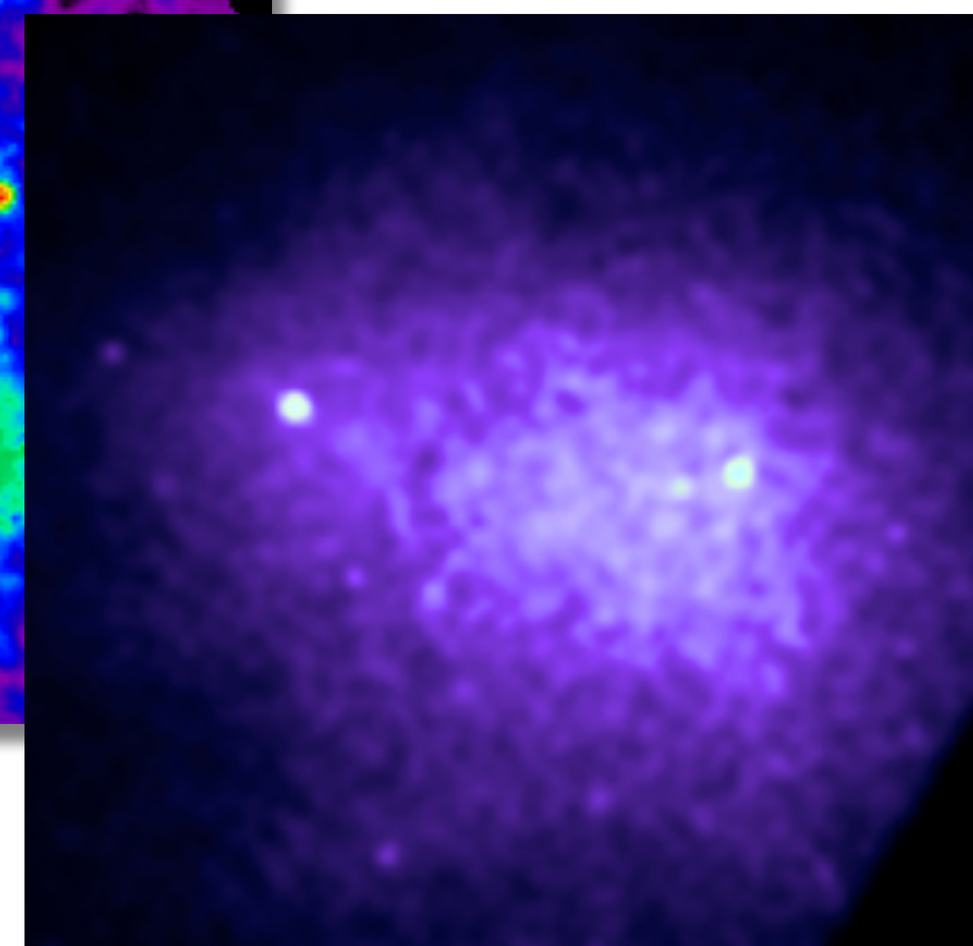

Chandra

Cúmulos de galaxias

- Los más grandes sistemas virializados en el Universo, con profundos pozos de potencial, determinados por la materia oscura, en los cuales quedan atrapados las galaxias y el medio intracúmulo.

- Medio Intracúmulo: gas caliente y difuso calentado por shocks de acreción cuando gas de relativamente baja temperatura se incorpora al cúmulo.

Los shocks generados durante la formación y fusión de cúmulos de galaxias son sitios potencialmente interesantes para la aceleración de partículas de alta energía por el mecanismo de Fermi, incluyendo electrones y protones

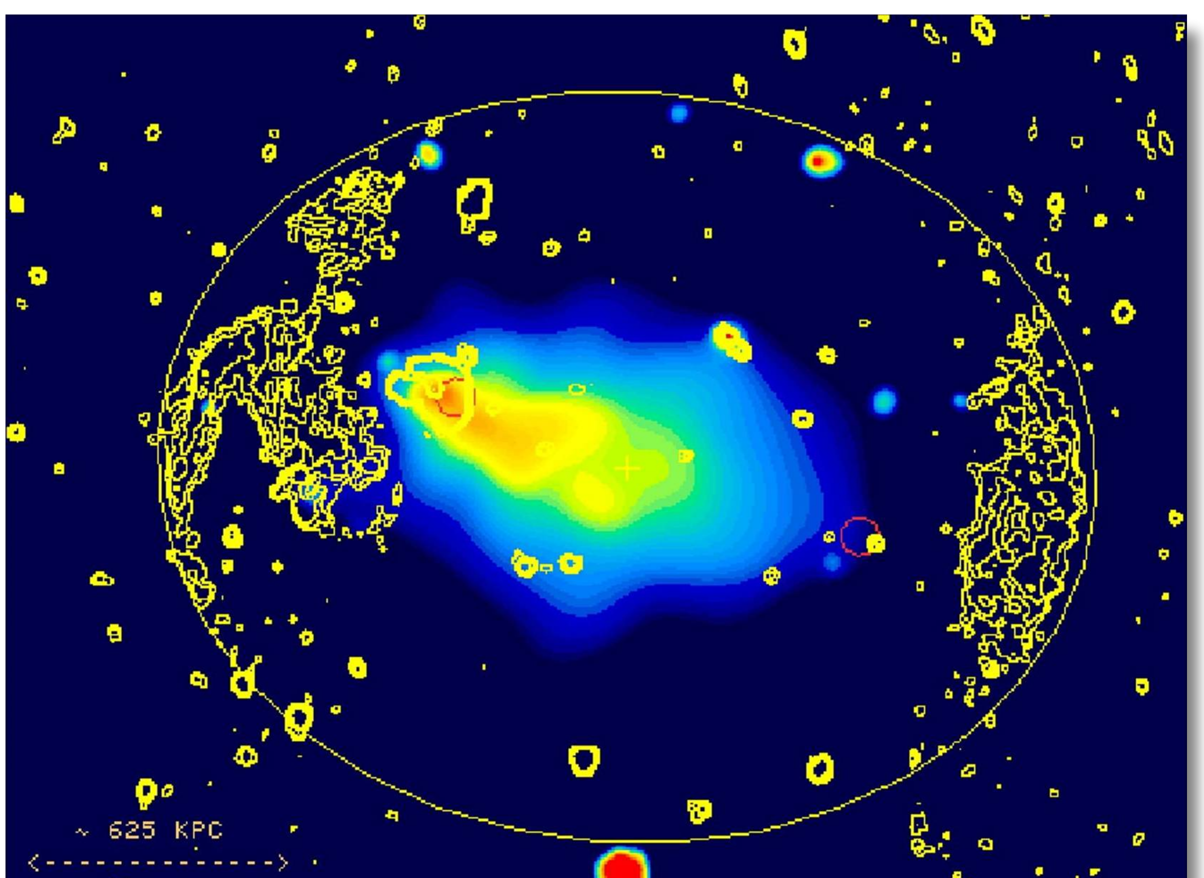

The rich cluster of galaxies Abell 3376 has been detected by *ROSAT* and *XMM*-Newton through its X-ray emission revealing strong evidence for merger activity of subclusters.

Cúmulo de galaxias A3376

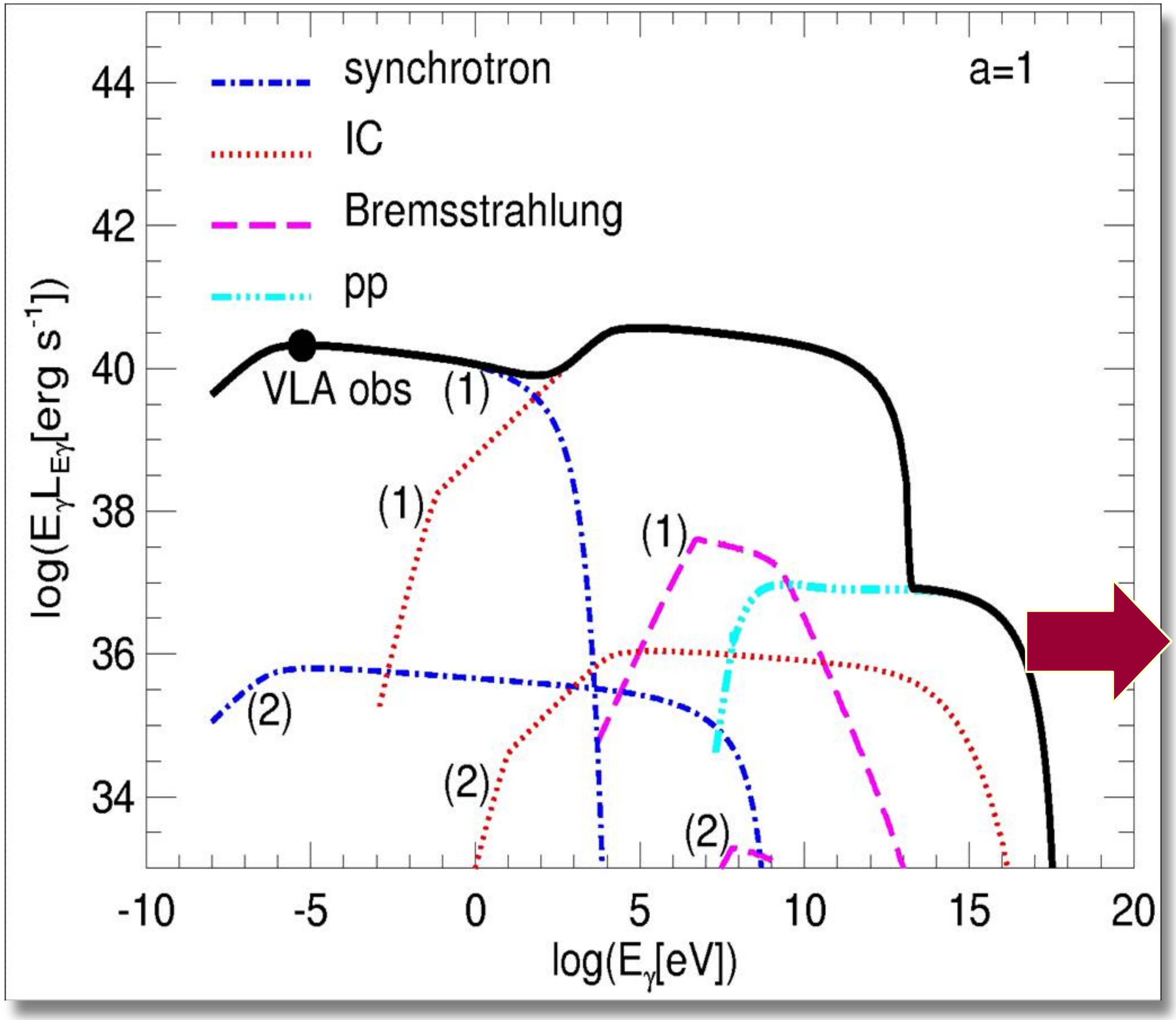

Araudo, Cora, Romero MNRAS 2008

decay from *pp* interactions contribute to the gamma-ray emission, being its luminosity smaller than that of IC interactions because of the low density of thermal protons at the location of radio relics

IC photons from cluster Abell 3376 could be detected by gamma-ray instruments such as *Fermi* satellite and the Cherenkov telescope HESS II, which operates in the ranges ~100 MeV to ~100 GeV, and 0.1 to 10 TeV, respectively

$$\text{Fuentes activas acretantes galácticas} \begin{cases} \text{Microquasars} \\ \text{X} - \text{ray binaries} \end{cases}$$

$$\text{Fuentes activas acretantes extragalácticas} \begin{cases} \text{AGNs} \\ \text{Gamma} - \text{Ray Bursts} \end{cases}$$

Jets are collimated outflows observed in a variety of astrophysics objects.

Heber Curtis (Lick Observatory) observed Messier 87 in 1918 and was the first to notice the polar jet which he described as a "curious straight ray ... apparently connected with the nucleus by a thin line of matter."

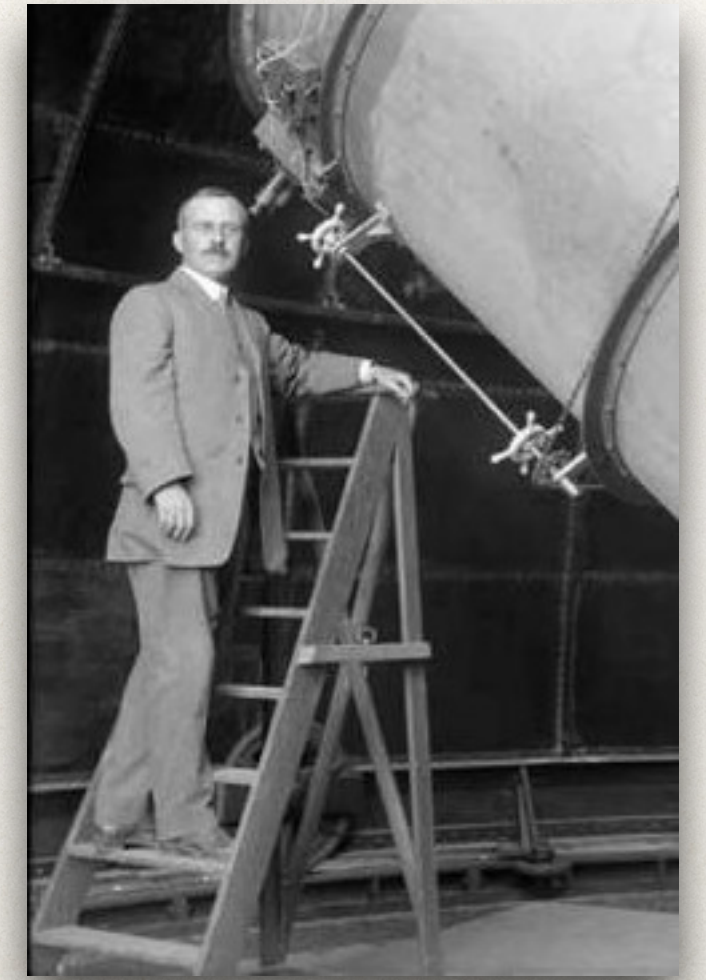

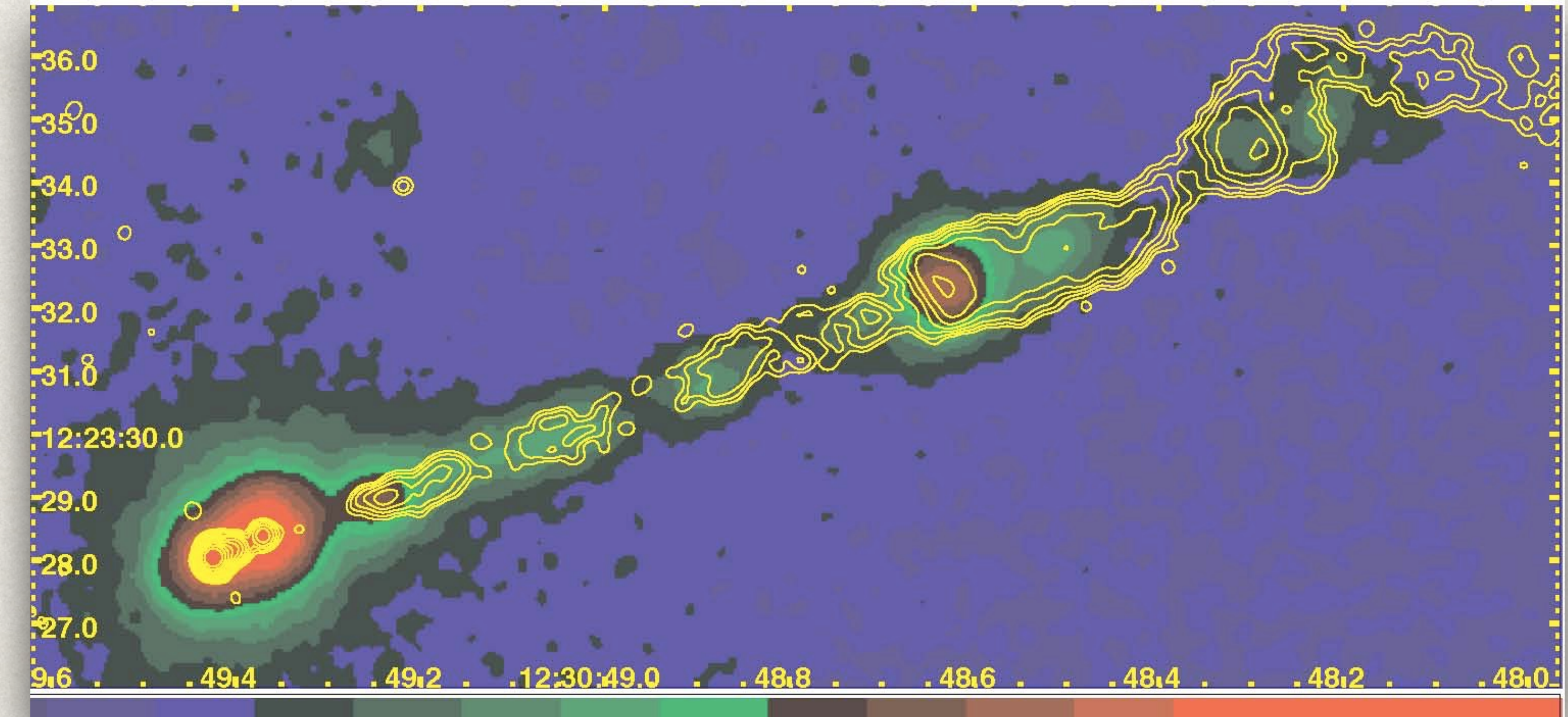
36.0
35.0
34.0
33.0
32.0
31.0
12:23:30.0
29.0
28.0
27.0
49.4
49.2
12:30:49.0
48.8
48.6
48.4
48.2
48.0

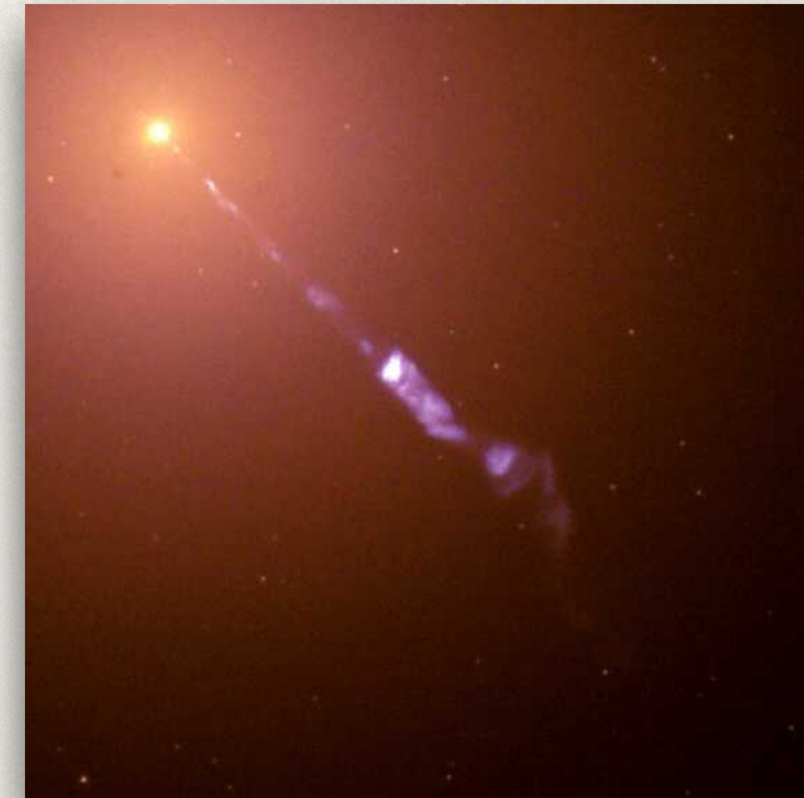

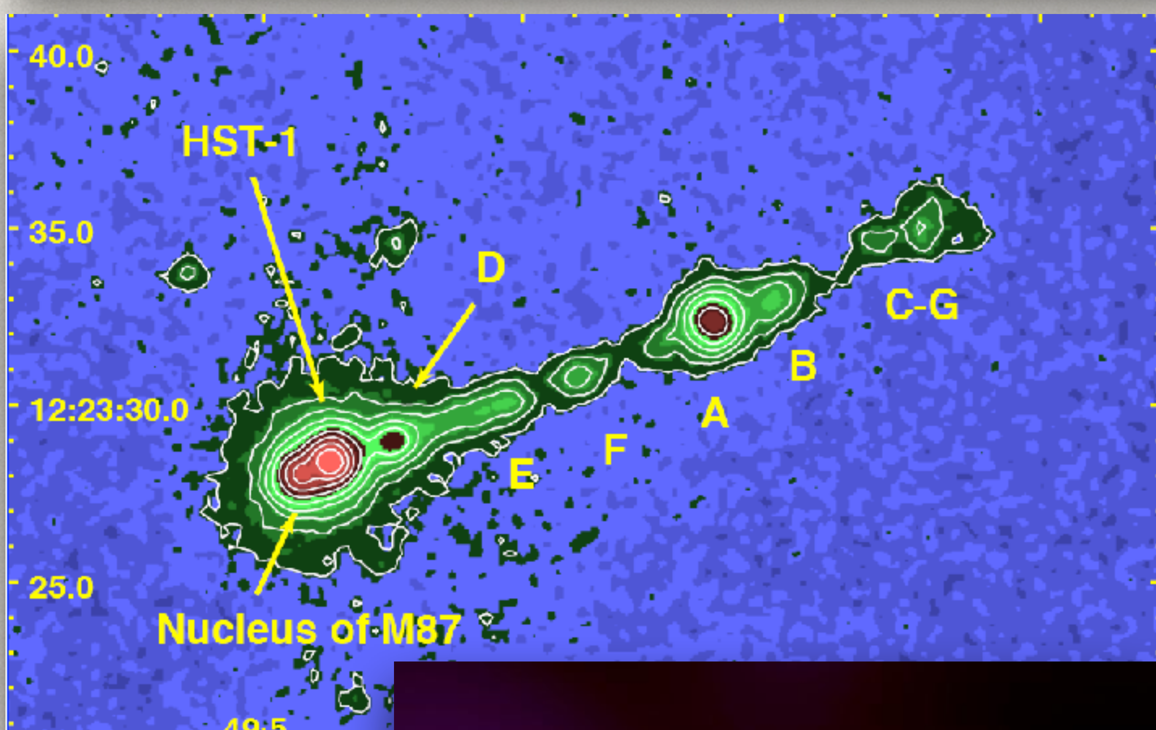
40.0
35.0
12:23:30.0
25.0
49.5
HST-1
D
C-G
B
A
F
E
Nucleus of M87


X-rays

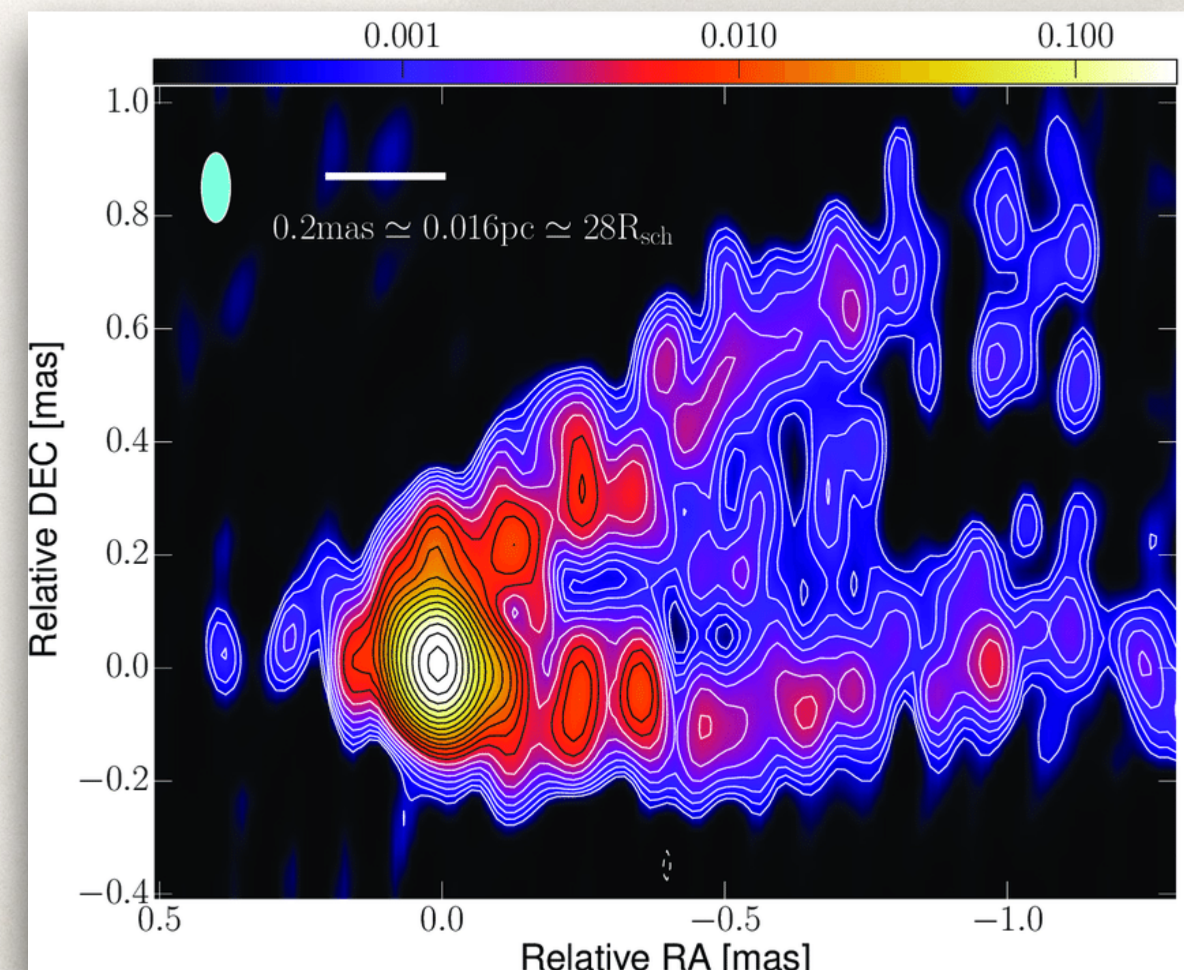
0.001
0.010
0.100
0.2mas ≃ 0.016pc ≃ 28R_sch
Relative DEC [mas]
Relative RA [mas]
1.0
0.8
0.6
0.4
0.2
0.0
−0.2
−0.4
0.5
0.0
−0.5
−1.0

M87

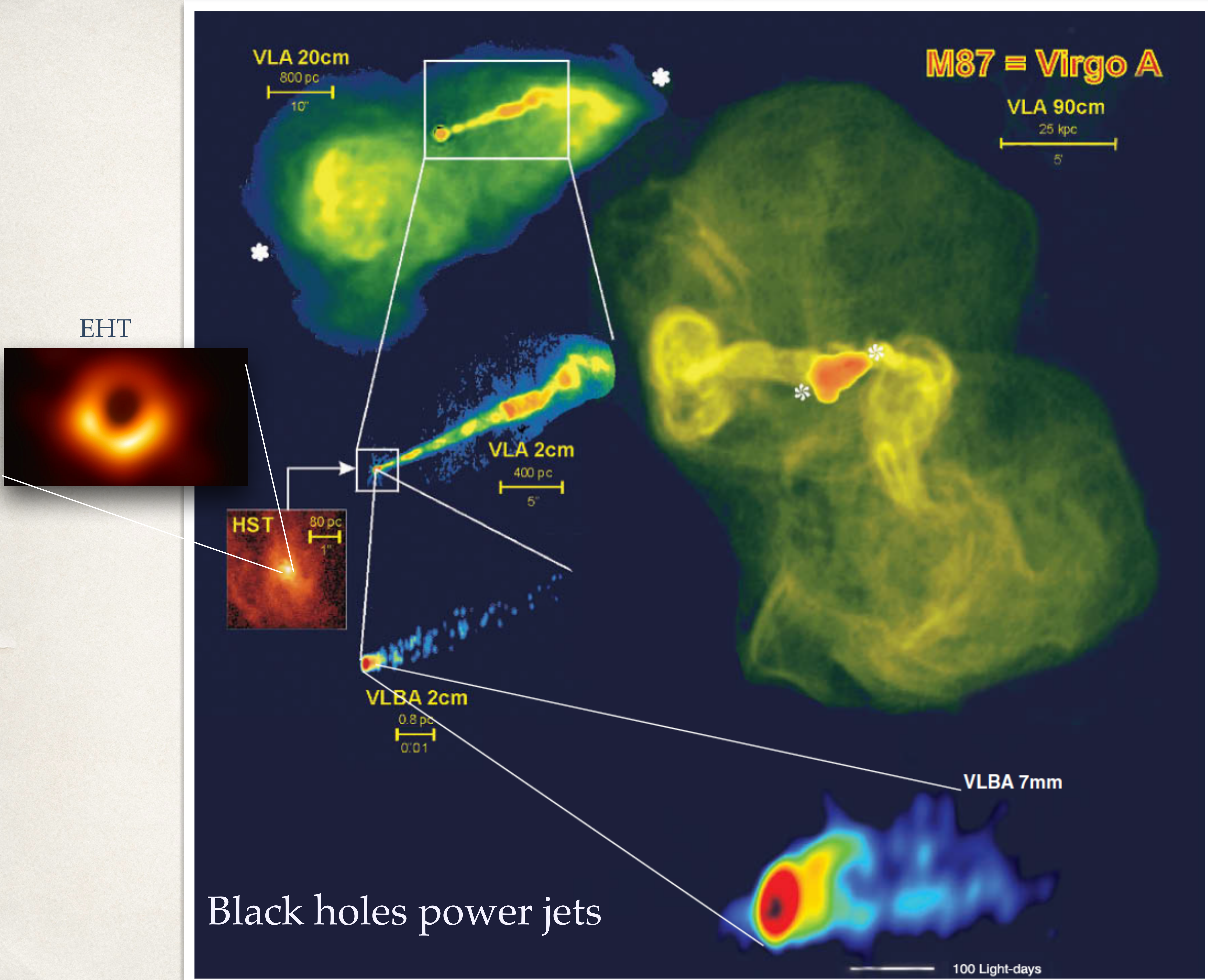

Black holes power jets

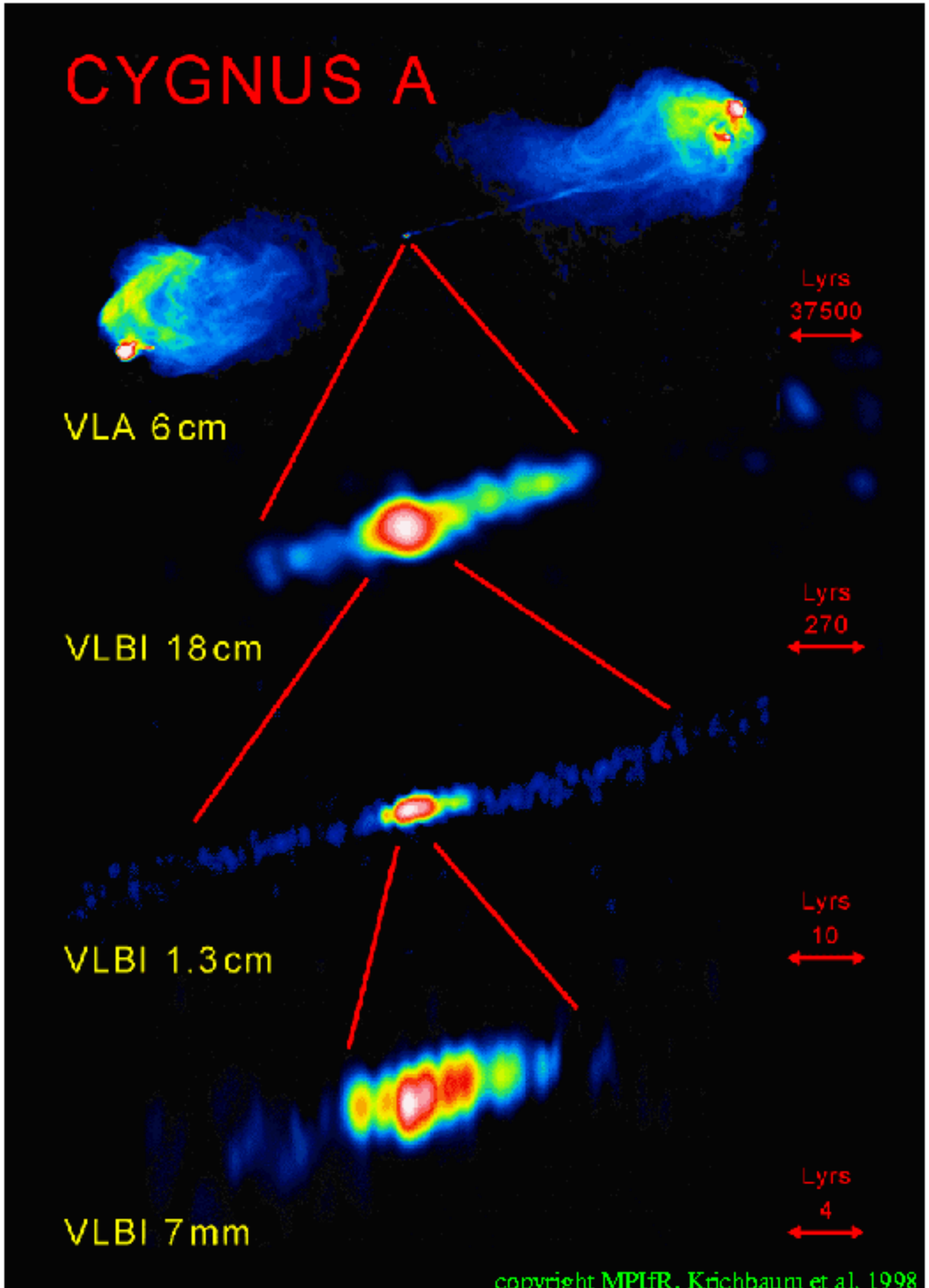

The jet remains self-similar and well collimated along more than 10^5 orders of magnitud in size.

Cygnus A

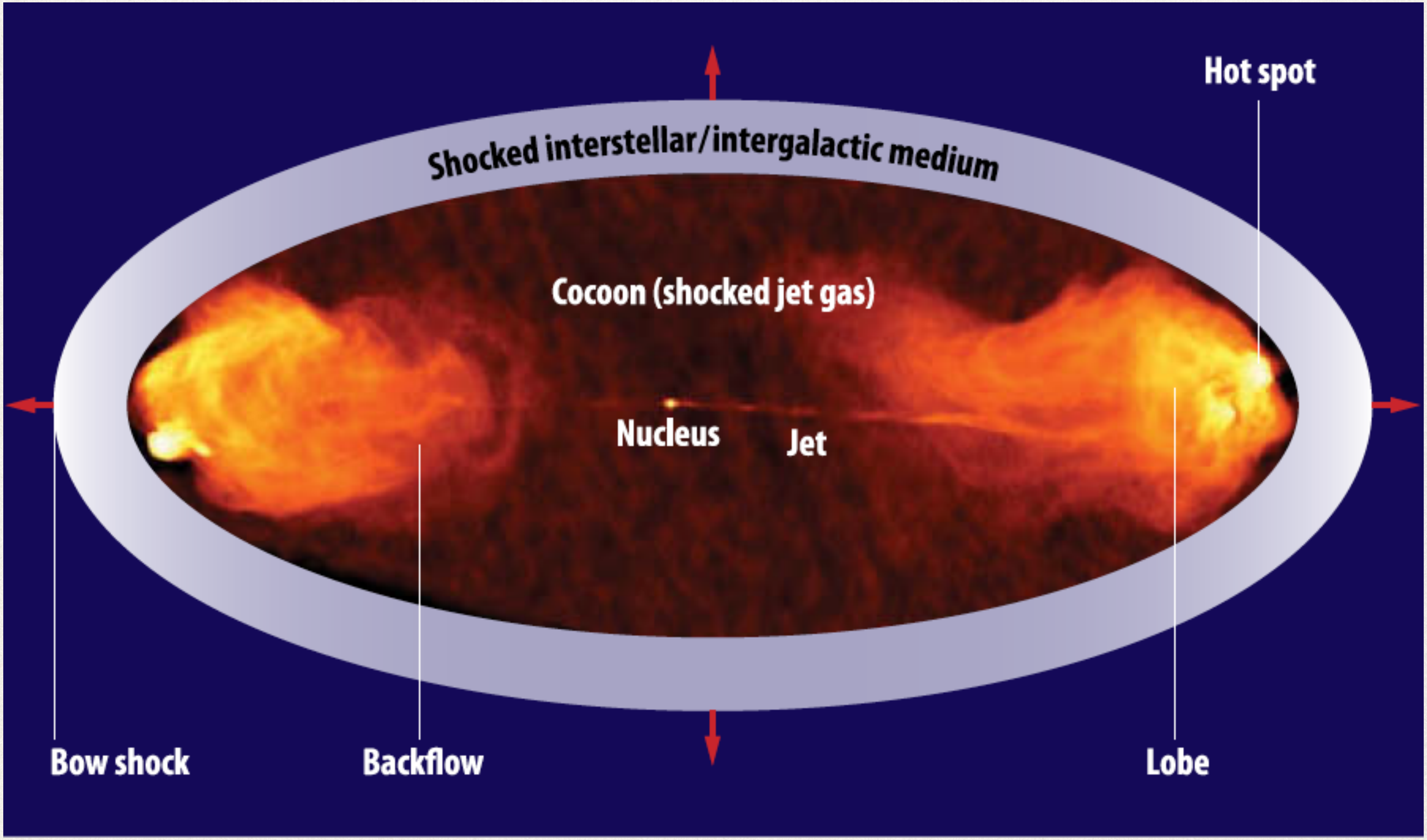

Hot spot
Shocked interstellar/intergalactic medium
Cocoon (shocked jet gas)
Nucleus
Jet
Bow shock
Backflow
Lobe

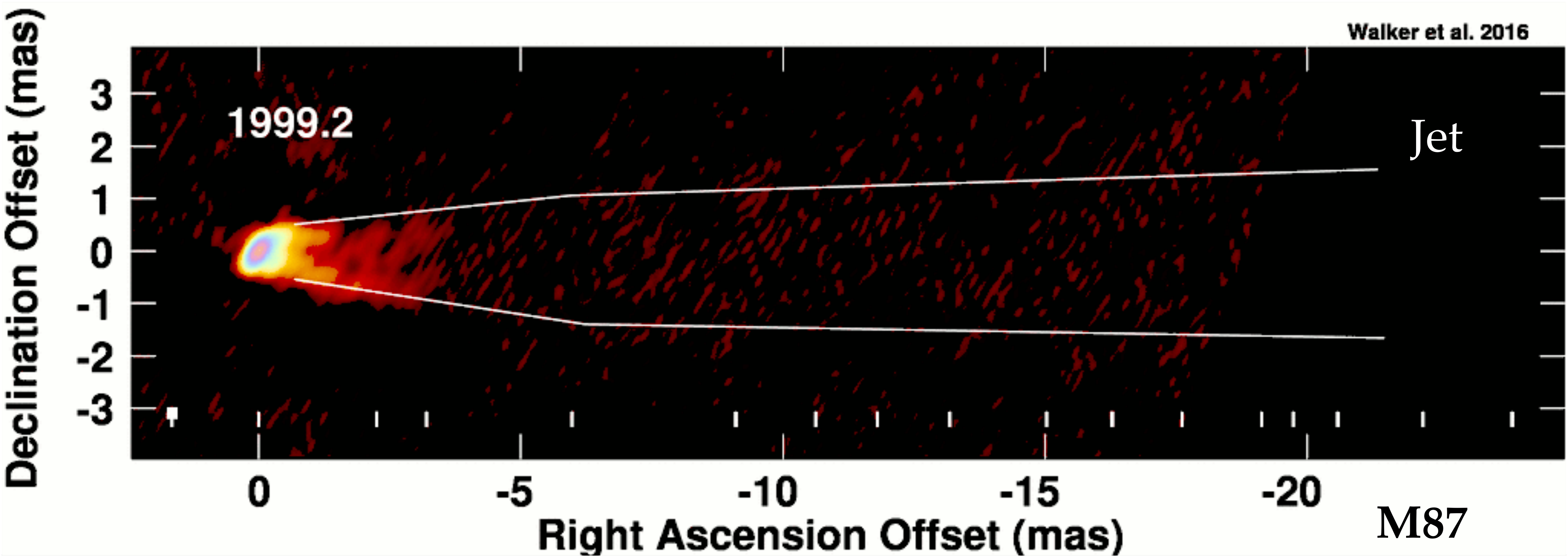

Mechanisms of Jet Dissipation

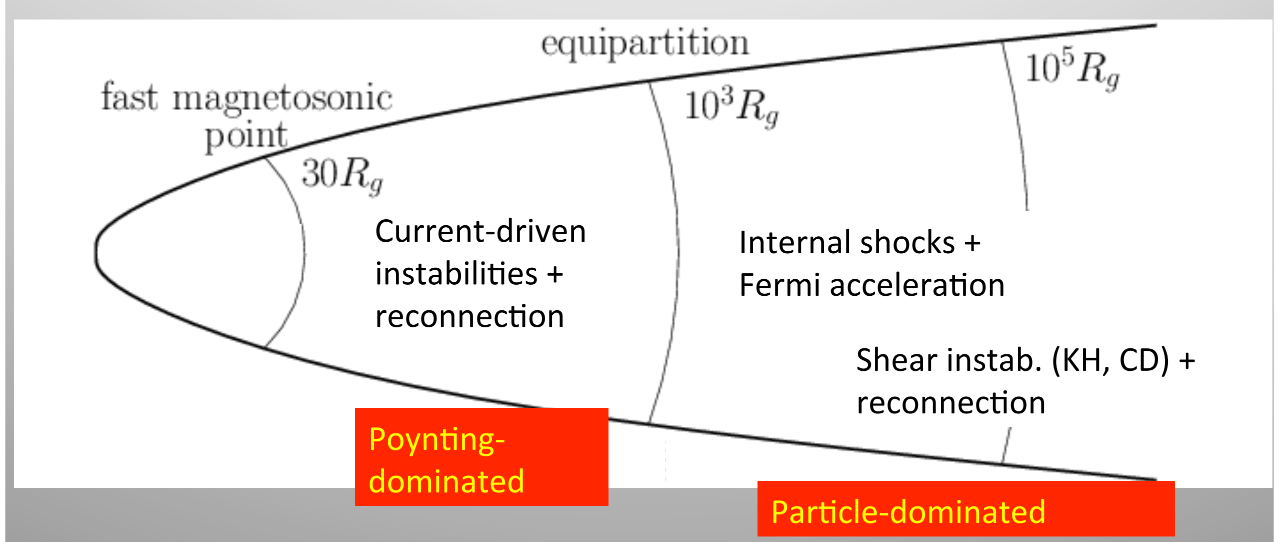

Jets: collimated outflows of particles and fields

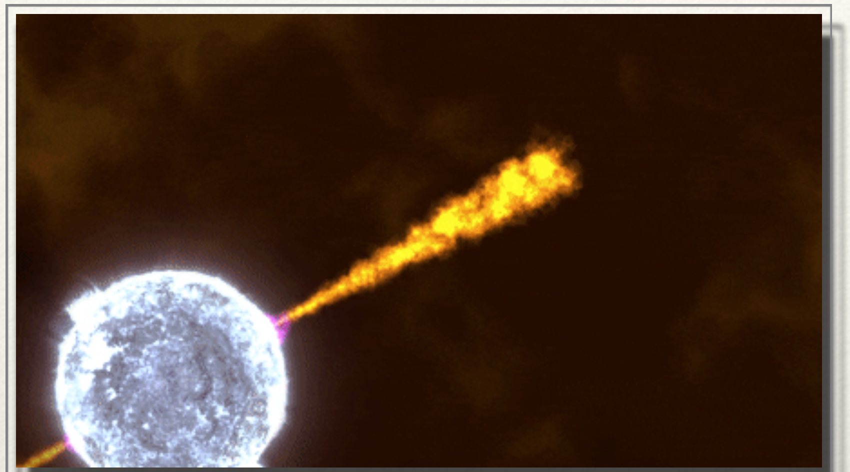

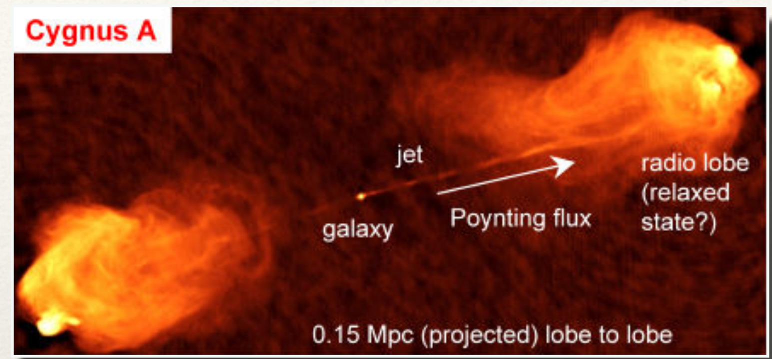

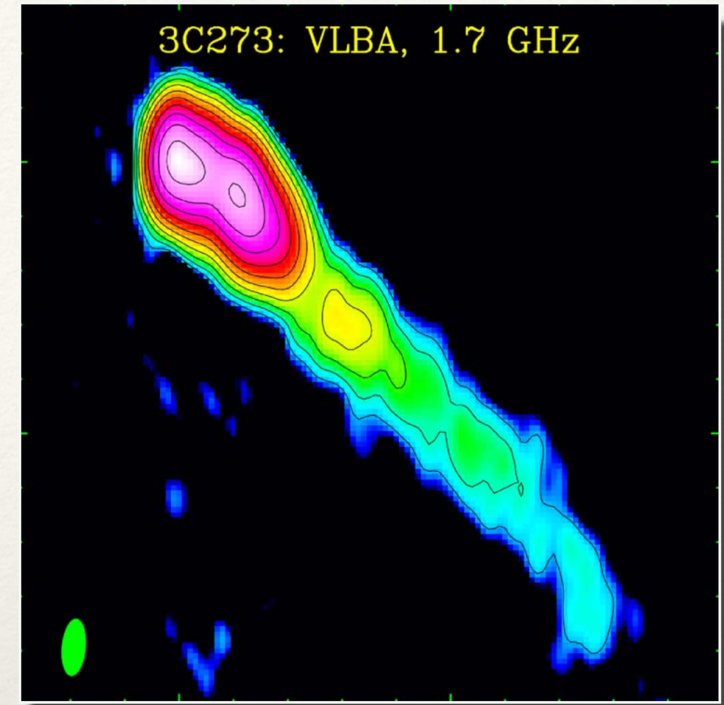

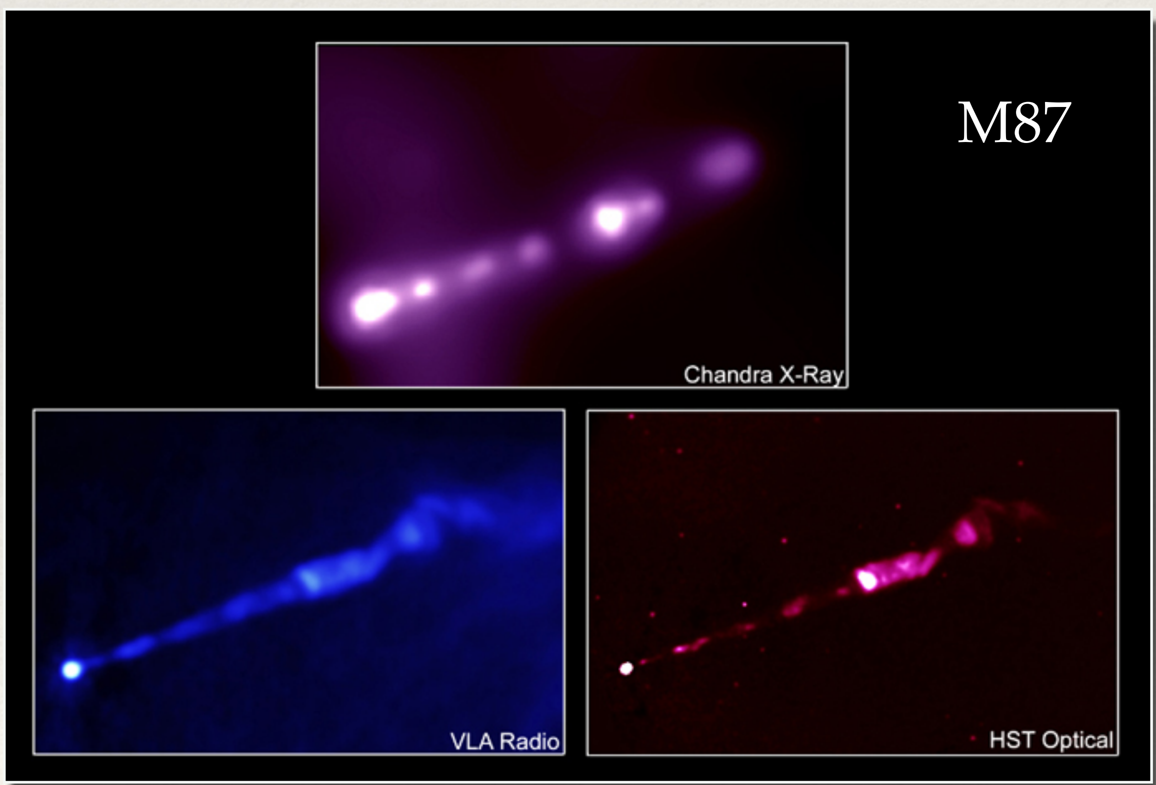

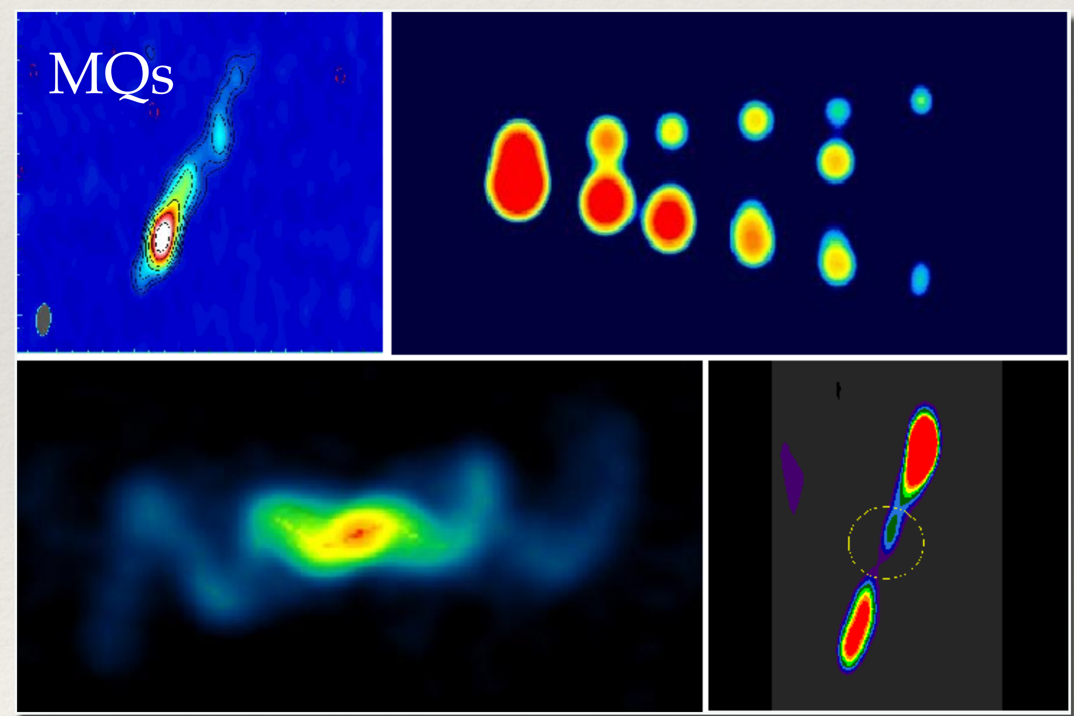

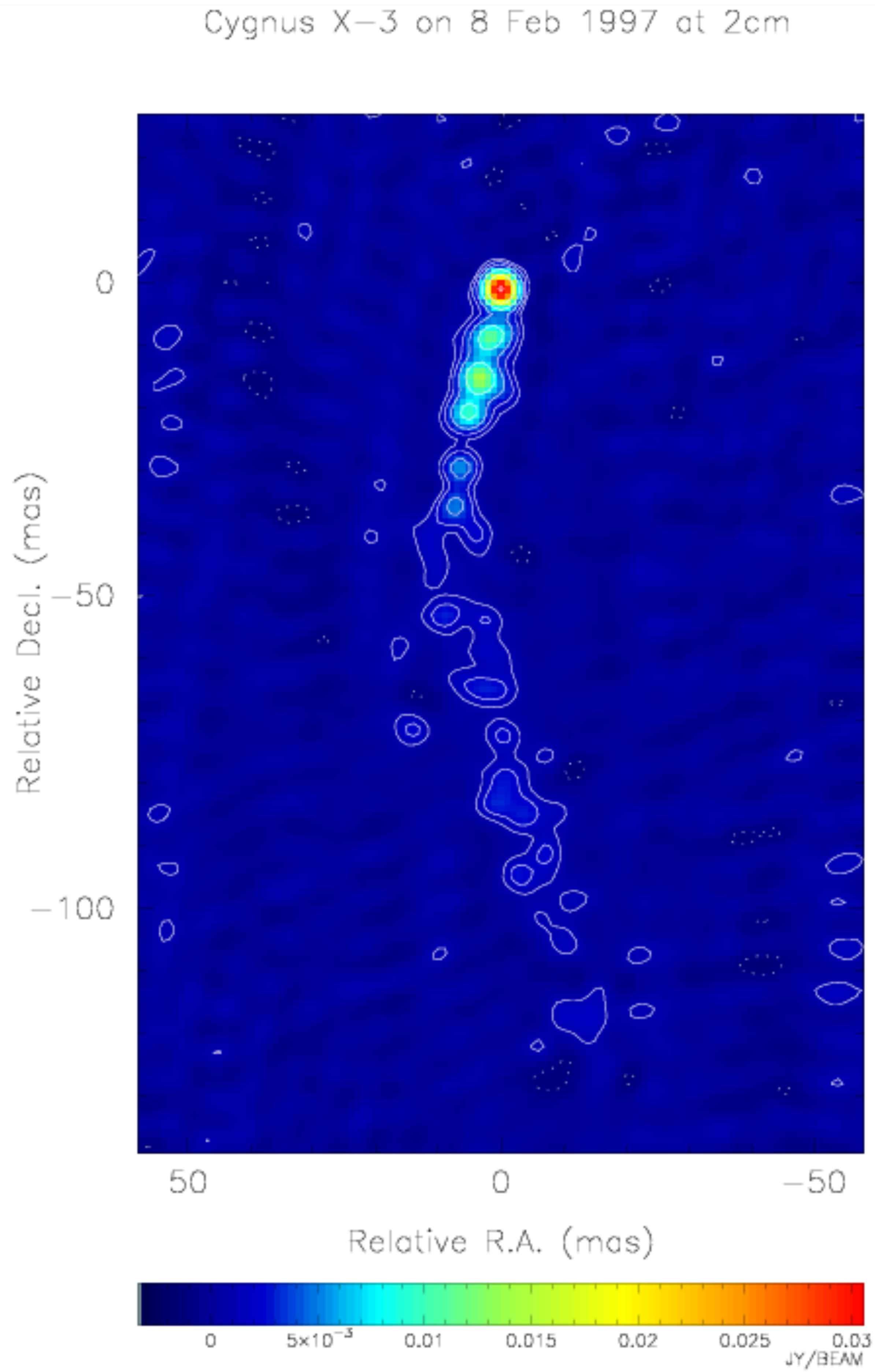

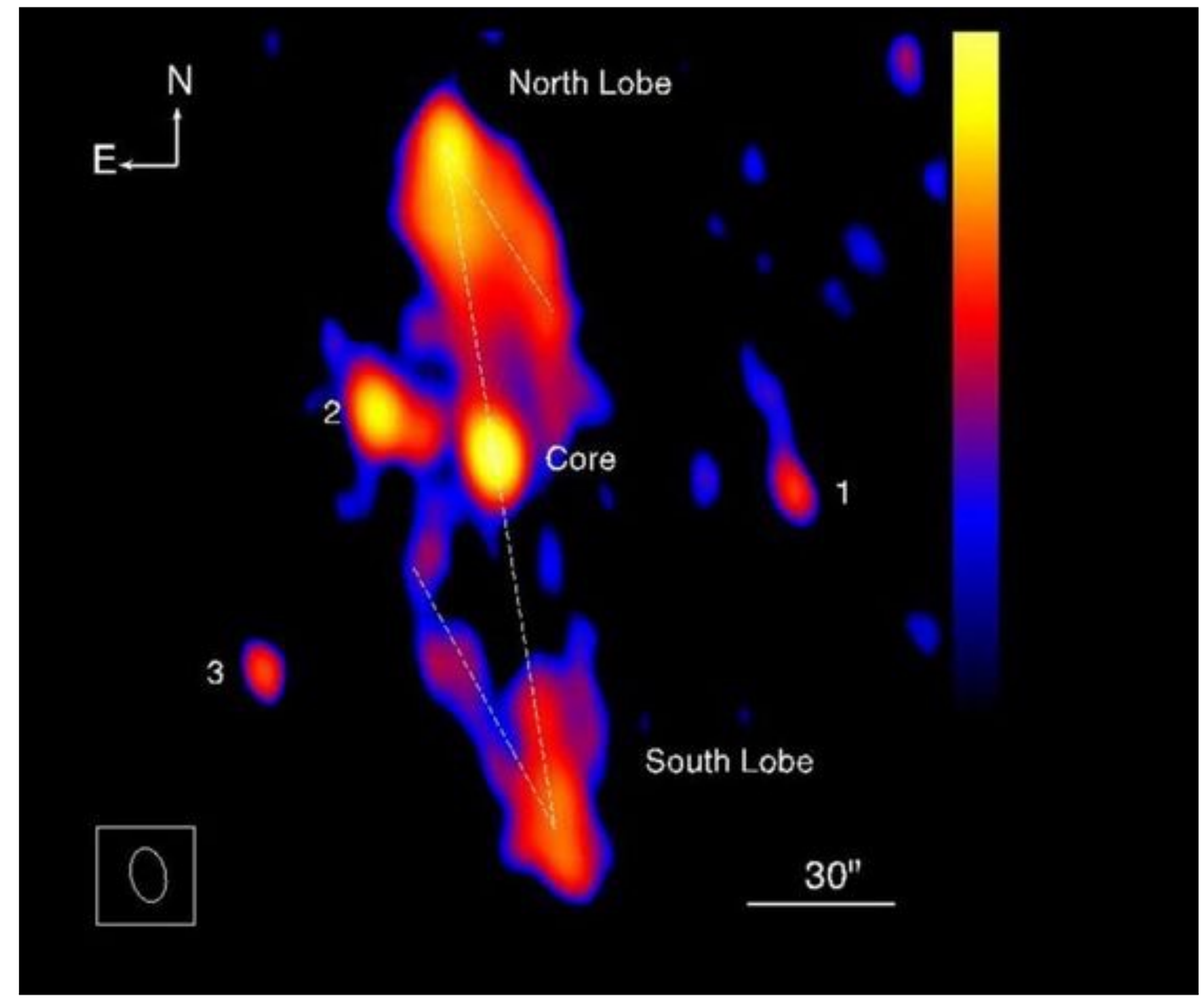

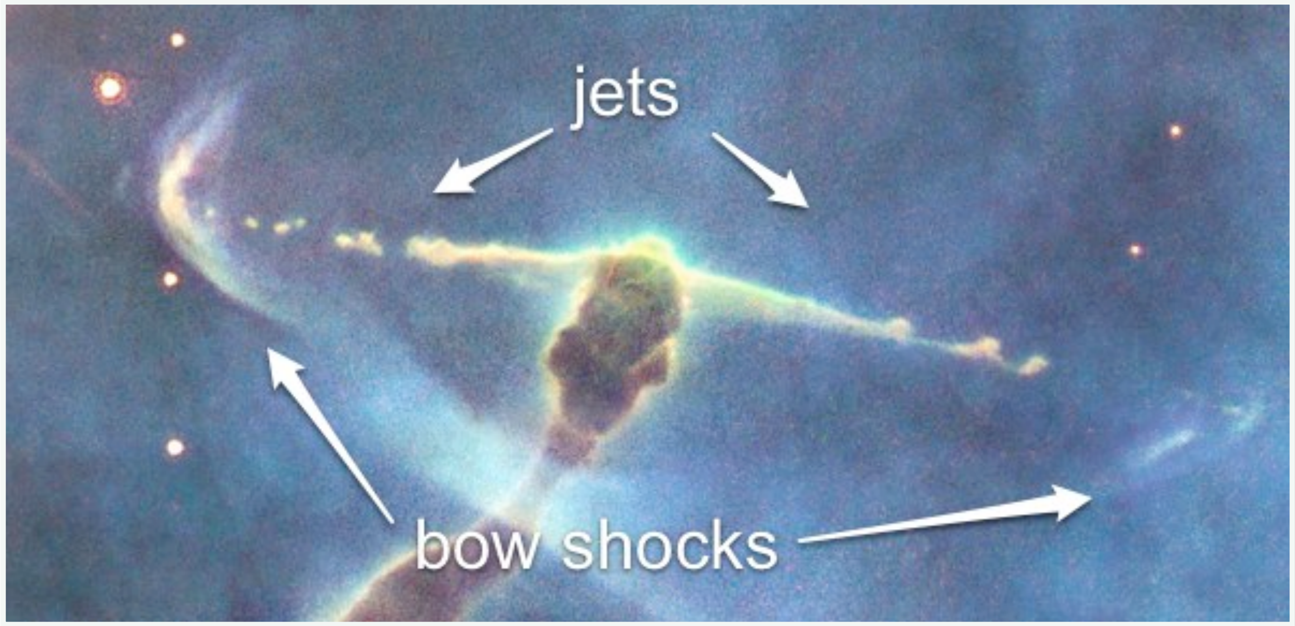

Also observed in micoquasars and protostars

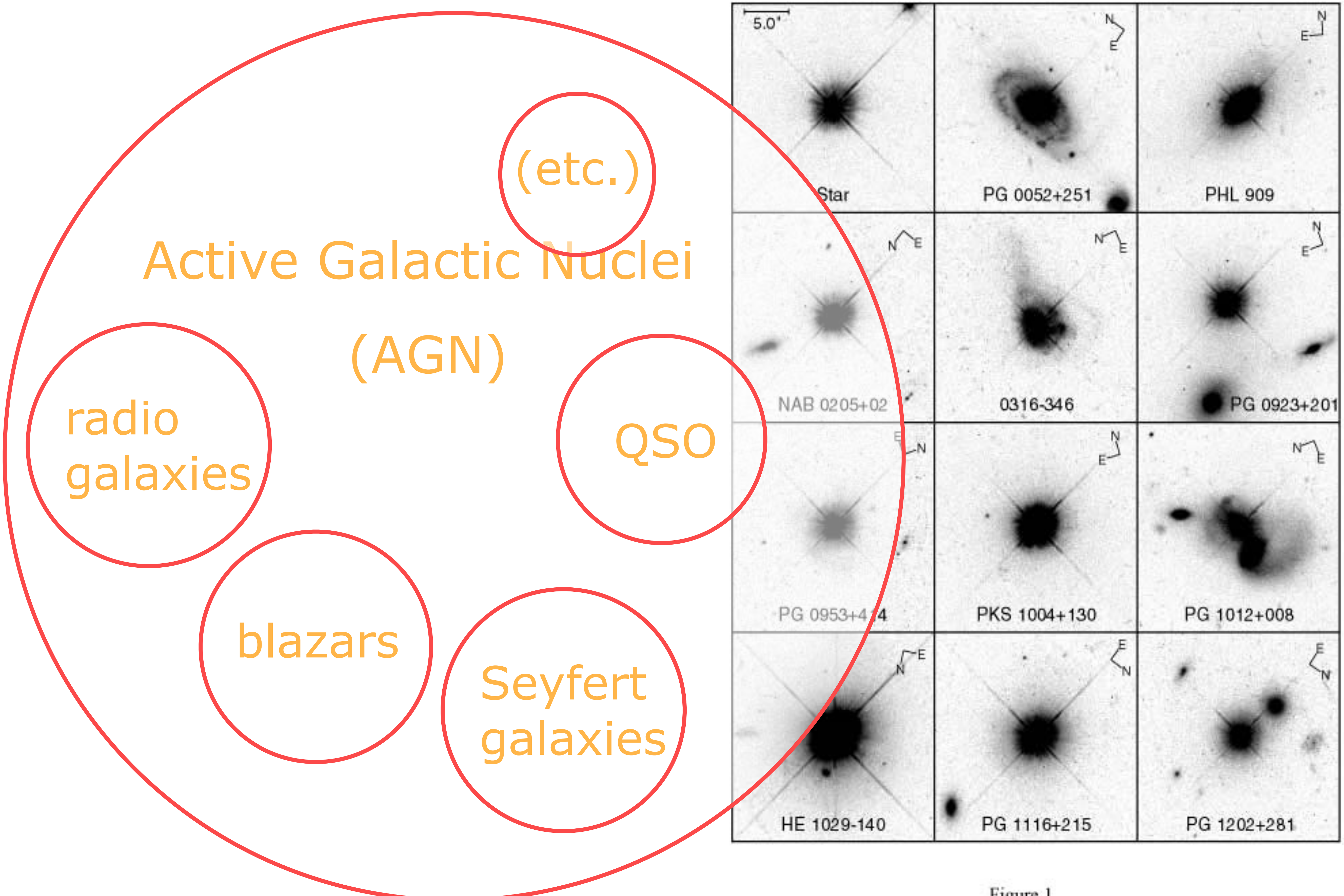
Active Galactic Nuclei
(AGN)
(etc.)
radio galaxies
QSO
blazars
Seyfert galaxies
5.0"
Star
PG 0052+251
PHL 909
NAB 0205+02
0316-346
PG 0923+201
PG 0953+414
PKS 1004+130
PG 1012+008
HE 1029-140
PG 1116+215
PG 1202+281

Figure 1

Radio "quiet" quasars were afterwards discovered (in fact, ~90% of all quasars are radio quiet)

↓

Quasi Stellar Objects (QSO)

Today, the name **quasar**
is used for objects in both classes, either
radio loud (RLQ) or **radio quiet (RQQ)**.

Main characteristics of QSOs:

- High redshift ⇒ high luminosity (-29.5 < M_B < -21.5)
- Strong, often broad, emission lines (not "HII region")
- Continuum and emission line variability
- Broad spectral energy distribution (SED) from radio to γ-rays

Seyfert galaxies

Radio galaxies

Galaxies (mostly ellipticals) hosting an **active nucleus**, and strong **radio emission**, usually with a core + jet + lobes morphology

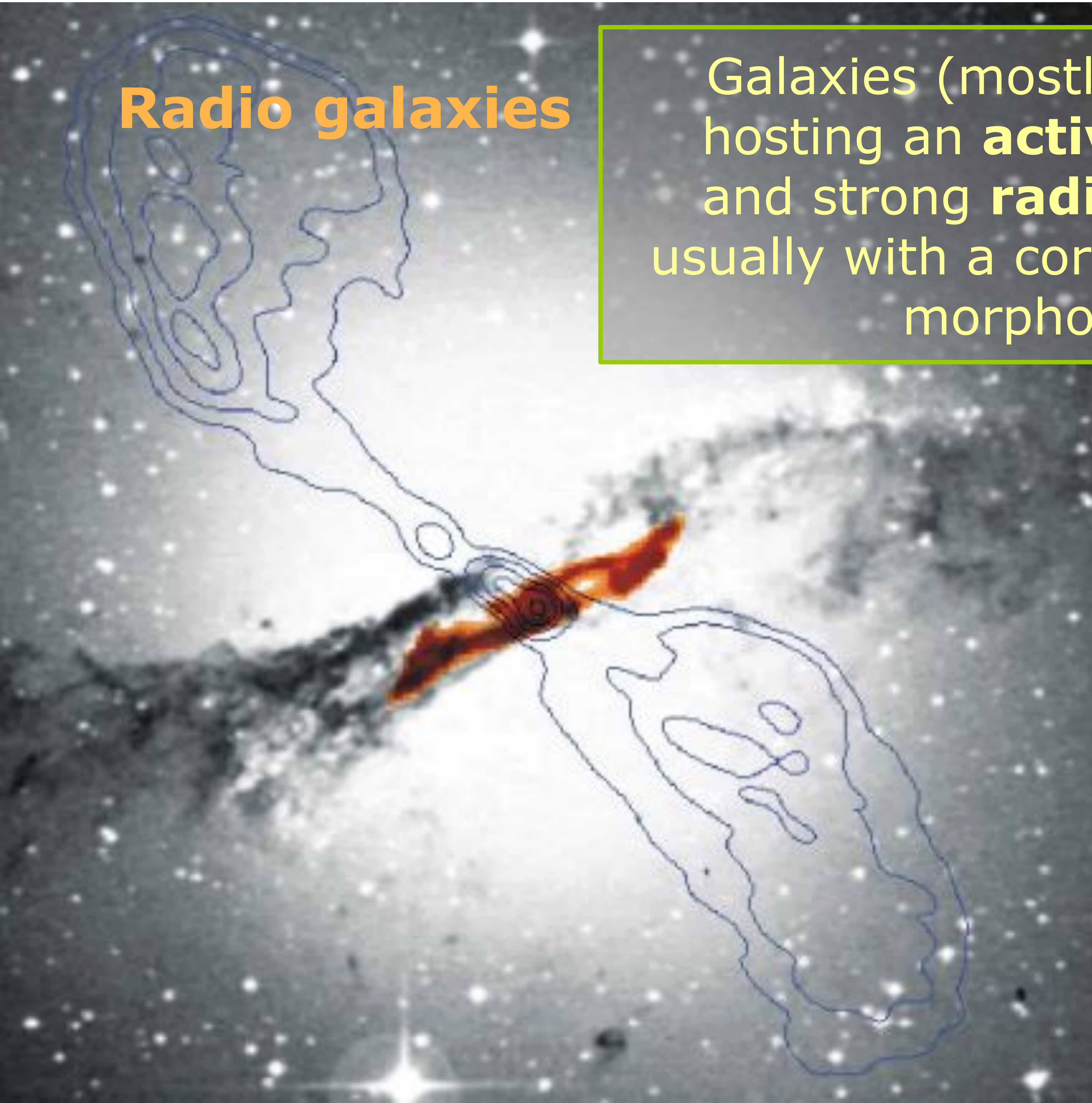

What is the engine of AGNs?

- Fast variability → small size

$$\Delta x < c \cdot \Delta t$$

- High energy output → large mass

$$L \leq L_E = (4\pi G\, c\, m_p\, M) / \sigma_e$$

Up to several 10^{13} L_o are generated within a few pc^3

Nuclear fusion is insufficient

Conversion of gravitational energy is more efficient

Super Massive Black Hole (SMBH): $M \leq 10^9\, M_o$

Active Galactic Nuclei (AGN) -- a schematic view --

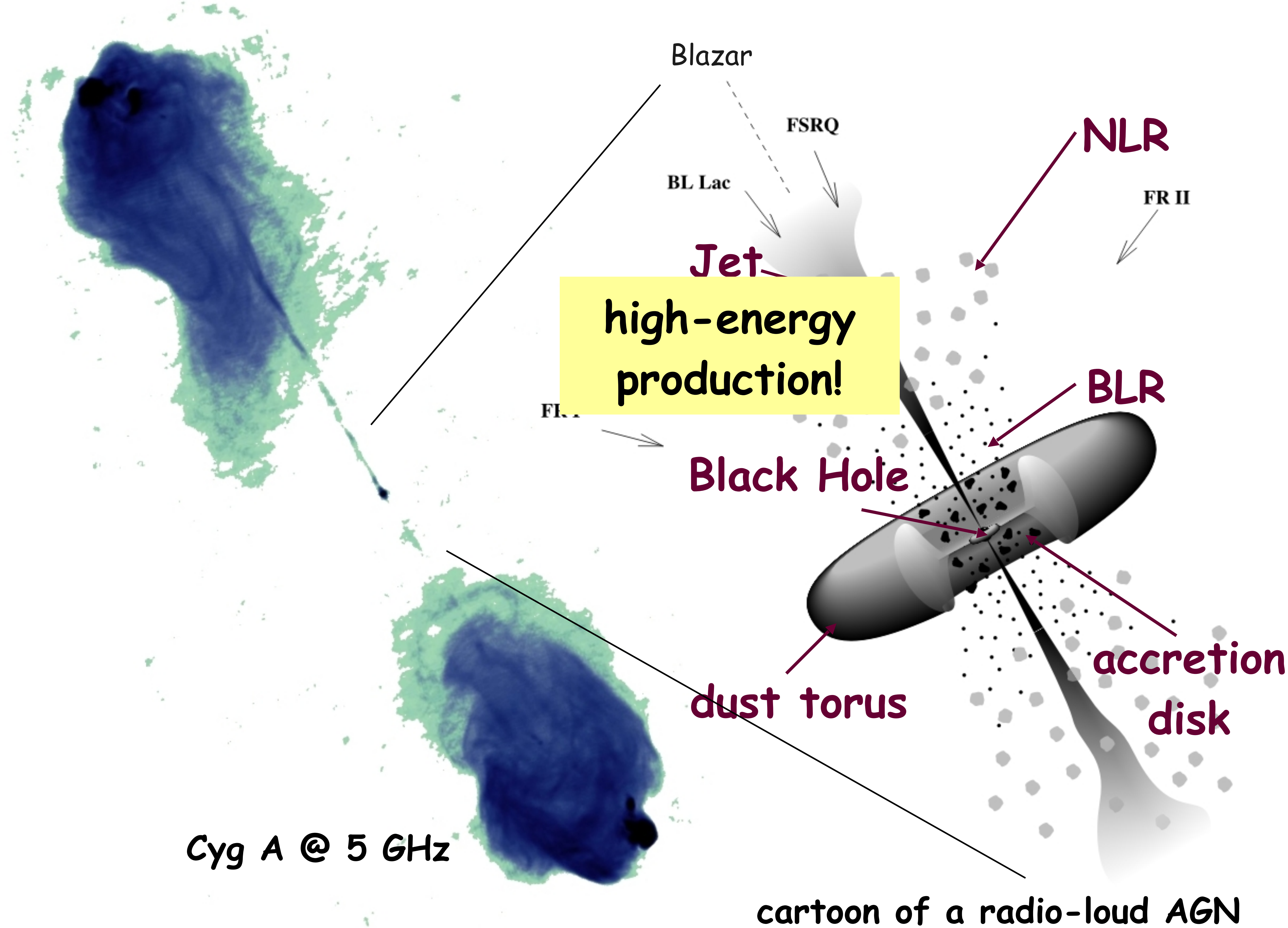

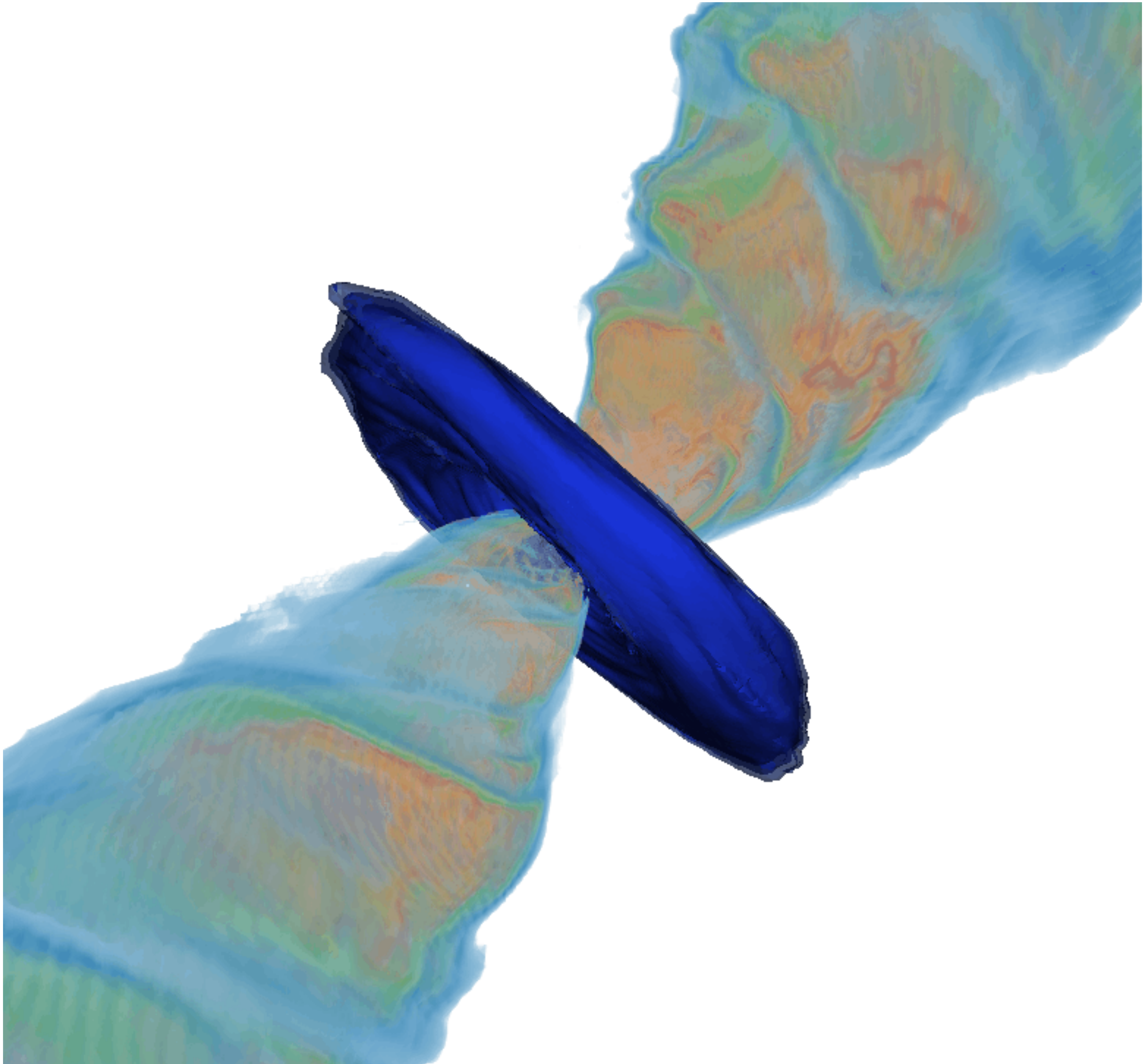

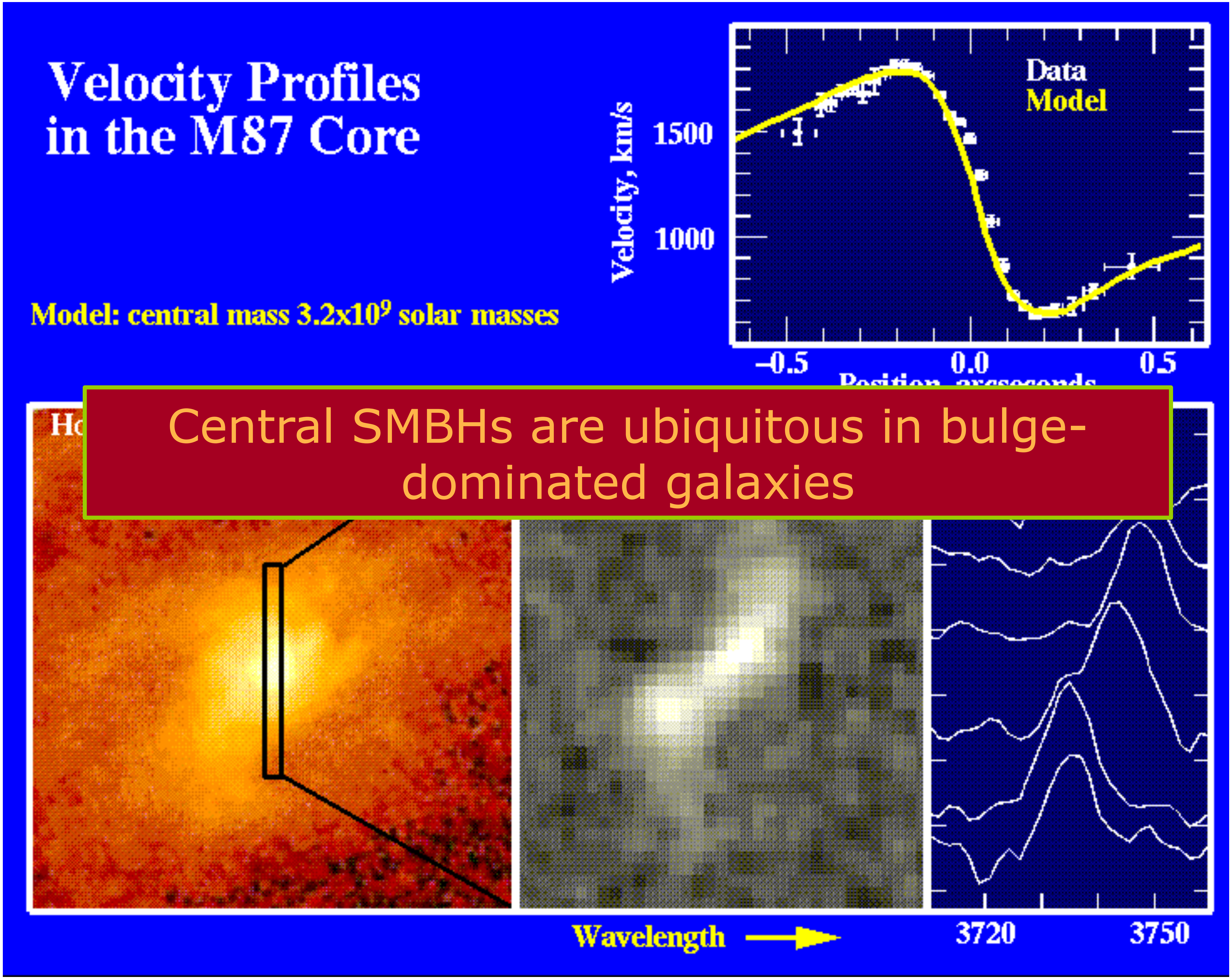

Central SMBHs are ubiquitous in bulge-dominated galaxies

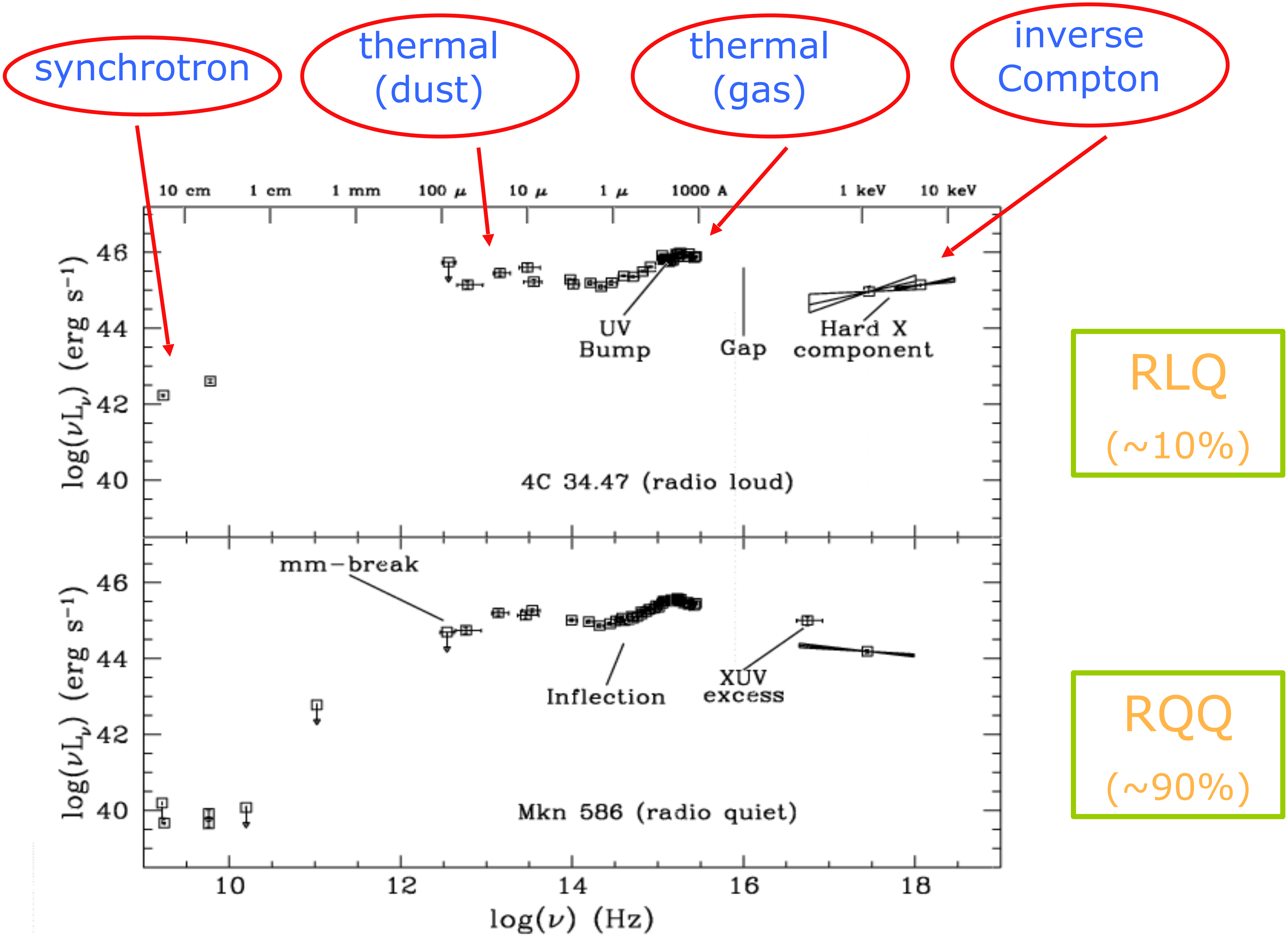
synchrotron
thermal (dust)
thermal (gas)
inverse Compton
10 cm
1 cm
1 mm
100 μ
10 μ
1 μ
1000 A
1 keV
10 keV
UV Bump
Gap
Hard X component
4C 34.47 (radio loud)
mm−break
Inflection
XUV excess
Mkn 586 (radio quiet)
log(νLν) (erg s−1)
log(ν) (Hz)
RLQ
(~10%)
RQQ
(~90%)

(Why) are there RL and RQ quasars?

Wilson & Colbert (1995, ApJ 438, 62)

- RL AGN never occur in spiral hosts *(and few RQ AGN in elliptical hosts)*
- Radio luminosity functions of Seyferts and radio galaxies are different
- RL and RQ AGN have similar emission properties from IR to X $\Rightarrow$ accretion is similar

SMBH spin $\rightarrow$ RL AGN

Projected gas density

left: xy

right: xz

Isolated Disk (Sbc) Galaxy
Run: execute/G3G2r-u3
T.J. Cox & Patrik Jonsson, UC Santa Cruz
UC Santa Cruz, 2004

A subset of RLQs with:

- "Flat" optical continuum
- Rapid variability
- Usually high and variable polarization
- Superluminal motions

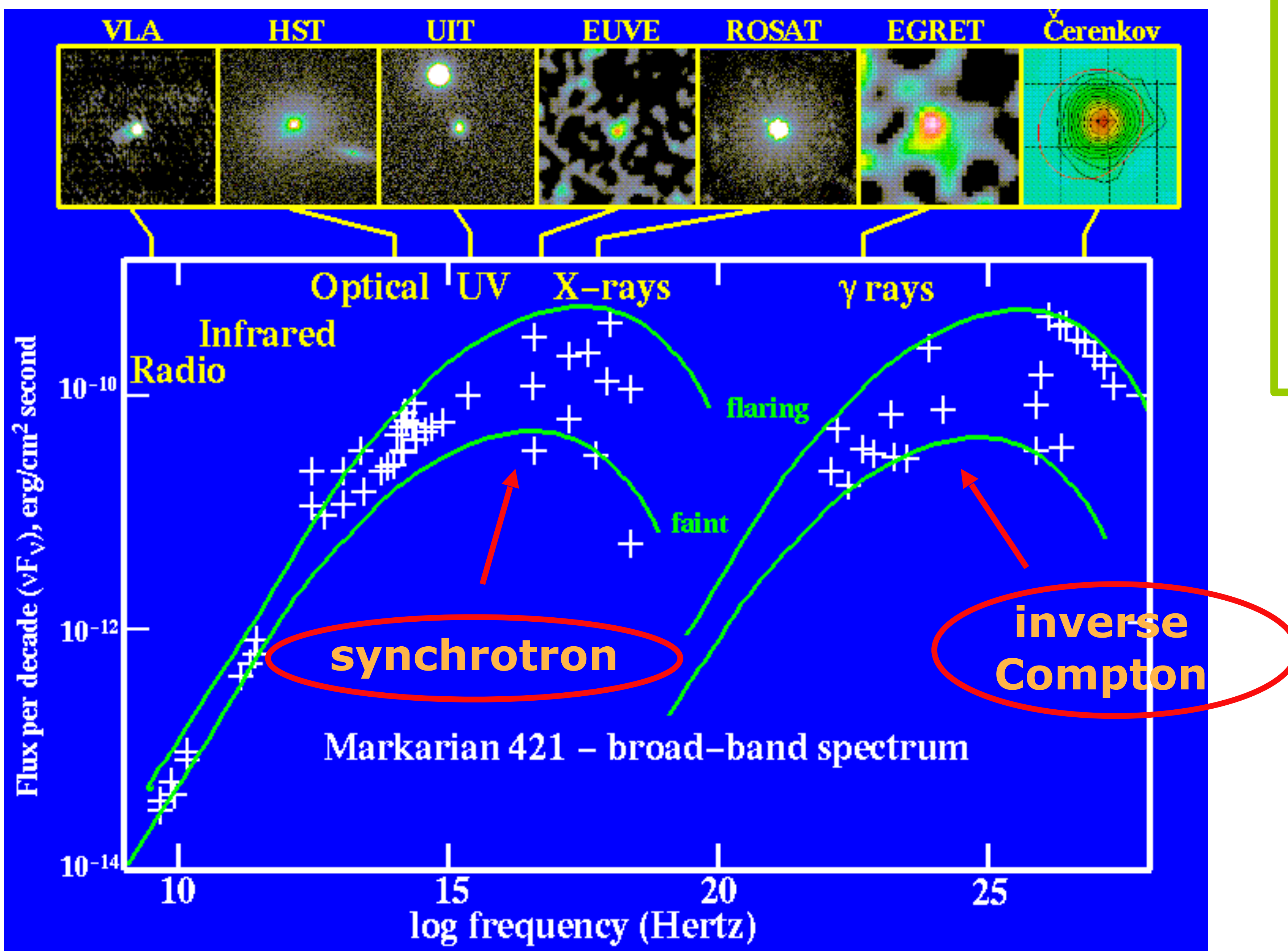

blazars

=

Flat Spectrum Radio Quasars (**FSRQ**)

+

BL Lac objects (faint or absent emission lines)

Blazars: looking down the jet …

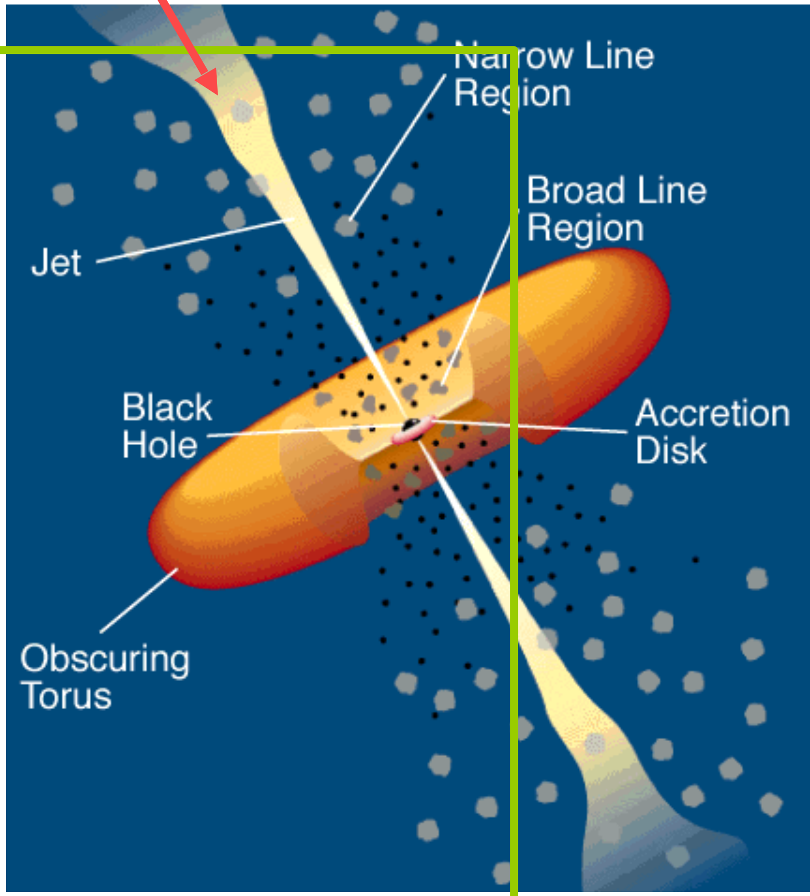

Relativistic effects are important

Doppler boosting: $F = \delta^4 F'$

(broadband flux)

$\delta = [\gamma\,(1-\beta\cos\theta)]^{-1}$ Doppler factor

$\beta = v/c$

$\gamma = (1-\beta^2)^{-1/2}$ Lorentz factor

Blazars: looking down the jet …

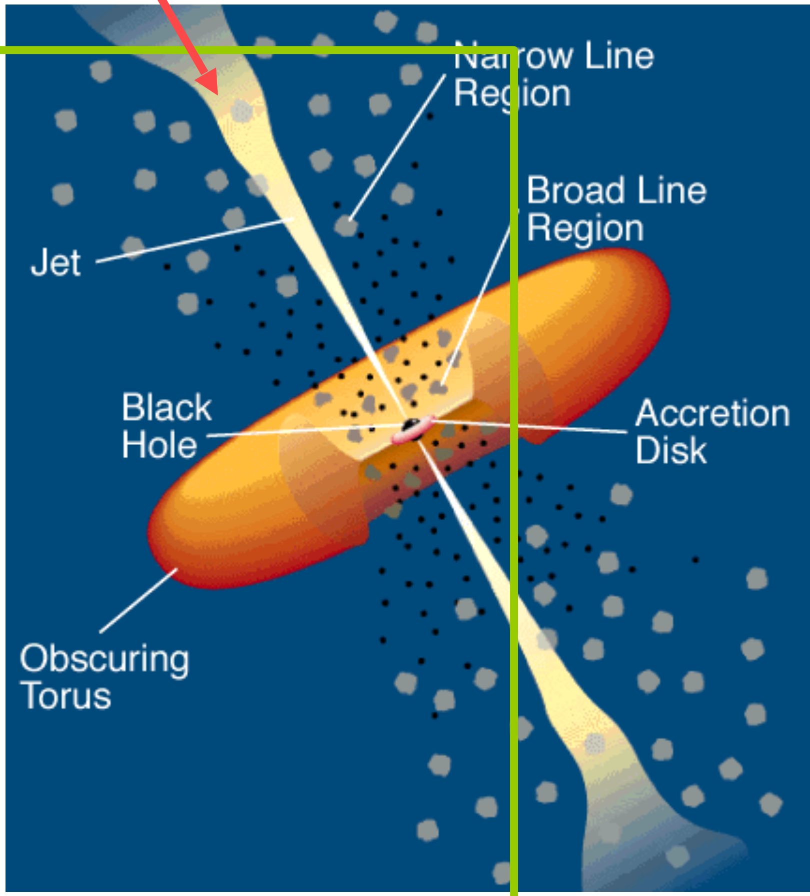

Relativistic effects are important

Doppler boosting: $F = 4\text{x}10^5\ F'$

(broadband flux)

$\delta = [\gamma\,(1-\beta\cos 1^\circ)]^{-1} = 13.9$ Doppler factor

$\beta = v/c = 0.99$

$\gamma = (1-\beta^2)^{-1/2} = 7.1$ Lorentz factor

Superluminal motion

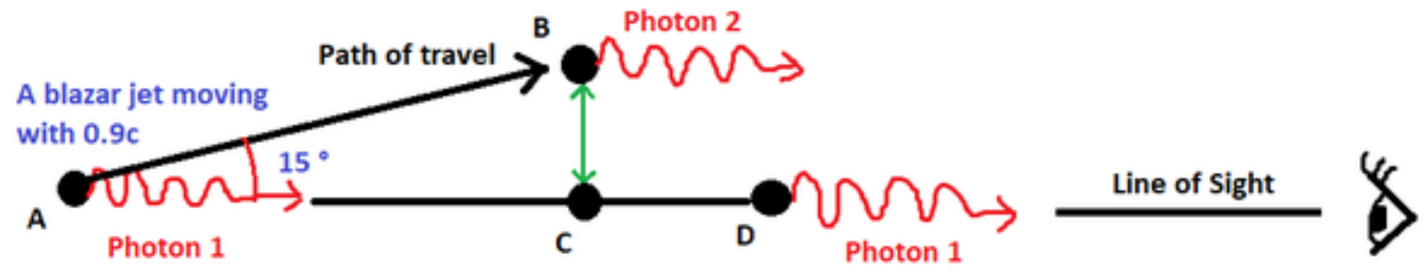

Superluminal Motion in the M87 Jet

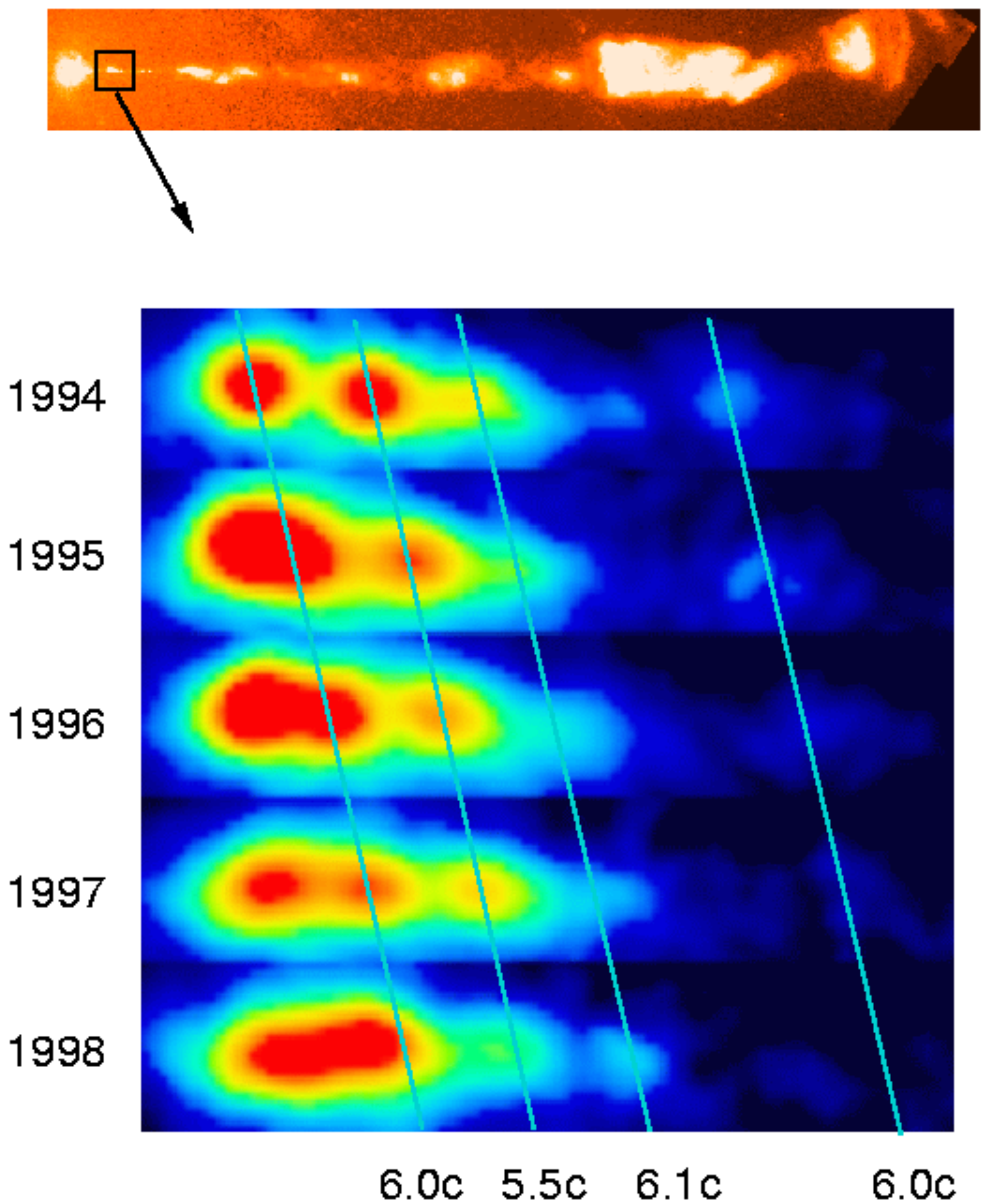

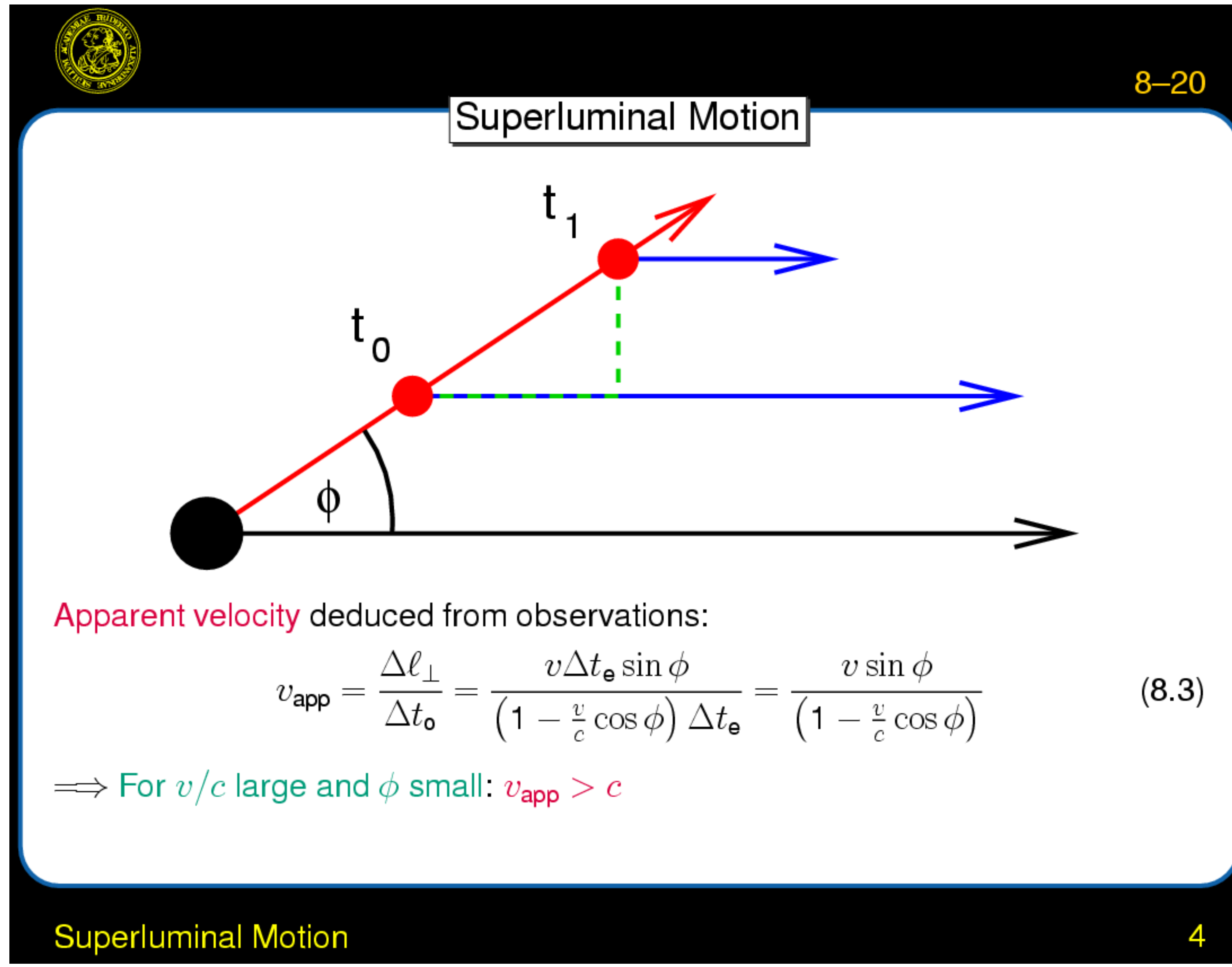

PKS 2155-304

Flux Variability

Big Flare: July 28 ~7 Crab

Aharonian et al, ApJ, 664L, 71A, 2007

- **Δt ~3min**
  - constraint on emission region size (if causality)
  - PDS: compatible with red noise
  - SF : Superina et al., Proc SF2A 2008

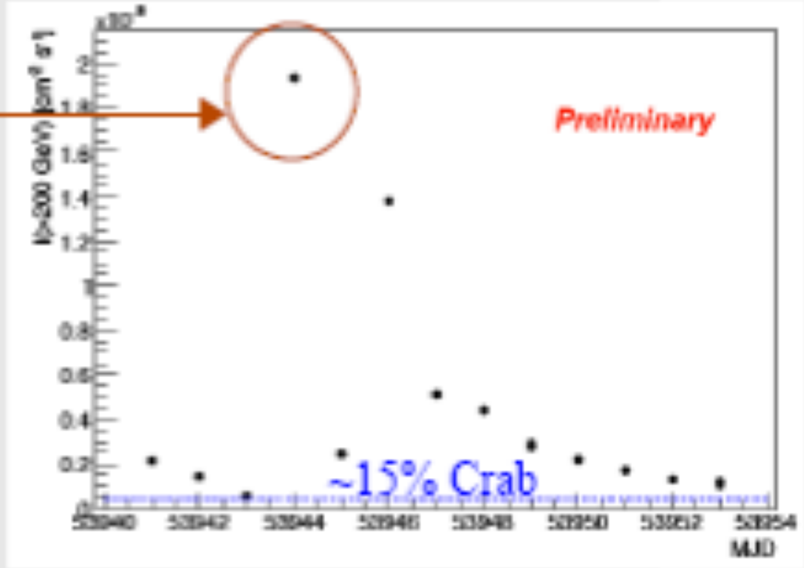

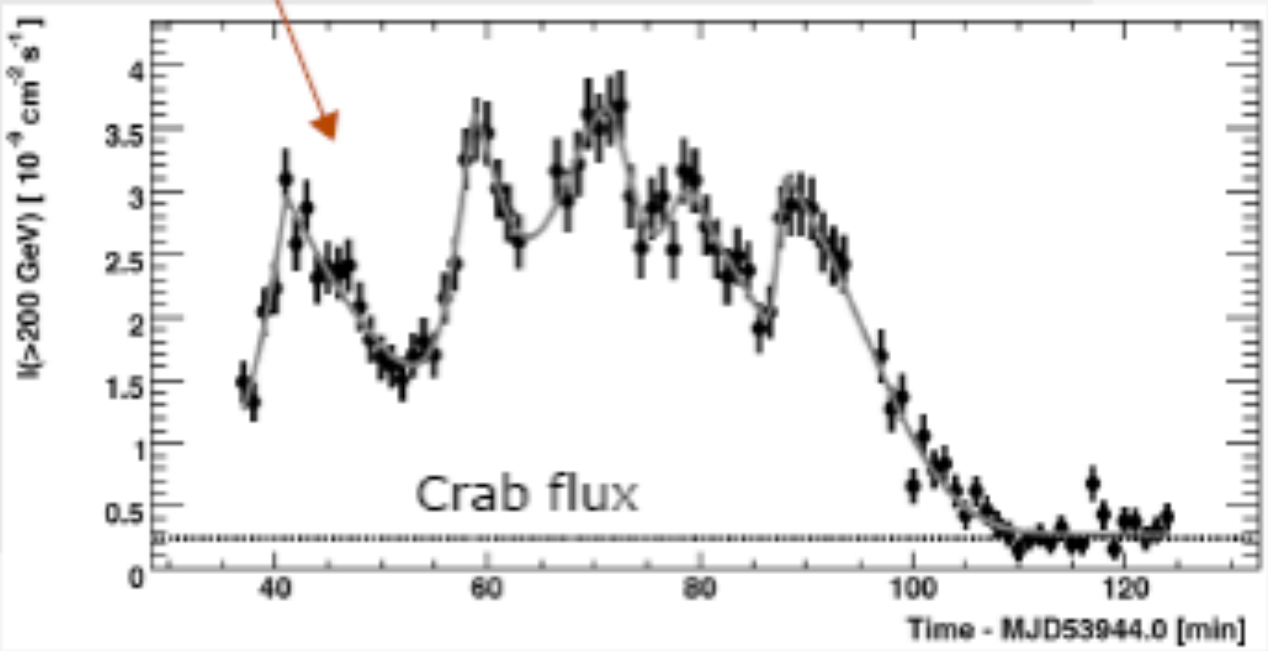

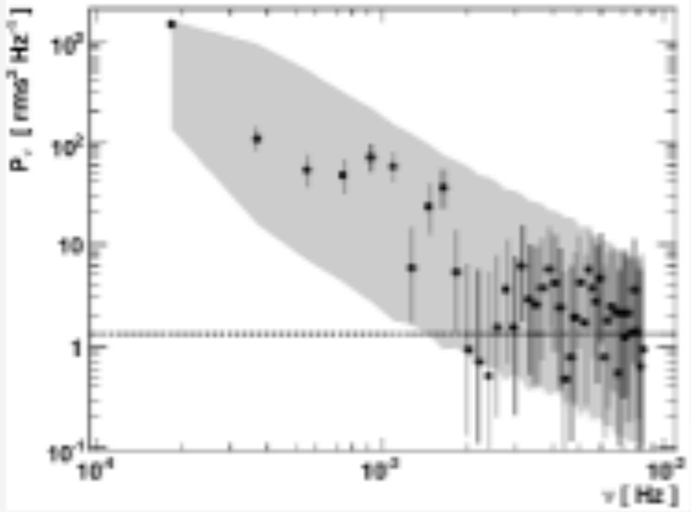

Whenever jets are observed, three ingredients are present:

A strong potential well, accretion of matter, and magnetic fields.

The most powerful jets are produced in the surroundings of black holes, the most compact objects in the universe.

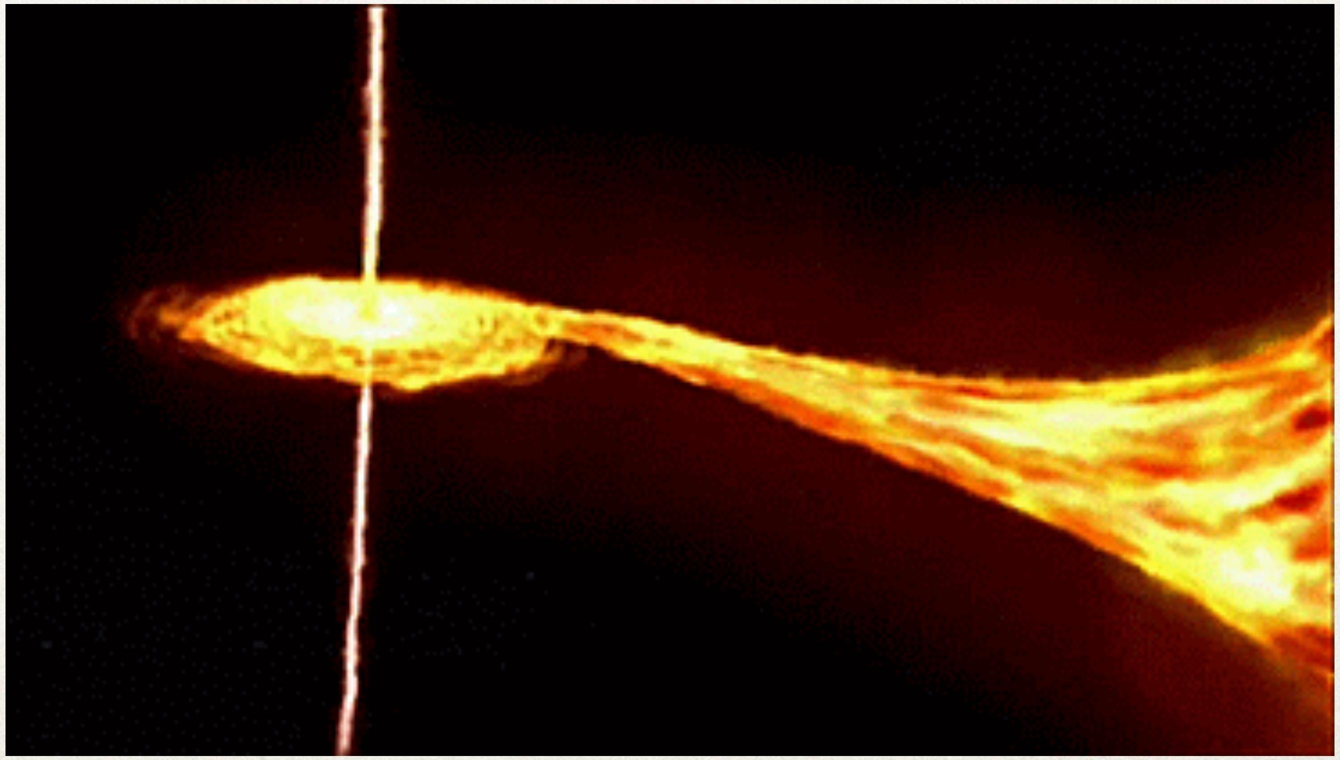

Axially symmetric black hole (Kerr)

$$
\begin{aligned}
ds^2 &= g_{tt}dt^2 + 2g_{t\phi}dtd\phi - g_{\phi\phi}d\phi^2 - \Sigma\Delta^{-1}dr^2 - \Sigma d\theta^2 \\
g_{tt} &= (c^2 - 2GMr\Sigma^{-1}) \\
g_{t\phi} &= 2GMac^{-2}\Sigma^{-1}r\sin^2\theta \\
g_{\phi\phi} &= [(r^2 + a^2c^{-2})^2 - a^2c^{-2}\Delta\sin^2\theta]\Sigma^{-1}\sin^2\theta \\
\Sigma &\equiv r^2 + a^2c^{-2}\cos^2\theta \\
\Delta &\equiv r^2 - 2GMc^{-2}r + a^2c^{-2}. \qquad a = J/M
\end{aligned}
$$

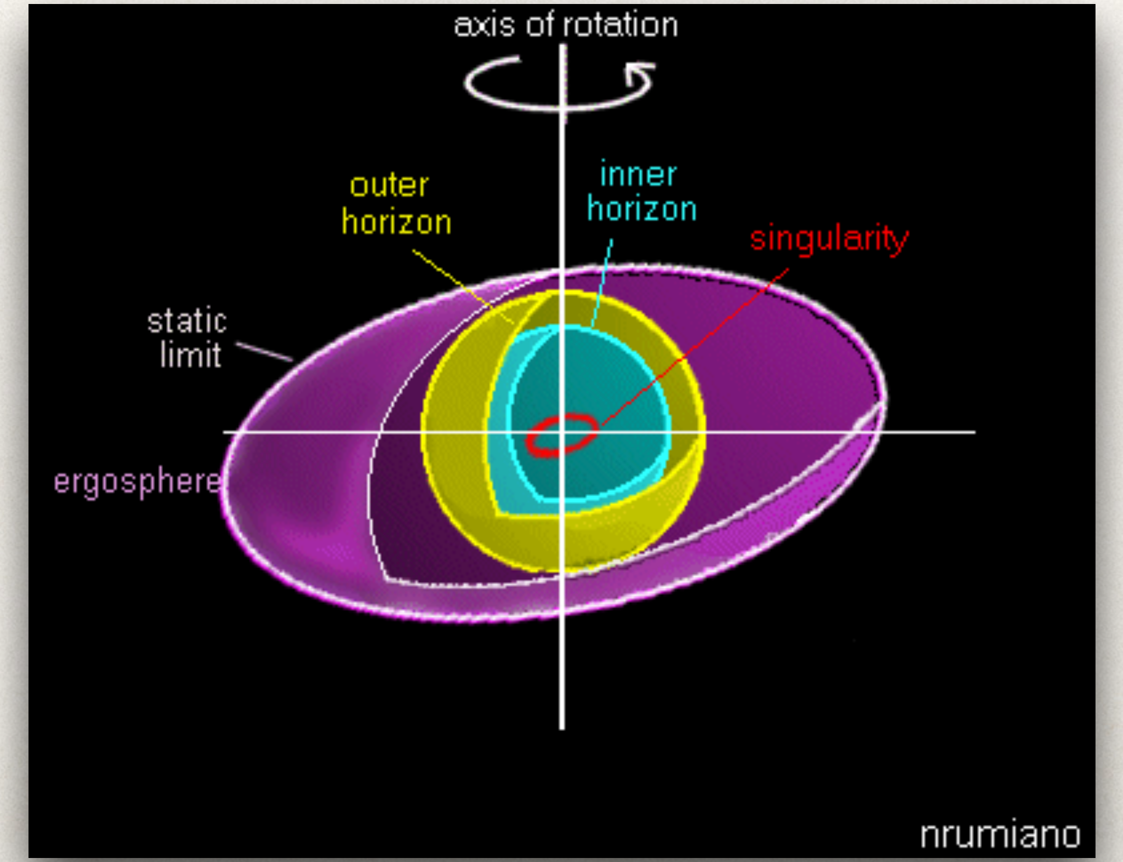

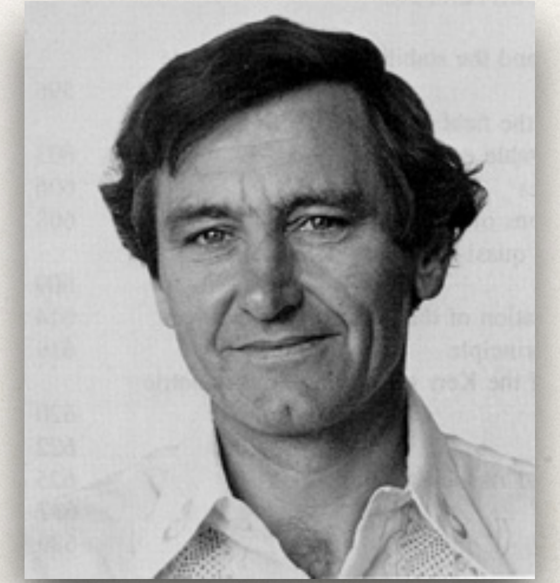

Roy Kerr

Kerr black hole

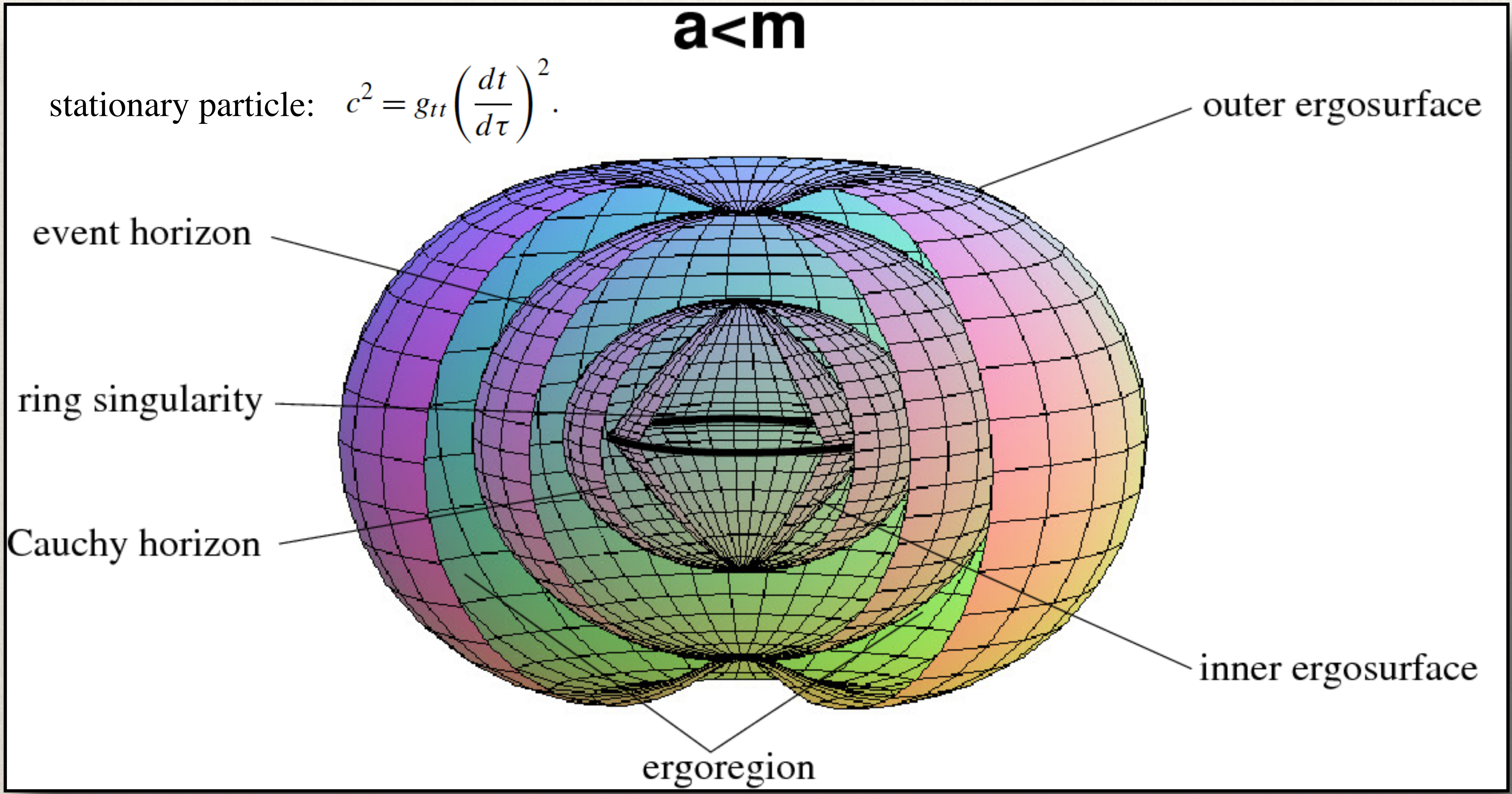

When $g_{tt} \leq 0$ the stationary condition cannot be fulfilled, and hence a massive particle cannot be stationary inside the surface defined by $g_{tt} = 0$ —> ergosphere

Accretion onto black holes

Standard disk model (Shakura & Sunyaev 1973): conservation of angular momentum leads to the formation of a disk around the BH. Energy is dissipated through radiation created by viscosity. Then angular momentum is removed and there is an inflow. If the disk is optically thick each ring radiates as a blackbody of different temperature.

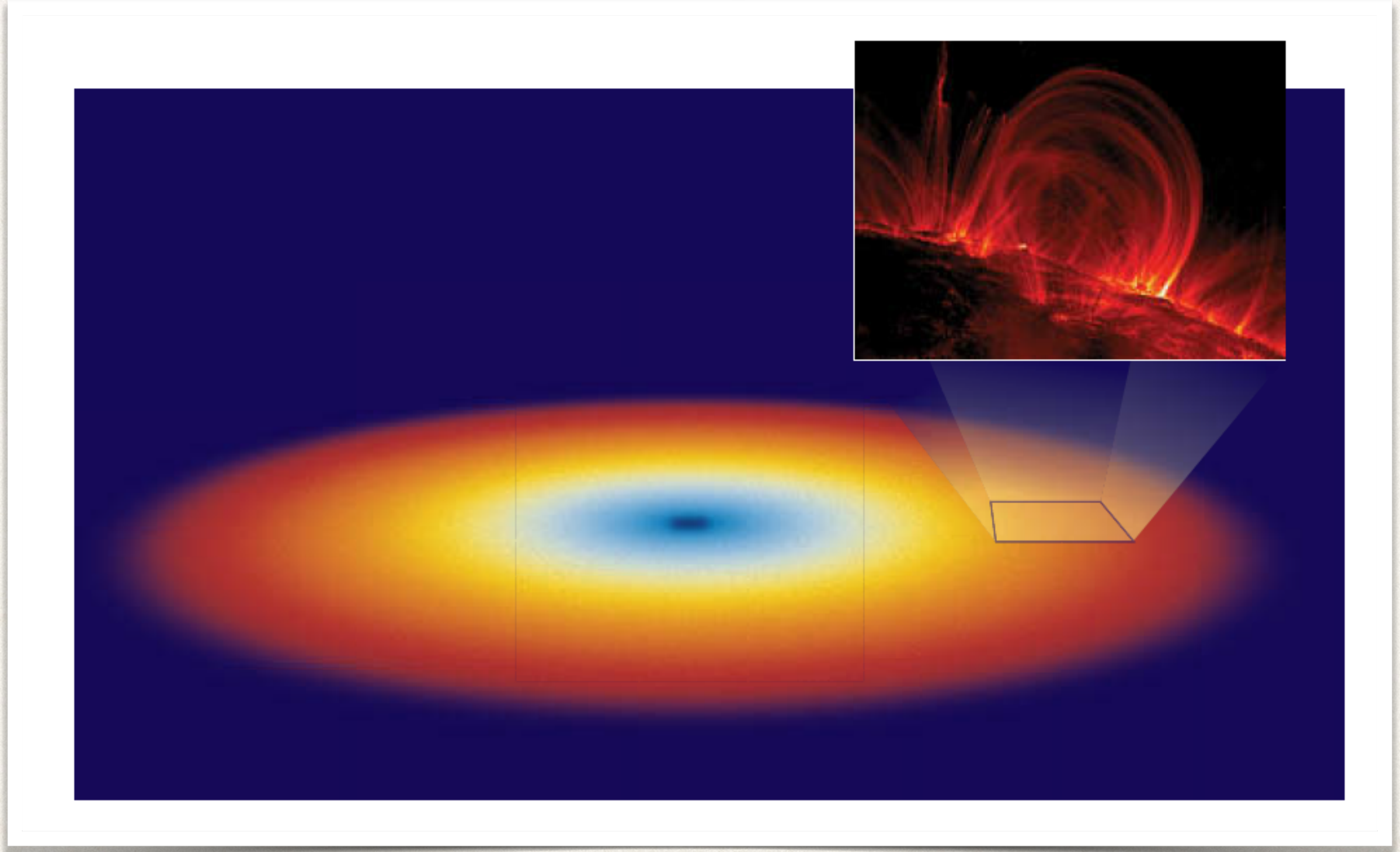

Basic equations for (thin) accretion disks

Simplifying assumptions:

1. The disk is axisymmetric, i.e. $\partial/\partial\varphi = 0$.
2. The disk is thin, i.e. its characteristic size scale in the z -axis is $H << R$.
3. The matter in the disk is in hydrostatic equilibrium in the z-direction.
4. The self-gravitation of the disk is negligible.

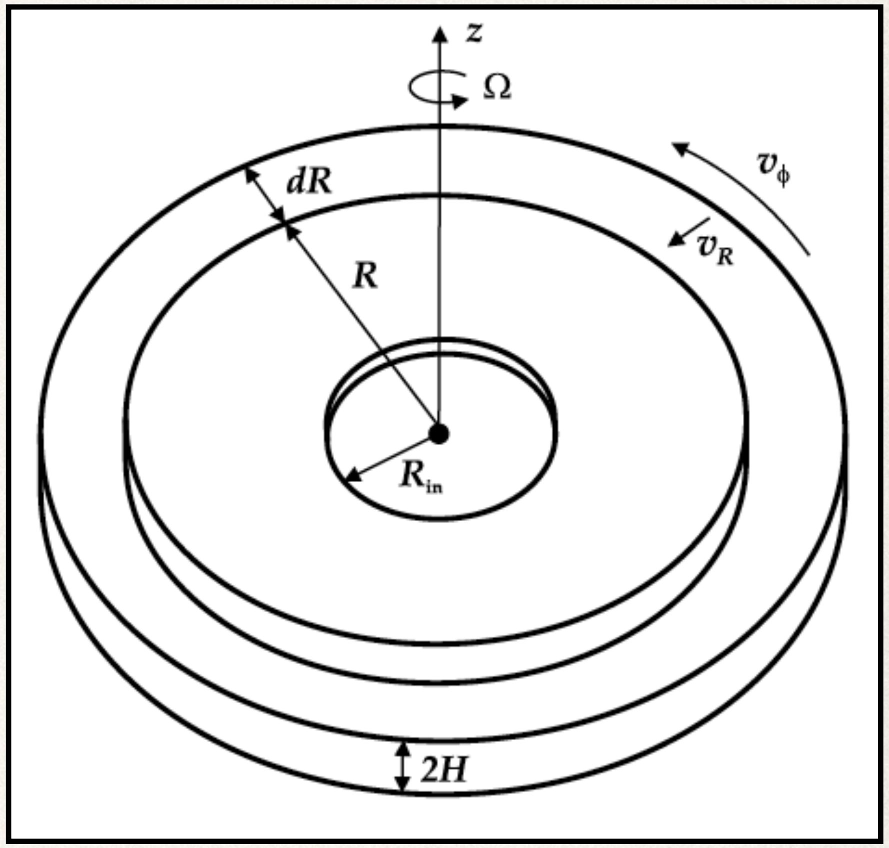

- Equation of continuity
- Equation of momentum transfer
- Energy dissipation in the disk
- Viscous stresses $\nu = \alpha a_{\rm s} H.$
- Equation of state $P = P_{\rm gas} + P_{\rm rad} = \frac{\rho k T}{\mu m_p} + \frac{4\sigma_{\rm SB}}{3c} T.$
- Opacity law $\kappa = \kappa\left(\rho, T\right).$
- Relation between electron and proton temperature.

Structure of the thin disks

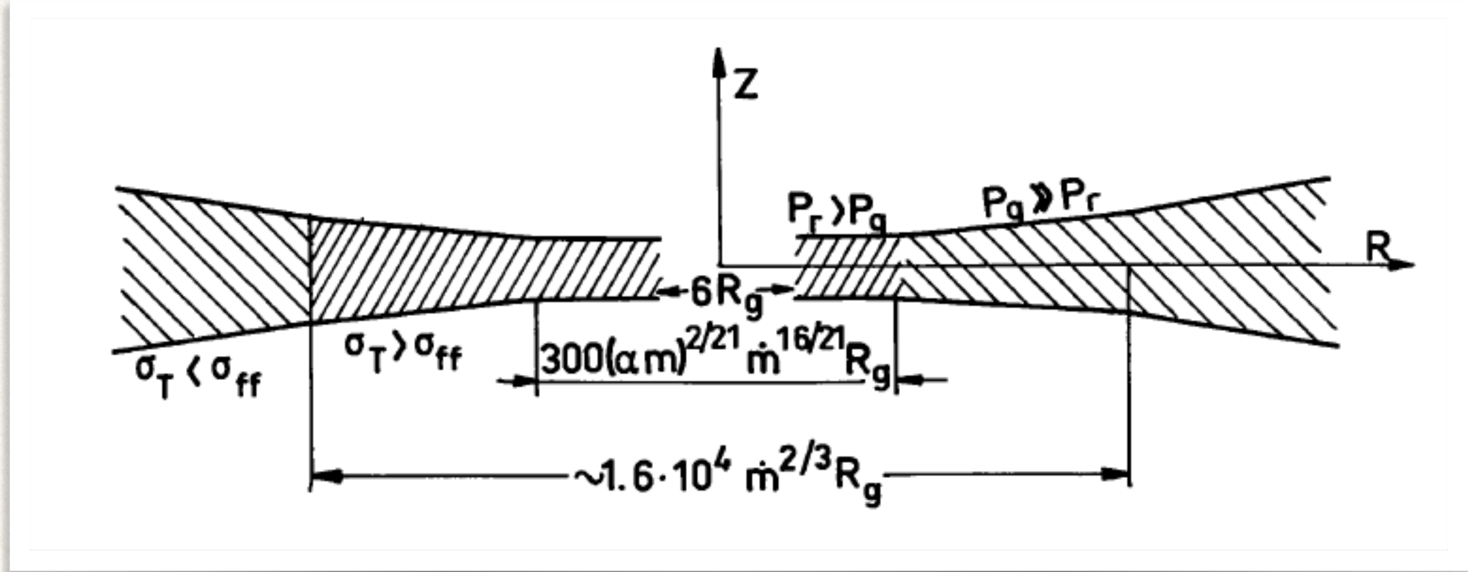

1. An outer region (large R) in which gas pressure dominates over radiation pressure and the opacity is due to free-free absorption.

2. A middle region (smaller R) in which gas pressure dominates over radiation pressure but opacity is due to Thomson scattering off electrons.

3. An inner region (small R) in which radiation pressure dominates over gas pressure and opacity is mainly due to scattering.

Thin accretion disk

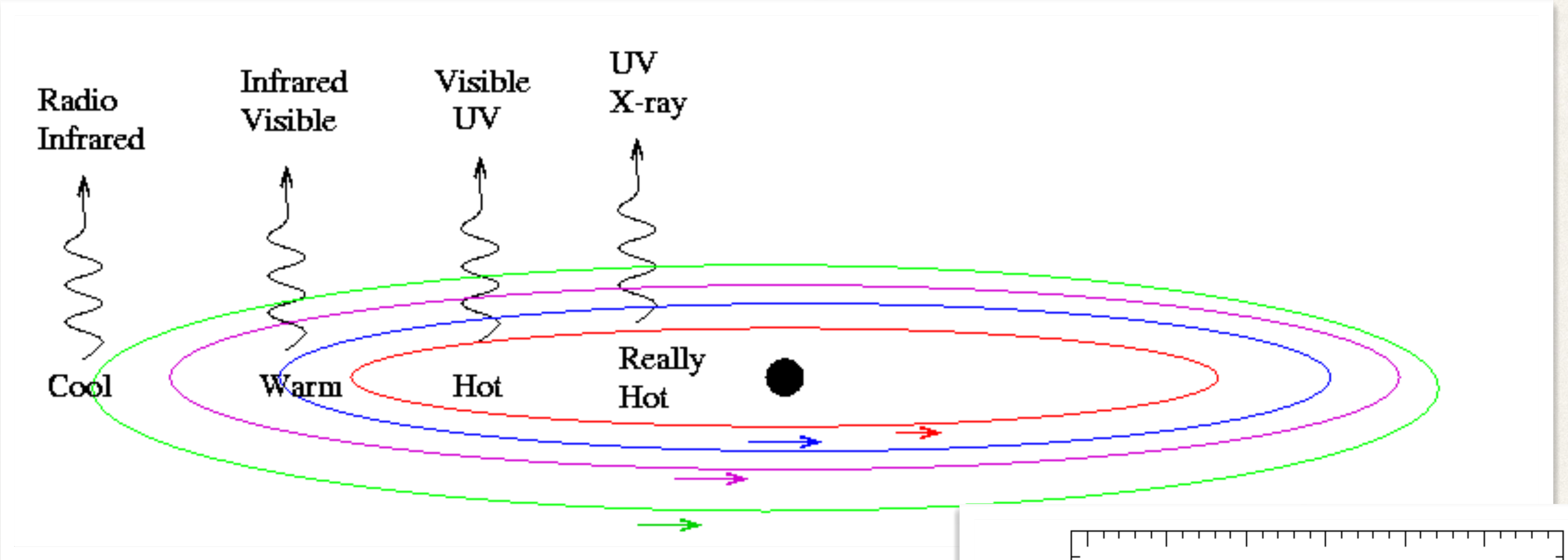

$$T(R) = \left[\frac{Q^+(R)}{\sigma_{SB}}\right]^{1/4} = \left(\frac{3GM\dot{M}}{8\pi\sigma_{SB}R^3}\right)^{1/4}\left(1-\sqrt{\frac{R_{in}}{R}}\right)^{1/4}.$$

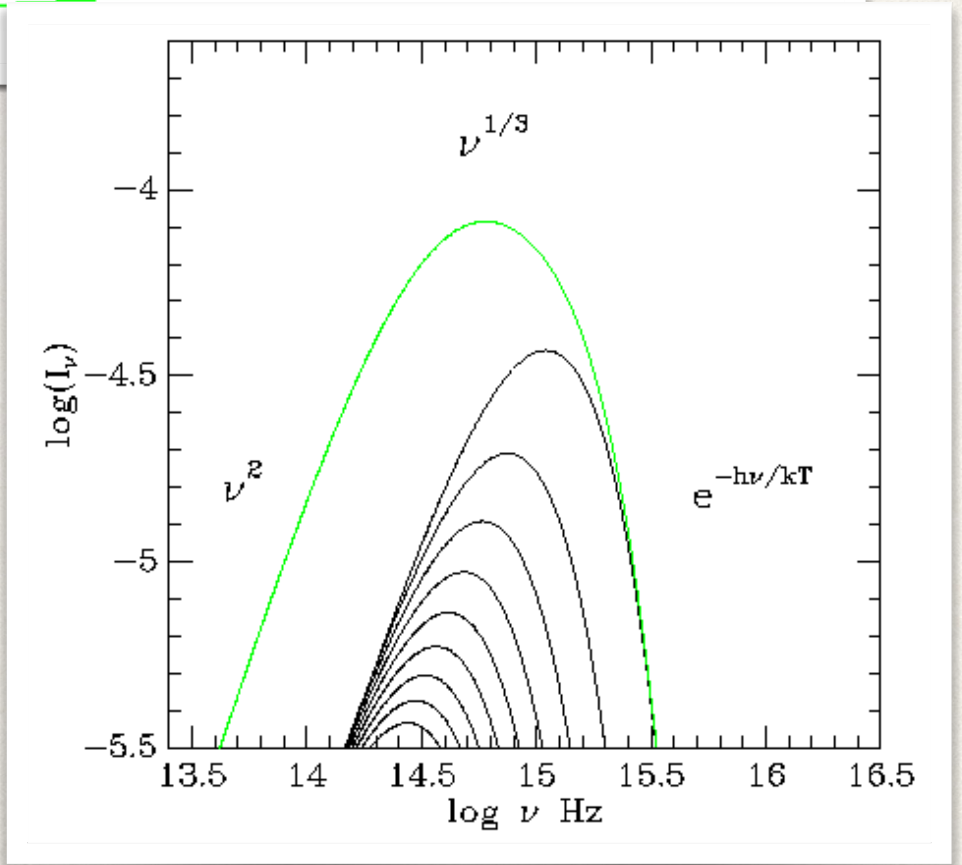

Spectrum

$$I_\nu(\nu, R) = B_\nu(\nu, R) \equiv \frac{2h\nu^3}{c^2[\exp(h\nu/kT)-1]}.$$

The total flux at frequency ν detected by an observer at a distance d whose line of sight forms and angle θ_d with the normal to the disk is:

$$F_\nu(\nu) = \frac{\cos\theta_\mathrm{d}}{d^2}\int_{R_\mathrm{in}}^{R_\mathrm{out}} 2\pi\, R\, I_\nu\, dR.$$

The flux grows as $F_\nu \propto \nu^2$ for photon energies $h\nu \ll kT(R_\mathrm{out})$, and decreases exponentially for $h\nu \gg kT(R_\mathrm{in})$. For intermediate energies the spectrum has the characteristic dependence $F_\nu \propto \nu^{1/3}$. As $T(R_\mathrm{out})$ approaches $T(R_\mathrm{in})$ this part of the spectrum narrows, and it becomes similar to that of a simple blackbody.

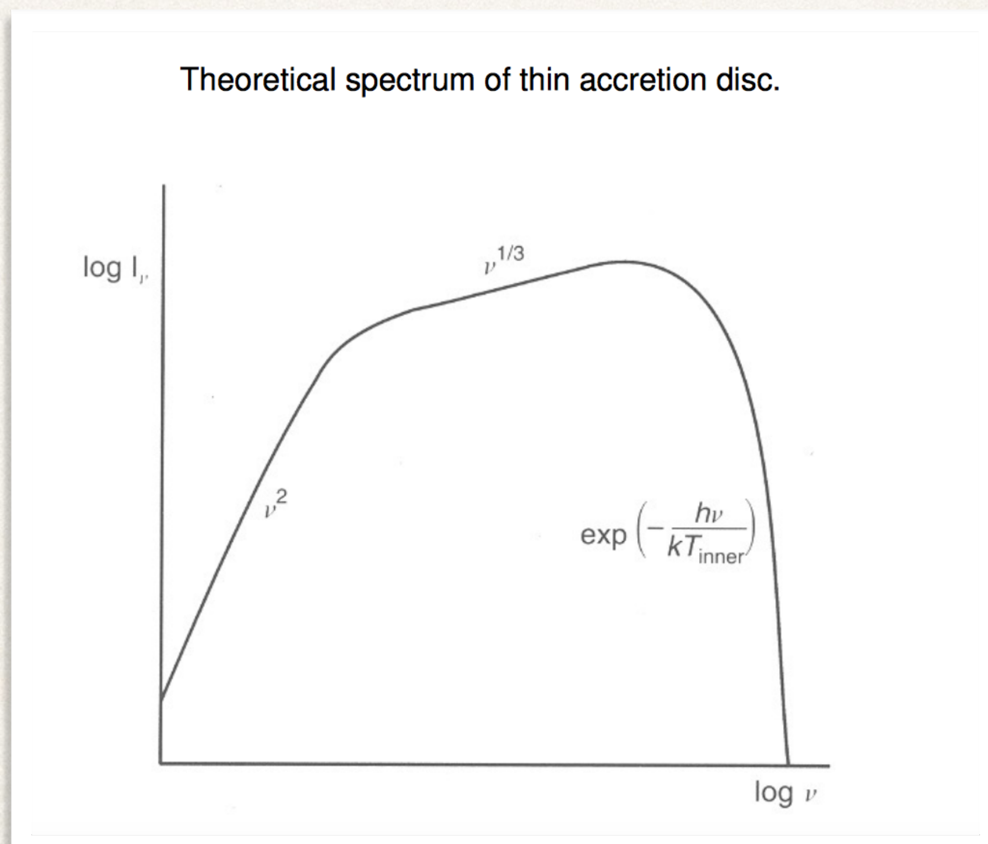

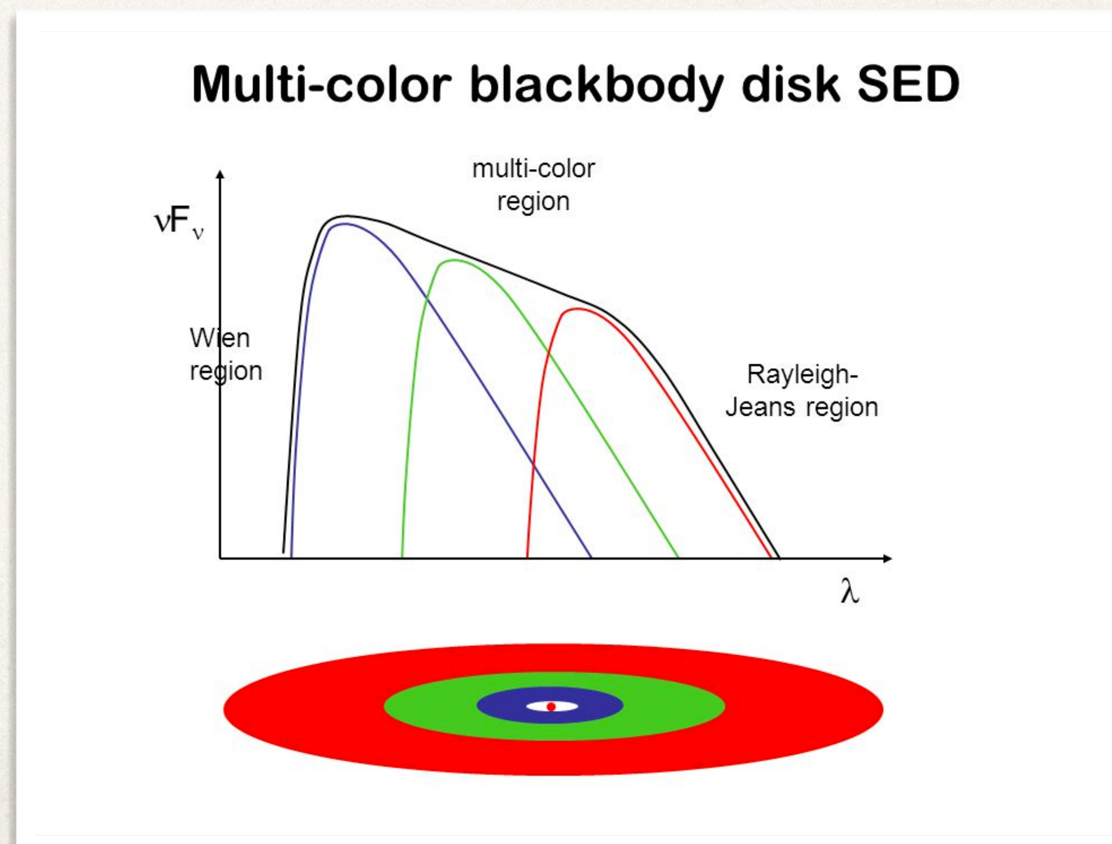

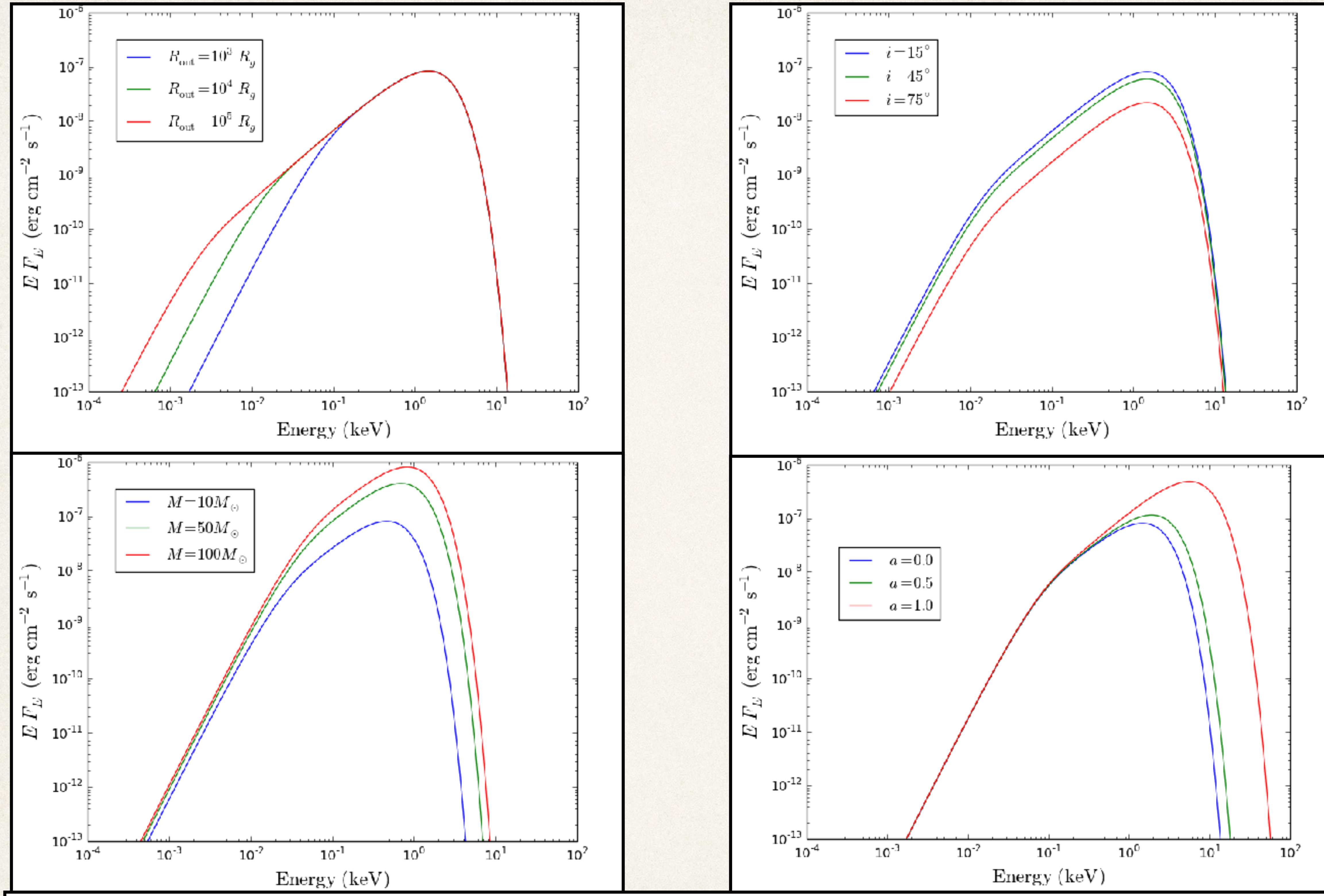

Changes in the accretion disk spectrum with different parameters

Diagnostics through Fe K-alpha lines

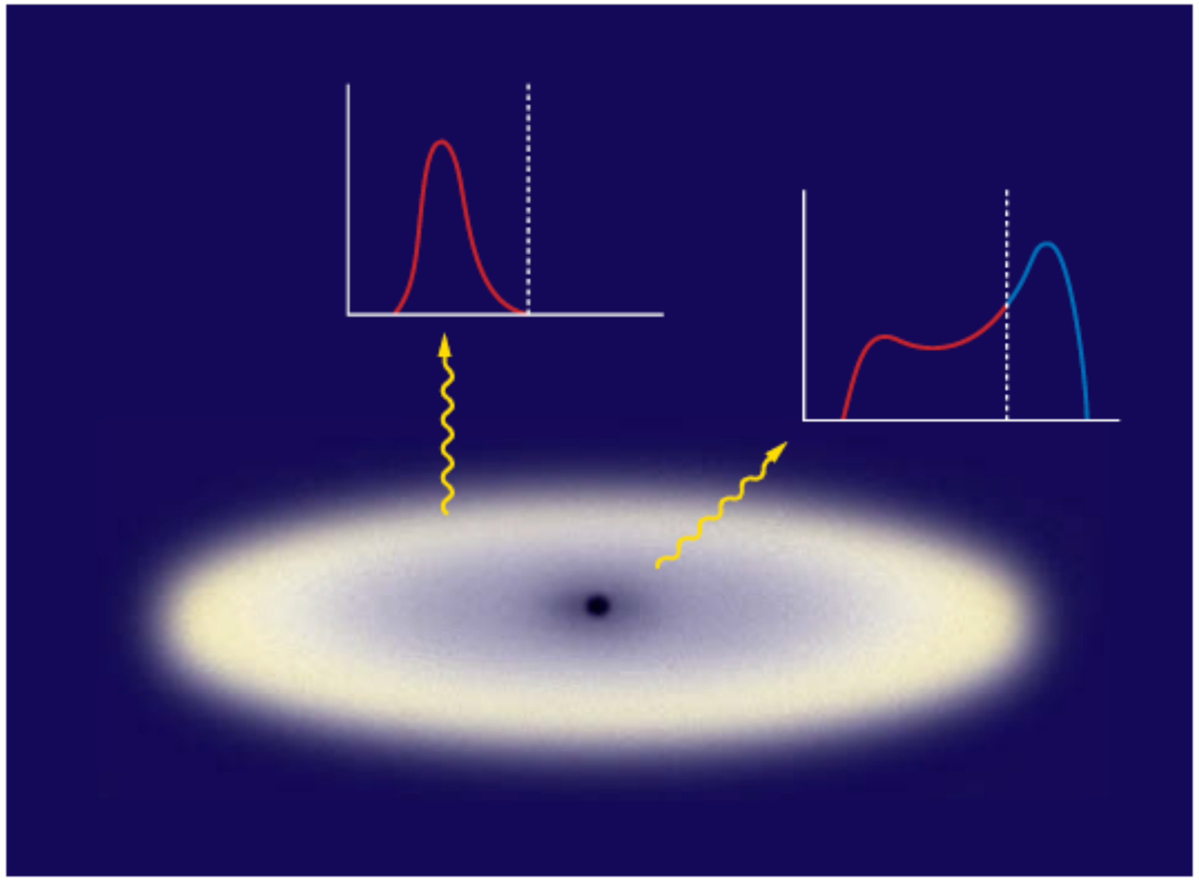

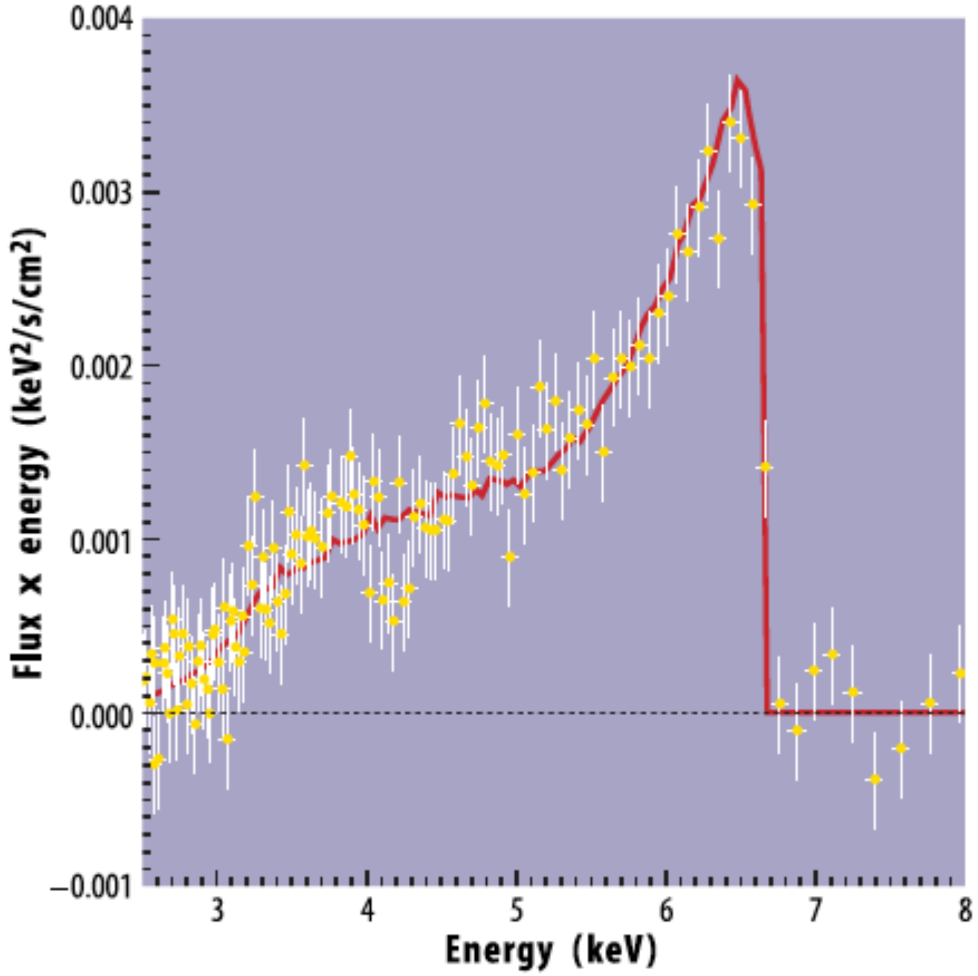

It is possible to determine the spin parameter a

$$r_{\rm isco} = \frac{GM}{c^2}\left(3 + Z_2 \pm \sqrt{(3 - Z_1)(3 + Z_1 + 2Z_2)}\right)$$

$$Z_1 = 1 + (1 - x^2)^{1/3}\left[(1 + x)^{1/3} + (1 - x)^{1/3}\right]$$

$$Z_2 = \sqrt{3x^2 + Z_1^2} \qquad x = a/M$$

The spectrum of X-ray binaries is more complex: more components

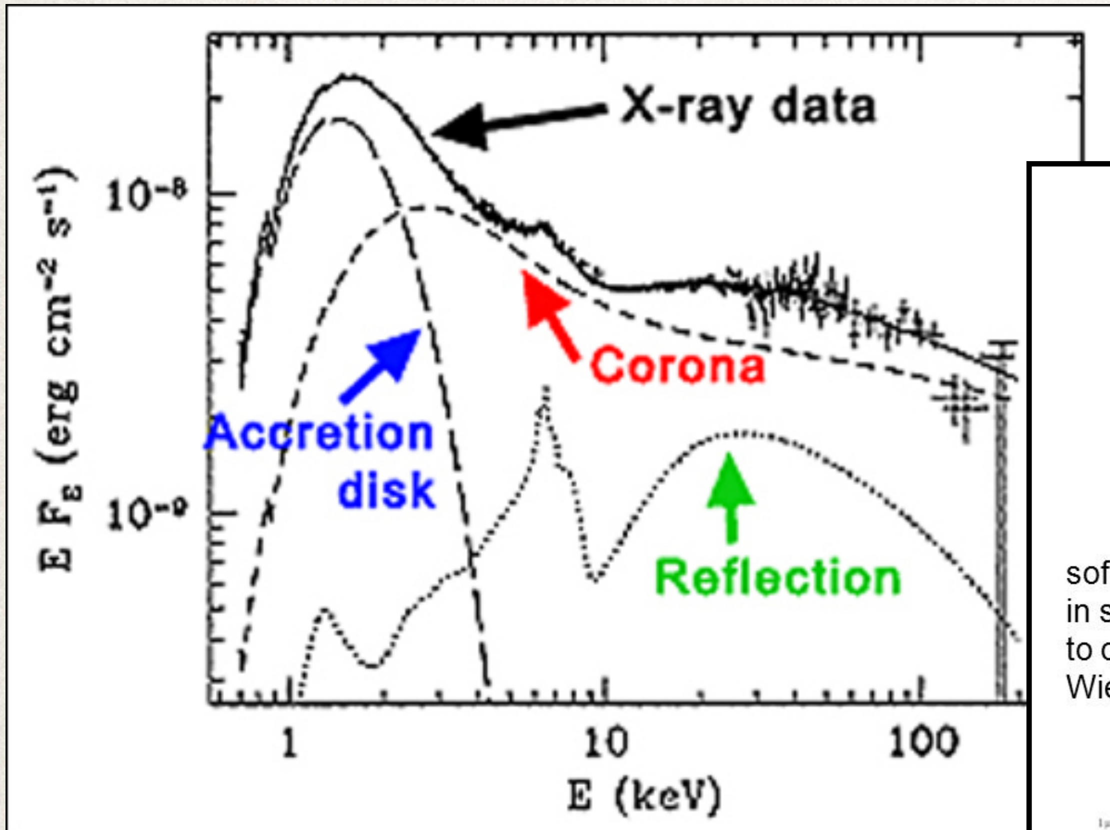

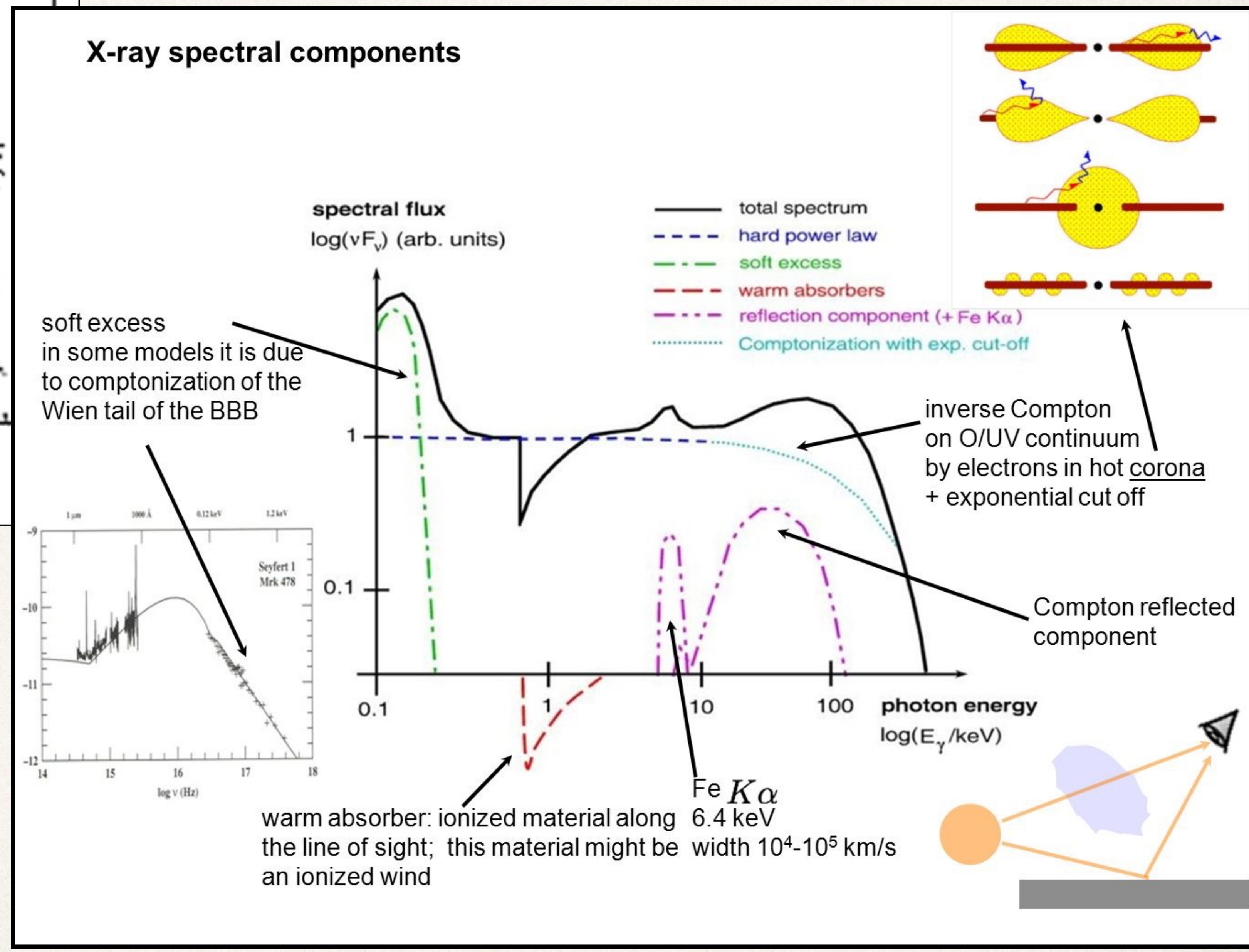

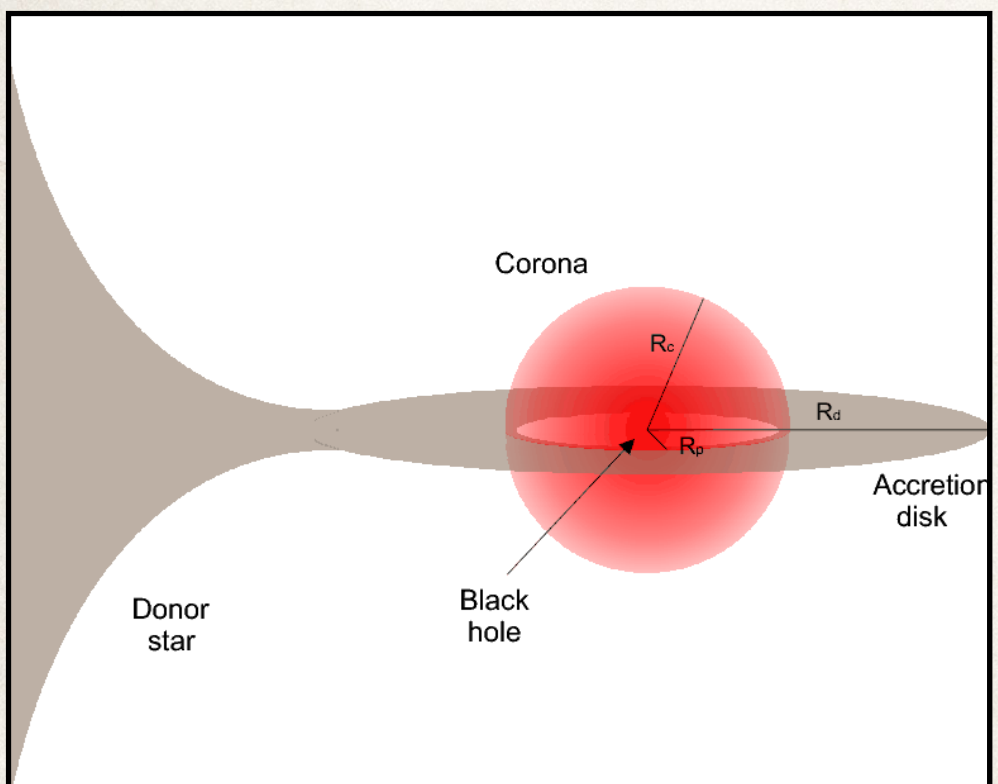

Eddington limits

The Eddington luminosity, also referred to as the Eddington limit, is the maximum luminosity that can be achieved when there is balance between the force of radiation acting outward and the gravitational force acting inward. The state of balance is called hydrostatic equilibrium.

$$L_{\mathrm{Edd}} = \frac{4\pi G M m_{\mathrm{p}} c}{\sigma_{\mathrm{T}}}$$
$$\cong 1.26 \times 10^{31} \left(\frac{M}{M_\odot}\right) \mathrm{W} = 1.26 \times 10^{38} \left(\frac{M}{M_\odot}\right) \mathrm{erg/s} = 3.2 \times 10^{4} \left(\frac{M}{M_\odot}\right) L_\odot$$

$$\dot{M}_{\mathrm{Edd}} = \frac{L_{\mathrm{Edd}}}{c^2} \approx 0.2 \times 10^{-8} \left(\frac{M}{M_\odot}\right)\ M_\odot\ \mathrm{yr}^{-1}.$$

$$T_{\mathrm{Edd}} = \left(\frac{L_{\mathrm{Edd}}}{4\pi\sigma_{\mathrm{SB}} R_{\mathrm{Schw}}^2}\right) \approx 6.6 \times 10^{7} \left(\frac{M}{M_\odot}\right)^{-1/4}\ \mathrm{K}.$$

ADAF

The assumption that all the heat generated by viscosity is radiated away does not hold for all accretion rates. Under some conditions the radial velocity of the accretion flow becomes large and the heat cannot be transformed into radiation and emitted fast enough. A significant fraction of the heat is stored as kinetic energy in the flow and advected onto the accretor. At the same time the disk "inflates", so that the thin disk assumption breaks down. This regime is known as "Advected Dominated Accretion Flow" (ADAF).

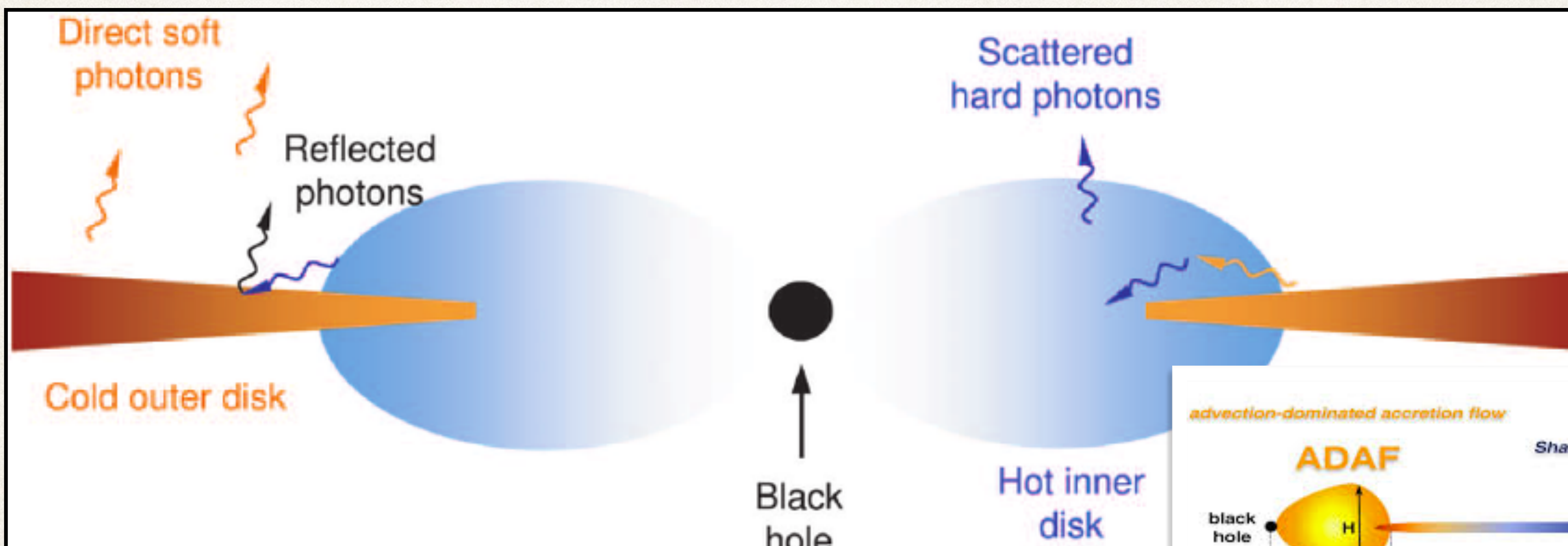

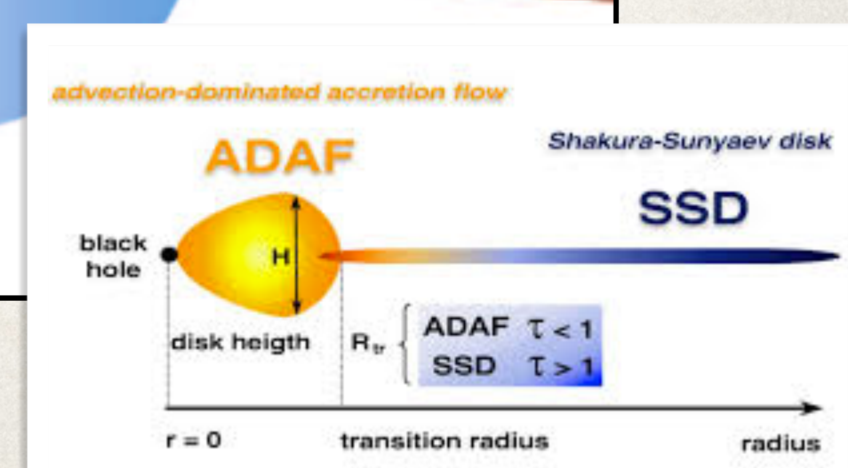

ADAF

There are two types of advection-dominated accretion flows. Optically thick ADAFs develop at very high accretion rates, typically larger than the Eddington value.

Optically thin ADAFs occur in the opposite limit of sufficiently low accretion rates. These models are similar to the disk + corona models.

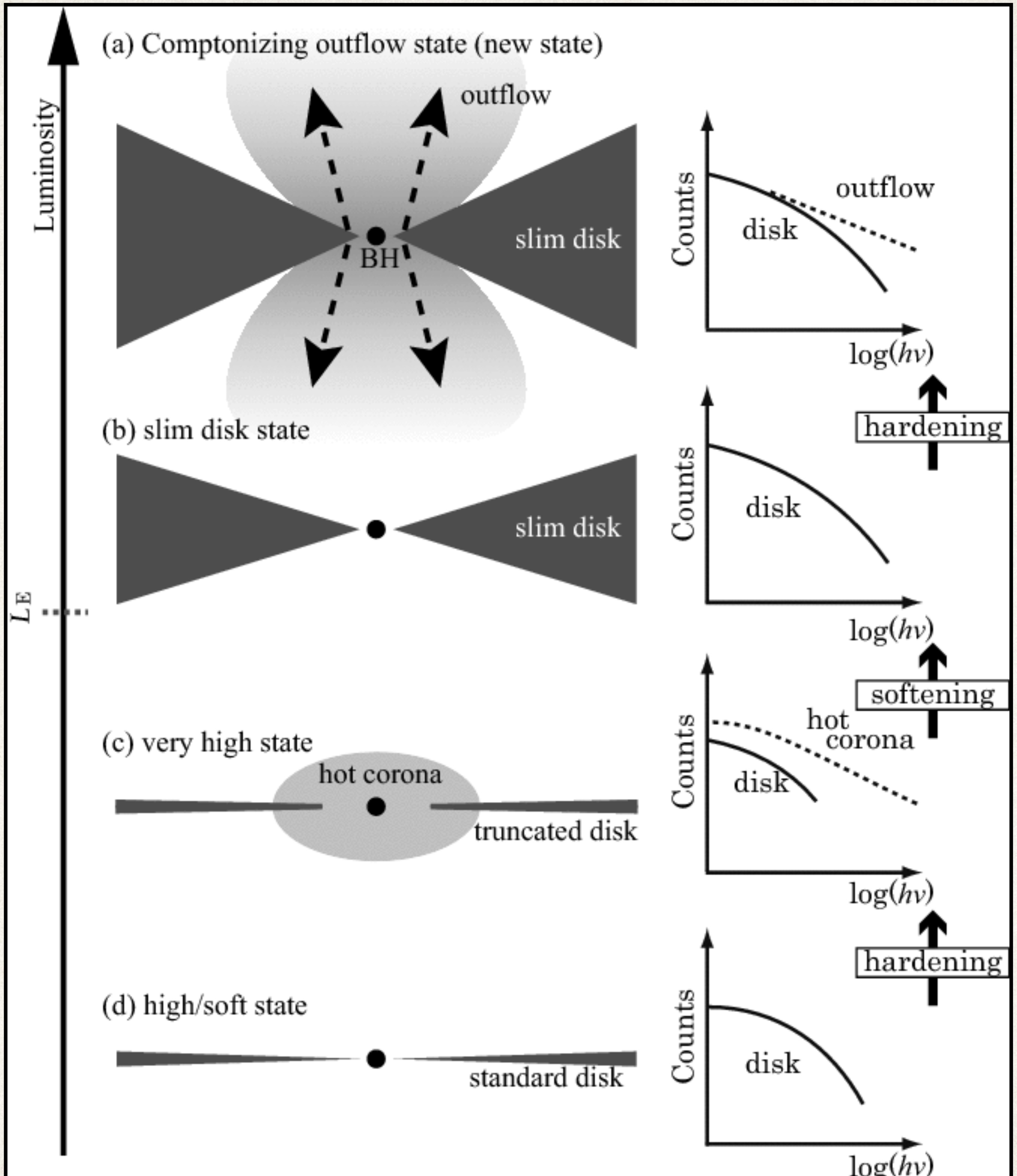

The super-Eddington wind is driven by radiation pressure.

Main ADAF assumptions:

- The total pressure is considered as the sum of the pressure of a two-temperature gas and the magnetic pressure.
- The heat generated by viscosity is preferably transferred to ions. Hence, $T_i >> T_e$
- Electrons cool completely.

$$q_e^- = q_{\rm Br}^- + q_{\rm synchr}^- + q_{\rm IC}^-.$$

$$q_{\rm IC}^- = q_{\rm IC,Br}^- + q_{\rm IC,\ synchr}^- + q_{\rm IC,ext}^-.$$

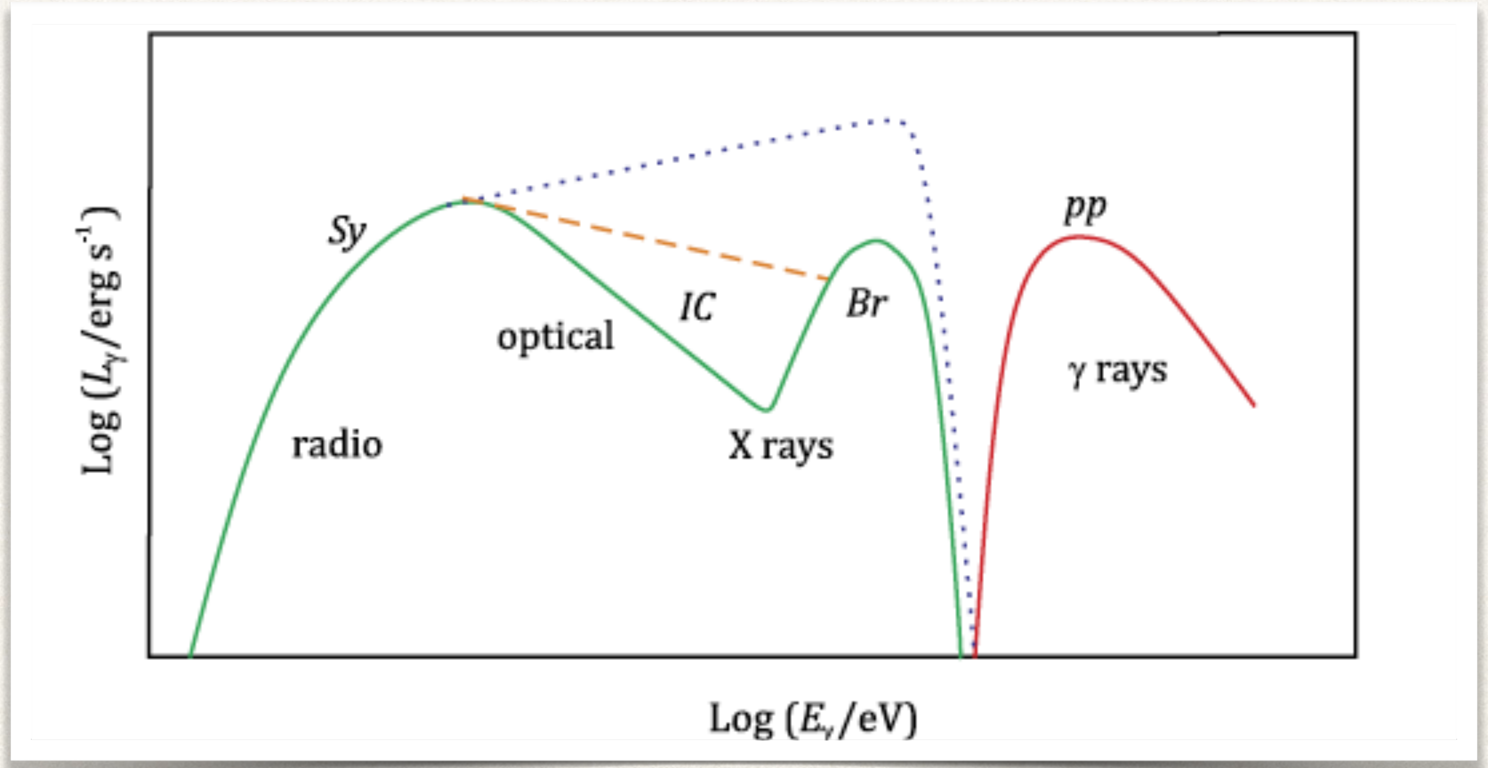

The spectrum of AGNs extends along the whole e.m. range: there is non-thermal emission

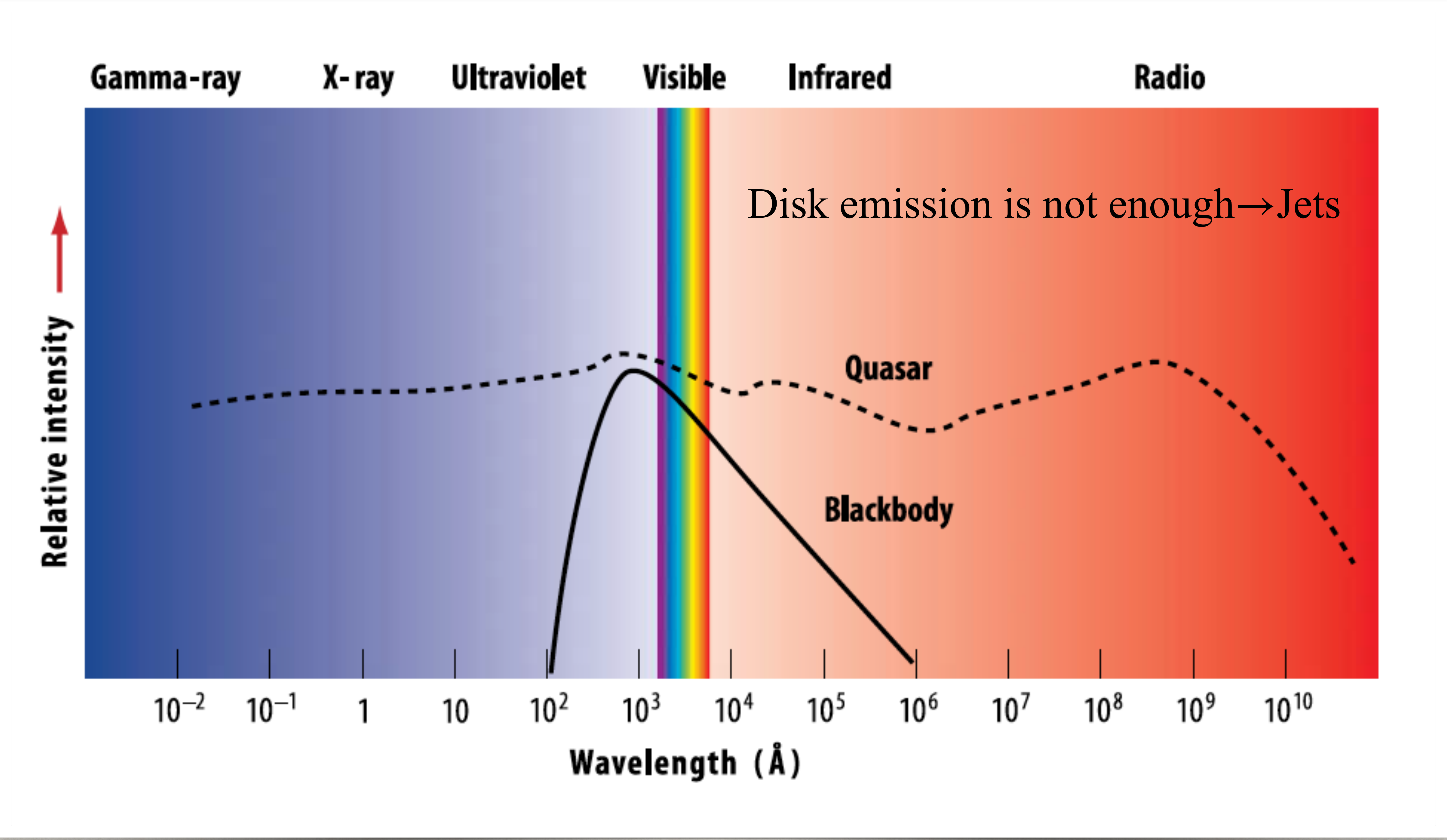

Basic equations that rule the outflow (ideal MHD)

$$
\begin{aligned}
\vec{\nabla} \cdot \vec{B} &= 0 \\
\vec{\nabla} \times \vec{E} + \frac{1}{c}\frac{\partial B}{\partial t} &= 0 \\
\vec{\nabla} \cdot \vec{E} &= 4\pi\rho \\
\vec{\nabla} \times \vec{B} - \frac{1}{c}\frac{\partial E}{\partial t} &= \frac{4\pi}{c}\vec{J}.
\end{aligned}
$$

$$\nabla \times \vec{B} = \frac{4\pi}{c}\vec{J},$$

$$\nabla \cdot \vec{B} = 0,$$

$$\nabla \times \vec{E} = 0,$$

$$\nabla \cdot \vec{E} = 4\pi\rho_{\rm e},$$

Maxwell

(steady state and conductivity of the plasma is very large).

$$\vec{E} + \frac{1}{c}\vec{v} \times \vec{B} = 0,$$ Ohm

$$\nabla \times \left(\vec{v} \times \vec{B}\right) = 0,$$ Induction

$$\nabla \cdot (\rho\vec{v}) = 0,$$ Continuity

$$\rho\,(\vec{v} \cdot \nabla)\,\vec{v} = -\nabla P - \rho\nabla\Phi + \frac{1}{4\pi}\left(\nabla \times \vec{B}\right) \times \vec{B}.$$ Euler

$$\vec{B} = \vec{B}_{\rm p} + B_\phi\hat{\phi}.$$

$$\vec{B}_{\rm p} \equiv B_r\hat{r} + B_z\hat{z}$$

$$B_r = -\frac{1}{r}\frac{\partial\Psi}{\partial z} \qquad B_z = \frac{1}{r}\frac{\partial\Psi}{\partial r}.$$

The poloidal component is given by the ***flux function***

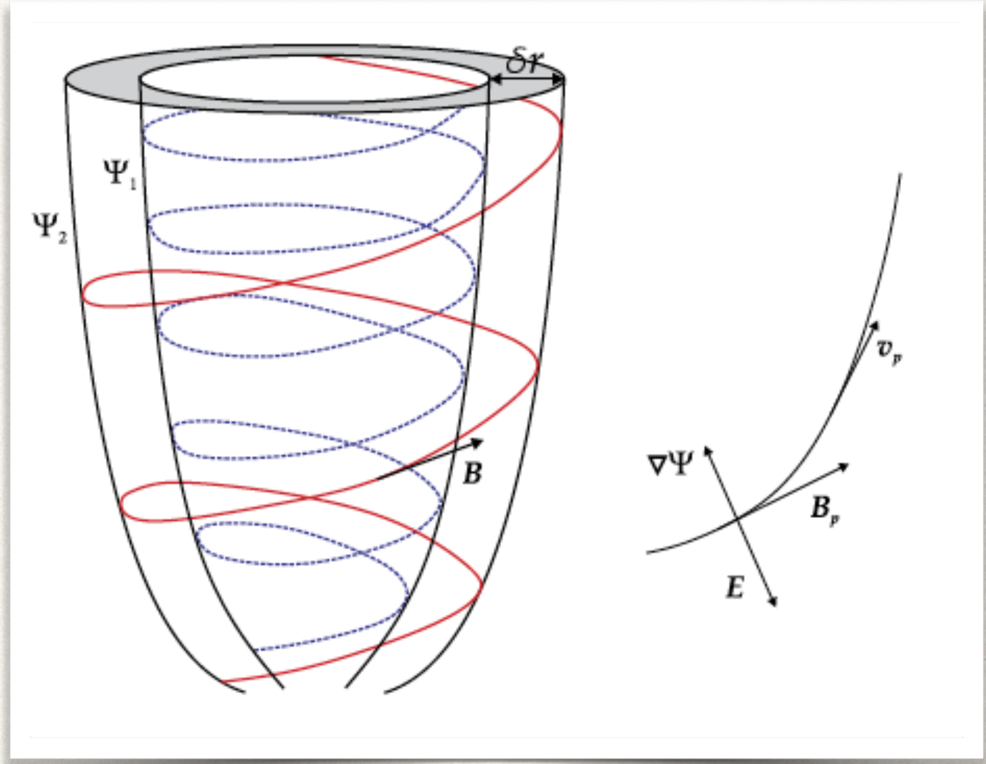

Ingredients for jet formation: compact object, accretion of matter, magnetic fields, rotation

The power of the jet is directly related to the accretion power

$$P_{\rm jet} = q\dot{M}c^2 \qquad \text{(jet-disk symbiosis)}$$

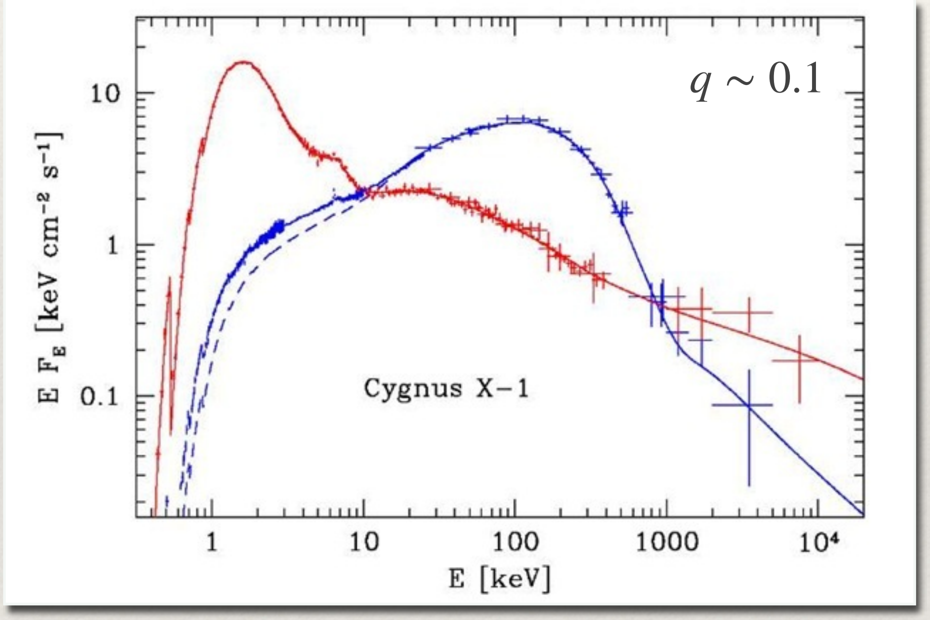

But in the case of many AGNs and GRBs we found

$$q > 1$$

This means that energy is extracted from the rotating black hole. The origin of the outflow is associated with the accretion of large-scale magnetic fields.

The origin of jets is related to the central compact object

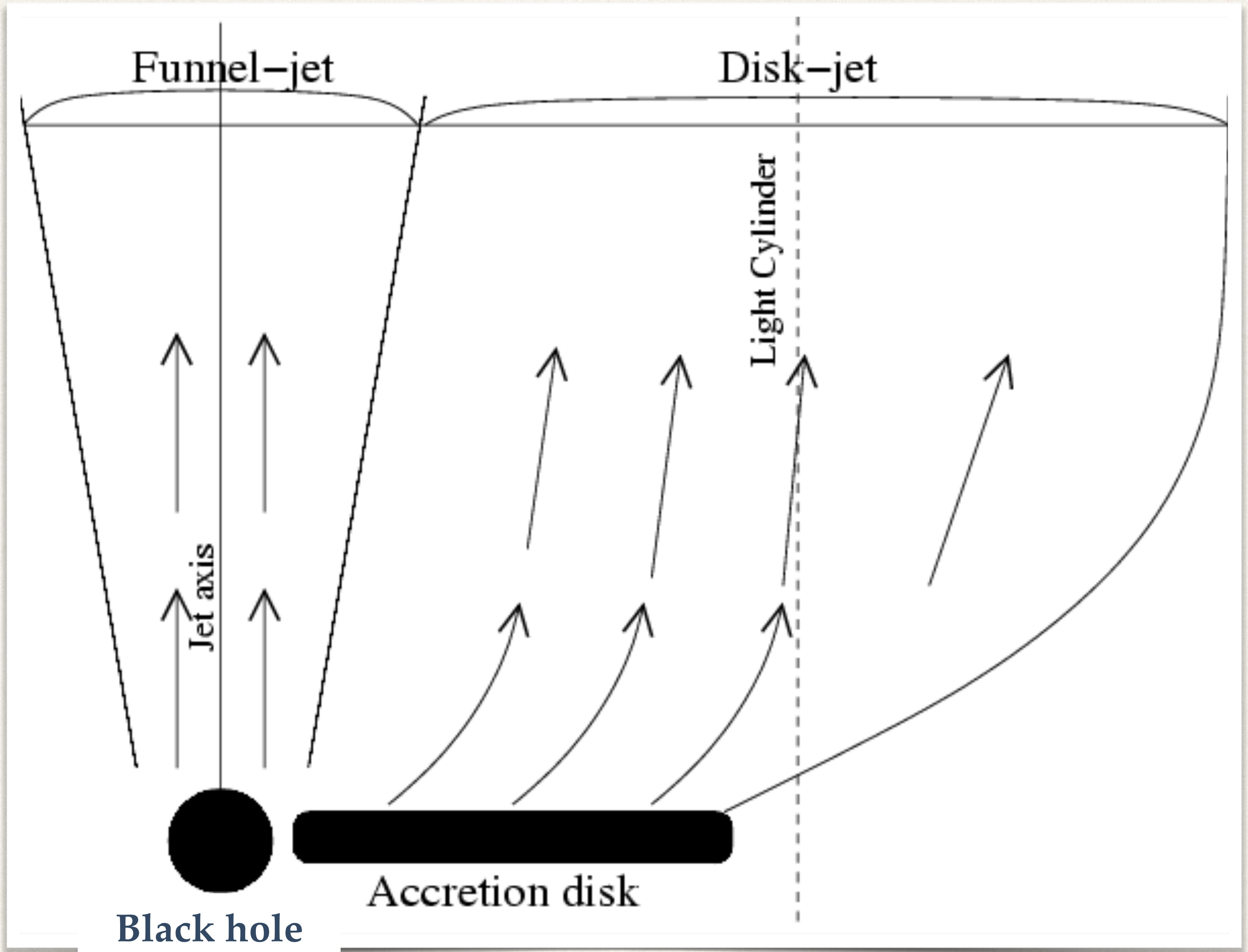

<u>Both the black hole itself and the accretion disk can launch outflows</u>

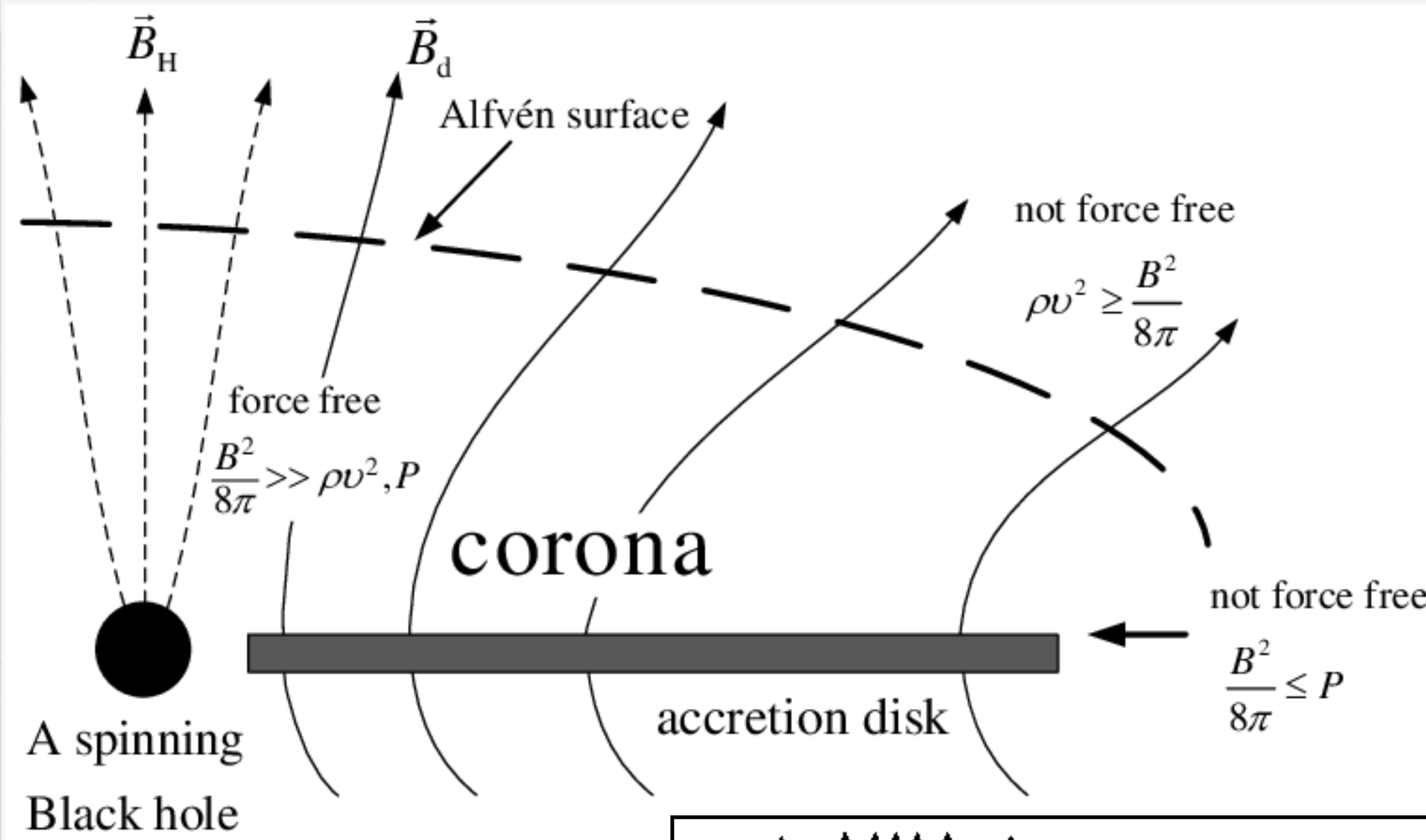

$\vec{B}_H$
$\vec{B}_d$
Alfvén surface
not force free
$\rho\upsilon^2 \geq \frac{B^2}{8\pi}$
force free
$\frac{B^2}{8\pi} >> \rho\upsilon^2, P$
corona
not force free
$\frac{B^2}{8\pi} \leq P$
accretion disk
A spinning
Black hole

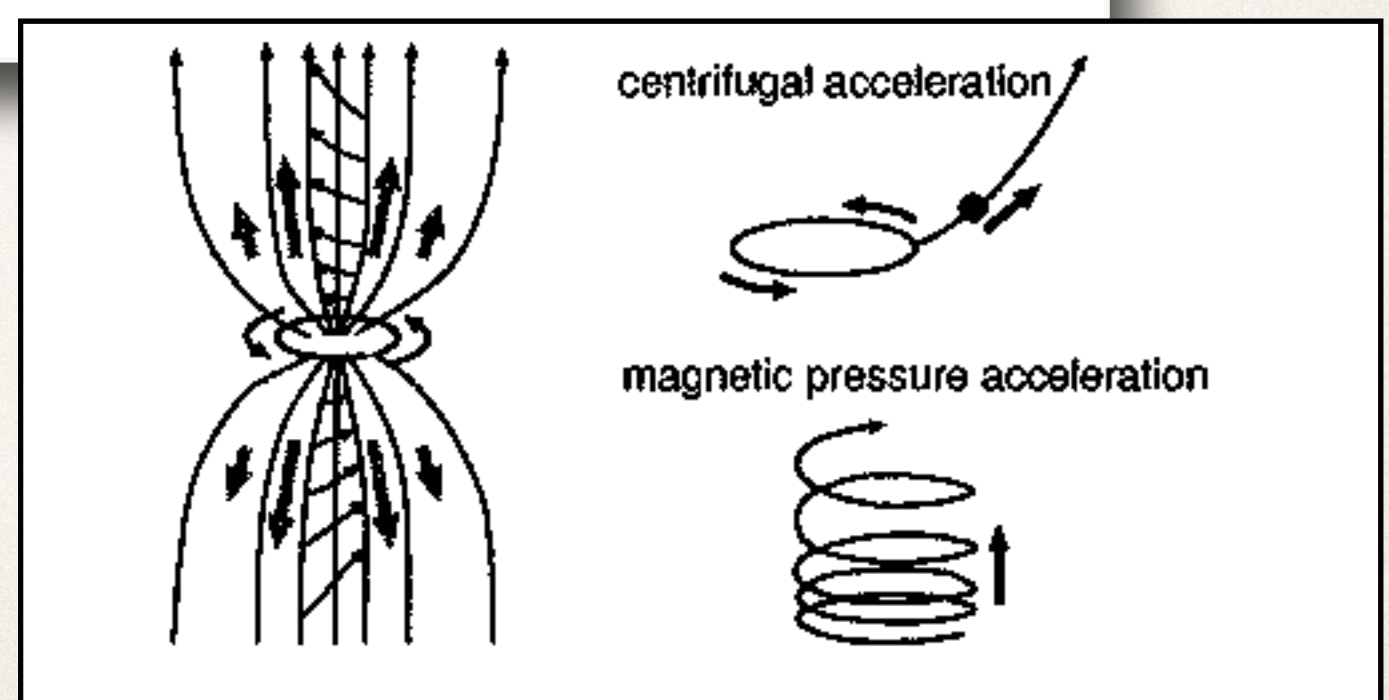

centrifugal acceleration
magnetic pressure acceleration

Accretion-disk driven jets

$$\Phi_{\rm off} = -\frac{GM_{\rm BH}}{\sqrt{r^2+z^2}} - \frac{1}{2}\Omega_{\rm m}^2 r^2.$$

$$\Phi_{\rm off} = -GM_{\rm BH}\left[\frac{r_0}{\sqrt{r^2+z^2}} + \frac{1}{2}\left(\frac{r}{r_0}\right)^2\right].$$

$$\frac{\partial^2\Phi_{\rm off}}{\partial s^2}(r_0,0) = -\frac{GM_{\rm BH}}{r_0^3}\left(3\sin\theta^2 - \cos\theta^2\right) < 0.$$

$$\theta > 30^\circ$$

$$\Omega_{\rm K}(R) = \left(\frac{GM}{R^3}\right)^{1/2}.$$

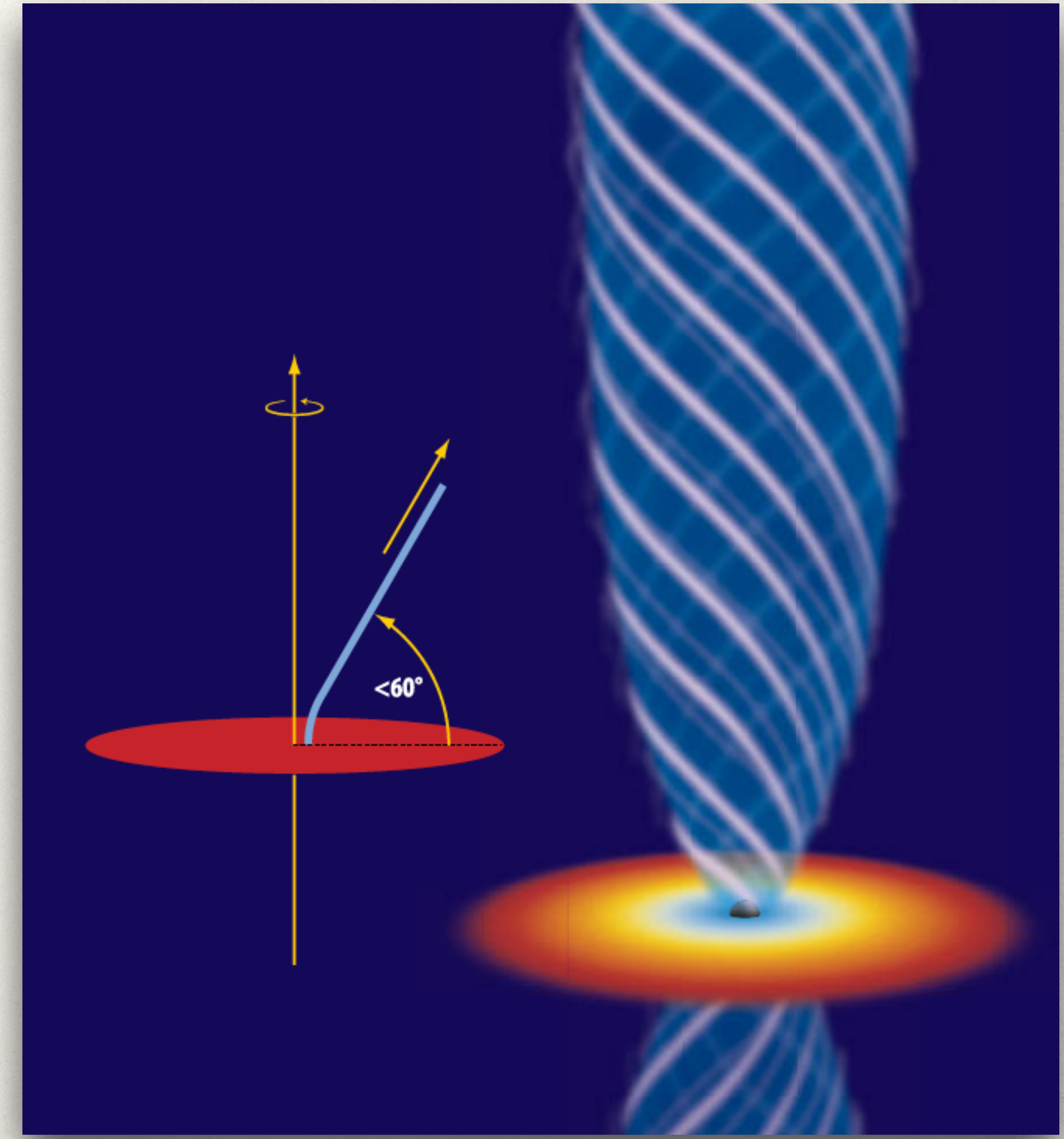

Jets in Young Stellar Objects

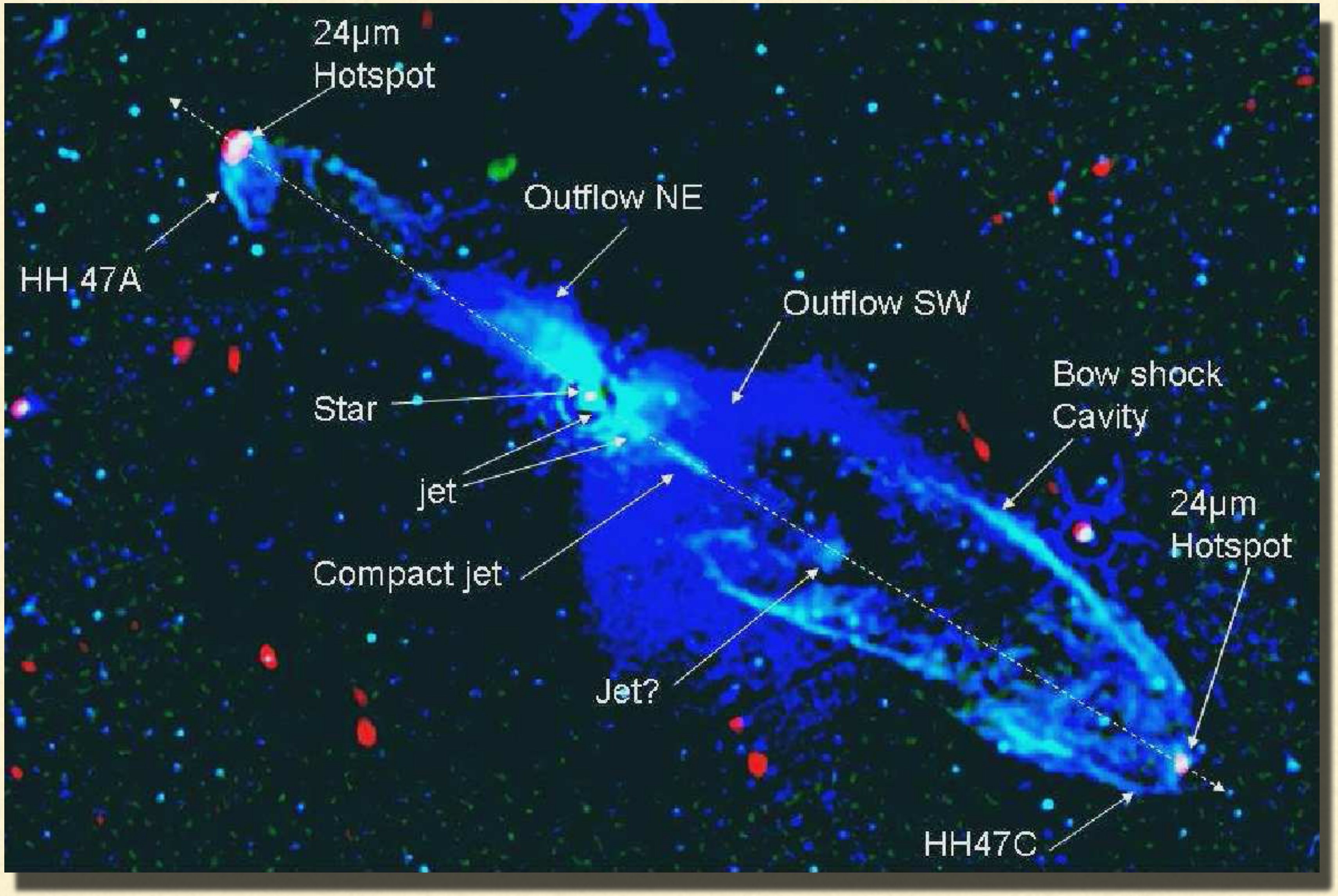

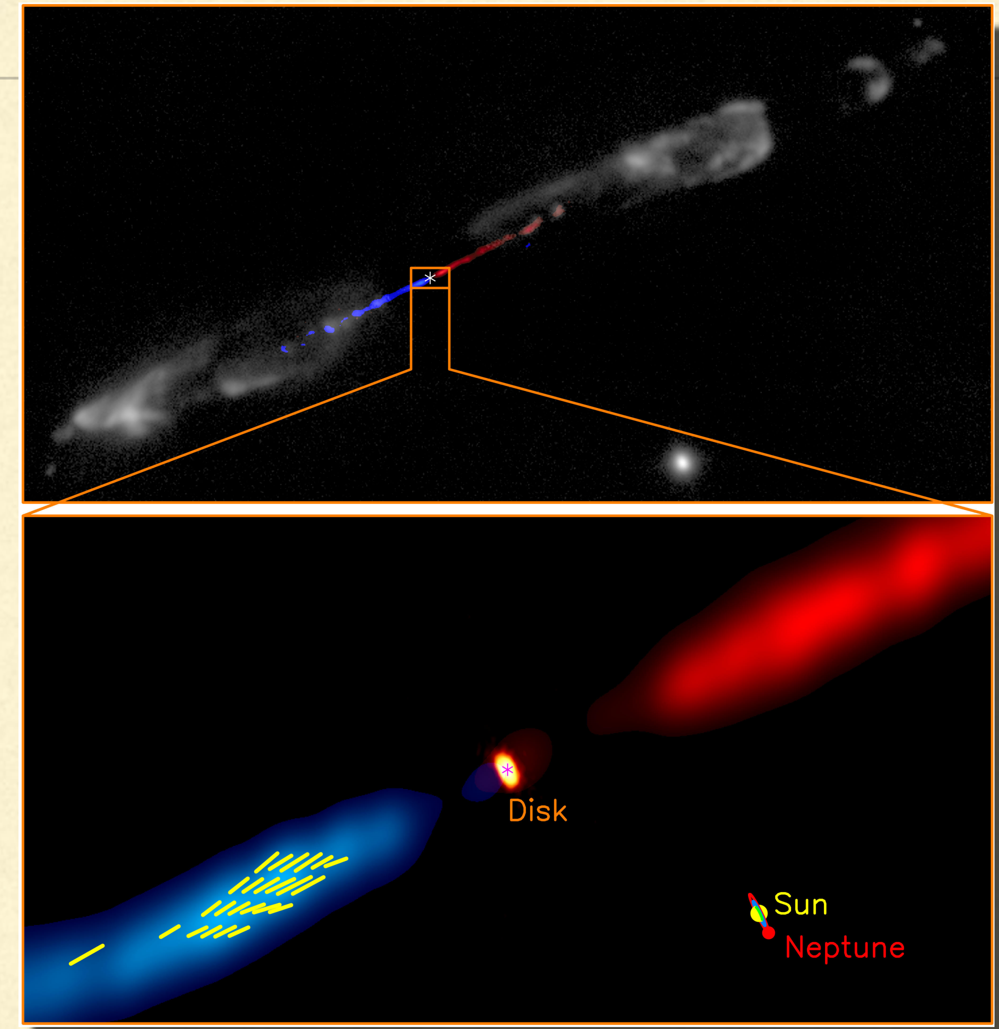
Disk
Sun
Neptune

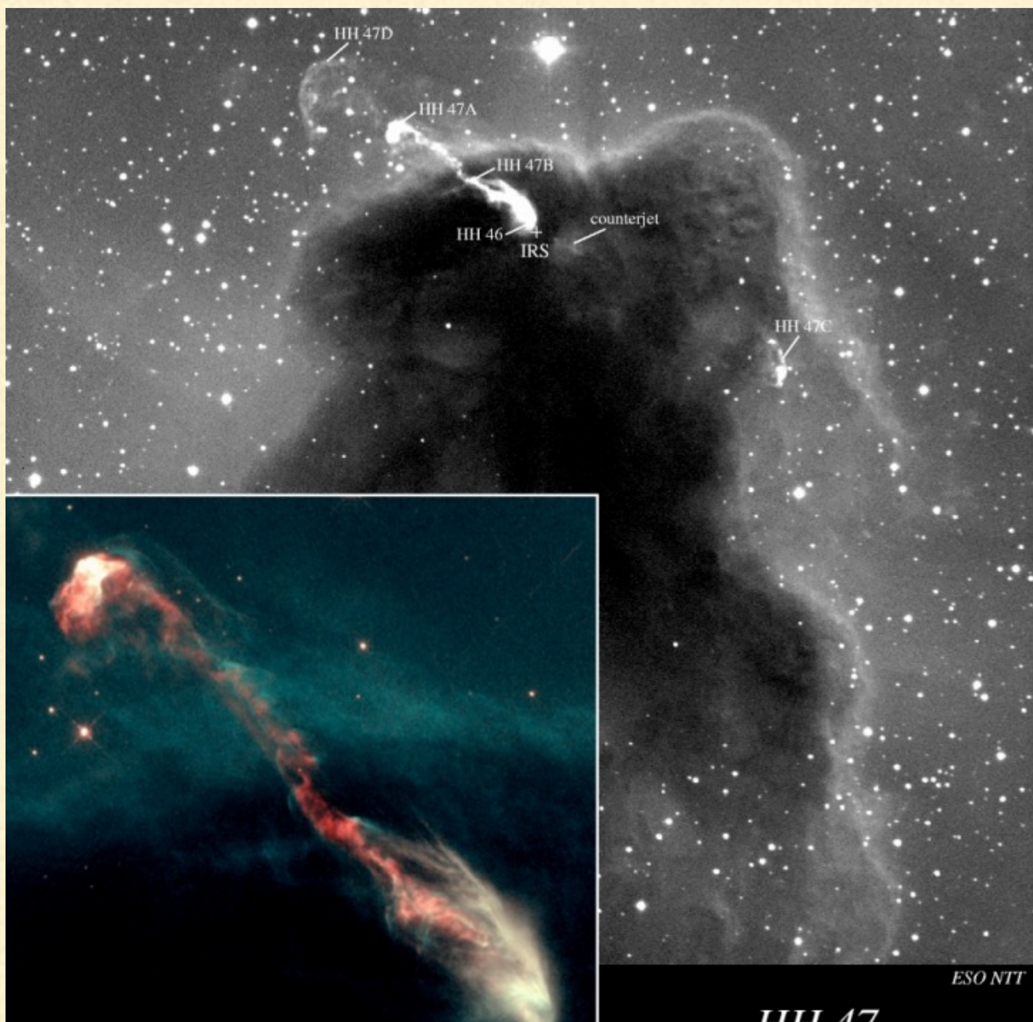
HH 47D
HH 47A
HH 47B
HH 46
IRS
counterjet
HH 47C
ESO NTT
HH 47

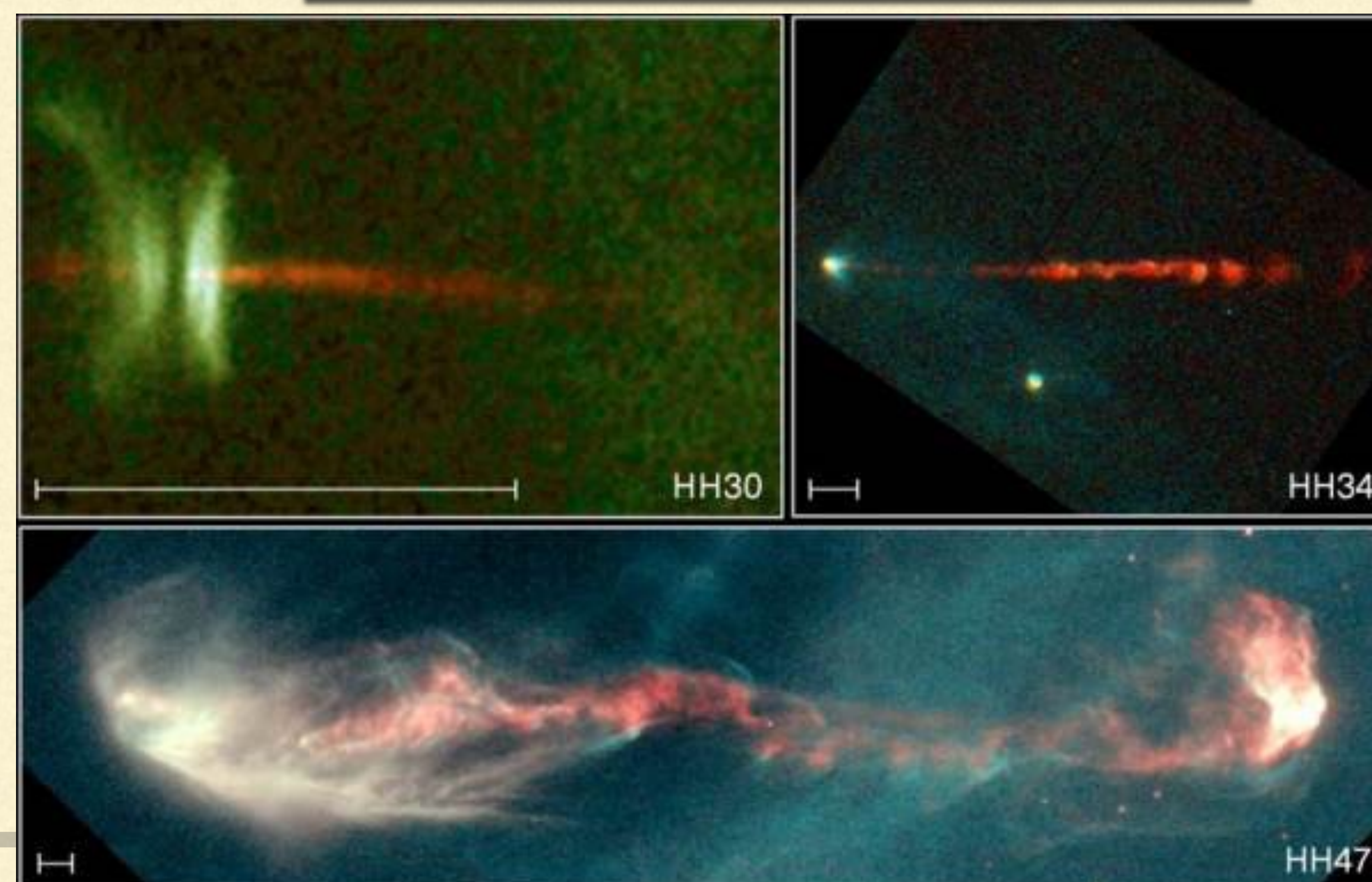
HH30
HH34
HH47

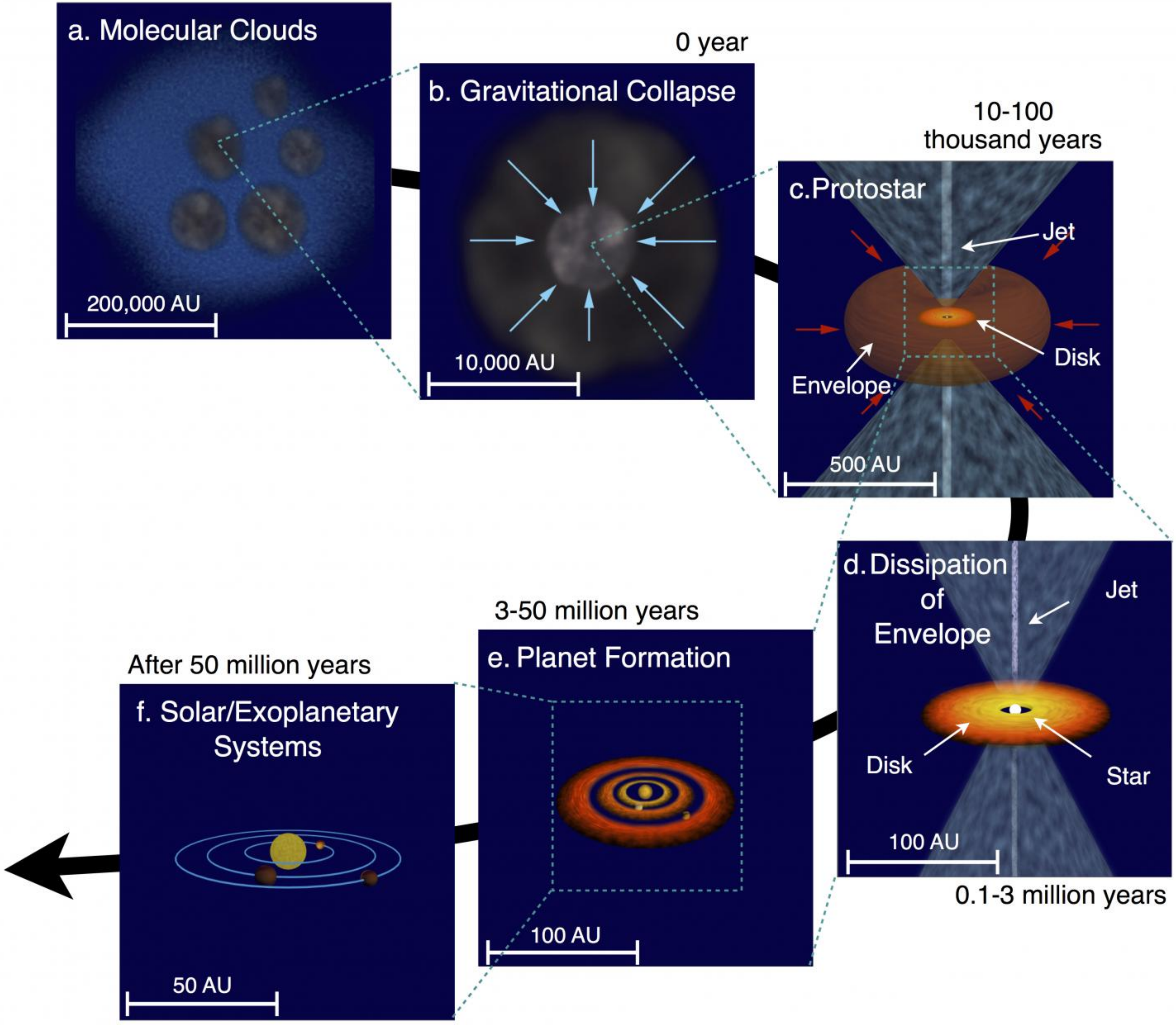
a. Molecular Clouds
200,000 AU
0 year
b. Gravitational Collapse
10,000 AU
10-100
thousand years
c.Protostar
Jet
Disk
Envelope
500 AU
d. Dissipation
of
Envelope
Jet
Disk
Star
100 AU
0.1-3 million years
3-50 million years
e. Planet Formation
100 AU
After 50 million years
f. Solar/Exoplanetary
Systems
50 AU

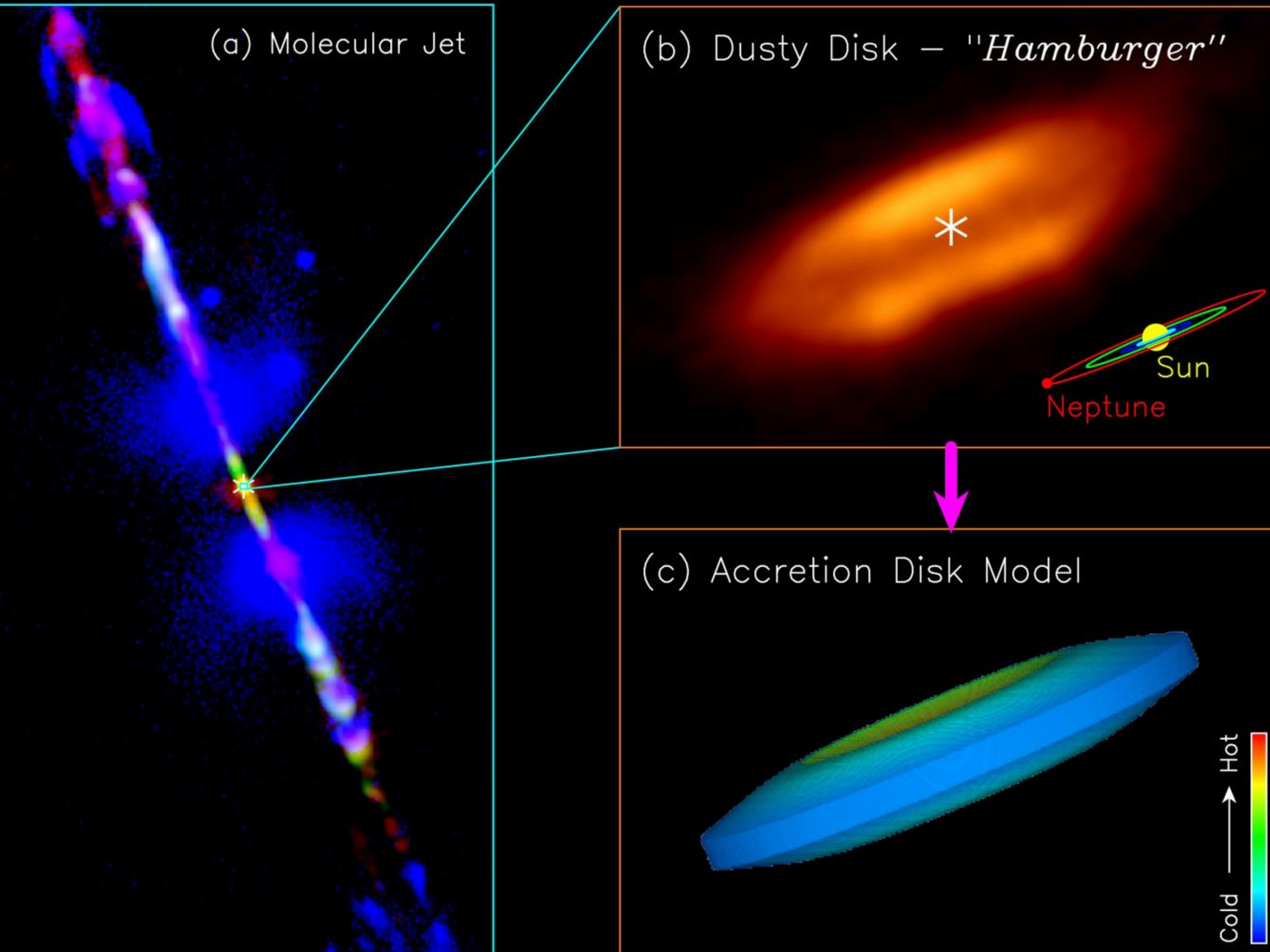
(a) Molecular Jet
(b) Dusty Disk – "Hamburger"
Sun
Neptune
(c) Accretion Disk Model
Cold
Hot

Termination of the jet

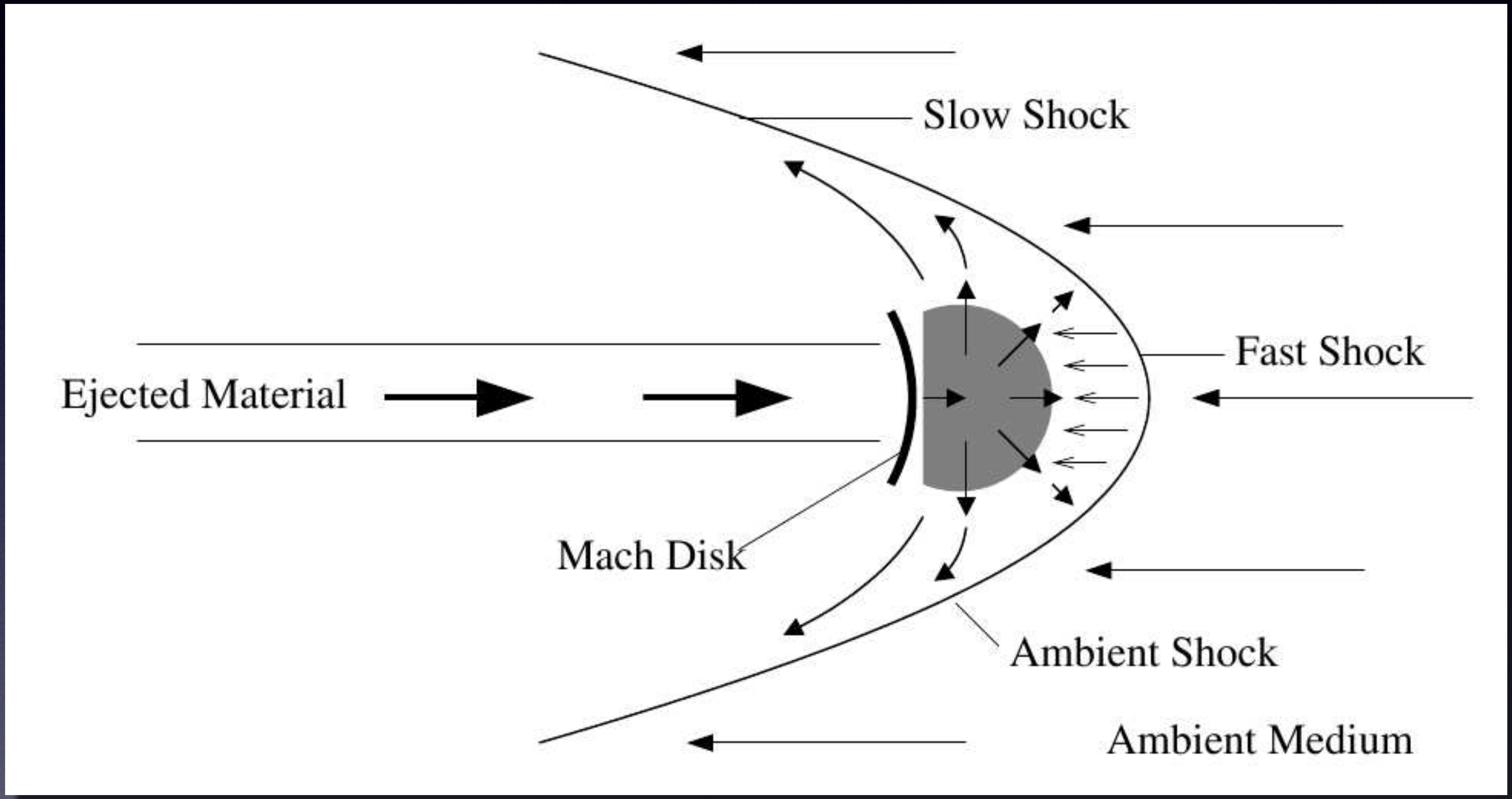

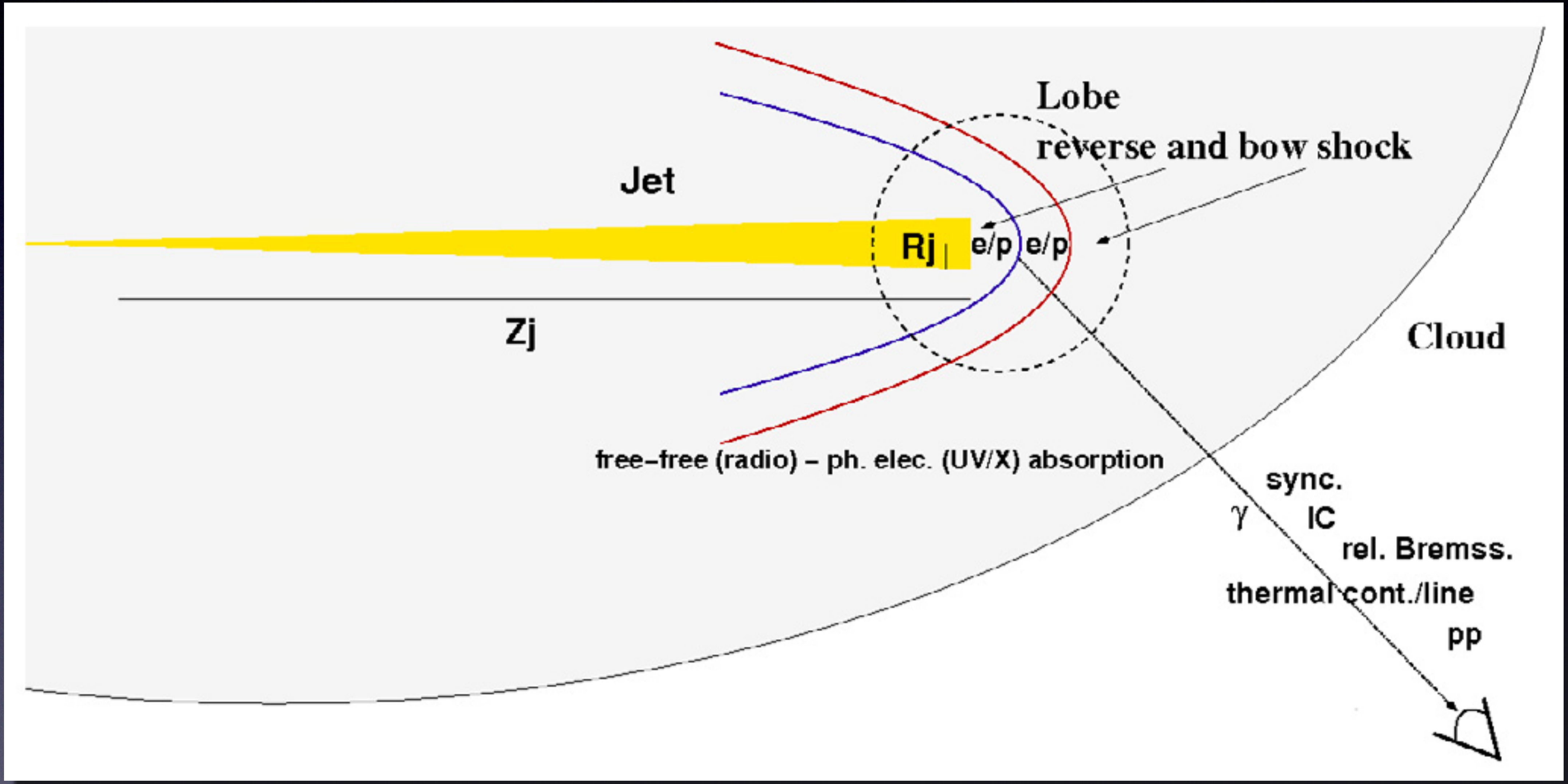

Bosch-Ramon, Romero, Araudo 2010, A&A

HH 80 and IRAS 16547-4247

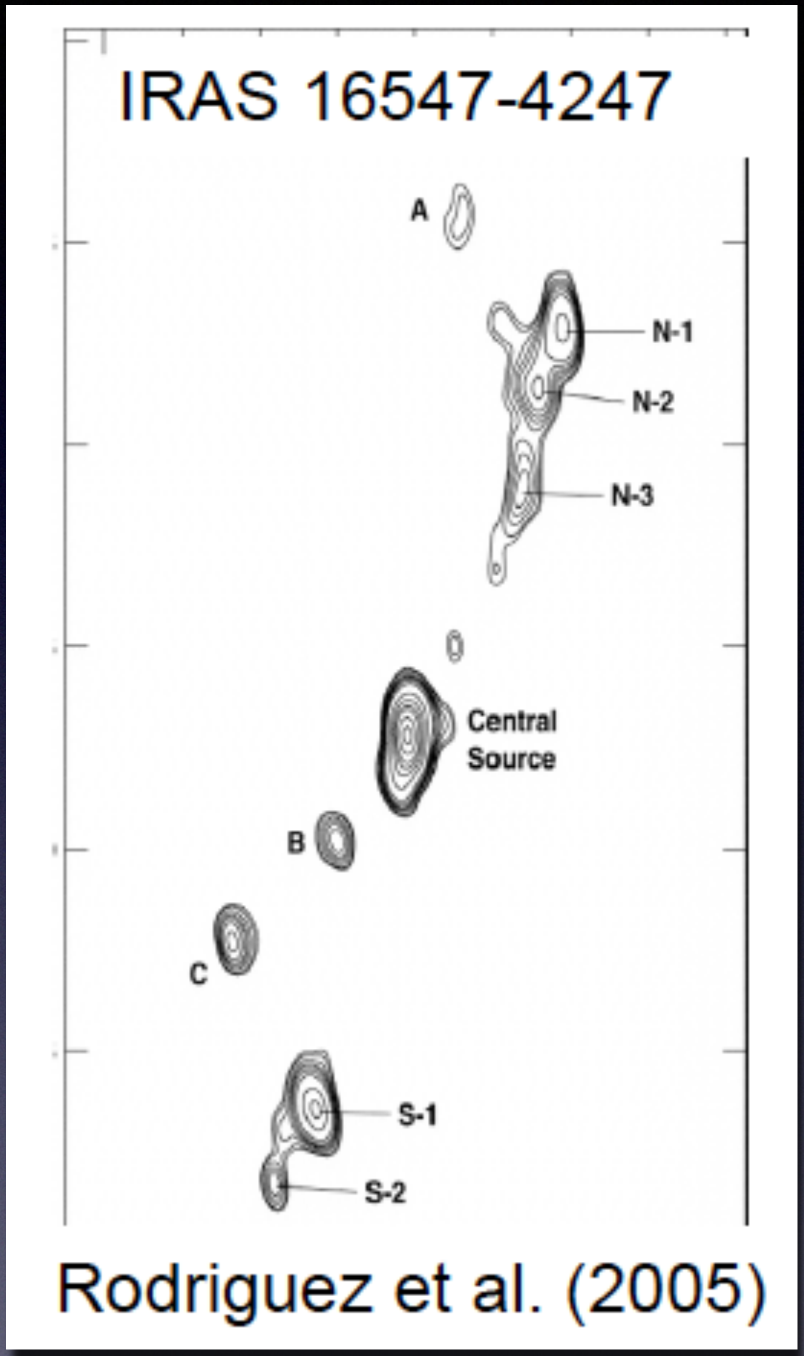

Martí et al. 1993, 1995

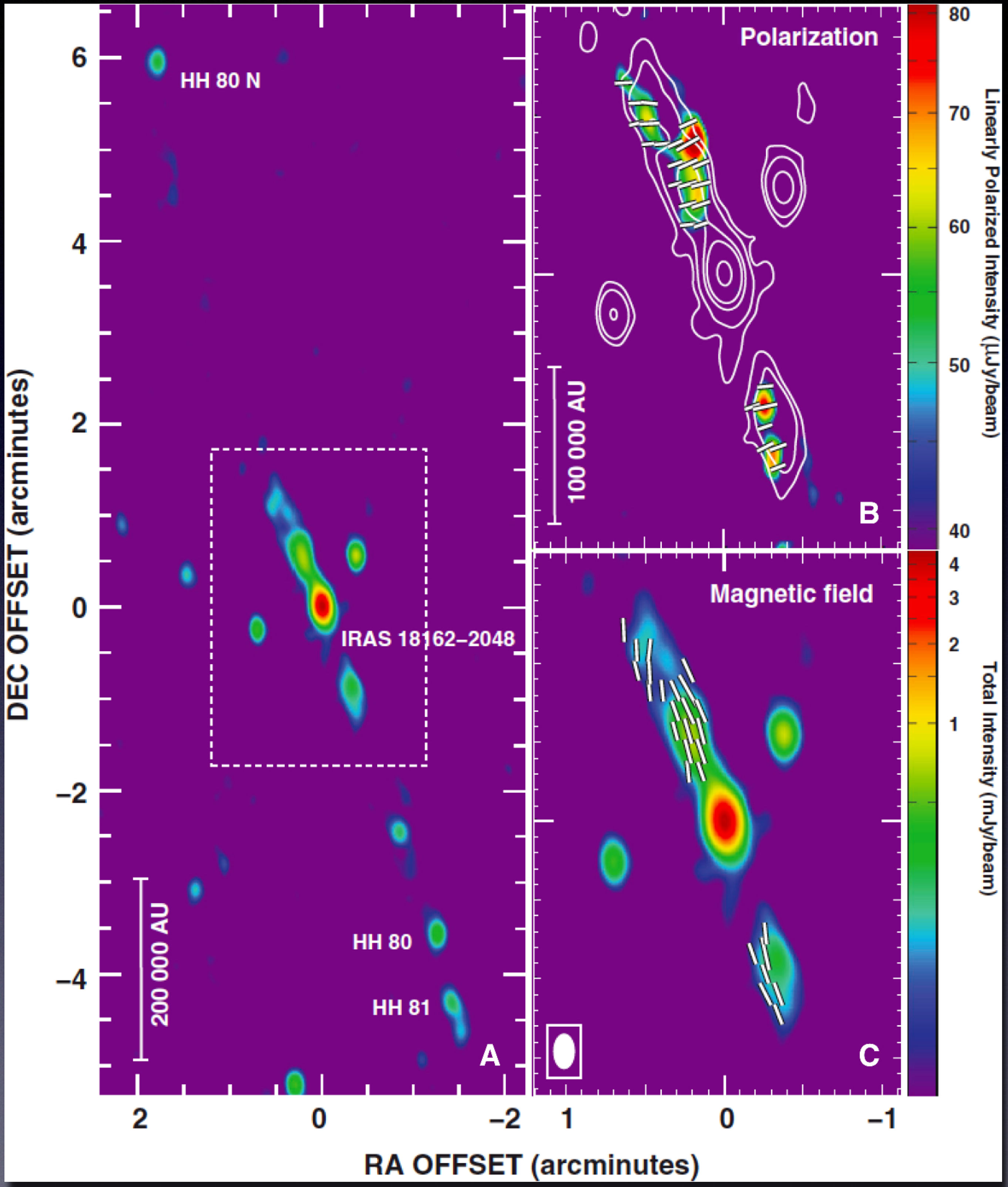

C. Carrasco-González et al.

	IRAS-N	HH 80
$n_{\rm c}$ [cm^{-3}]	5×10^{5}	4×10^{2}
d [kpc]	2.9	1.7
L_{*} [erg s^{-1}]	5×10^{38}	8×10^{37}
u [erg cm^{-3}]	2×10^{-9}	2×10^{-12}
$Z_{\rm j}$ [cm]	5×10^{17}	10^{19}
$n_{\rm j}$ [cm^{-3}]	5×10^{5}	4×10^{2}
$R_{\rm j}$ [cm]	1.6×10^{16}	5×10^{16}
$v_{\rm j}$ [cm s^{-1}]	5×10^{7}	10^{8}
$v_{\rm bs}$ [cm s^{-1}]	5×10^{6}	5×10^{7}
$v_{\rm r}$ [cm s^{-1}]	5×10^{7}	5×10^{7}
$t_{\rm life}$ [s]	10^{11}	3×10^{11}
$n_{\rm j}$ [cm^{-3}]	5×10^{3}	4×10^{2}
χ	0.01	1
$L_{\rm j}$ [erg s^{-1}]	5×10^{35}	2×10^{36}

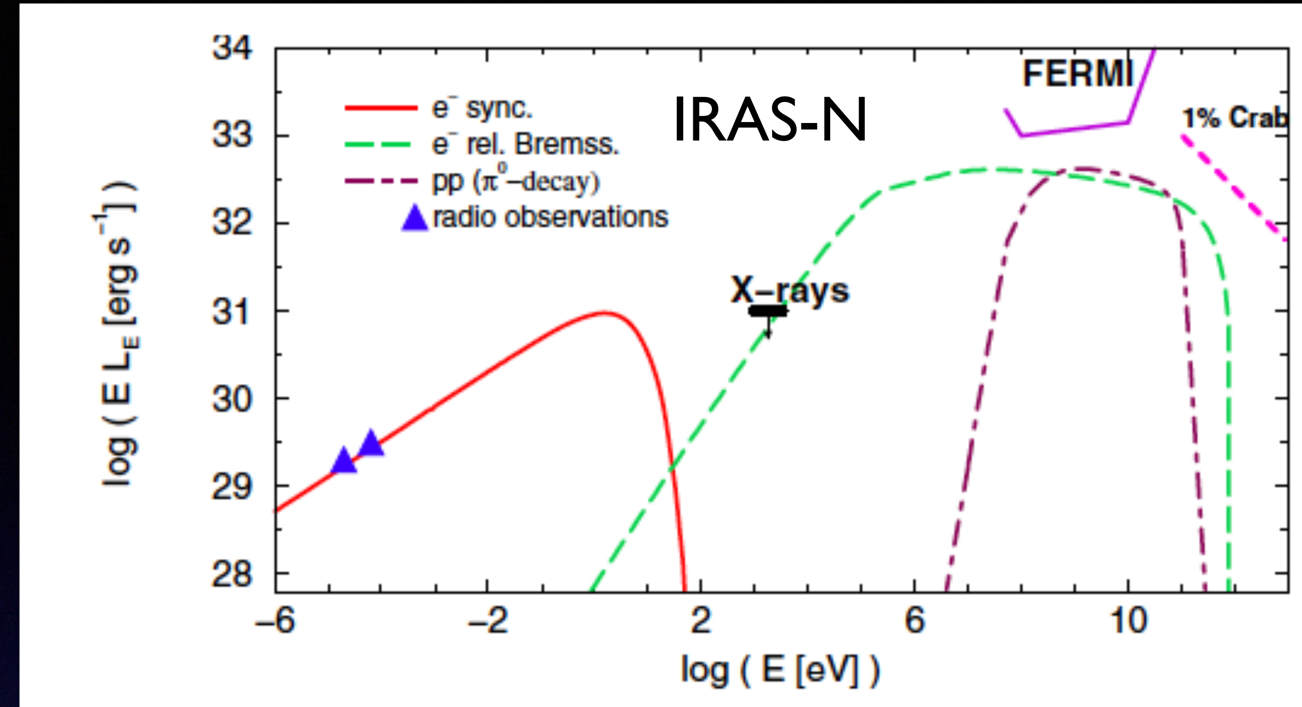

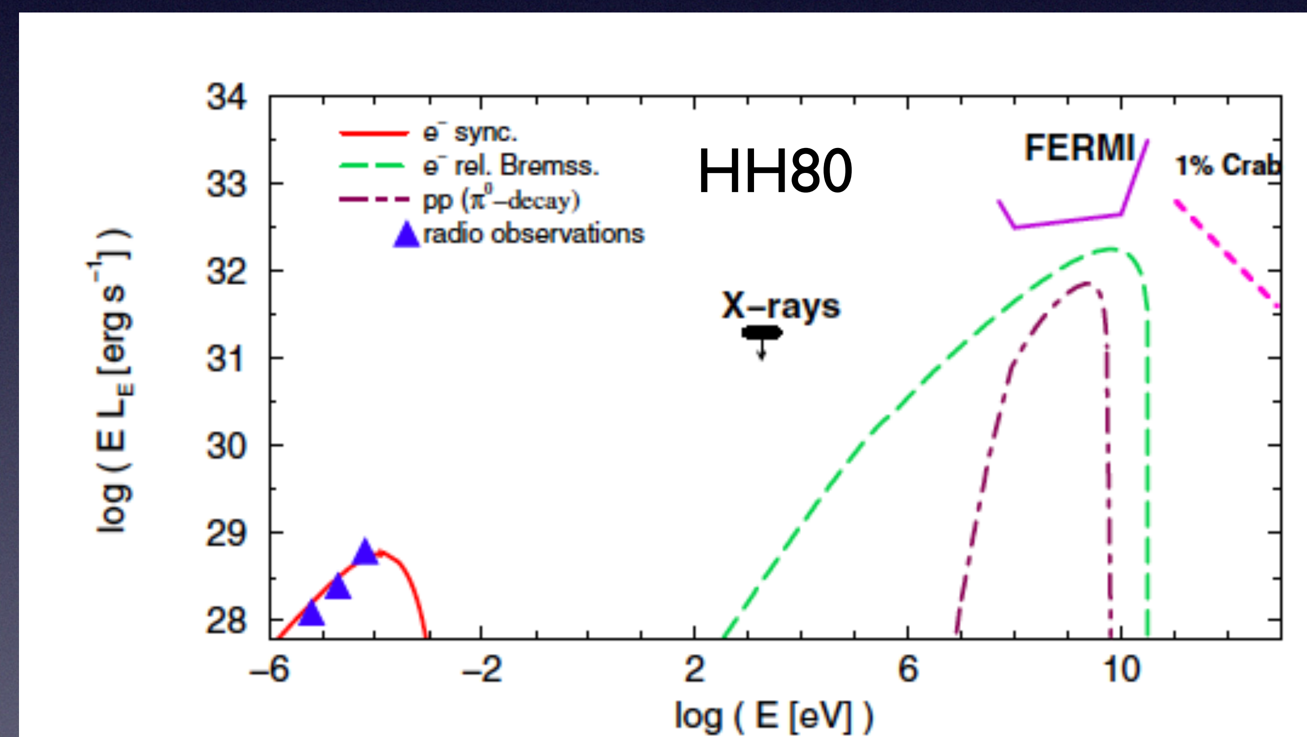

$$E_\gamma L_{E_\gamma} = E_\gamma^2 \int q_\gamma(E_\gamma, E_{e,p}) N_{e,p}(E_{e,p}) dE_{e,p},$$

Bosch-Ramon, Romero, Araudo 2010, A&A

Magnetic model of jets

- Powerful and relativistic jets are produced by rapidly rotating BHs with magnetized accretion disks.
- Power source - the rotational energy.
- The energy is extracted via magnetic torque as Poynting flux.
- Jet collimation is due to external medium.
- Jet acceleration is via conversion of electromagnetic energy into bulk kinetic energy.
- Jet emission is via energy dissipation at shocks (kinetic energy) and/or reconnection sites (magnetic energy).

What is the origin of the particles?

Rotation + poloidal field —> outflow

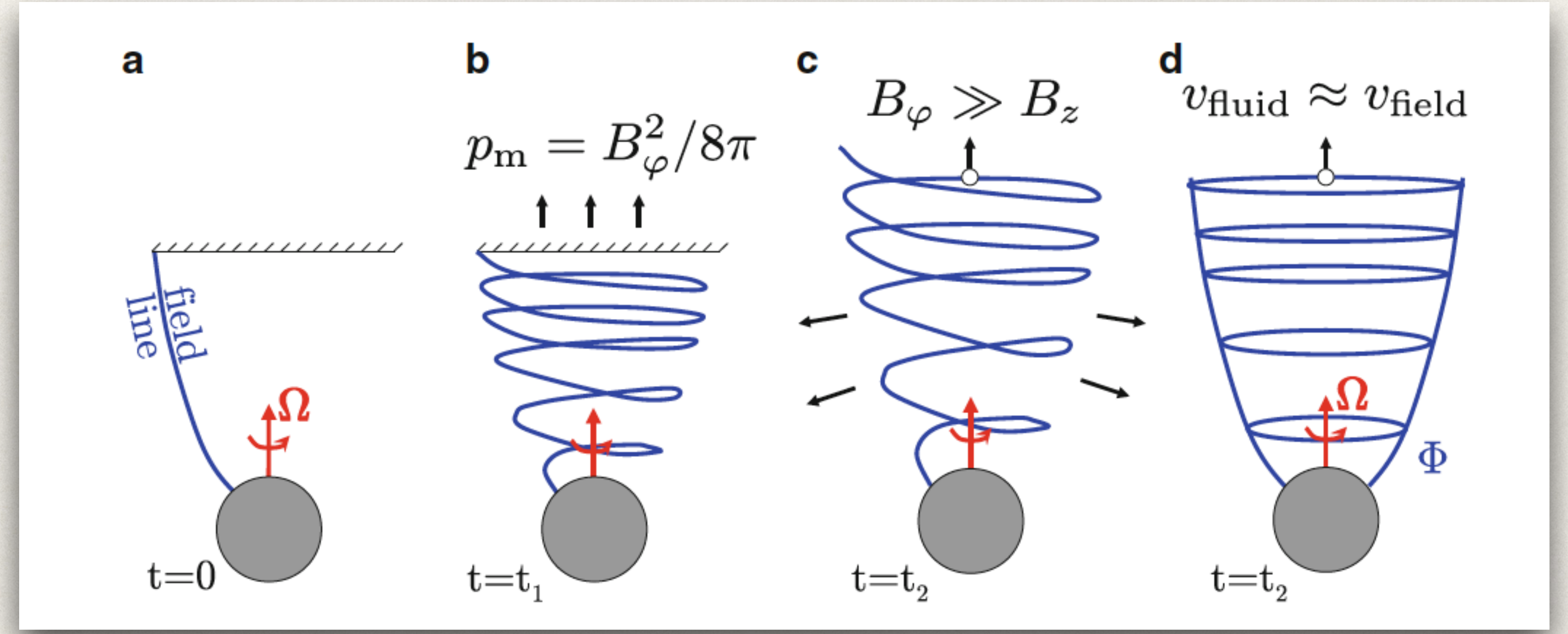

A. Tchekhovskoy

Initial collimation of relativistic jets requires a “nozzle”, external confining medium.

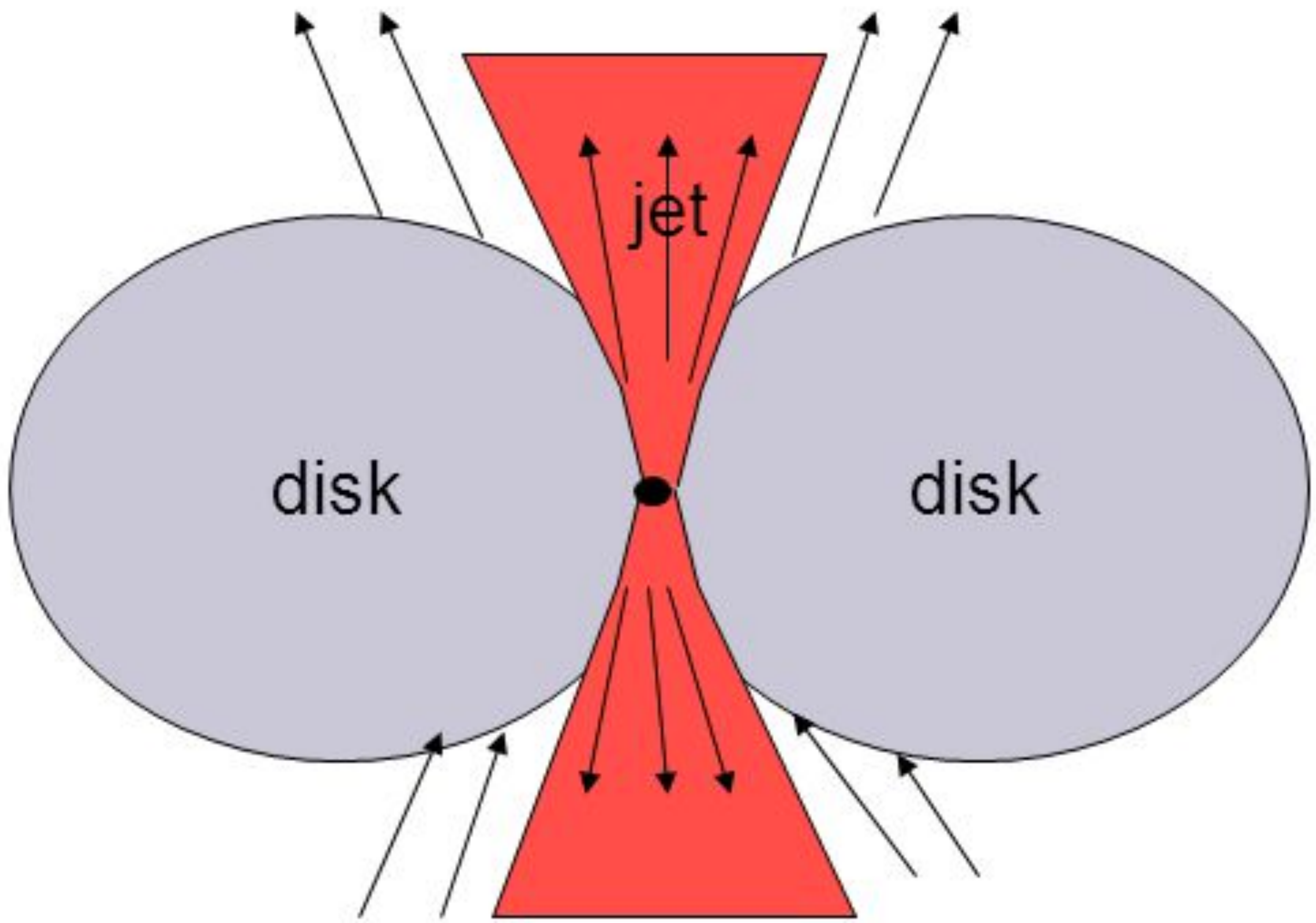

Suspects:

- Thick disk (torus)
- Disk corona
- Disk wind
- ISM

Ergospheric jets

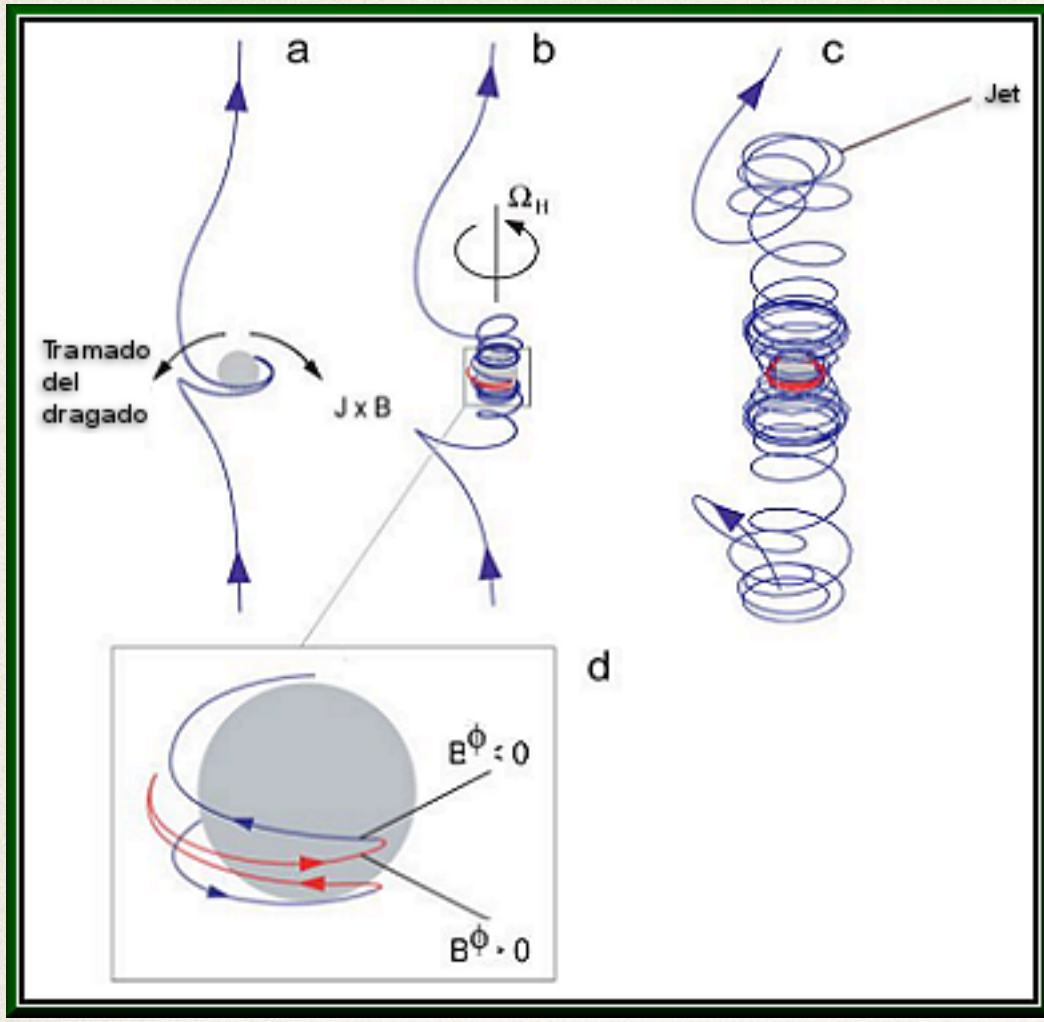

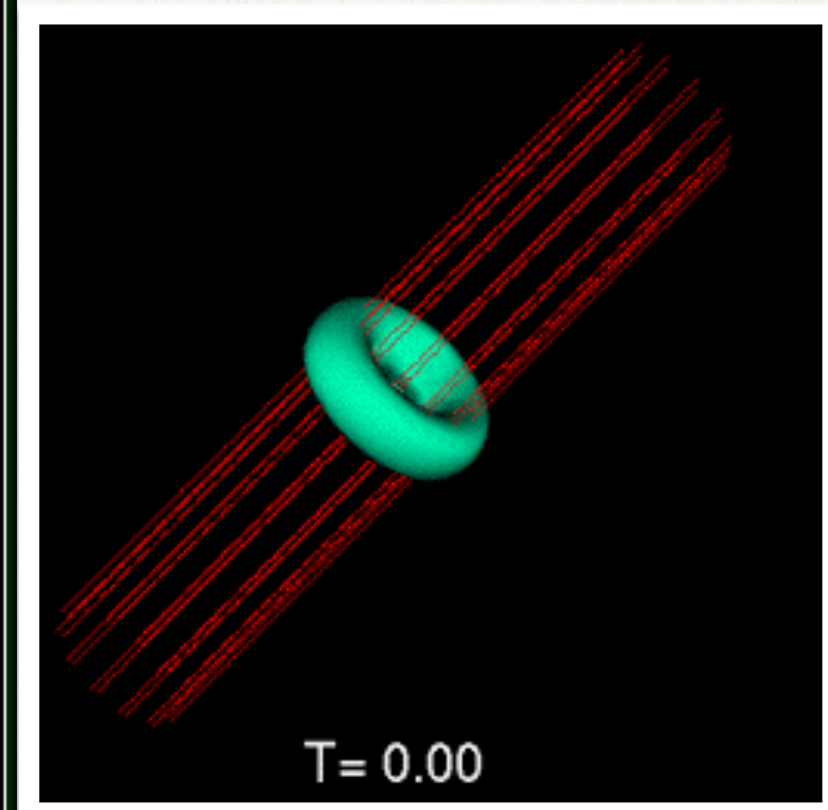

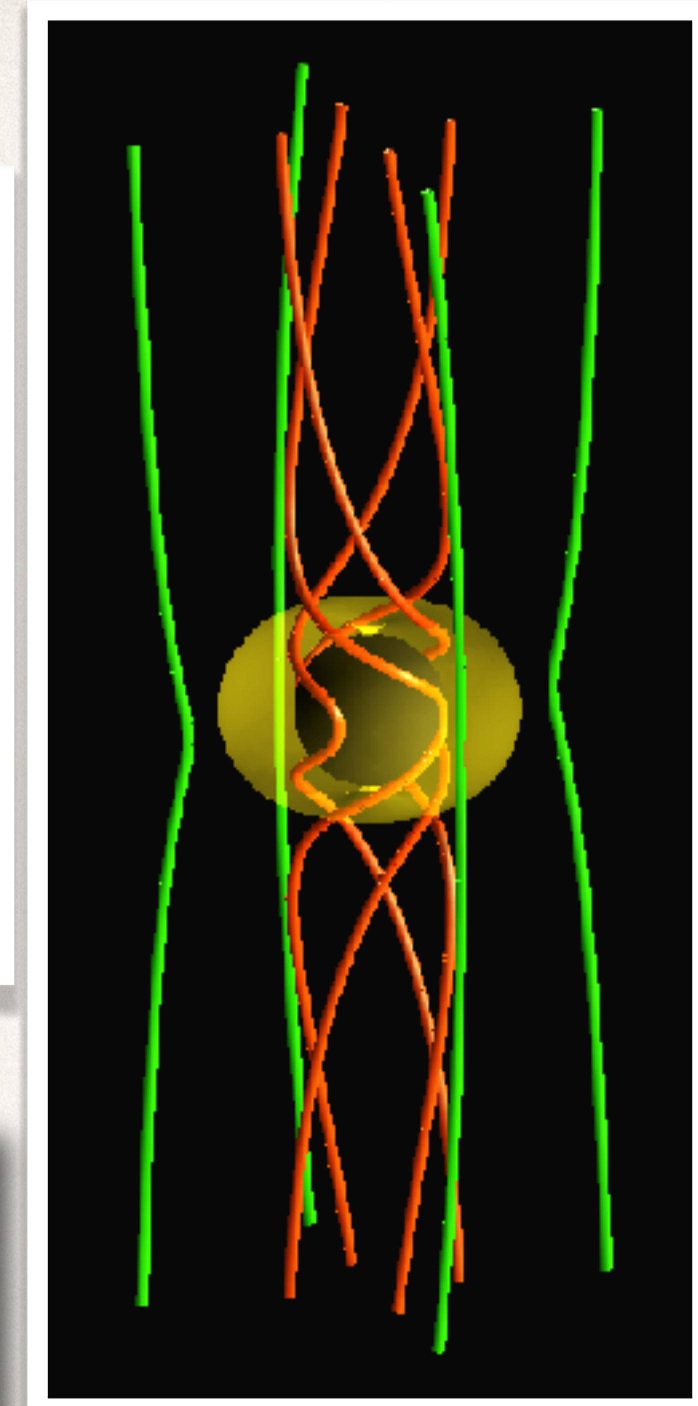

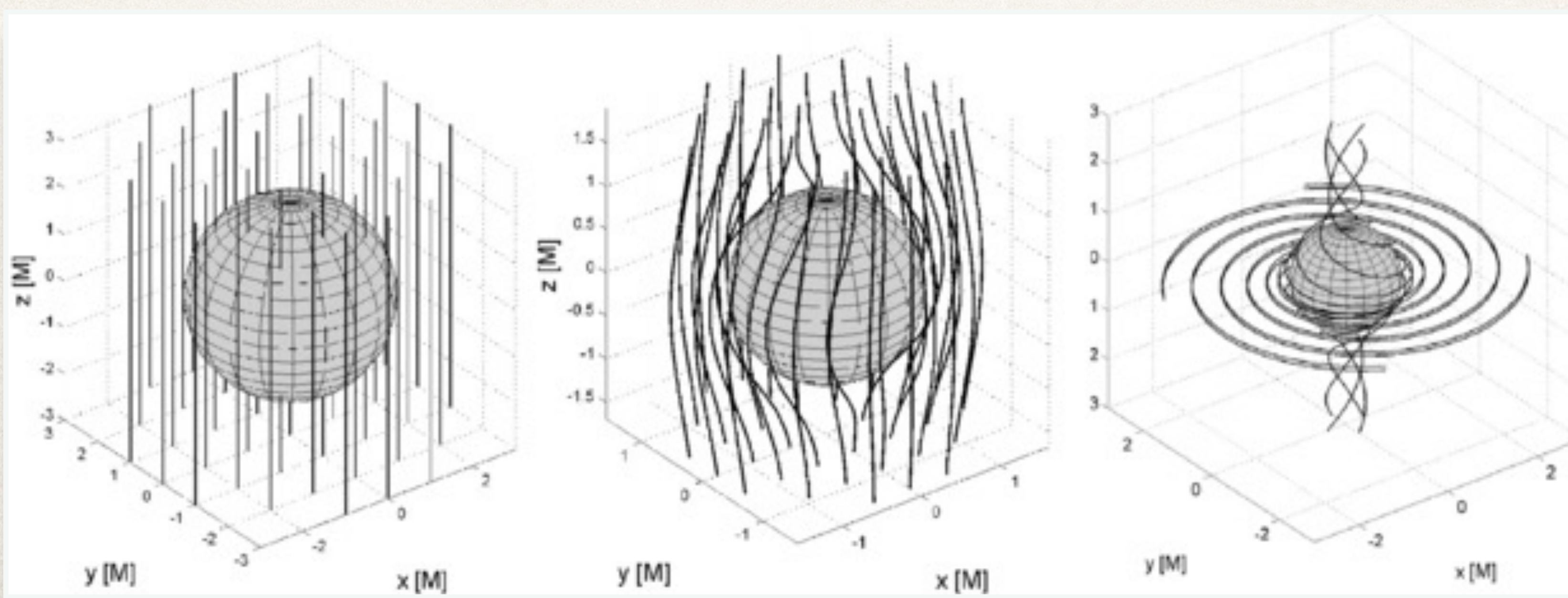

Relativistic Outflow driven by Magnetic Field from Ergosphere

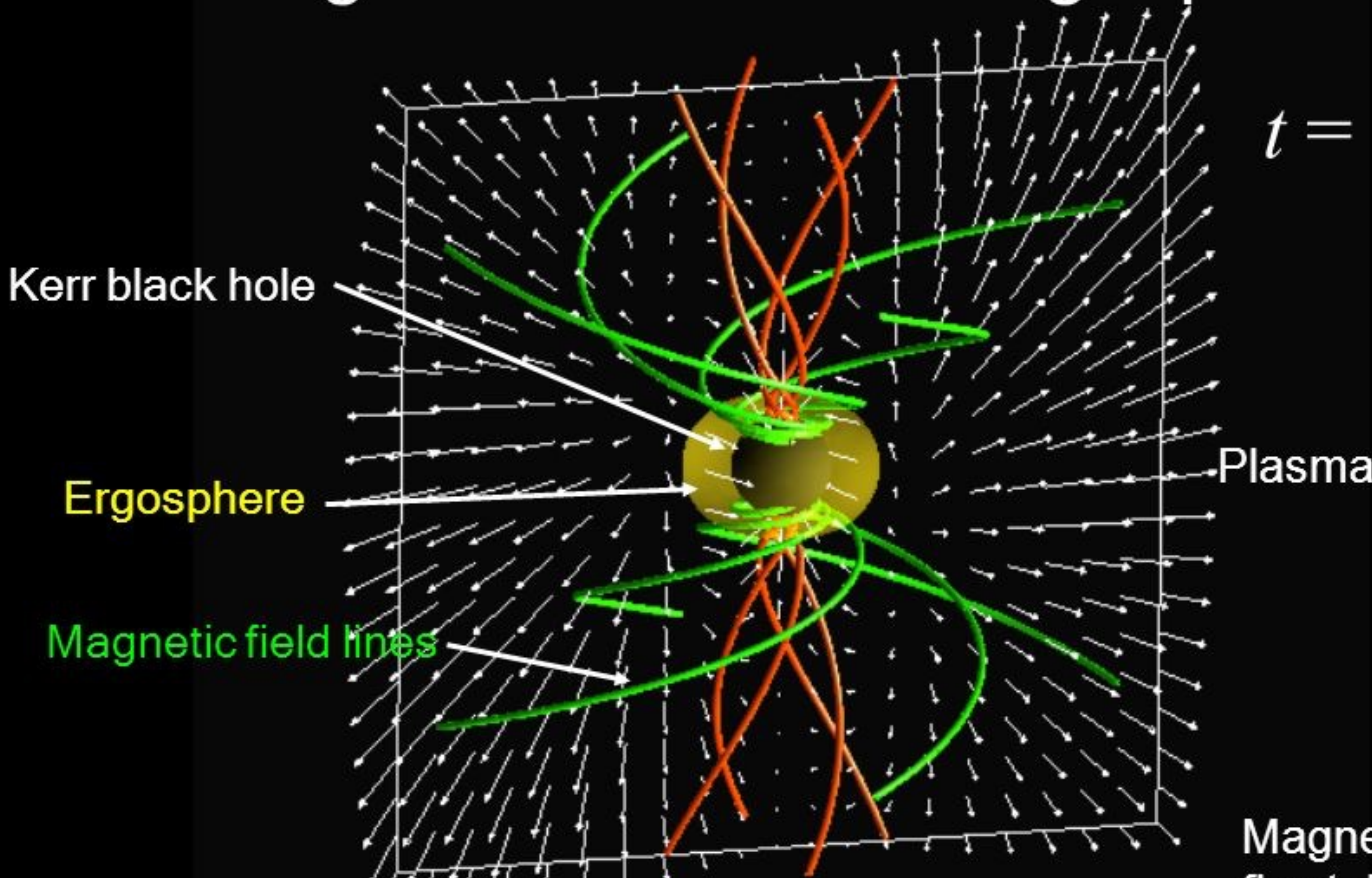

$t = 10.7\,\tau_S$

Magnetic field flux tube acts as propeller screw!

$$L_{\mathrm{EM}} \sim 4\pi \frac{B^2}{8\pi} c R_g^2 \sim c B^2 R_g^2$$

$$L \approx 10^{46} \left(\frac{B_n}{10^4\ \mathrm{G}}\right)^2 \left(\frac{M}{10^9 M_\odot}\right)^2 a_*^2\ \mathrm{erg\,s^{-1}}.$$

- While plasma is carried into the hole only (not ejected), electromagnetic power is ejected along the rotation axis.

- This Poynting power should eventually be turned into particles and a very fast jet. How??

- Magnetic field is tied to infalling plasma, not horizon.

- Frame dragging in the ergosphere twists up the field lines just as in the non-relativistic accretion disk case.

- Back-reaction of the magnetic field accelerates the ergospheric plasma to relativistic speeds counter to the hole's rotation: negative energy plasma.

- Accretion of negative energy plasma spins down the hole

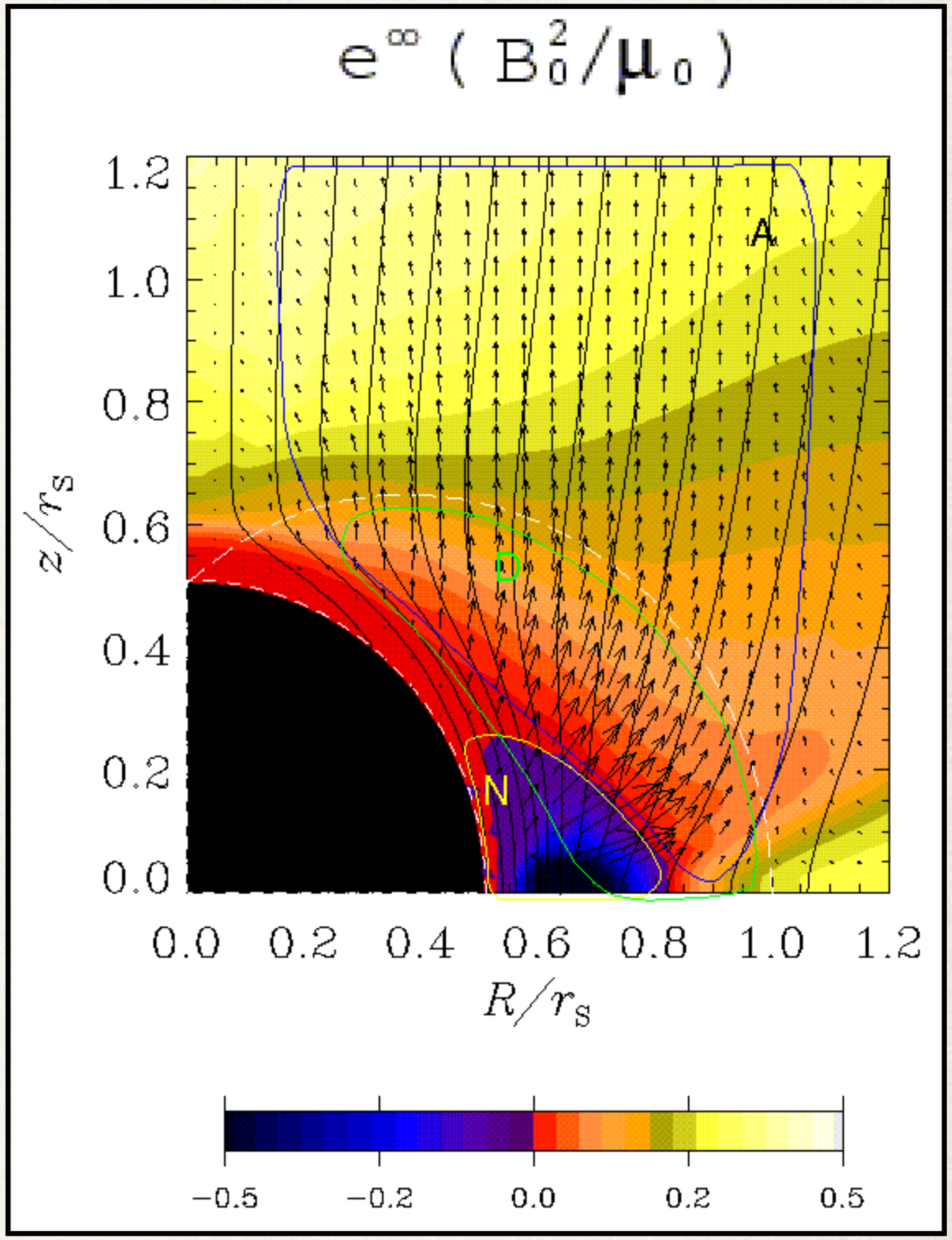

Issues with the magnetic model for generation of relativistic jets

$$B_{\rm MAD} \sim 4 \times 10^5 \ {\rm G}$$

$$r_{\rm L} = \frac{\gamma_p m_p c^2}{eB} \simeq 3 \times 10^4 \gamma_p \left(\frac{B}{10^4 \ {\rm G}} \right)^{-1} \ {\rm cm}\,.$$

The Schwarzschild radius $r_{\rm S} = 2r_{\rm g}$ of the SMBH in M87 is of ~ 10^{15} cm. Clearly protons, even highly relativistic ones, cannot be directly injected from outside: the base of the jet is shielded by the magnetic fields. For *e* is much worst.

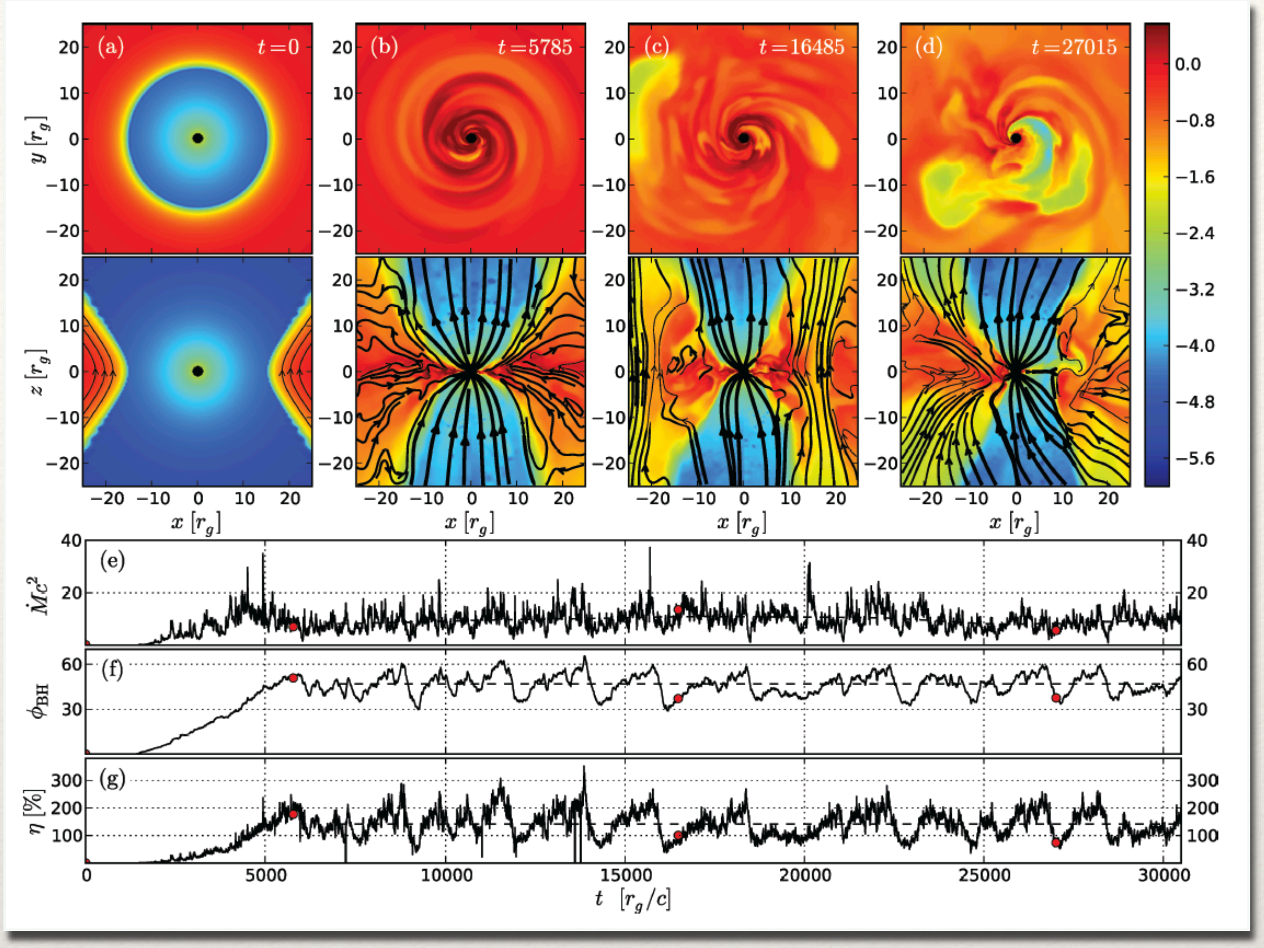

A. Tchekhovskoy, R. Narayan and J. C. McKinney (2011)

What is the origin of the matter present close to the base of the jets?

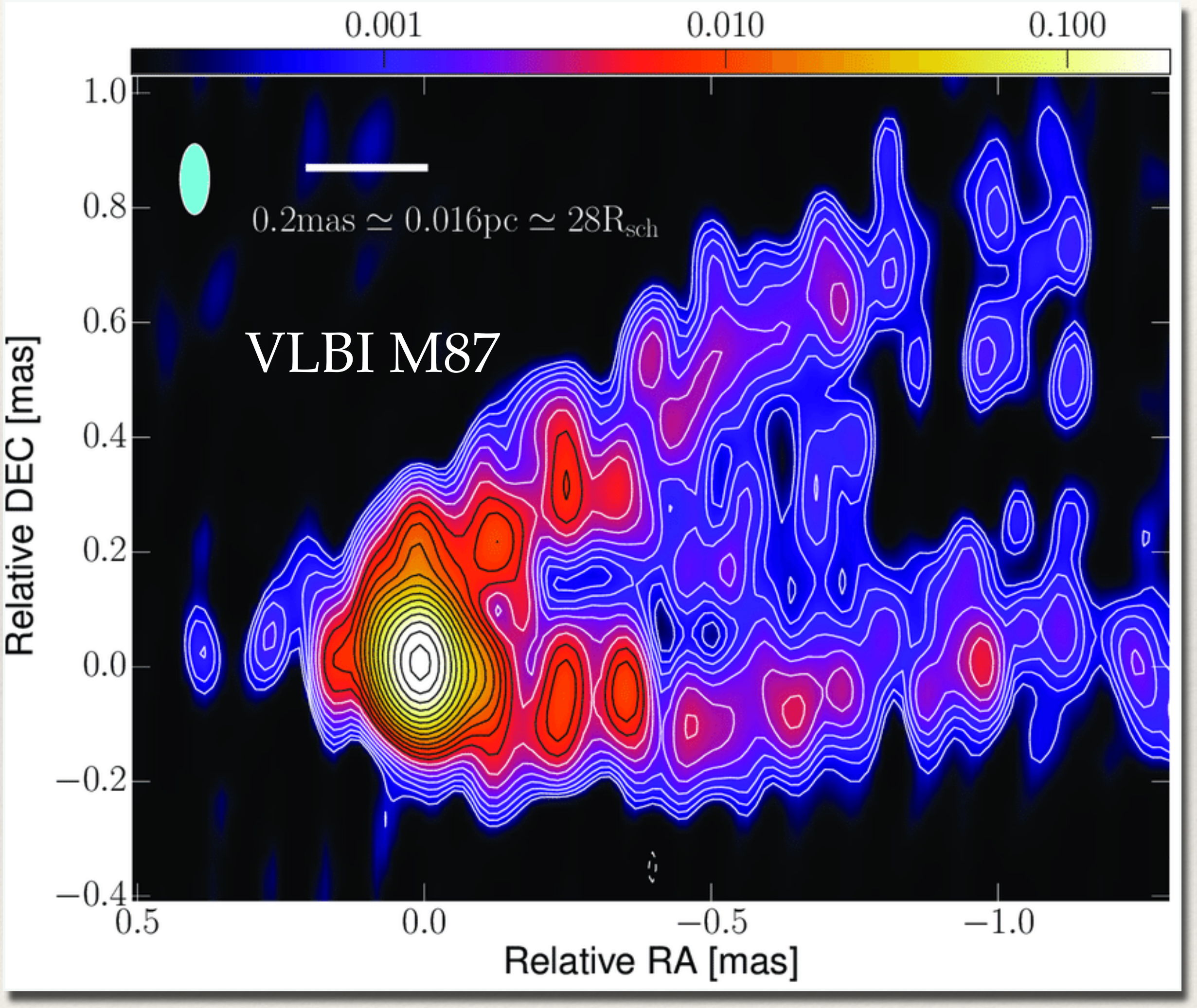

Romero & Gutiérrez (2020): Neutral particles from the hot accretion flow.

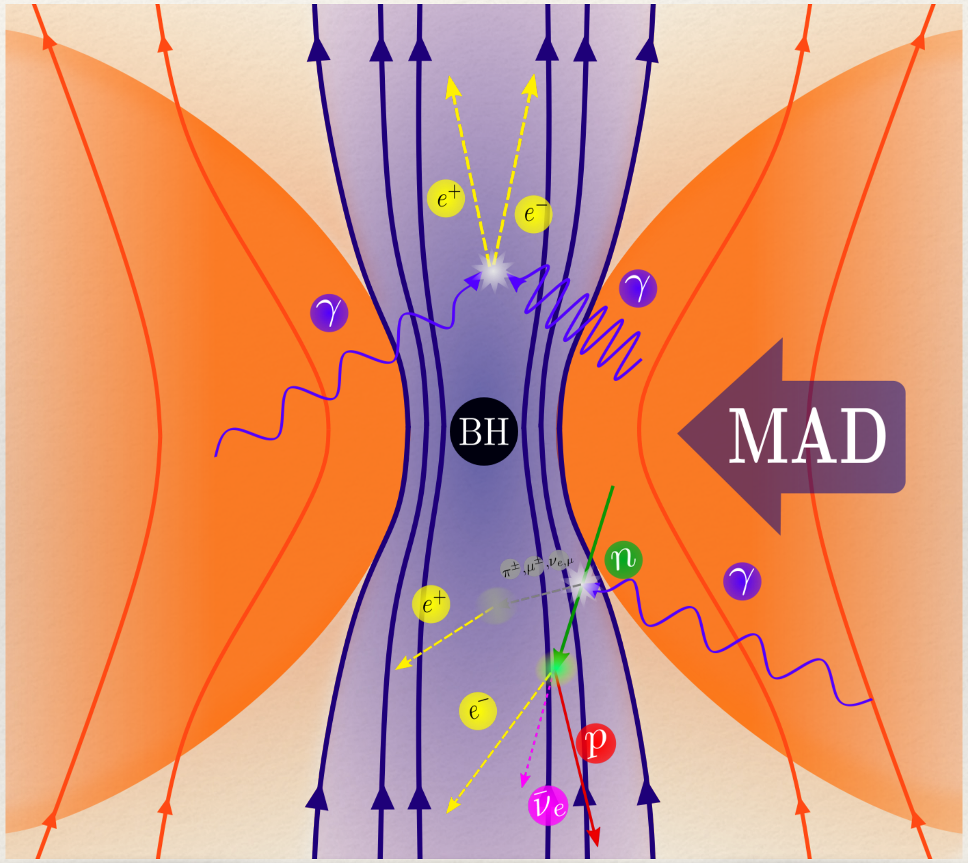

- At low accretion rates, the thin disk is truncated at large distances from the hole.
- The plasma in the inner region forms a Radiatively Inefficient Accretion Flow (RIAF).
- This is a hot, inflated, optically thin plasma.
- The hot electrons Compton up-scatter not only photons from the thin disk but also low-energy photons produced by synchrotron radiation.
- The hot plasma lies in the so-called collisionless regime where particles can be far out of thermal equilibrium.

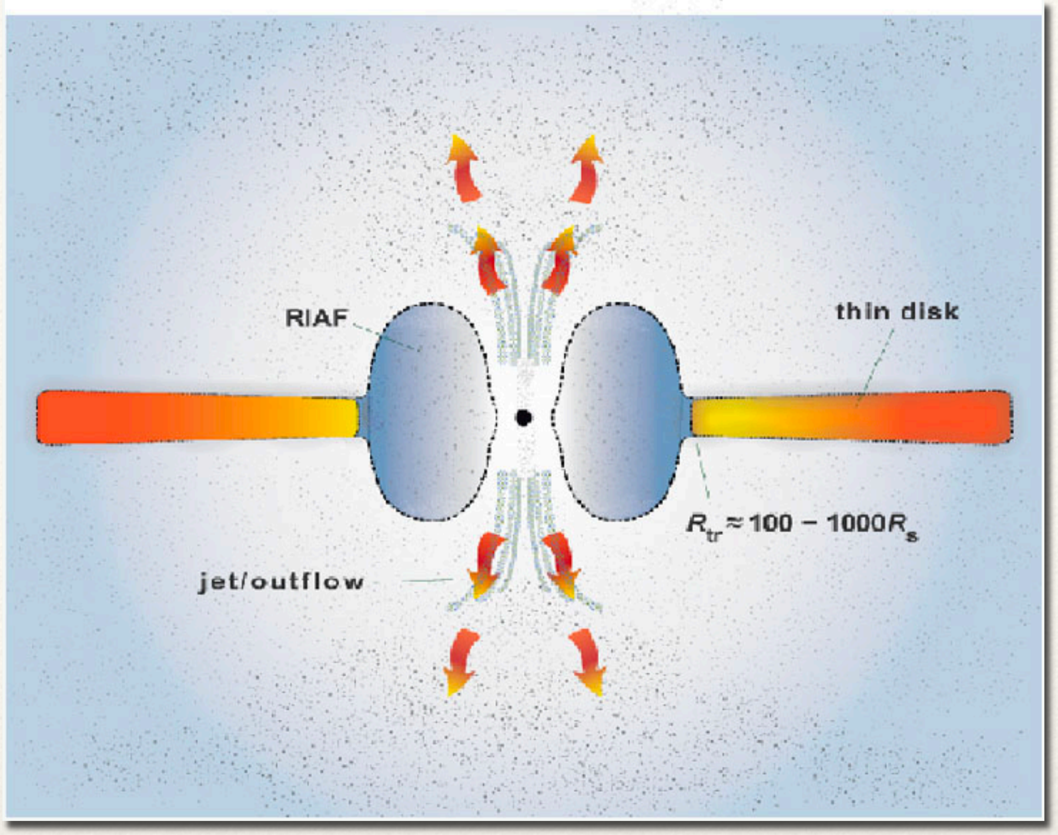

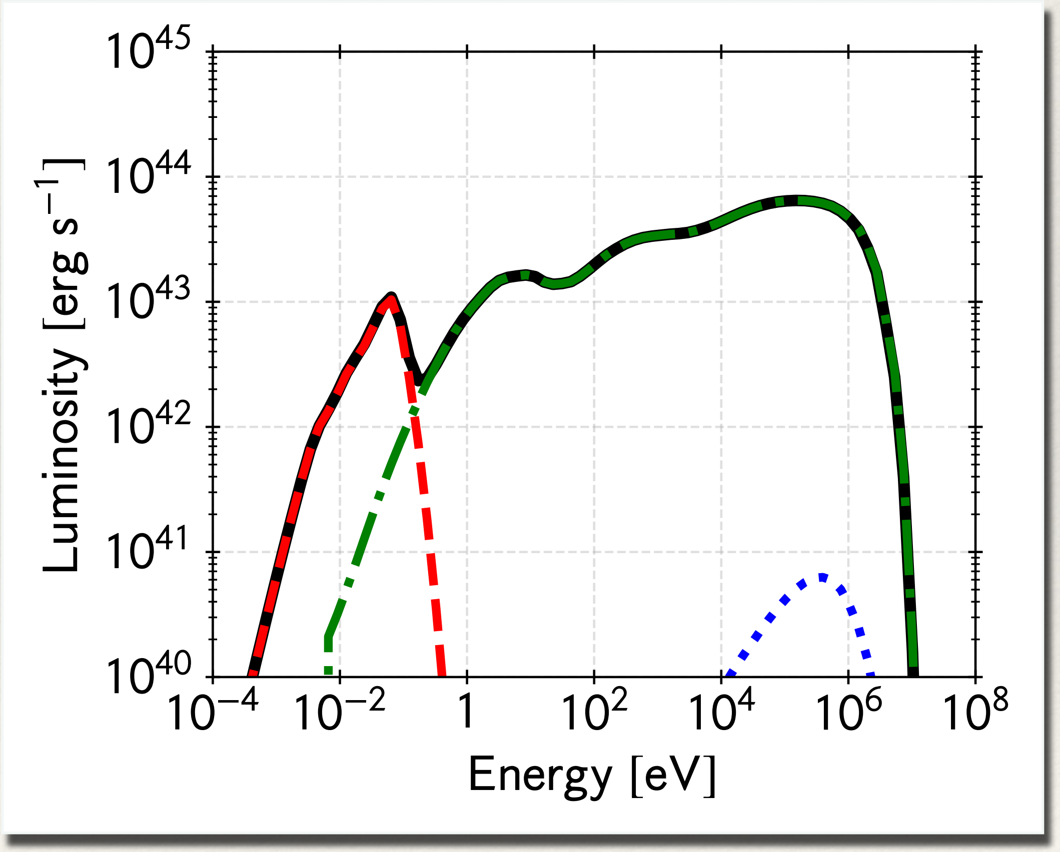

Romero & Gutierrez (2020)

Non-thermal particles in the RIAF

5% of the accretion power to NT particles

$$\frac{1}{r^2}\frac{\partial}{\partial r}\left[v_r(r) r^2 N(E,r)\right] + \frac{\partial}{\partial E}\left[b(E,r)N(E,r)\right] + \frac{N(E,r)}{t_{\rm diff}} = Q(E,r)\,.$$

$$Q(E) = Q_0 E^{-\alpha} e^{-E/E_{\rm cut}},$$

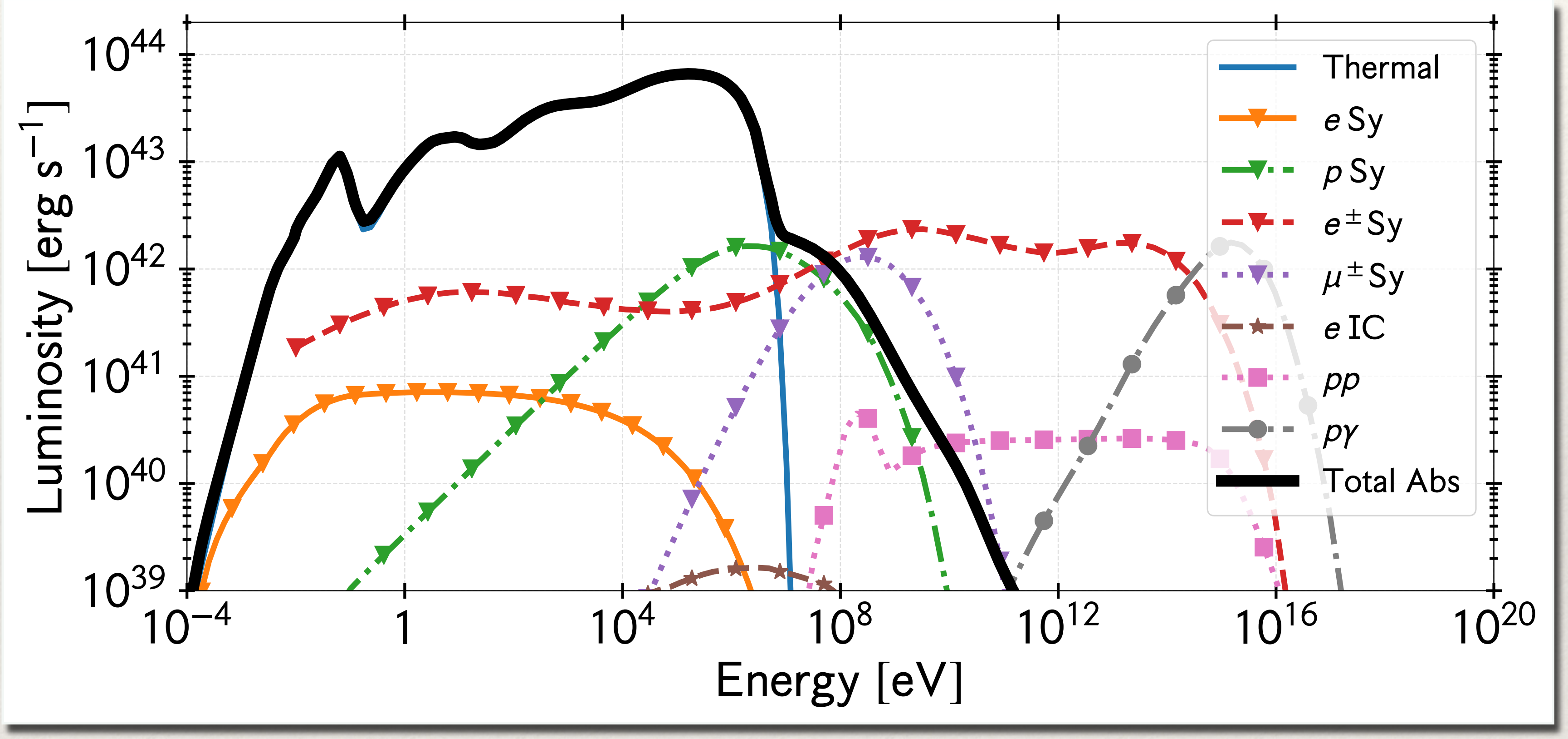

$$t_{\rm acc} = E/\eta_{\rm acc} eBc,$$

$$\eta_{\rm acc} = 10^{-3}$$

$$\gamma + \gamma \rightarrow e^+ + e^-$$

$$\tau_{\gamma\gamma}(E_\gamma) = \frac{1}{2}\int_l \int_{\epsilon_{\rm th}}^{\epsilon_{\rm max}} \int_{-1}^{\mu_{\rm max}} (1-\mu)\,\sigma_{\gamma\gamma}(E_\gamma,\epsilon,\mu)\, n_{\rm ph}(\epsilon,r)\,{\rm d}\mu\,{\rm d}\epsilon\,{\rm d}l\,.$$

Romero & Gutierrez (2020)

$$\gamma + \gamma \rightarrow e^{+} + e^{-}$$

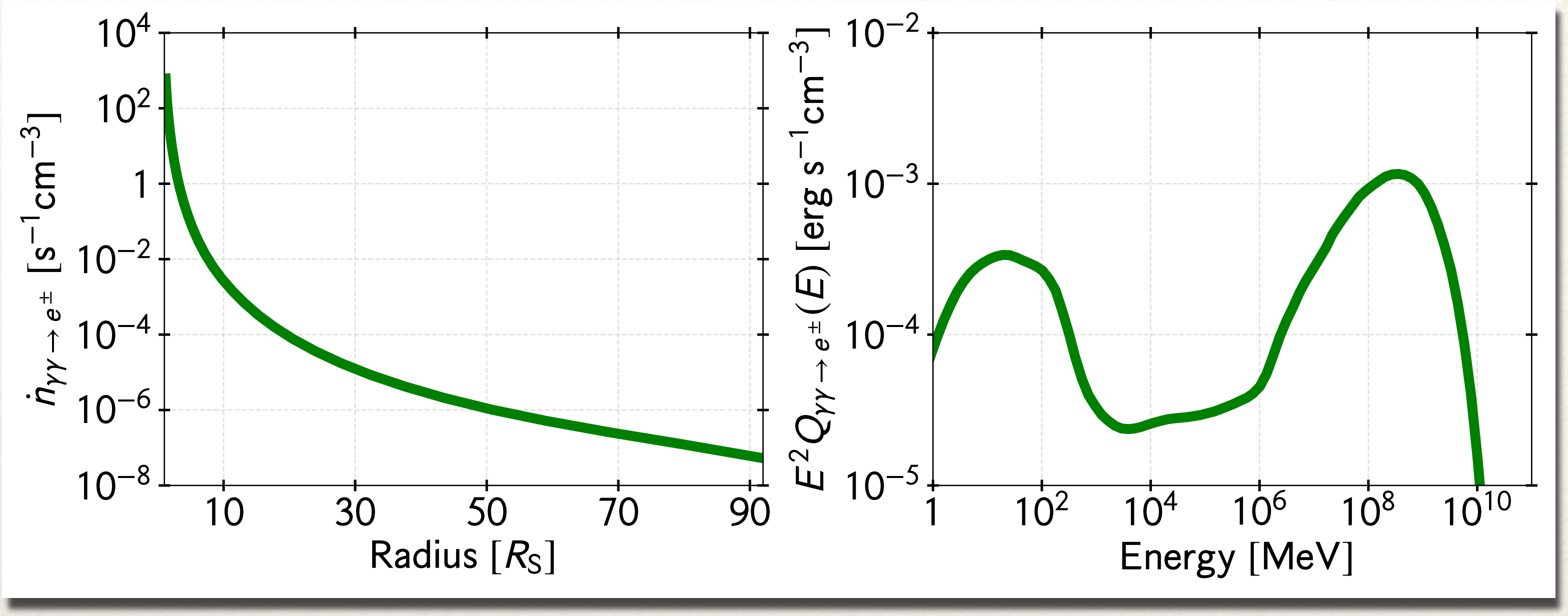

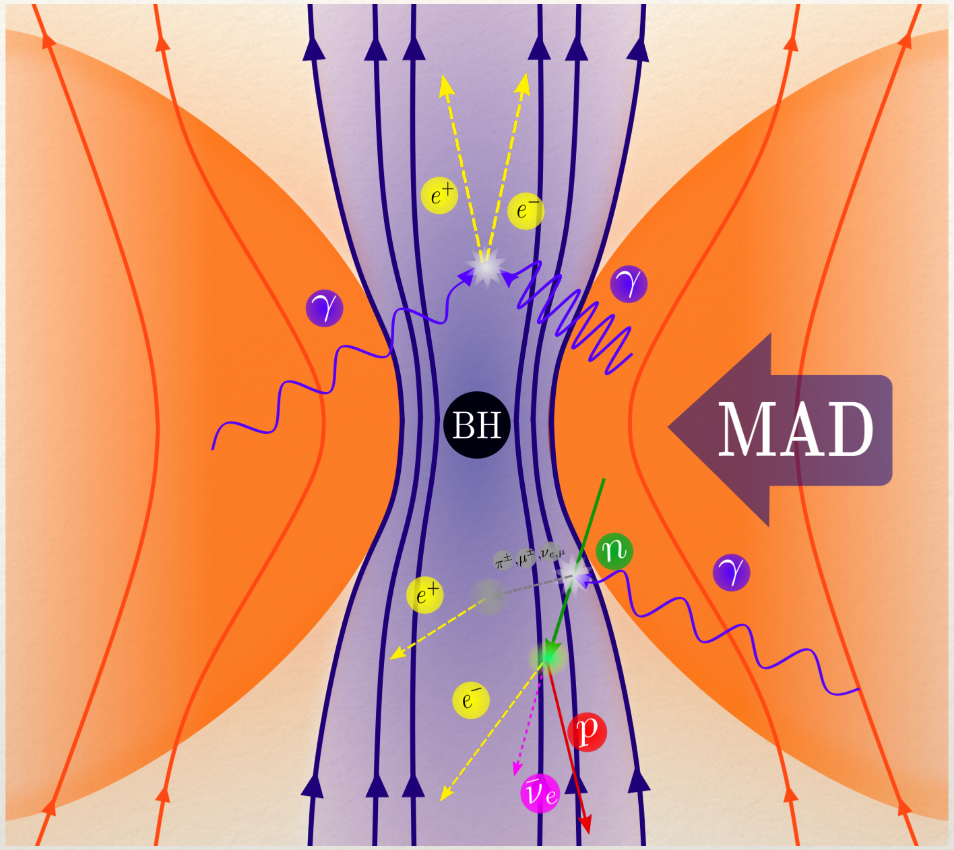

$$N_{e^{\pm}} \approx \dot{n}_{\gamma\gamma\rightarrow e^{\pm}} V_{\rm base}(R_S/c) \sim 10^{55}$$

The production rate is $\sim 10^{48}$ s^{-1}. Photon annihilation, then, might be a significant lepton loading mechanism as long as non-thermal acceleration processes are active and efficient in the flow around the black hole.

Romero & Gutierrez (2020)

Neutrons

$$p + p \rightarrow p + n + \pi^+ + a\pi^0 + b(\pi^+ + \pi^-),$$
$$p + p \rightarrow n + n + 2\pi^+ + a\pi^0 + b(\pi^+ + \pi^-),$$
$$p + \gamma \rightarrow n + \pi^+ + a\pi^0 + b(\pi^+ + \pi^-).$$

$$n \rightarrow p + e^- + \bar{\nu}_e$$
$$n + \gamma \rightarrow p + \pi^-$$

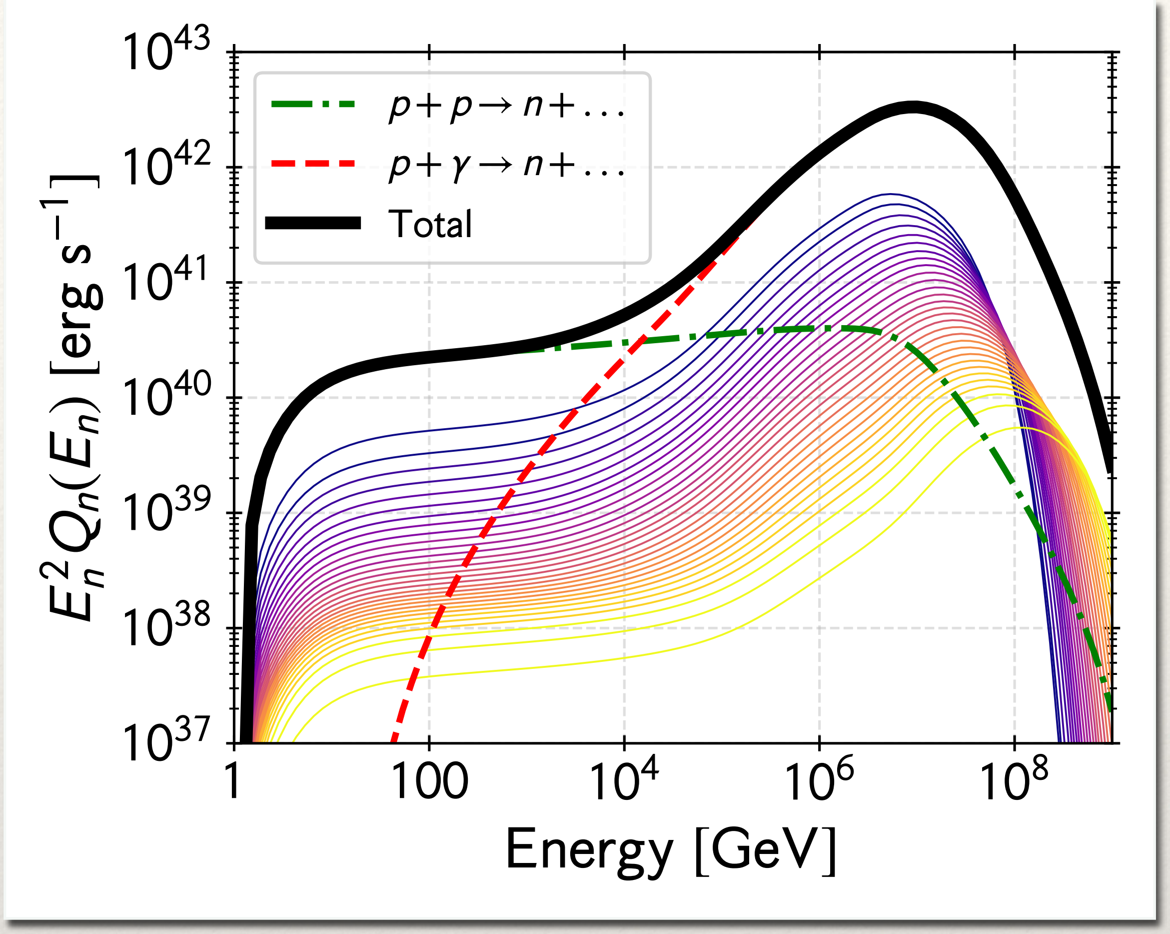

Once inside the jet, the protons will inject additional pairs by Bethe-Heitler interactions

Entrainment?

Large-scale fully three-dimensional GRMHD simulations of rapidly rotating, accreting black holes producing jets have shown that the accretion of non-dipolar magnetic fields resulting from turbulence in the accretion disk leads to weak, turbulent outflows, with important matter loading.

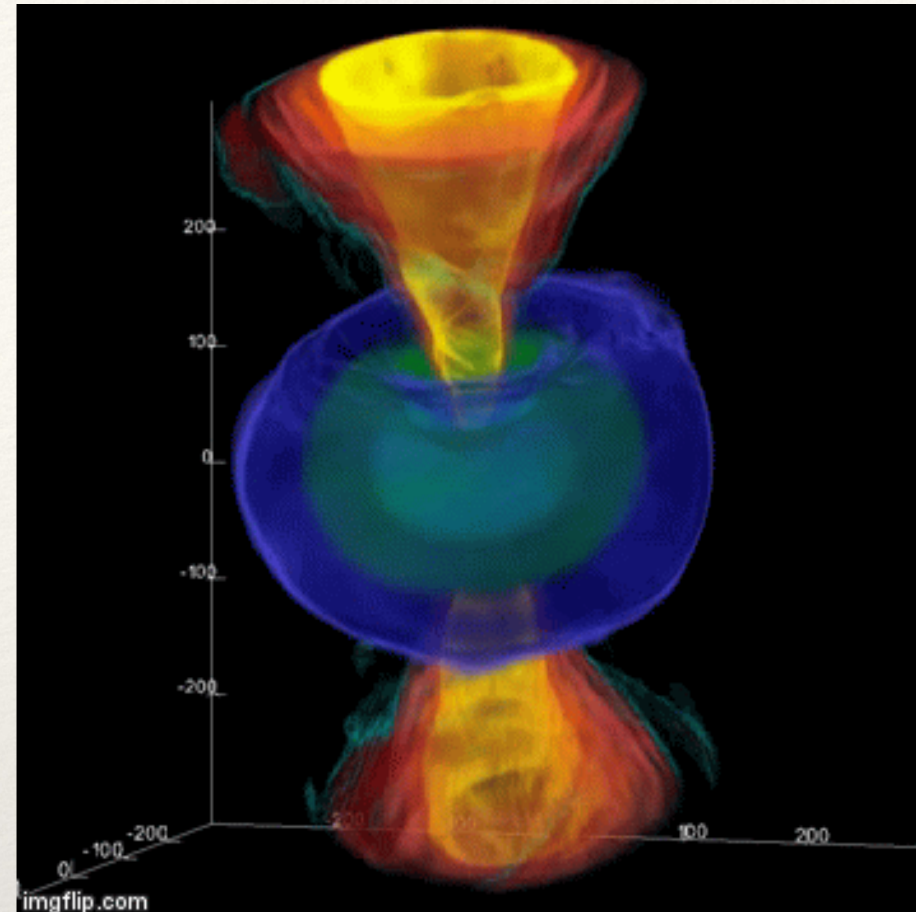

McKinney and Blandford (2009)

Disk winds tend to be clumpy

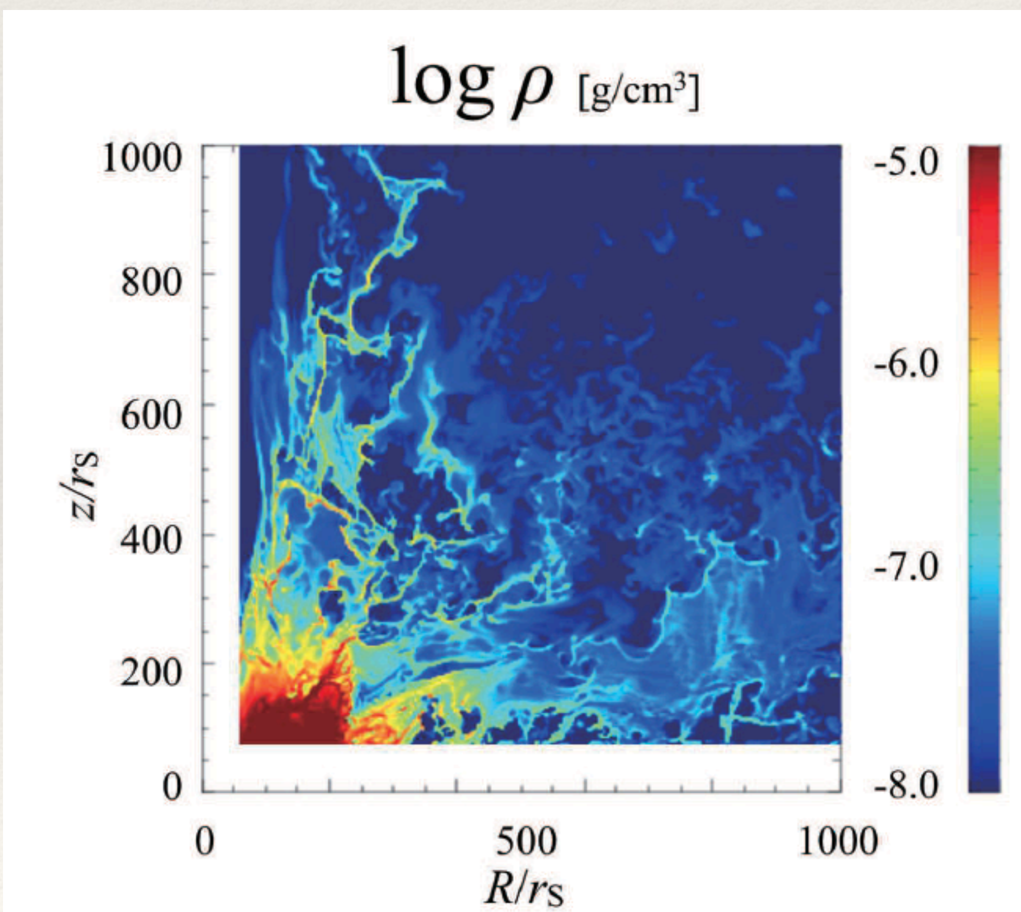

Kobayasi et al. (2014)

$$\rho_{\rm cloud} v_{\rm cloud}^2/2 > B_{\rm j}/8\pi$$

$$\rho_{\rm cloud} \gtrsim 10^{-7}\ {\rm g\ cm^{-3}}$$

Clouds

Stars

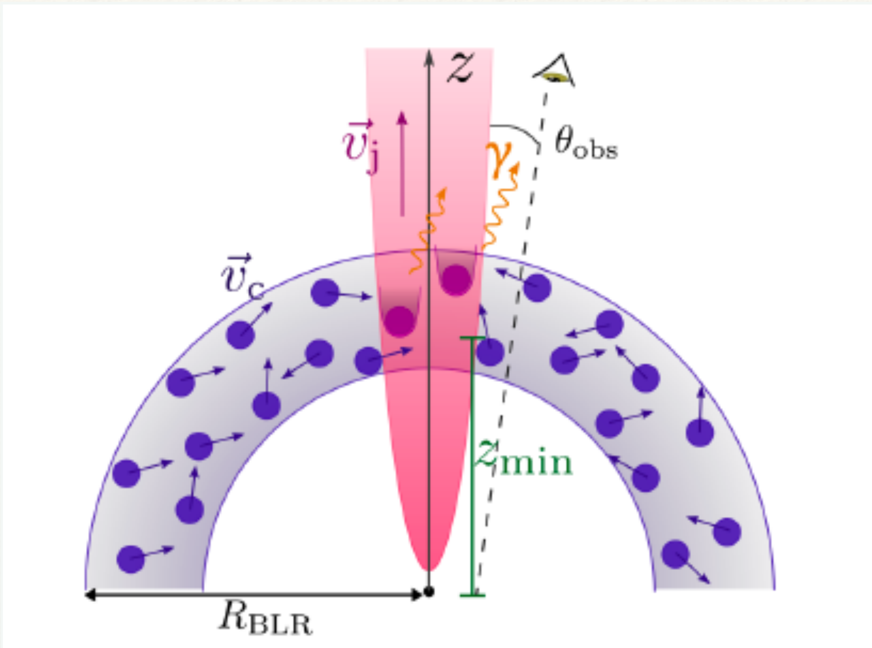

del Palacio et al. (2019)

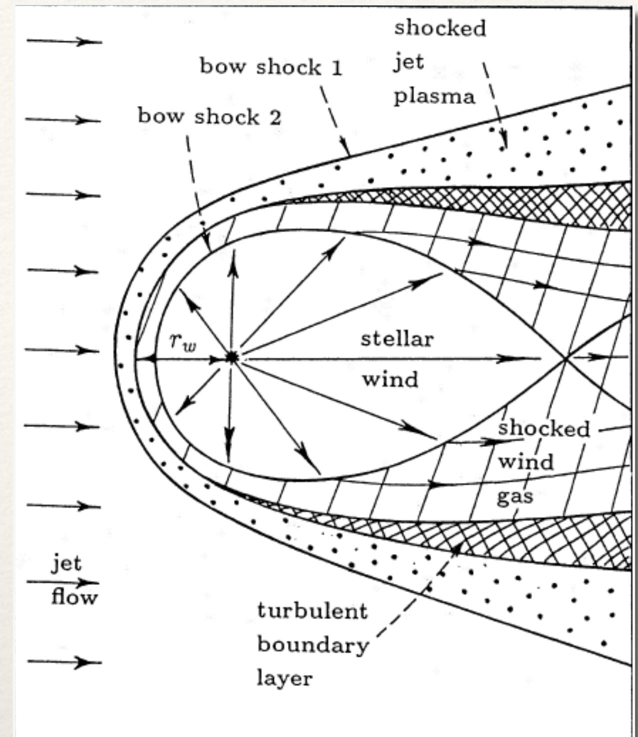

Komissarov 1994

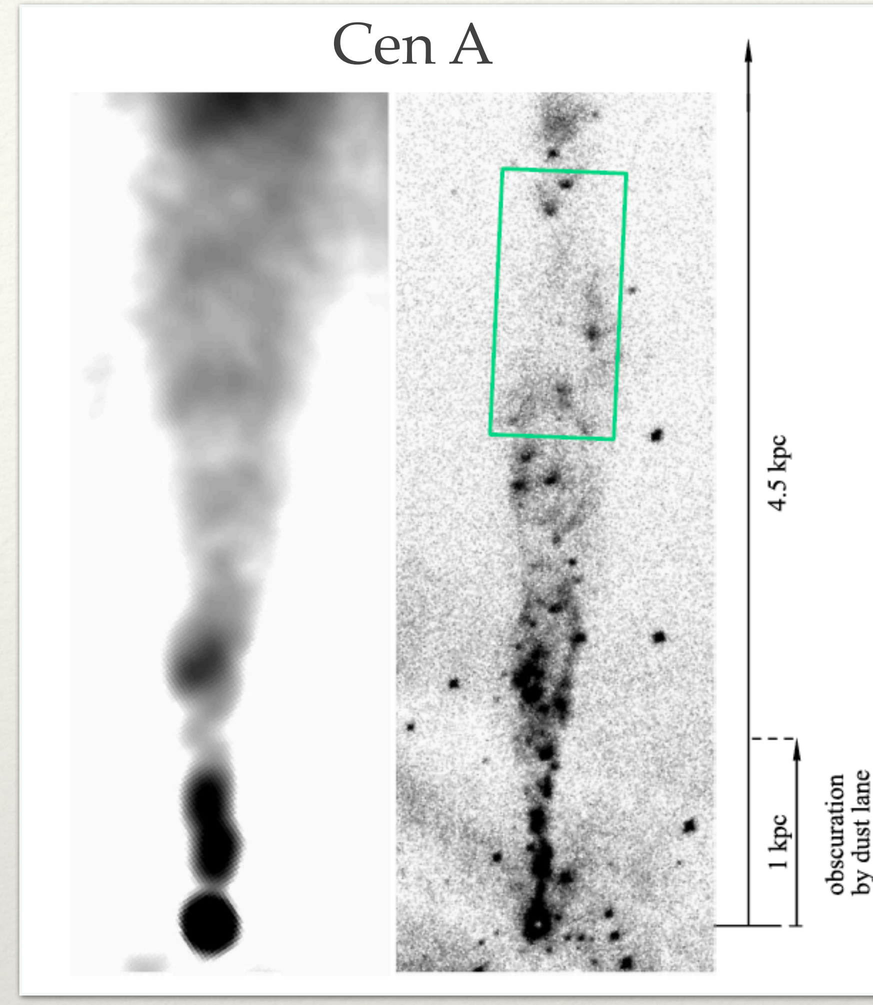

Wykes et al (2015)

Araudo et al. (2013)

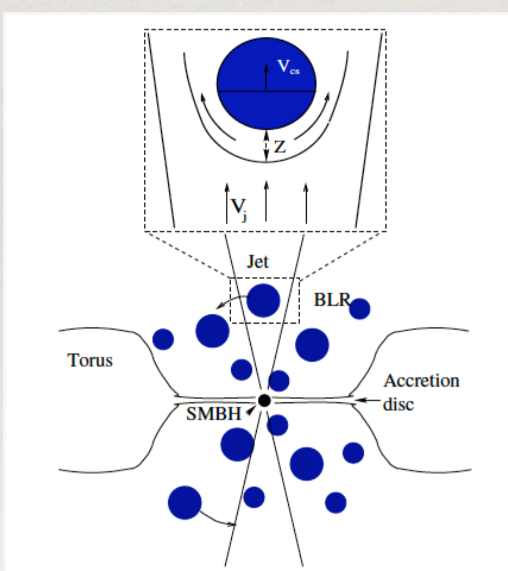

Araudo et al. (2010)

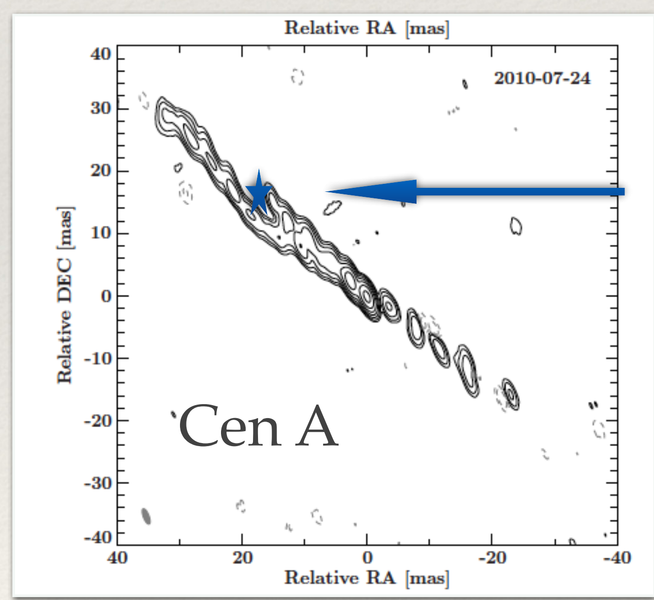

Multi-epoch VLBI 8.4 GHz

Müller et al. A&A 2014

Gamma-ray bursts

Las erupciones de rayos γ (Gamma-Ray Bursts, GRB) son un fenómeno astronómico caracterizado por un *rápido y breve* *incremento* *de la radiacion* γ

Puede llegar a superar a toda otra fuente γ del Universo.

Rango:
10^{-3} seg. - 10^{3} seg.

✳ La duración de este fenómeno es muy corta:
- unos pocos segundos a algunas decenas de segundos;
- duraciones extremas: milisegundos a decenas de minutos.

✳ En promedio se detecta entre 1 y 2 GRB por día.

✳ Descubiertos por los satélites militares Vela en 1967.

La misión de la serie de satélites Vela Hotel era descubrir las explosiones nucleares en el espacio, mientras que la serie de Vela Avanzada era no sólo descubrir estas explosiones espaciales sino, también, las producidas en la atmósfera. Fueron situados en órbitas entre 100.000 y 113.000 km, bastante por encima de los cinturones de Van Allen.

2 de julio de 1967: El satélite Vela 4a, b realiza la primera observación de un estallido de rayos gamma.

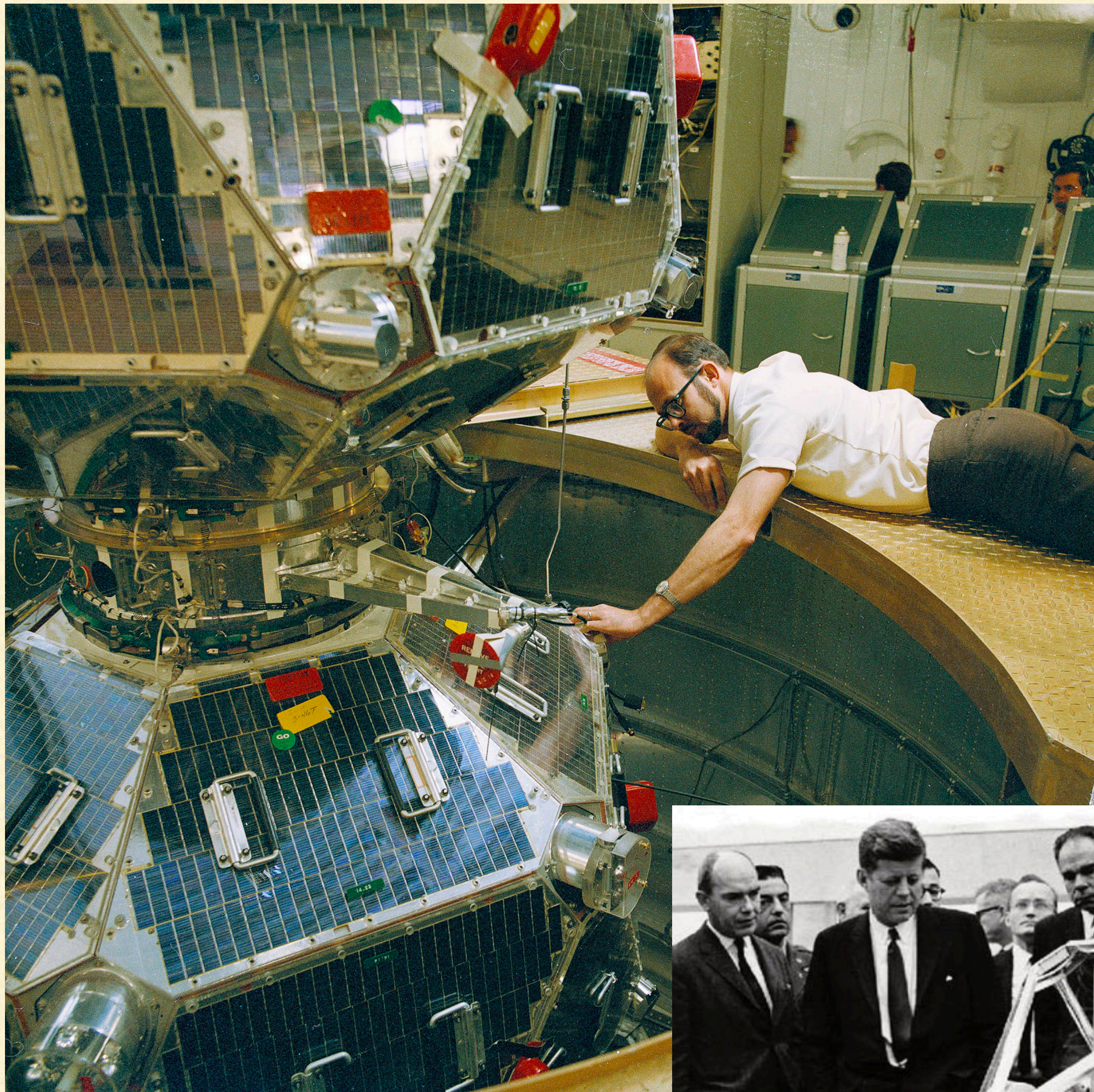

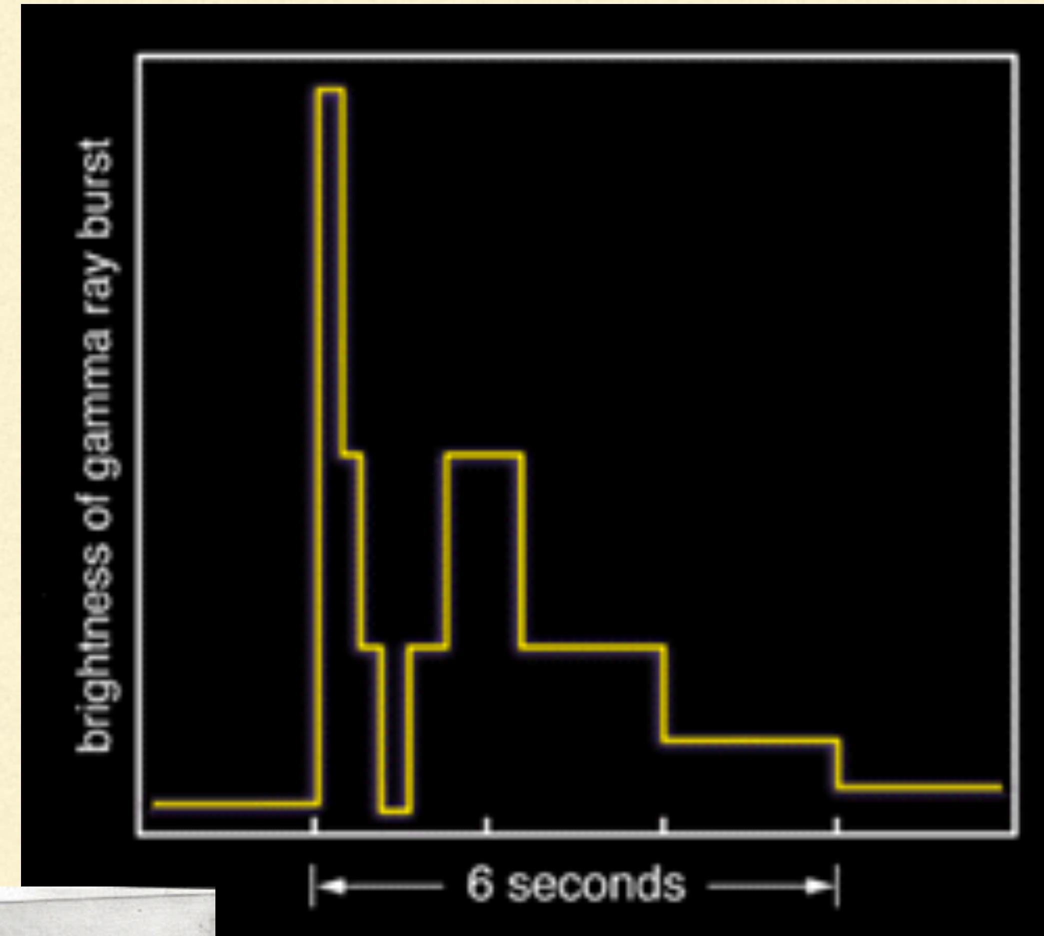

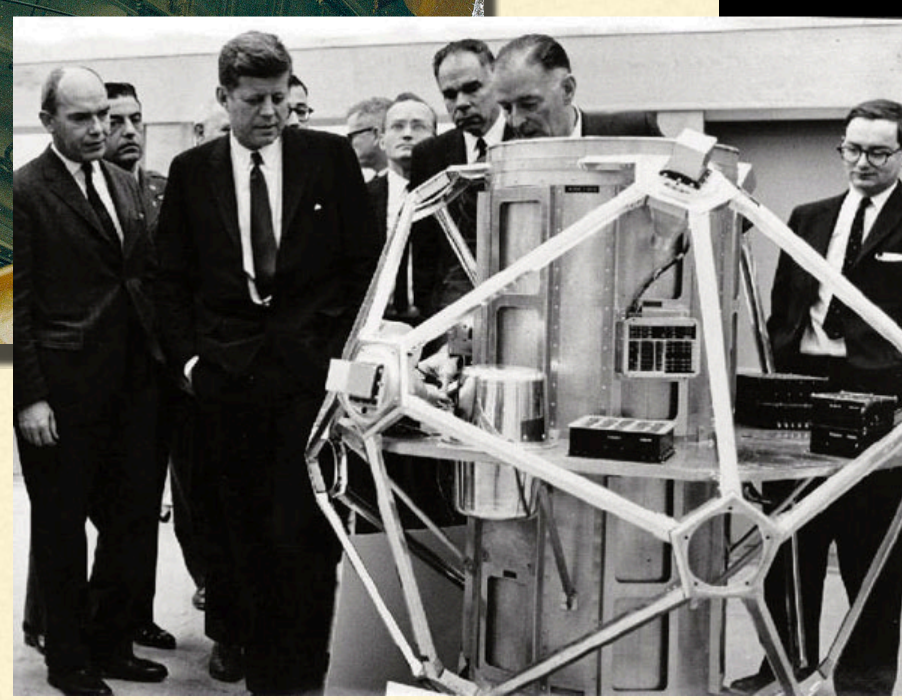

JFK inspecciona los primeros satélites Vela

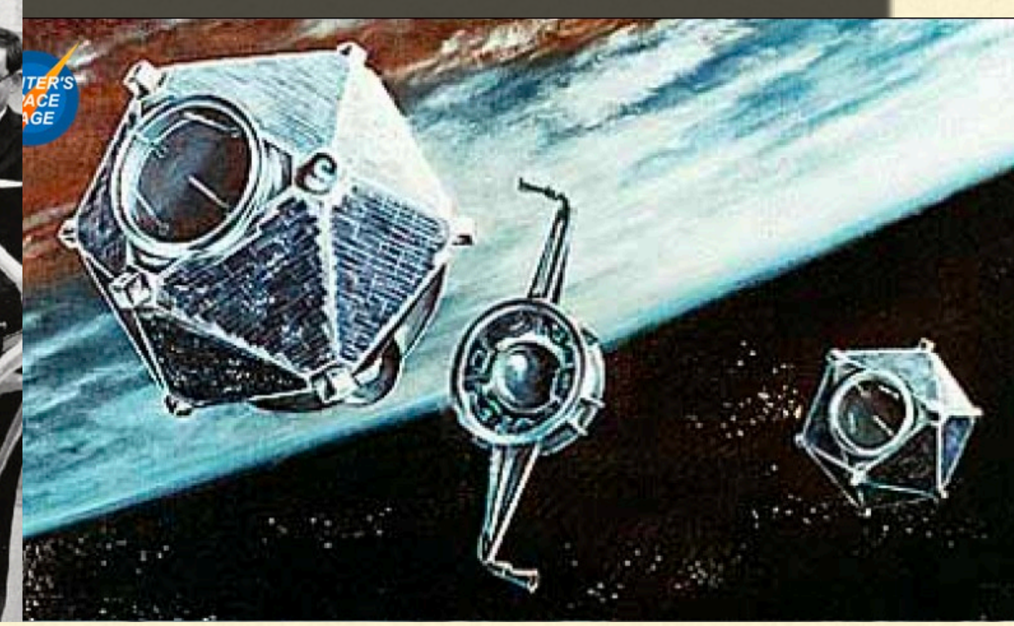

The Astrophysical Journal, **182**:L85–L88, 1973 June 1

OBSERVATIONS OF GAMMA-RAY BURSTS OF COSMIC ORIGIN

Ray W. Klebesadel, Ian B. Strong, and Roy A. Olson

University of California, Los Alamos Scientific Laboratory, Los Alamos, New Mexico
Received 1973 March 16; revised 1973 April 2

ABSTRACT

Sixteen short bursts of photons in the energy range 0.2–1.5 MeV have been observed between 1969 July and 1972 July using widely separated spacecraft. Burst durations ranged from less than 0.1 s to ~30 s, and time-integrated flux densities from $\sim 10^{-5}$ ergs cm^{-2} to $\sim 2 \times 10^{-4}$ ergs cm^{-2} in the energy range given. Significant time structure within bursts was observed. Directional information eliminates the Earth and Sun as sources.

Subject headings: gamma rays — X-rays — variable stars

En 1973, 6 años después de la primera detección, Ray Klebesadel (responsable del programa **VELA** en Los Álamos) y sus colegas Ian Strong y Roy Olsen publicaron en el Astrophysical Journal la lista de los 16 brotes que se había detectado hasta entonces con las misiones **VELA**5 y **VELA**6 (con una estimación de posición) dando indicios de su origen cósmico.

1991-2000: BATSE, en el satélite COMPTON, detecta miles de GRBs.

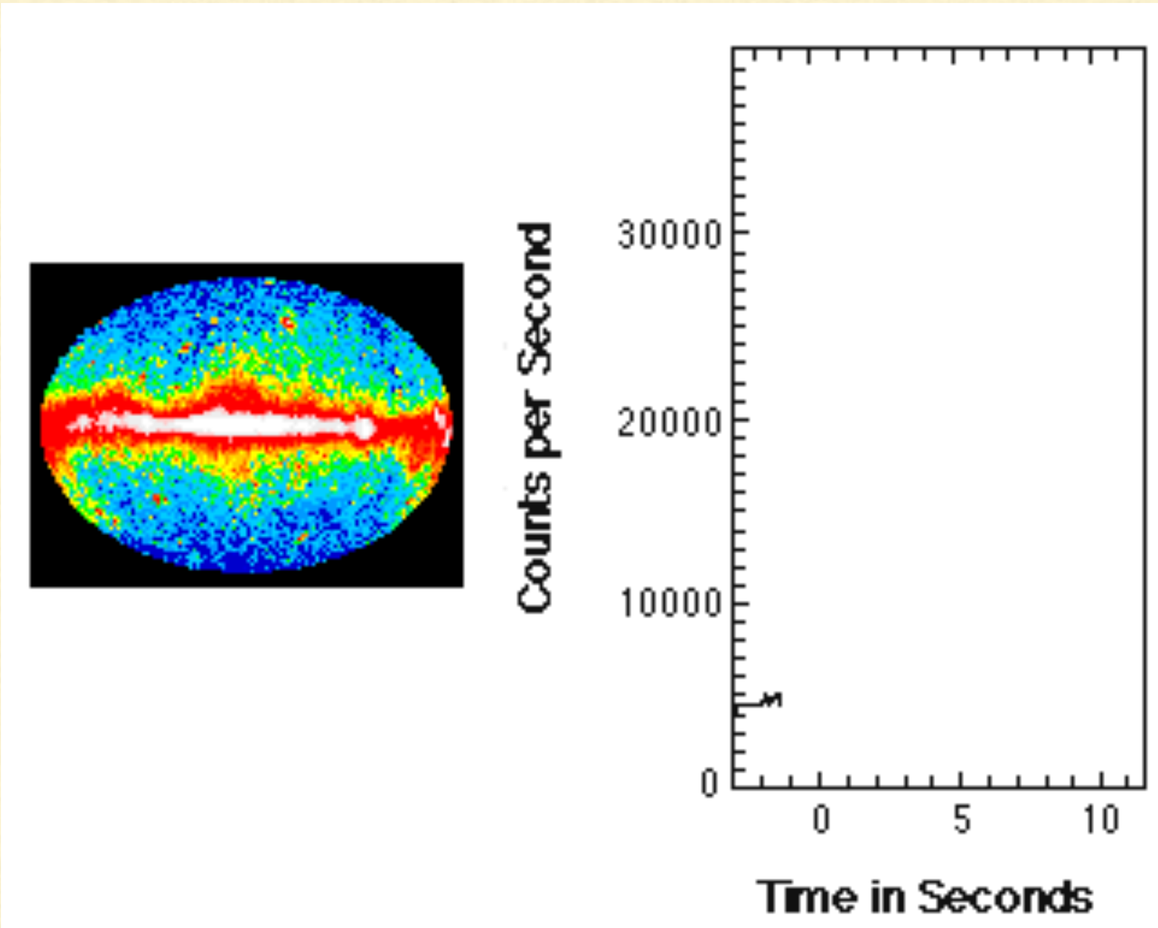

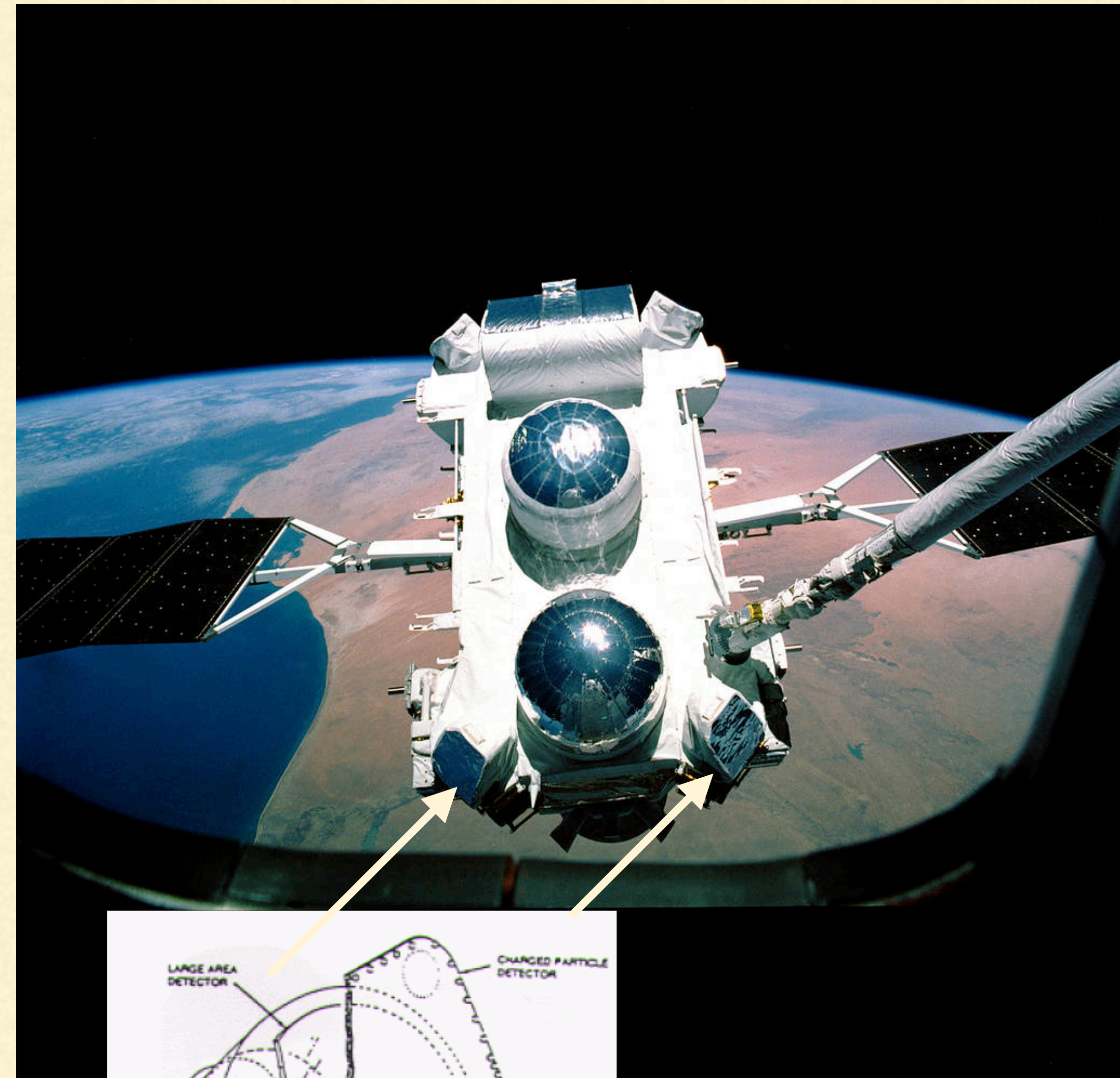

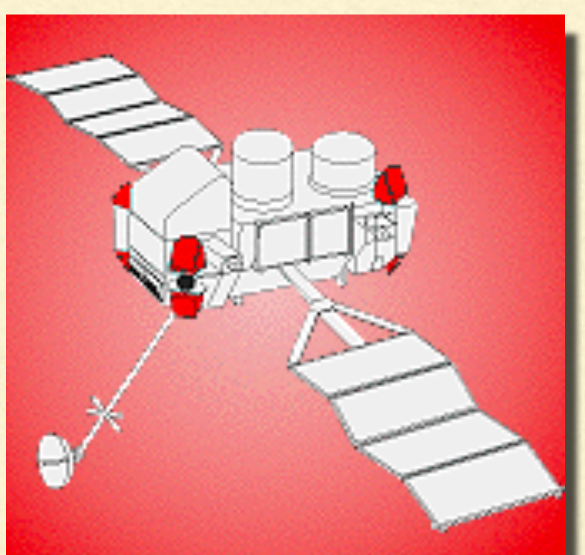

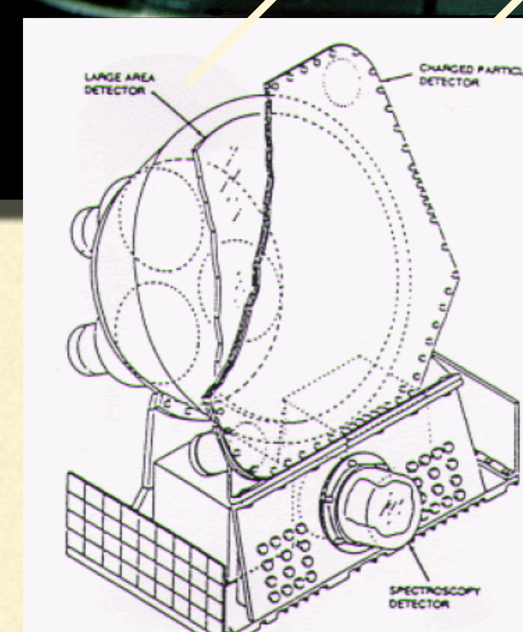

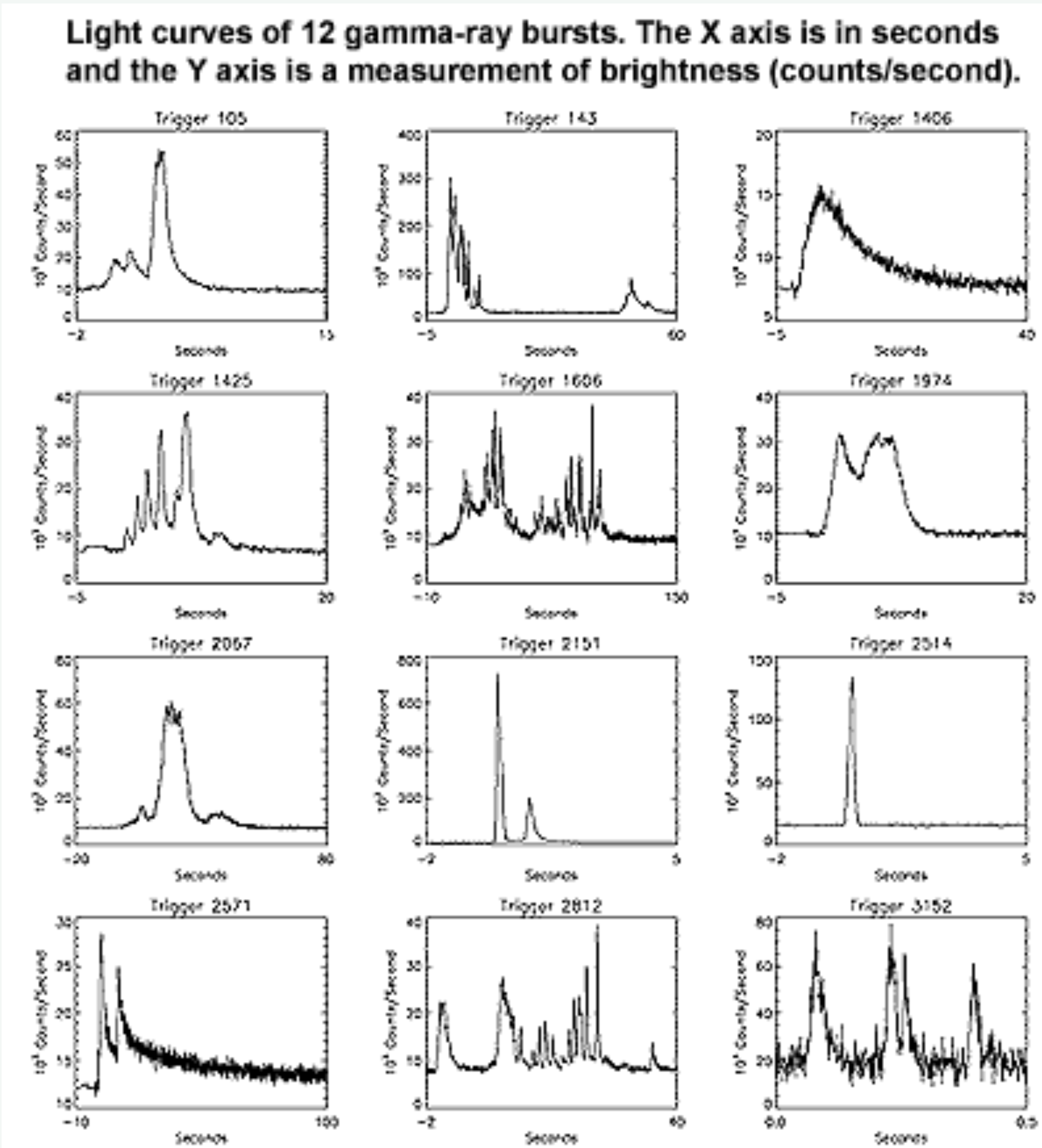

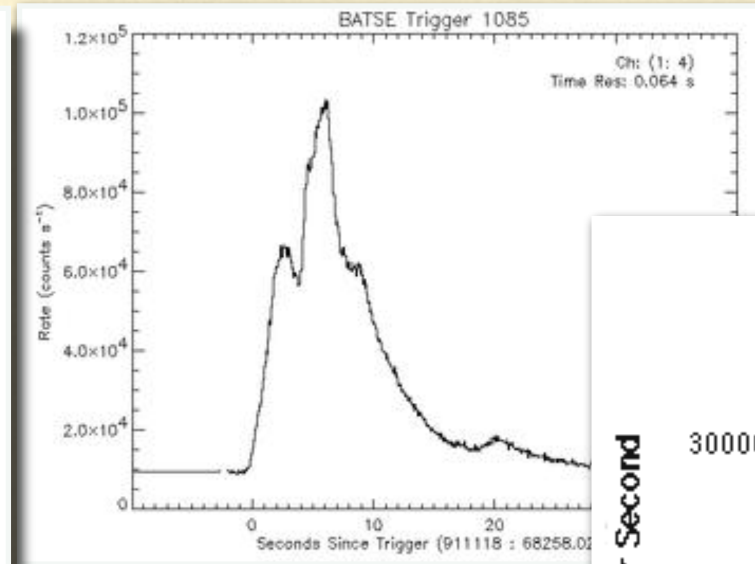

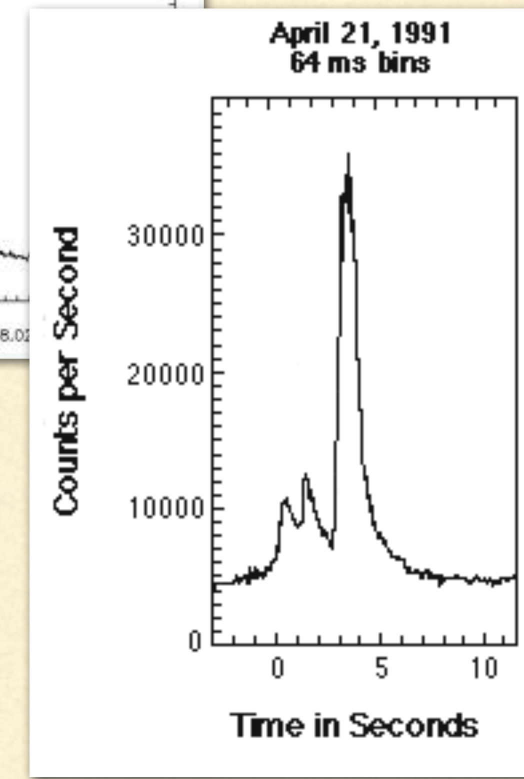

Los pulsos simples tienen poca o ninguna estructura.

Una subclase particular de estos eventos son los llamados FREDs (Fast Rise, Exponential Decay).

En muchos de los eventos de múltiple picos, los tiempos de subida y de bajada tienden a ser similares.

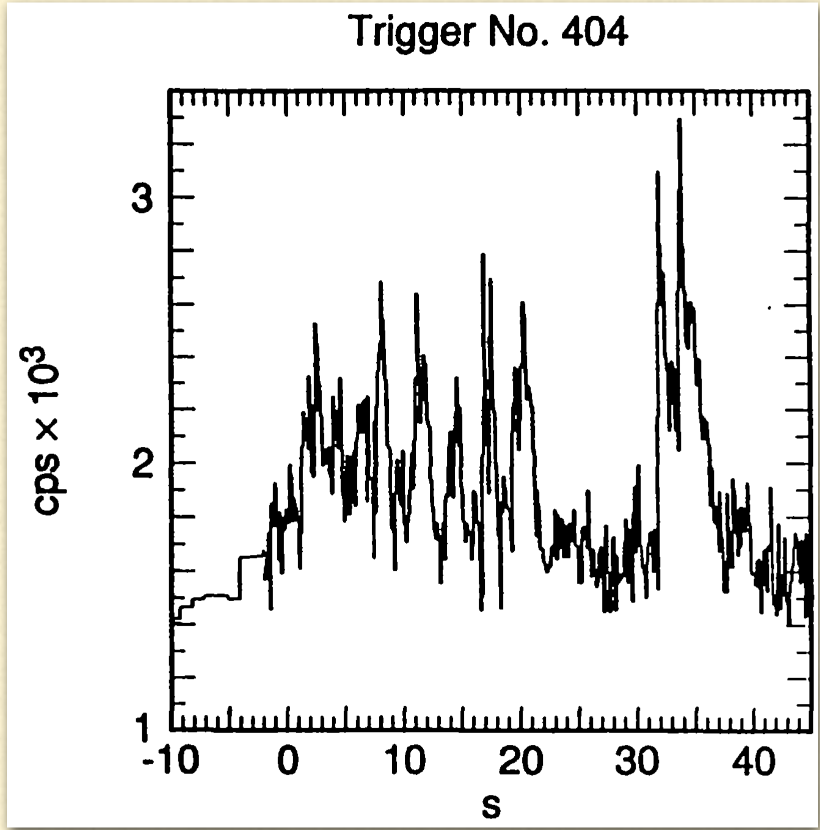

GRBs con perfiles temporales altamente estructurados a nivel de milisegundo, con muchos picos angostos.

En muchos de estos casos parecería haber una "capa" subyacente de emisión de dónde provienen los picos.

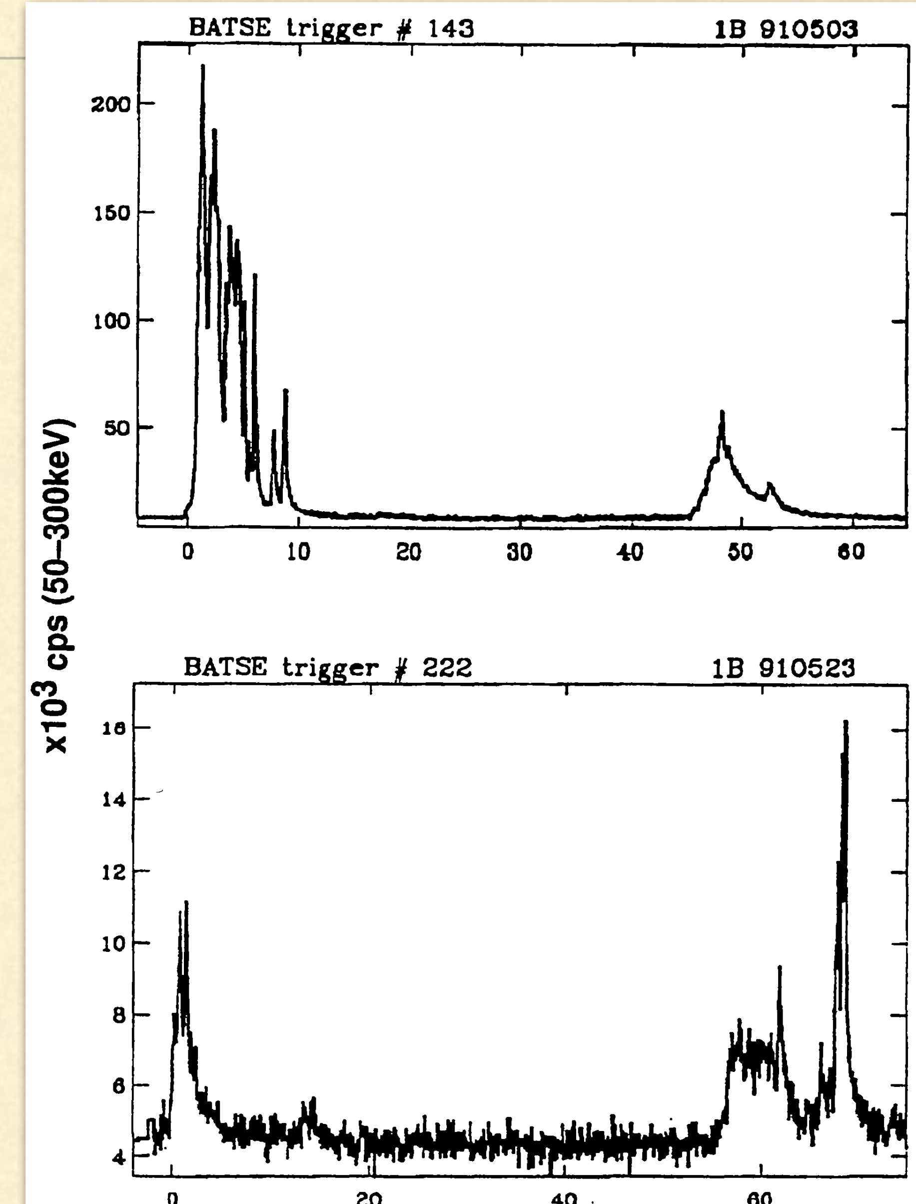

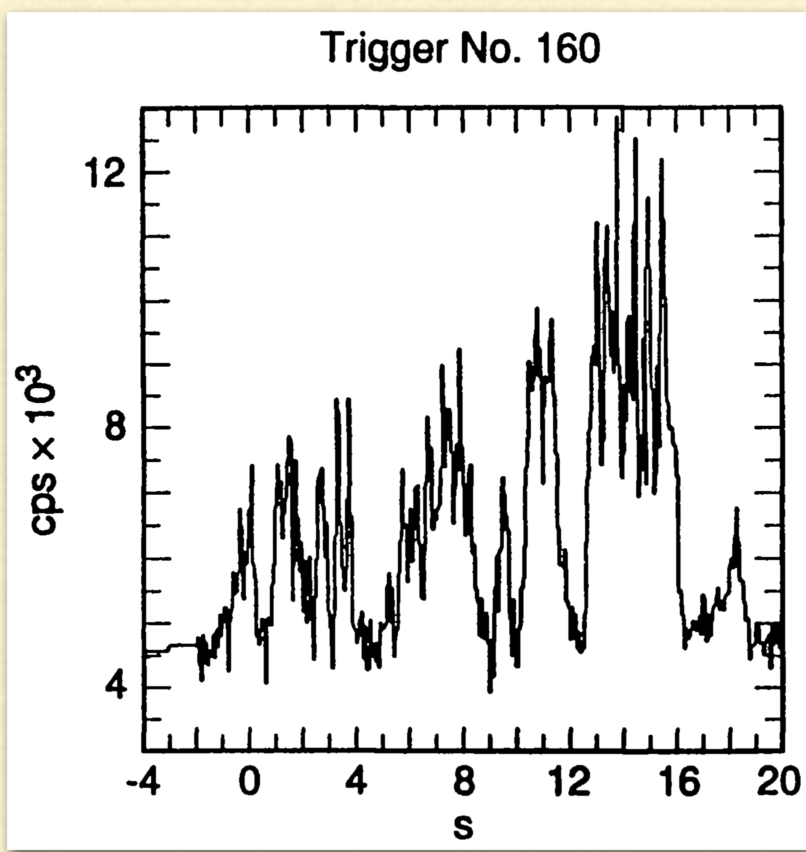

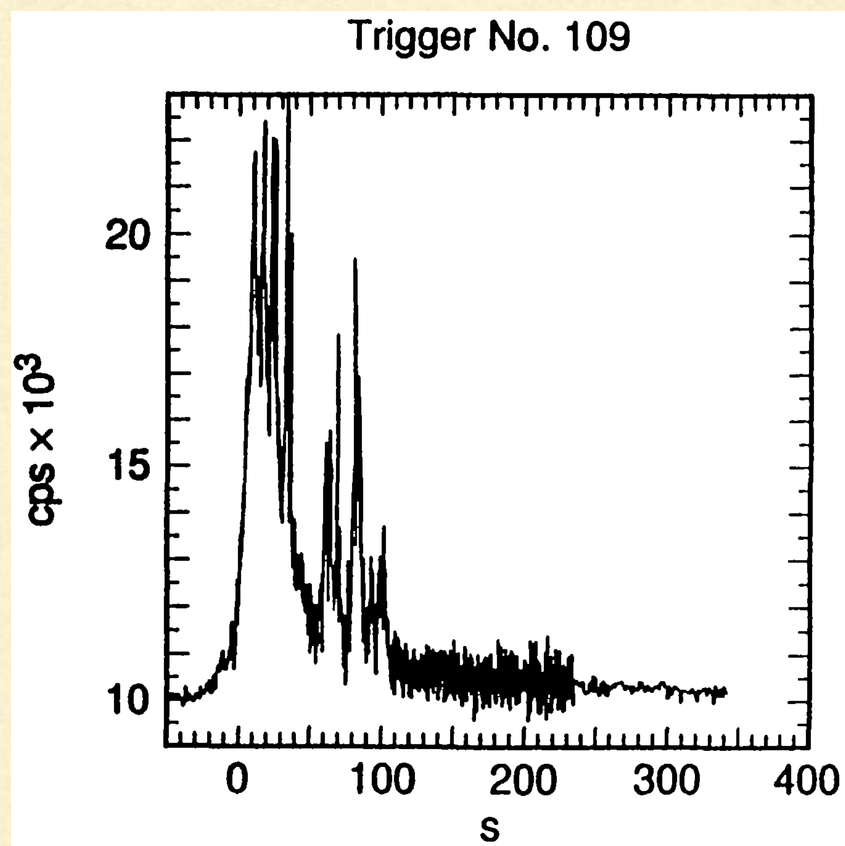

GRB con episodios de emisión distintos y bien separados.

Exhiben relativamente largos períodos de tiempos entre picos donde no hay emisión detectable.

Perfiles temporales

La distribución de los tiempos de duración de los GRB parece ser *bimodal* (descubrimiento importante de BATSE).

➡ Los GRB pueden clasificarse de acuerdo a su duración:

- ✦ GRB cortos, con duración $T < 2$ seg.
- ✦ GRB largos, con $T \geq 2$ seg.

Se supone que esta dicotomía refleja una diferencia intrínseca en el mecanismo que genera ambas clases de eventos.

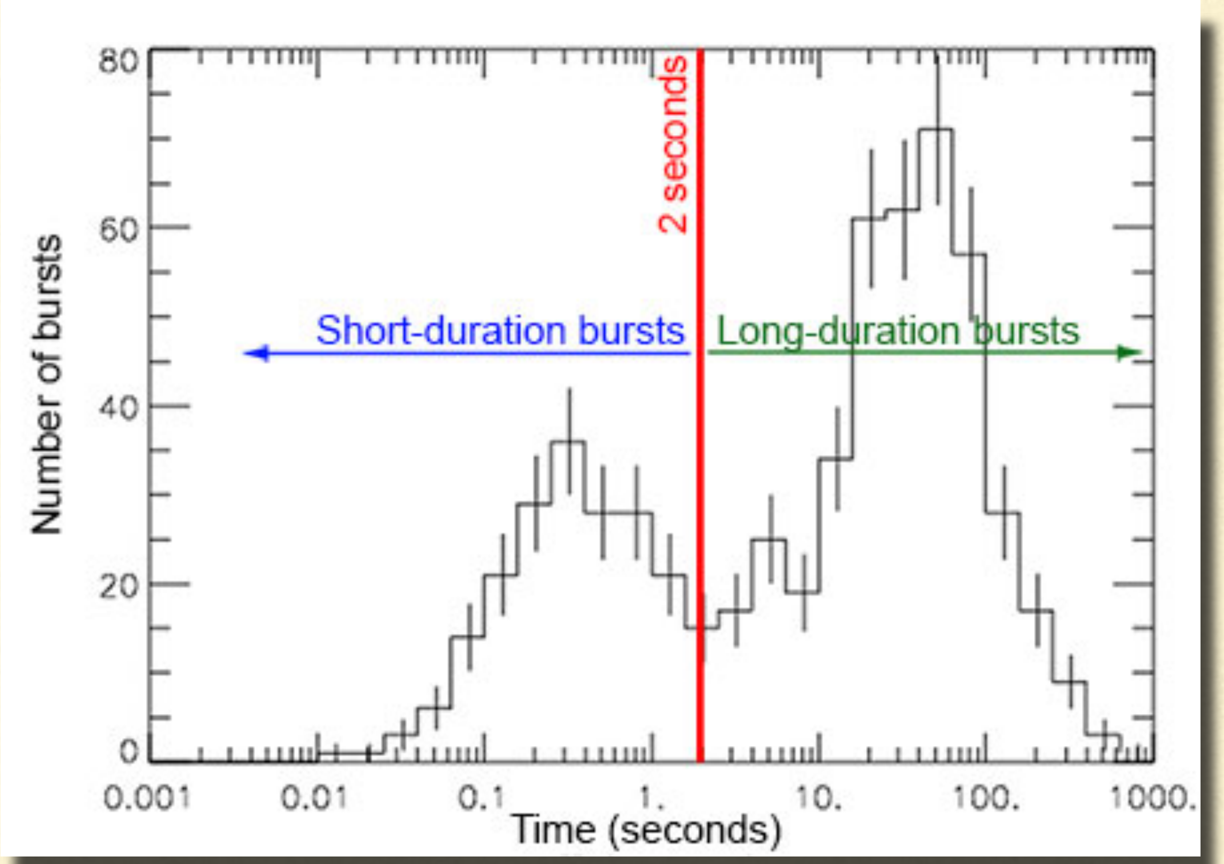

Propiedades espectrales

La energía de los fotones que caracterizan a los GRB esta típicamente en el rango que va de algunas decenas de keV a unos pocos MeV.
En algunos casos excepcionales se han observado fotones de hasta 10 GeV.

El espectro es claramente no térmico y puede representarse por (Band et al. 1993):

$$n(E)dE = n_0 \begin{cases} AE^{-\alpha}e^{-(E/E_0)} & E < E_0 \\ BE^{\beta} & E > E_0 \end{cases}$$

con

$\alpha \in (\sim 0.1, \sim 1)$ índice espectral (bajas energías)

$\beta \in (\sim -2, -3)$ índice espectral (altas energías)

$E_0 \in (\sim 0.1, \sim 1)$ MeV energía de quiebre

Estos parámetros varían de brote a brote sin un valor universal.

La intensidad integrada en el tiempo T es de

$F \sim (0.1 - 10) \times 10^{-6}$ erg cm^{-2}

Ejemplo de un ajuste espectral.
El modelo es ajustado al espectro promedio del GRB 1B 911127.

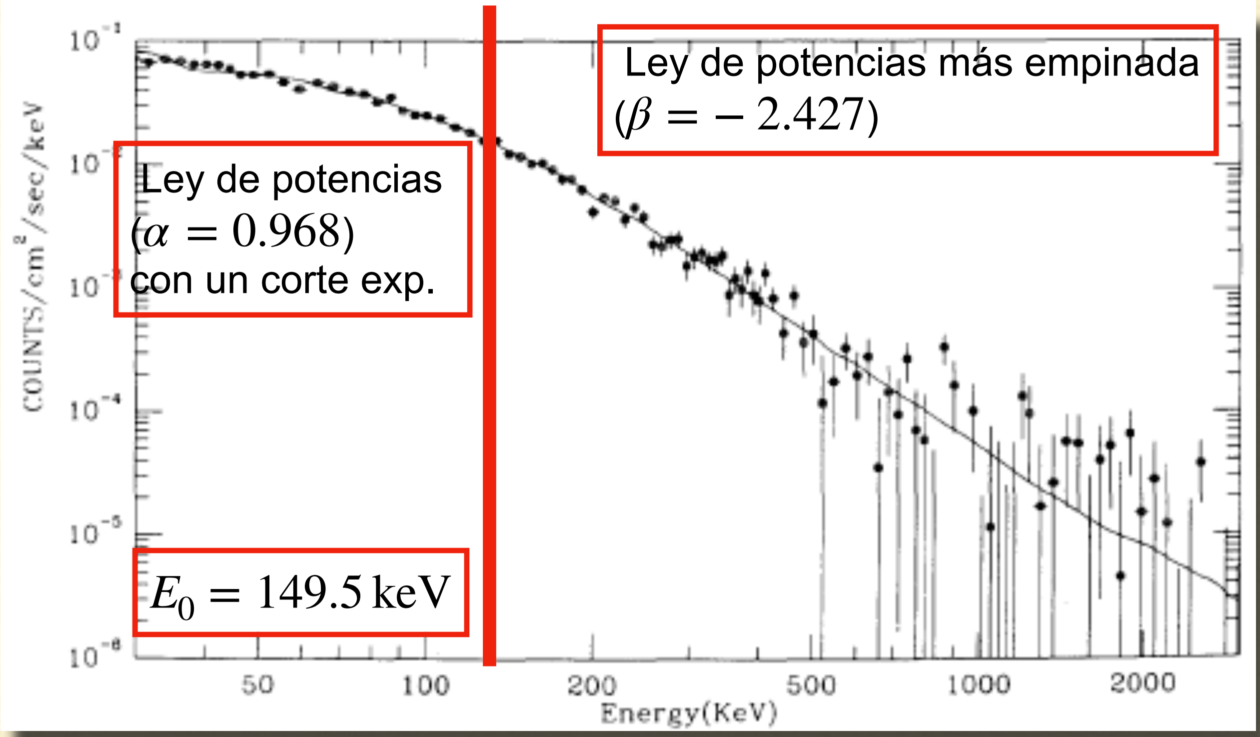

Band et al. ApJ, 413, 281 (1993); Apunte Introducción a la Astrofísica Relativista, G. E. Romero

Propiedades espectrales

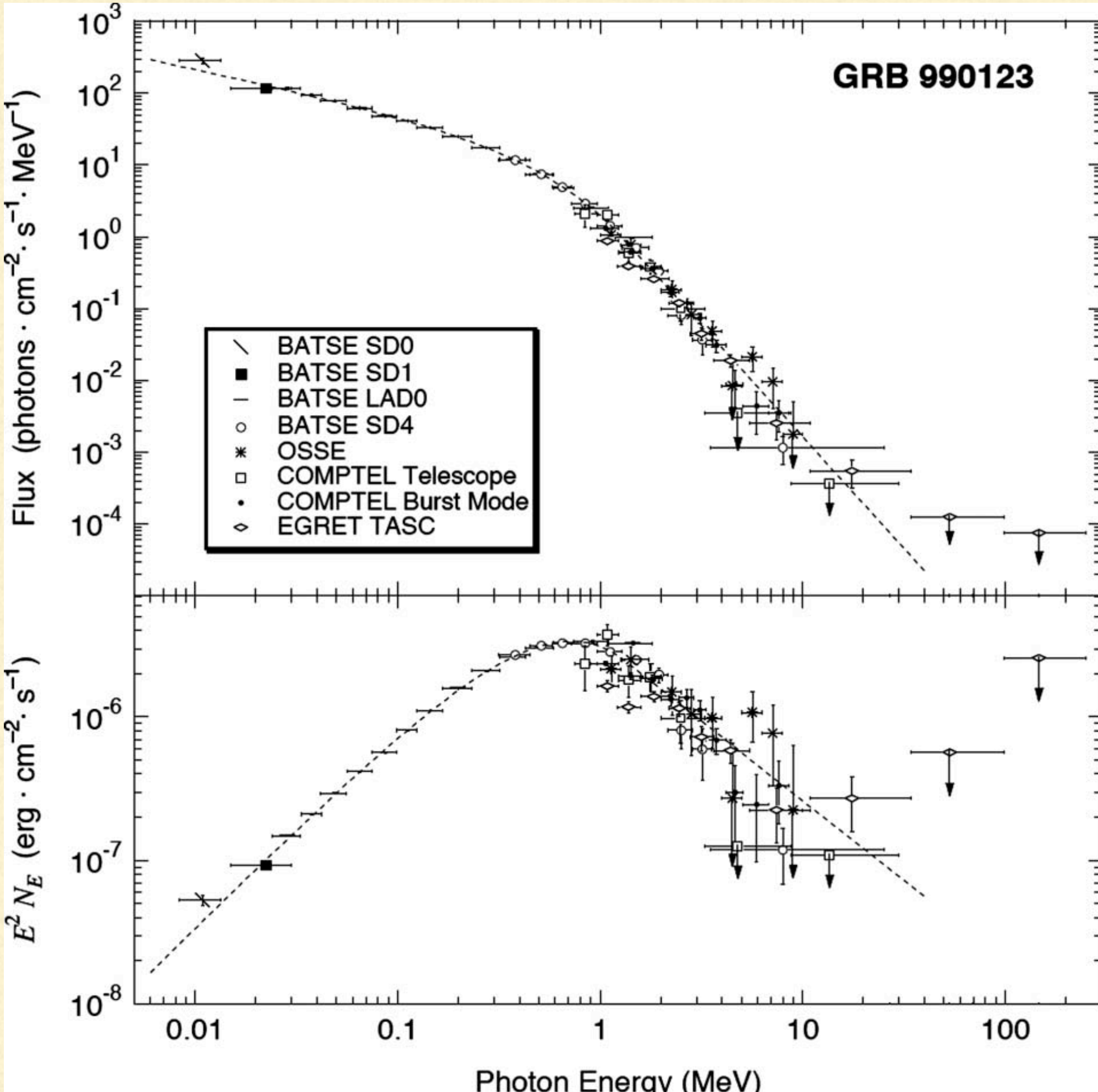

Ejemplo del ajuste al espectro de un GRB detectado por BATSE, mostrado

- como cuenta de fotones N_E,
- y en unidades in E^2N_E,
  where E es la energía de los fotones detectados.

La cantidad E^2N_E indica la cantidad de potencia emitida en una cierta banda de energía.

Distribución espacial

El instrumento BATSE mostró claramente que la distribución de los GRBs es **altamente isotrópica.**

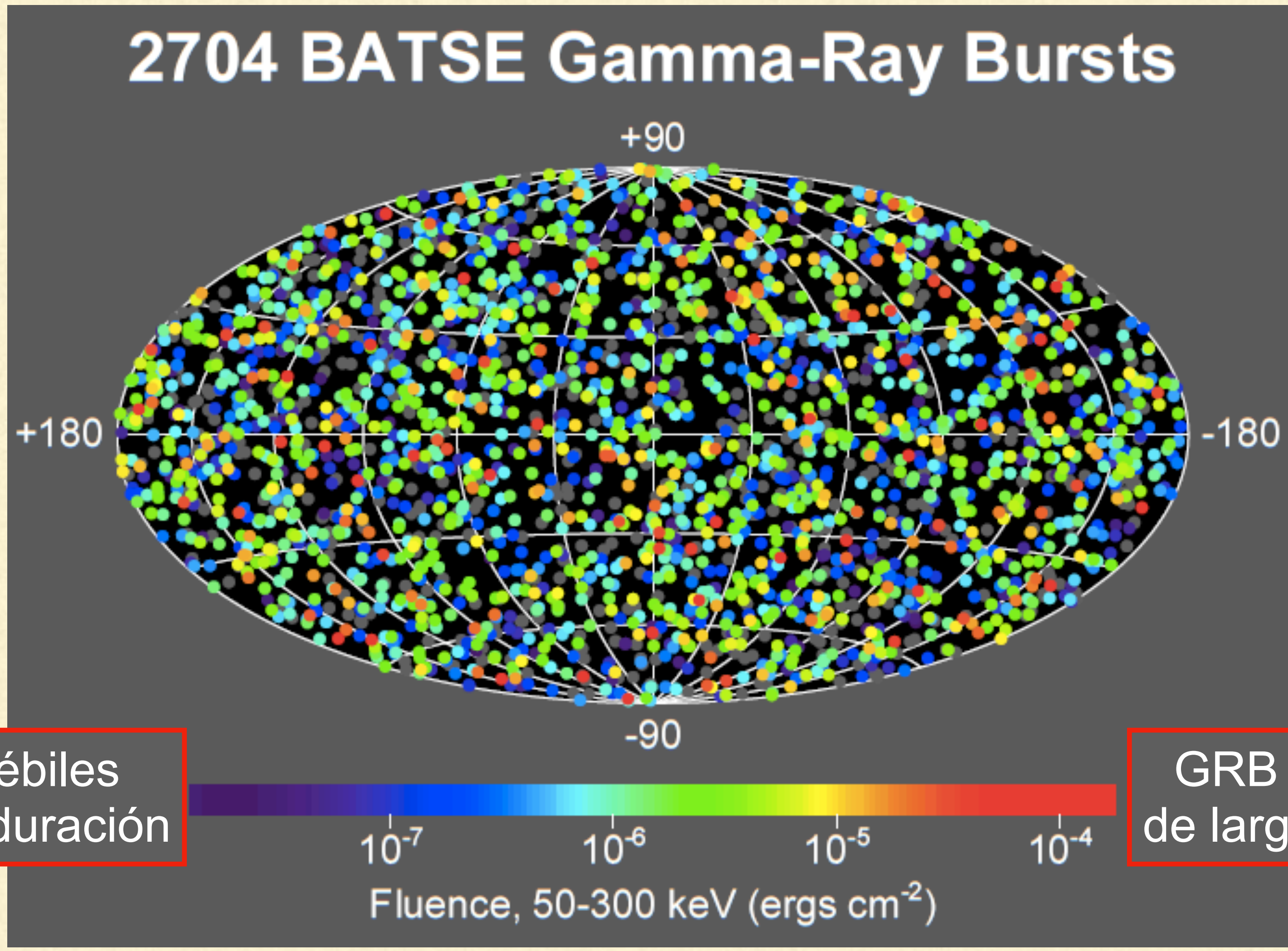

Distribución espacial de los GRB detectados por el instrumento BATSE.

Las ubicaciones de los brotes están codificadas por color de acuerdo a su fluencia (flujo de energía del brote integrado sobre la duración total del evento).

BATSE:

- Observaciones de GRB limitadas a rayos-γ
- No eran posibles observaciones subsiguientes (*follow-up*) al brote en otras longitudes de onda.

Ubicaciones de los GRB tenían cajas de error de unos pocos grados: contenían un gran número de posibles contrapartidas a bajas energías.

Contrapartidas a bajas energías

Descubrimiento de post-luminicencia (*afterglow*) en rayos-X de un GRB (28/02/97) por el satélite BeppoSAX:

- observatorio espacial de rayos X, 30/04/96 - 29/04/03, 1 a 200 keV;
- detección de eventos transitorios en el rango entre 2 a 30 keV;
- Combinación de instrumentos (*Gamma-Ray Burst Monitor* y 2 *Wide Field Cameras*) con capacidad para detectar GRB y posicionarlos rápidamente (orden de arcmin) para posterior seguimiento.

→ Ocho horas después de GRB 970228, BeppoSAX detectó una fuente de rayos-X que se debilitaba, coincidente con el GRB (Costa et al. 1997).

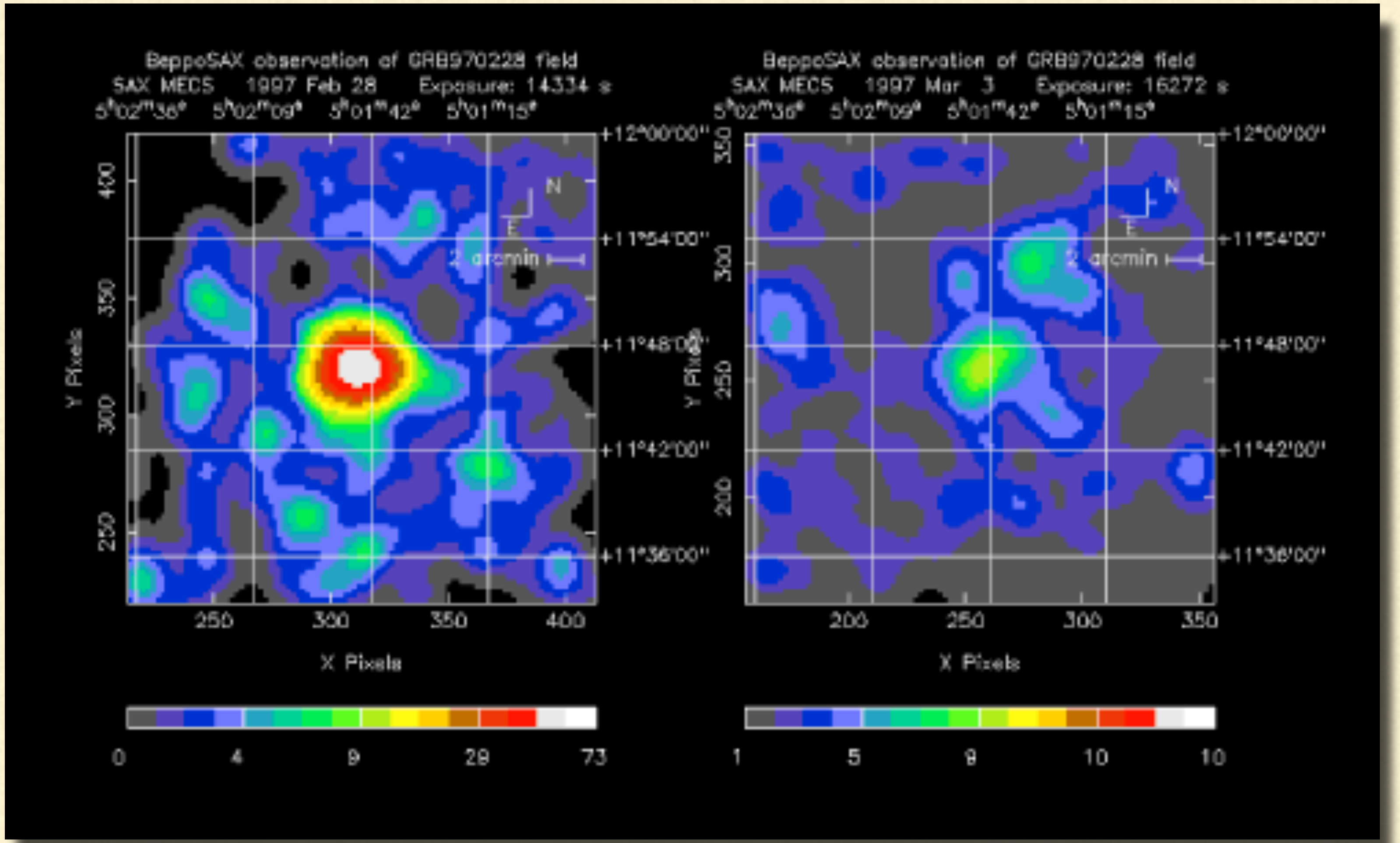

Flujo de la fuente, 1SAX J0501.7+114, detectada por Beppo-SAX dentro de la caja de error de GRB970228.
Izquierda: Observación original del brote el 28/02/97.
Derecha: fuente observada tres días después debilitada en un factor 20.

Cota et al., Nature, 387, 783 (1997); Mészáros, ARAA, 40, 137, (2002); Gomboc, Contemporary Physics, 53, 339 (2012)

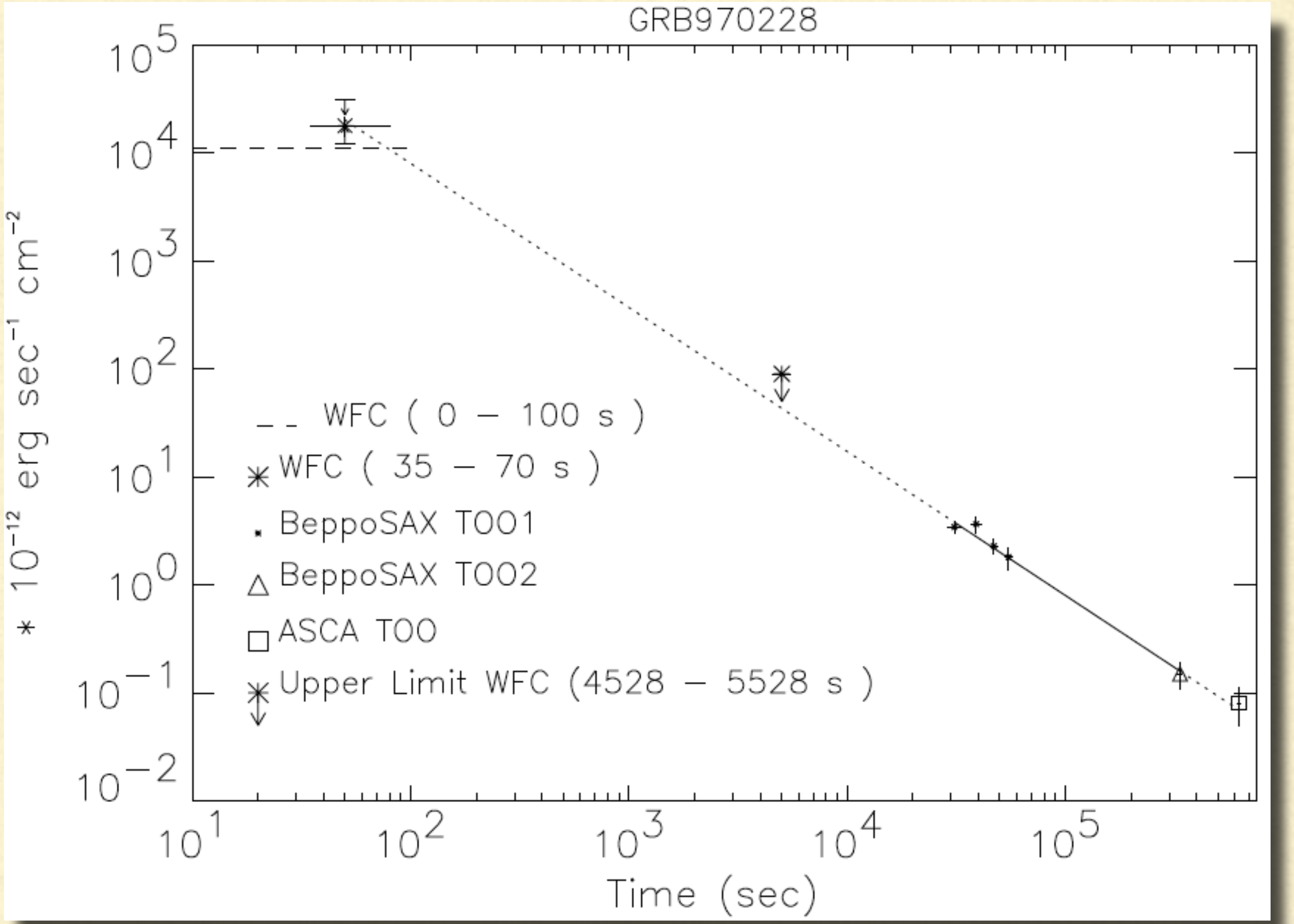

Flujo de la fuente 1SAX J0501.7+114 en función del tiempo en el rango 2-10 keV.

Los datos son ajustados por una ley de potencias ($\propto t^{-1.32}$; línea sólida).

La extrapolación hacia adelante en el tiempo es consistente con el flujo detectado por ASCA (Advanced Satellite for Cosmology and Astrophysics; 20/02/92 - 02/03/01).

Cota et al., Nature, 387, 783 (1997); Mészáros, ARAA, 40, 137, (2002); Gomboc, Contemporary Physics, 53, 339 (2012)

Contrapartidas a bajas energías

Estas detecciones en rayos-X, luego de 4-6 horas de la erupción en rayos-γ:

- permitieron obtener posiciones del orden del minuto de arco,
- facilitando la detección de la contrapartida en el óptico y del seguimiento de la post-luminicesnia de los GRB a longitudes de onda más largas.

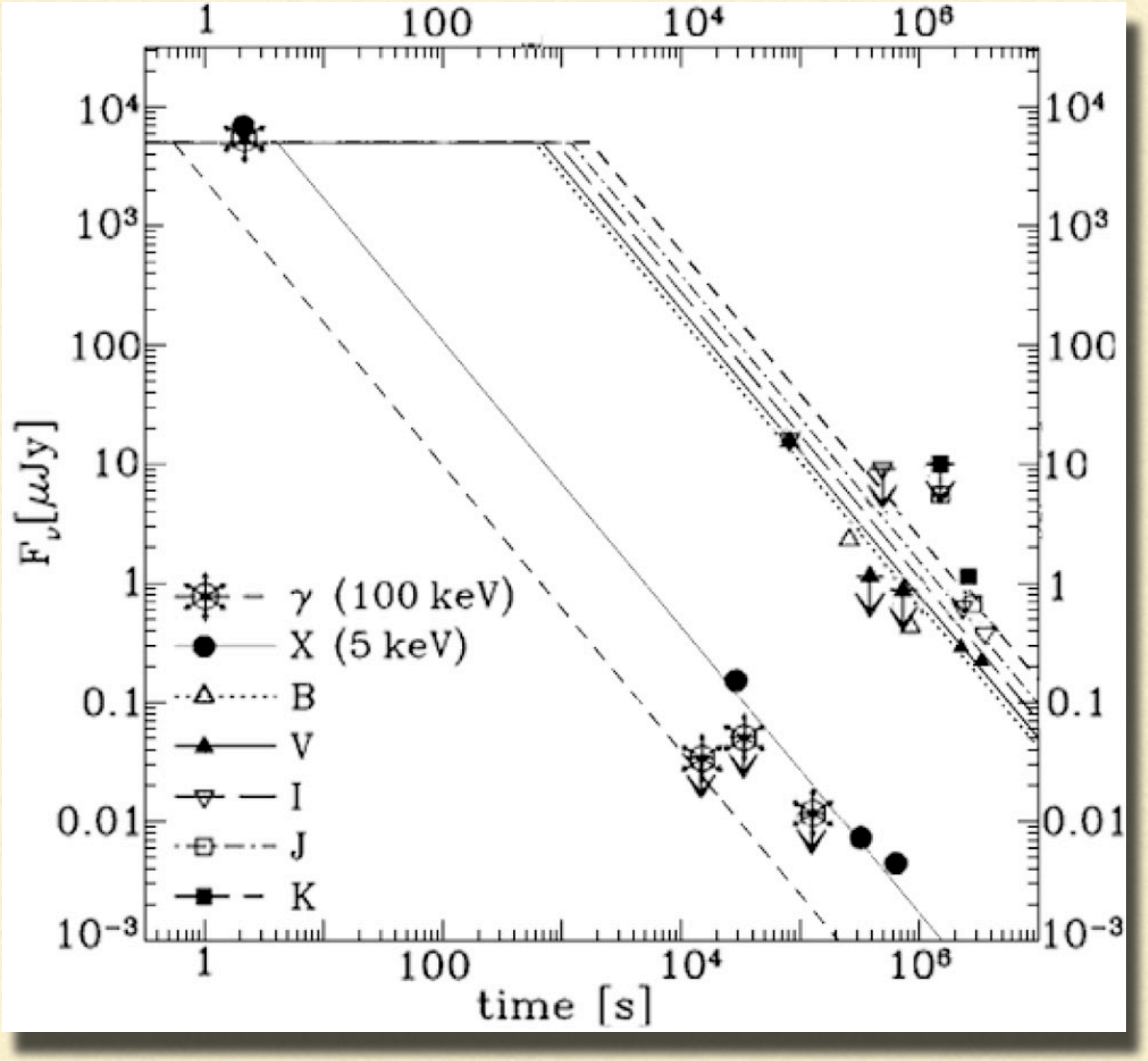

Curvas de luz de la post-luminiscencia de GRB970228 en bandas del óptico/infrarrojo.

Mészáros, ARAA, 40, 137, (2002)

Contrapartidas a bajas energías

✦ Detecciones de post-luminiscencia en rayos-X, óptico y radio.
✦ Las duraciones de los eventos son mayores a energías mas bajas,
✦ Las contrapartidas son variables y su intensidad decae como leyes de potencia: $F_\nu \propto t^{-\alpha}$ $(\alpha = 1.1 - 2.1)$

✦ La detección de post-luminiscencia en el óptico permitió:
- determinar con precisión la posición de los GRB y
- realizar observaciones espectroscópicas con grandes telescopios.

↓

Identificación de galaxias anfitrionas.
Medición de sus corrimientos al rojo (*redshifts*):
confirmación de que los GRB se encuentran a distancias cosmológicas.

Gomboc, Contemporary Physics, 53, 339 (2012)
Apunte Introducción a la Astrofísica Relativista, G. E. Romero

Distribución de corrimientos al rojo

El telescopio Swift permitió realizar observaciones de alta calidad de cientos de GRBs, con mejor cobertura temporal y de multi-banda de la post-luminiscencia.

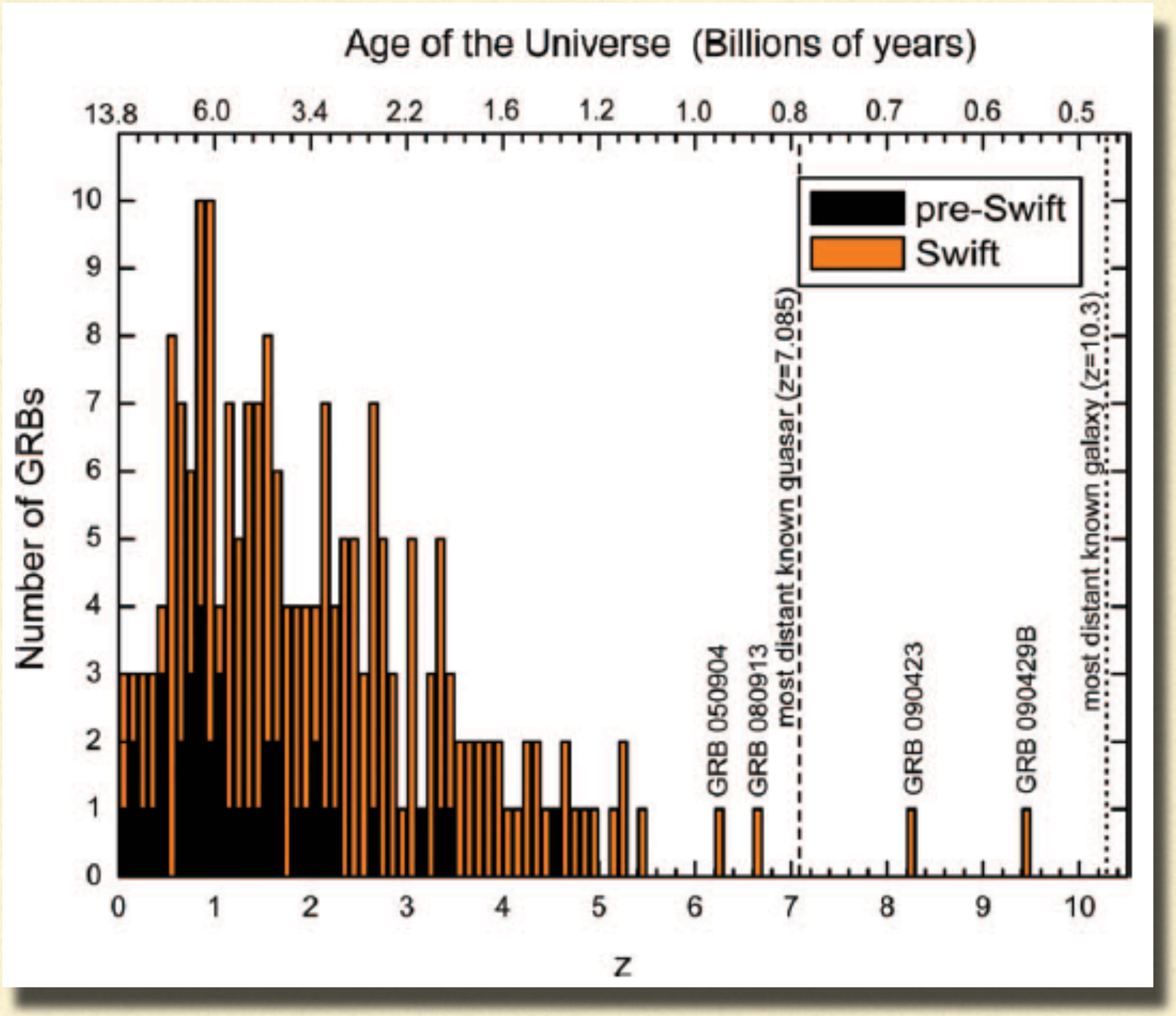

Distribución de redshifts de GRB
antes de la era Swift: $< z > \sim 1.4$,
y después de la era Swift: $< z > \sim 2.1$
(hasta 2012).

Diferencias debidas a la mayor sensibilidad de Swift (en comparación con BeppoSAX y HETE-2).

La mayoría de los redshifts de GRB fueron determinados usando observaciones espectroscópicas de post-luminiscencia en el óptico y de galaxias anfitrionas

→ la muestra presenta una tendencia (*bias*) a GRB ópticamente brillantes.

Gomboc, Contemporary Physics, 53, 339 (2012)

Galaxias anfitrionas

La observación directa de la galaxias anfitrionas de GRB revelan propiedades sobre los entornos en los que tienen lugar los brotes:

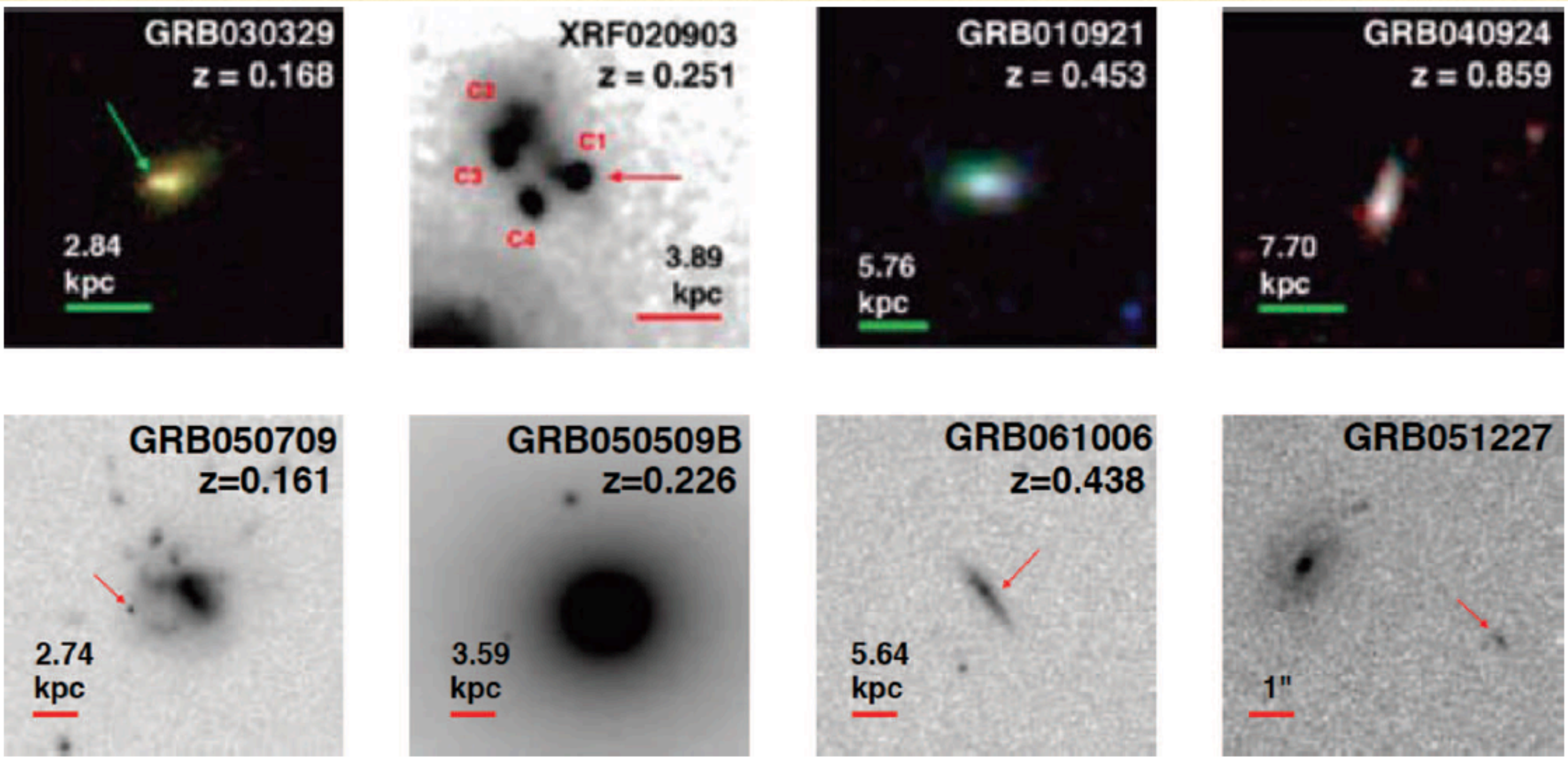

Selección de galaxias anfitrionas de GRB largos (arriba; Wainwright et al. 2007) y GRB cortos (abajo; Fox et al 2005), observadas por el Hubble Space Telescope.
Se eligieron pares de galaxias anfitrionas de GRB cortos y largos con redshifts comparables. Las flechas señalan la ubicación del brote.

Gomboc, Contemporary Physics, 53, 339 (2012)

Galaxias anfitrionas

Propiedades de galaxias anfitrionas de:

✦ GRB largos

- Galaxias mayormente débiles, azules e irregulares,
- de baja masa, con formación estelar,
- y bajas metalicidades.

✦ GRBs cortos

- Galaxias con luminosidades y metalicidades más altas.
- Algunas galaxias son viejas y masivas sin formación estelar reciente, pero la mayoría son galaxias con formación estelar.

Una comparación detallada entre las galaxias anfitrionas de GRB cortos y GRB largos revela diferencias sistemáticas, y las pruebas estadísticas muestran que no pertenecen a la misma población de galaxias.

Gomboc, Contemporary Physics, 53, 339 (2012)

Modelos para progenitores de GRB

El mecanismo que produce la liberación de la energía en forma de radiación está oculto por la "bola de fuego", que es opaca en su estado inicial.

Modelos más aceptados para progenitores de GRB:

★ GRB largos: modelo de *collapsar* → colapso de estrellas muy masivas

★ GRB cortos: La fusión de objetos en sistemas binarios compactos (2 estrellas de neutrones; 1 estrella de neutrones y 1 agujero negro) de período ultracorto: hipótesis respaldada por la reciente detección de ondas gravitacionales con un patrón característico de fusión asociadas a un GRB.

$$l = \frac{L_\gamma}{R}, \quad [l] = \mathrm{erg\,s^{-1}\,cm^{-1}}$$

$$L_\gamma = 4\pi D^2 F$$

$$\gamma + \gamma \rightarrow e^+ + e^-$$

$$\tau_{\gamma\gamma} \approx \sigma_{\gamma\gamma} n_\gamma R = \frac{\sigma_{\gamma\gamma}}{4\pi c \langle E_\gamma \rangle} l$$

$$\tau_{\gamma\gamma} \sim 10^{14}$$

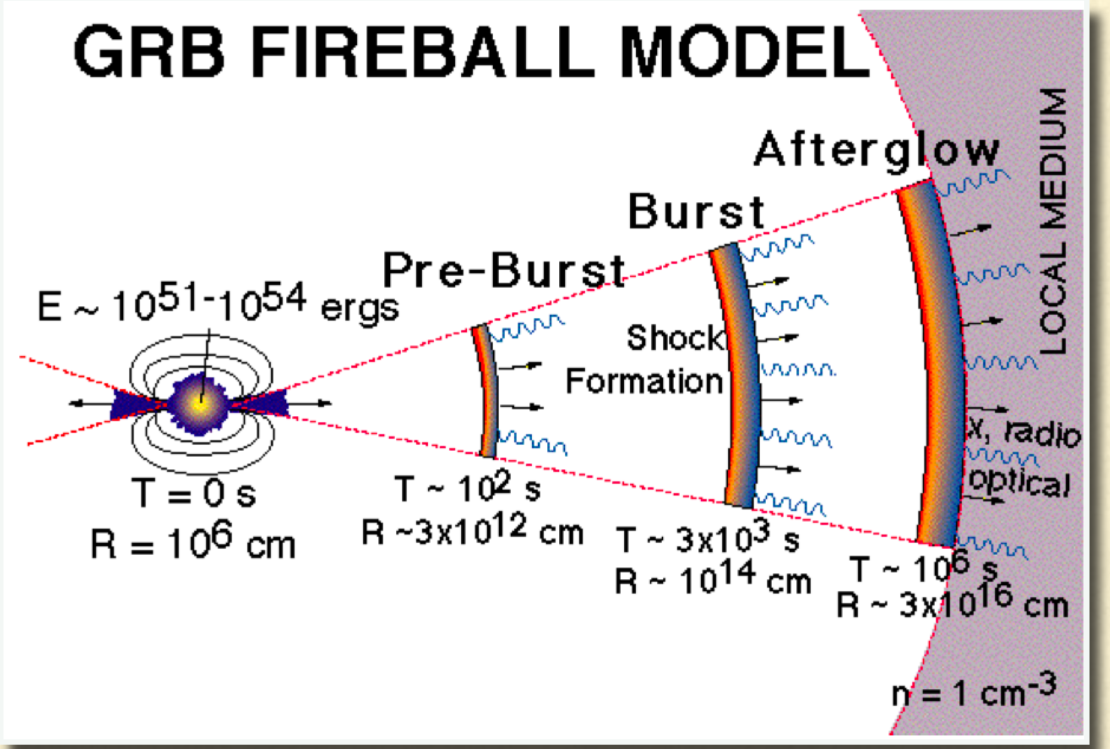

Gomboc, Contemporary Physics, 53, 339 (2012); Apunte Introducción a la Astrofísica Relativista, G. E. Romero

Gamma-ray bursts: Collapsar

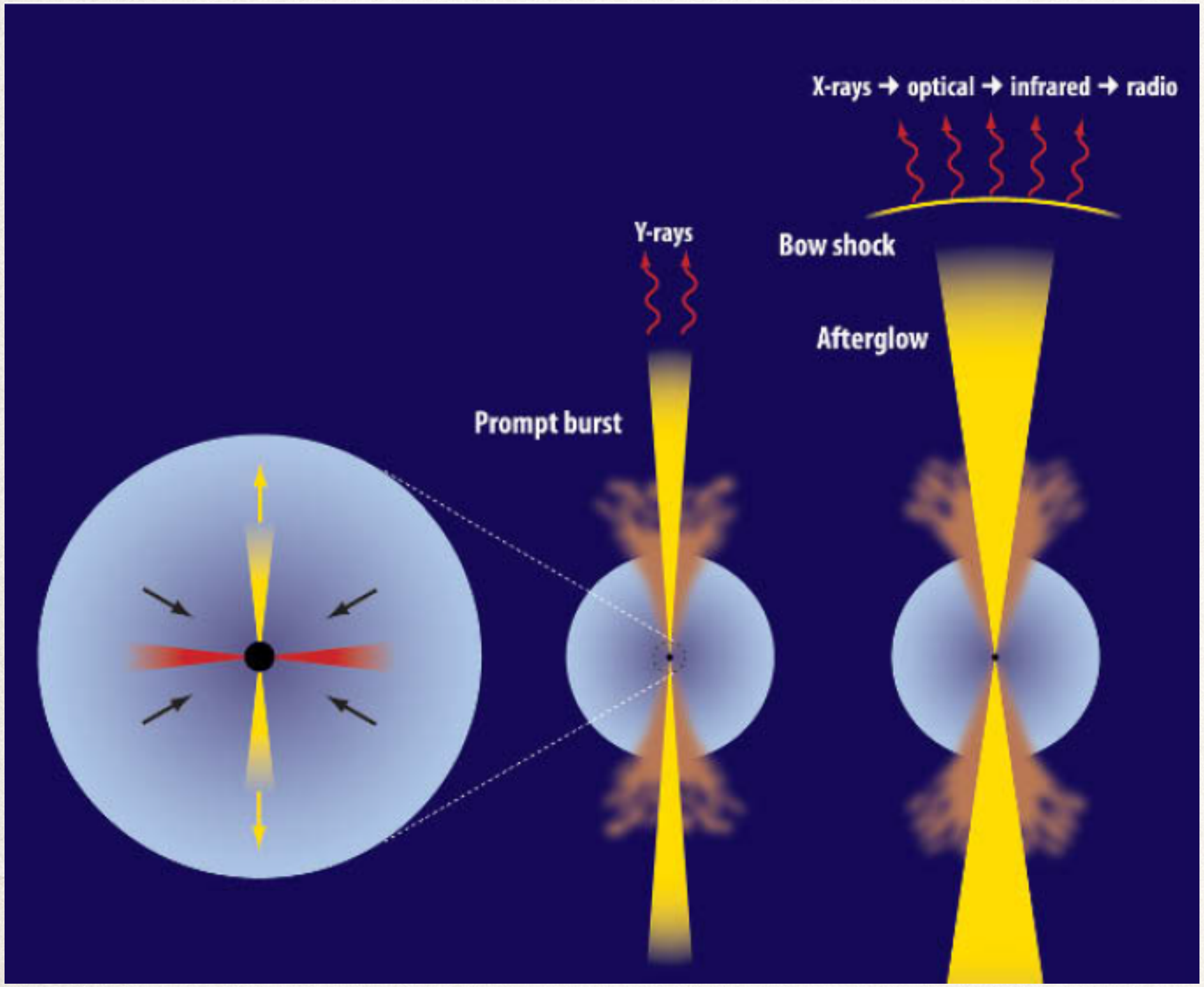

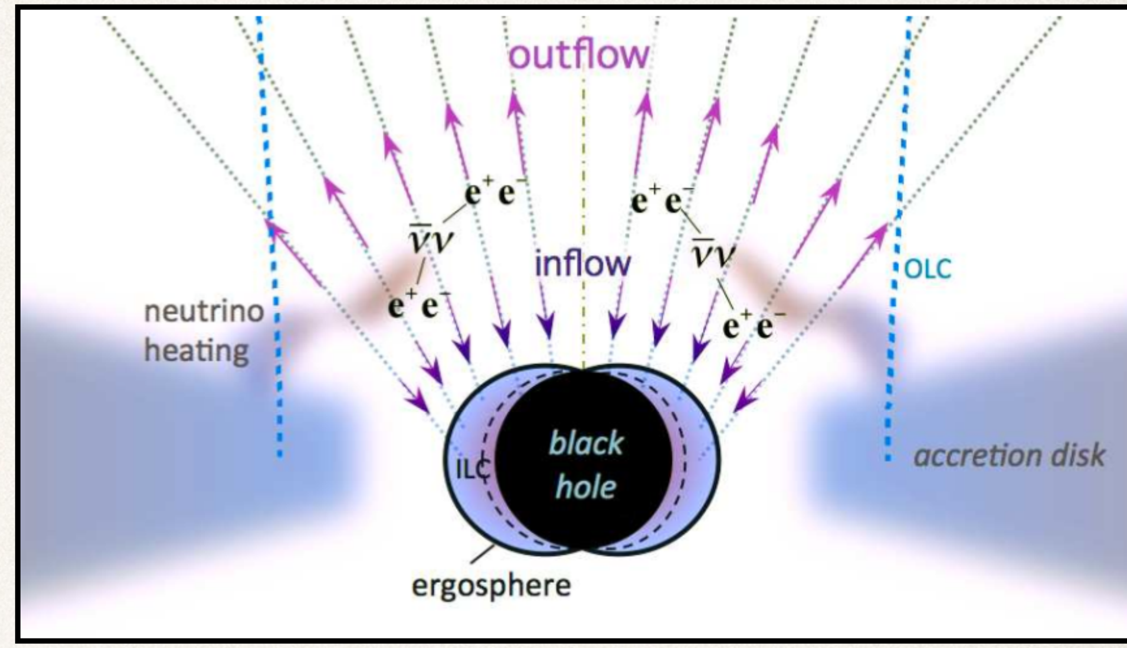

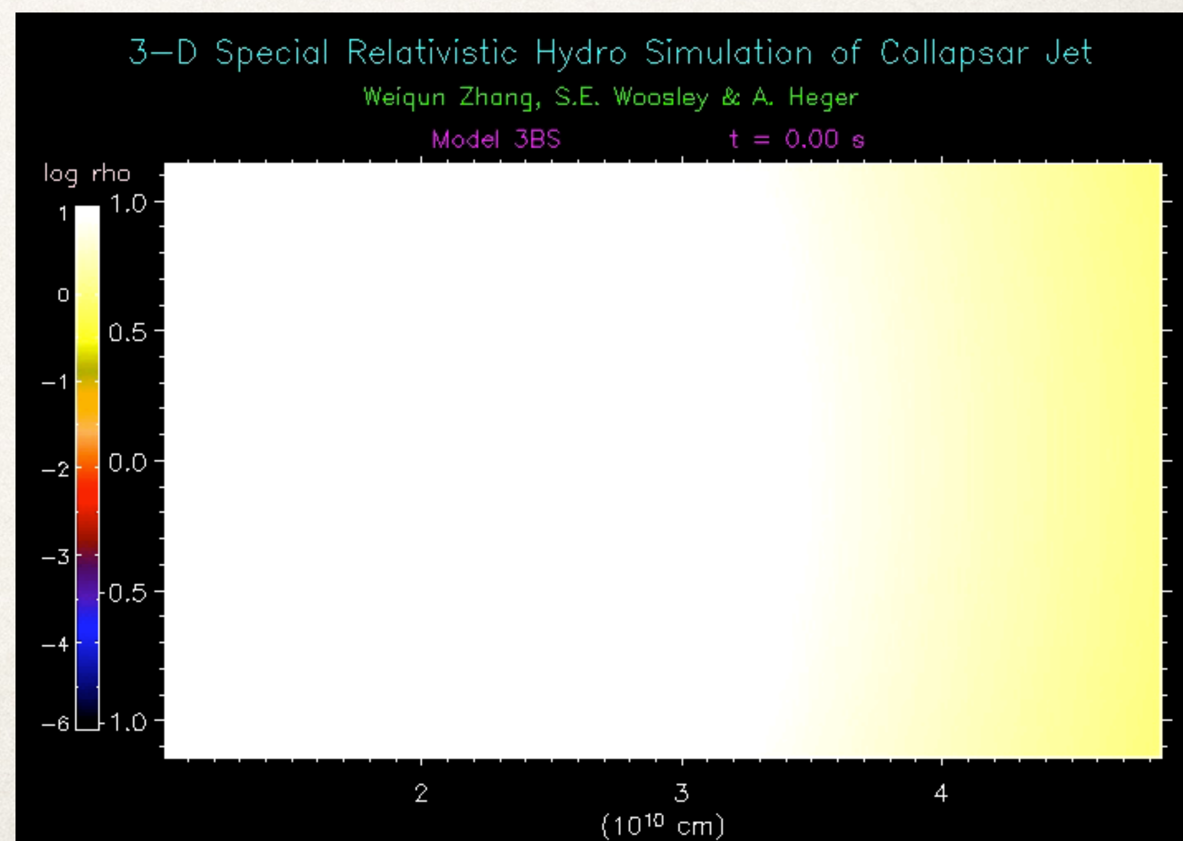

Pair load by neutrino annihilation

Neutron dragging?

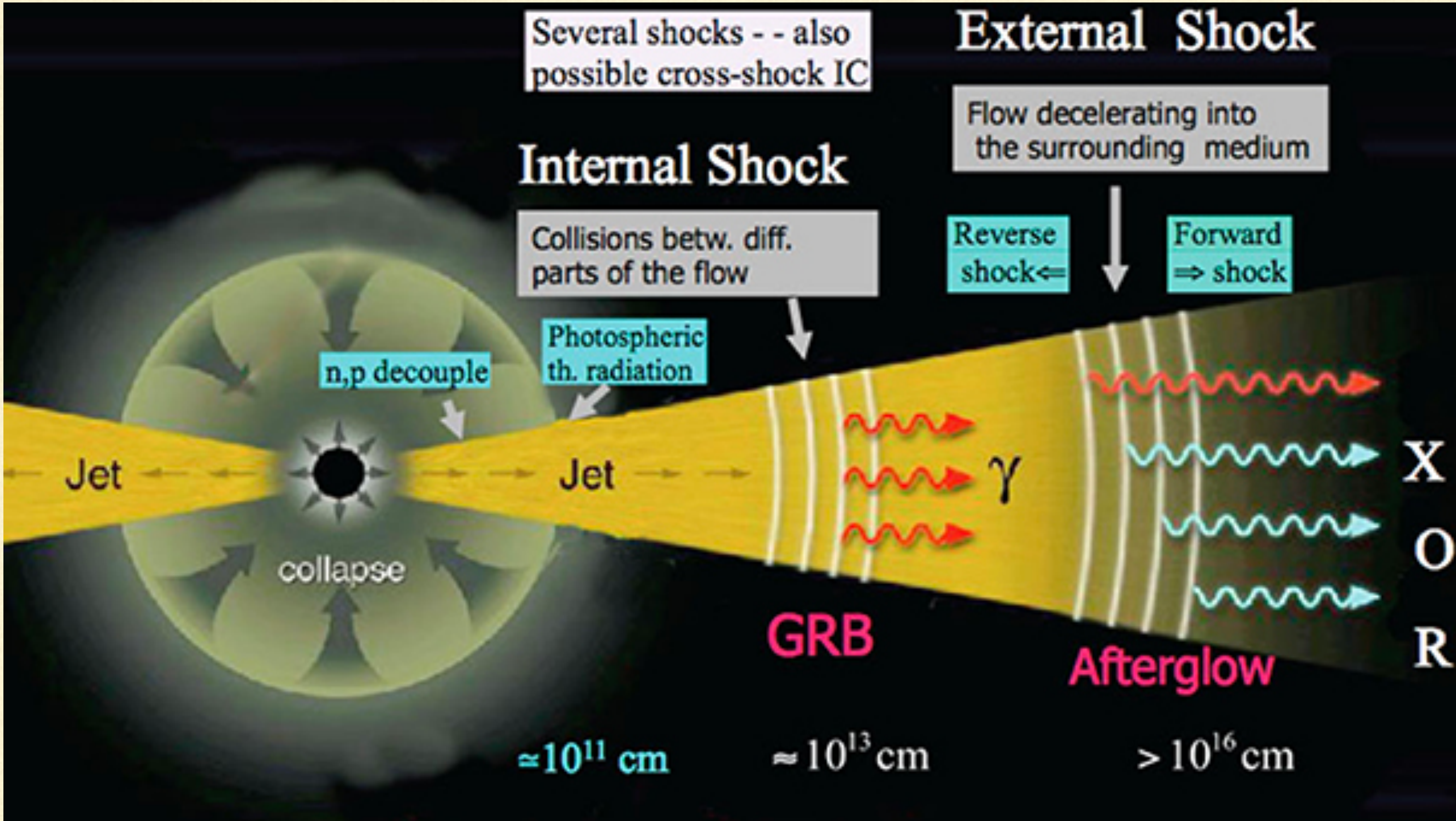
Several shocks - - also possible cross-shock IC
External Shock
Flow decelerating into the surrounding medium
Internal Shock
Collisions betw. diff. parts of the flow
Reverse shock⇐
Forward ⇒ shock
Photospheric th. radiation
n,p decouple
Jet
Jet
γ
X
O
R
collapse
GRB
Afterglow
≃10^11 cm
≈10^13 cm
>10^16 cm

sigma (magnetization) < 1 → shocks
if sigma > 1, the fluid is incompressible
and shocks are suppressed

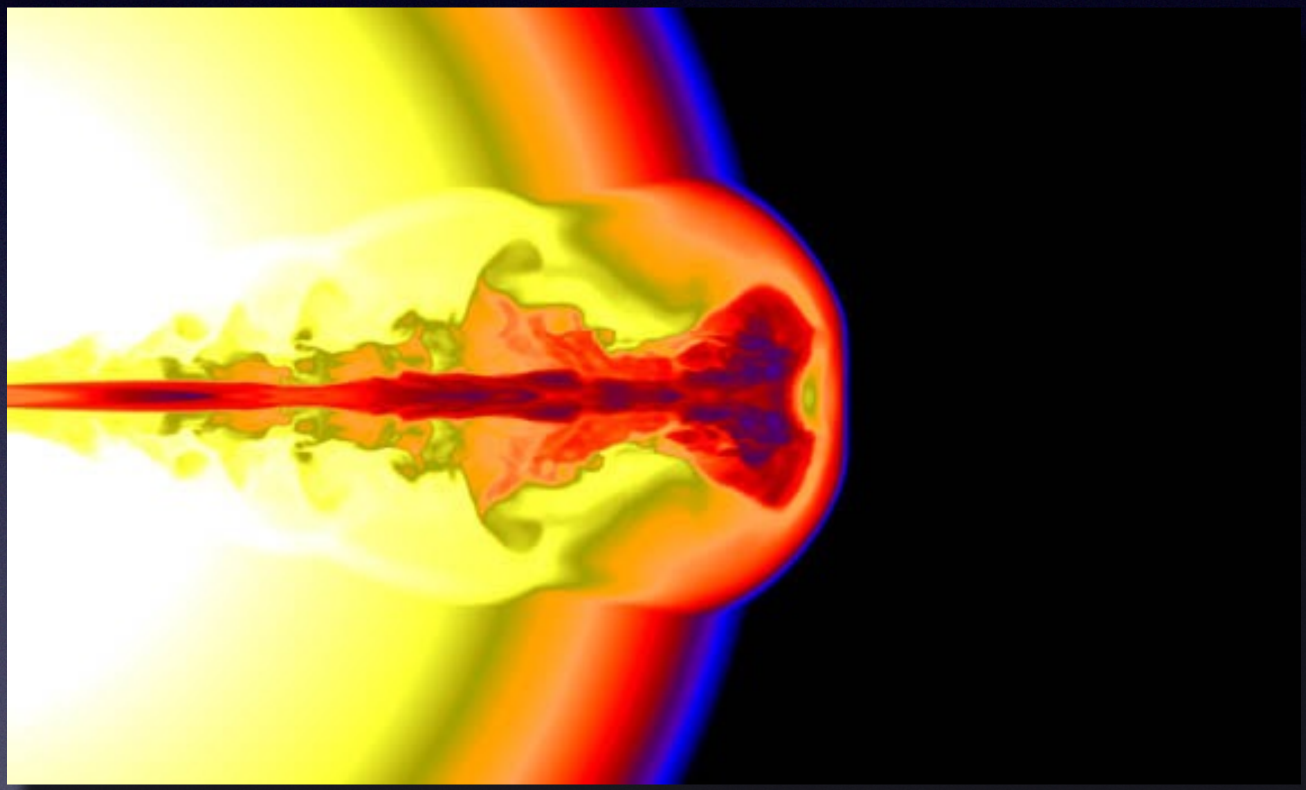

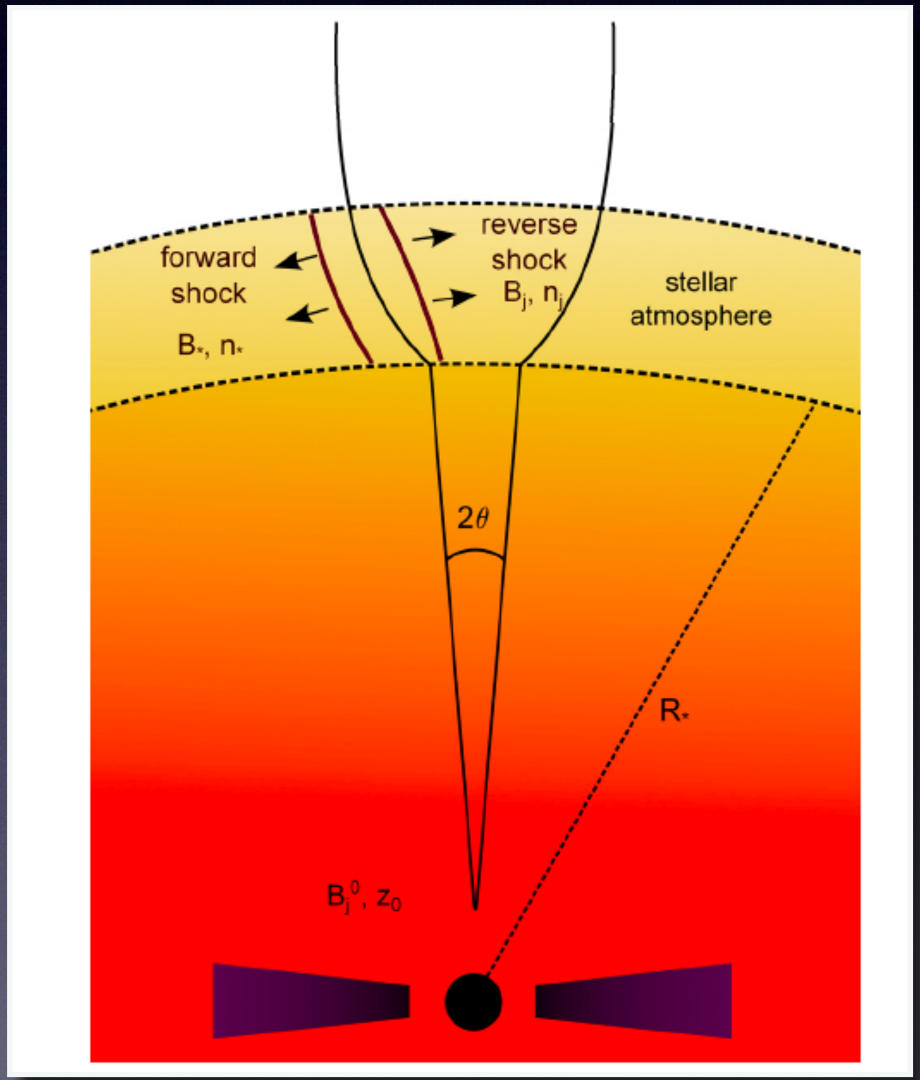

Vieyro, Romero & Peres 2013, A&A

GRB cortos

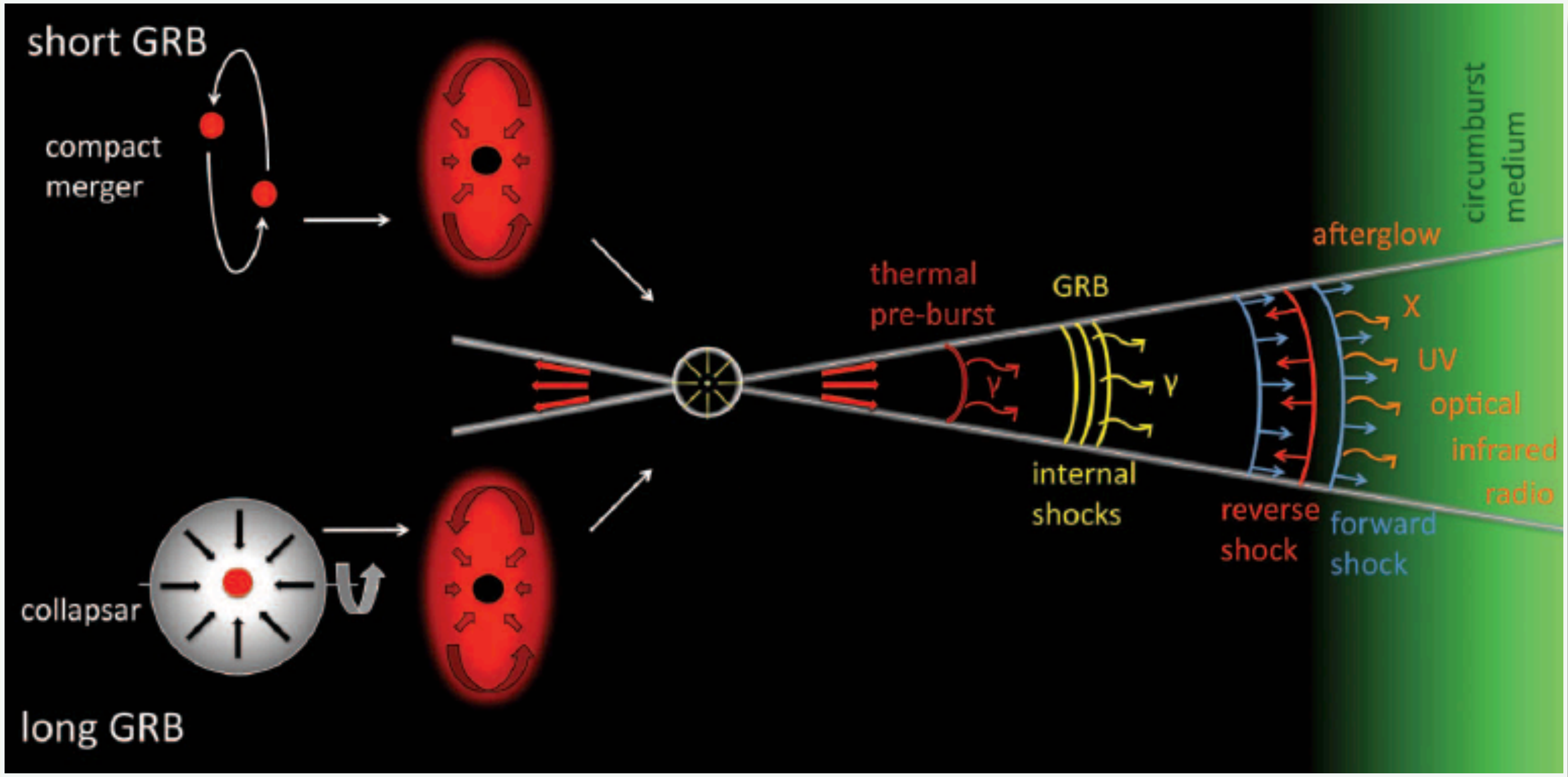

short GRB
compact
merger
collapsar
long GRB
thermal
pre-burst
GRB
γ
γ
internal
shocks
reverse
shock
forward
shock
afterglow
circumburst
medium
X
UV
optical
infrared
radio

GRB cortos

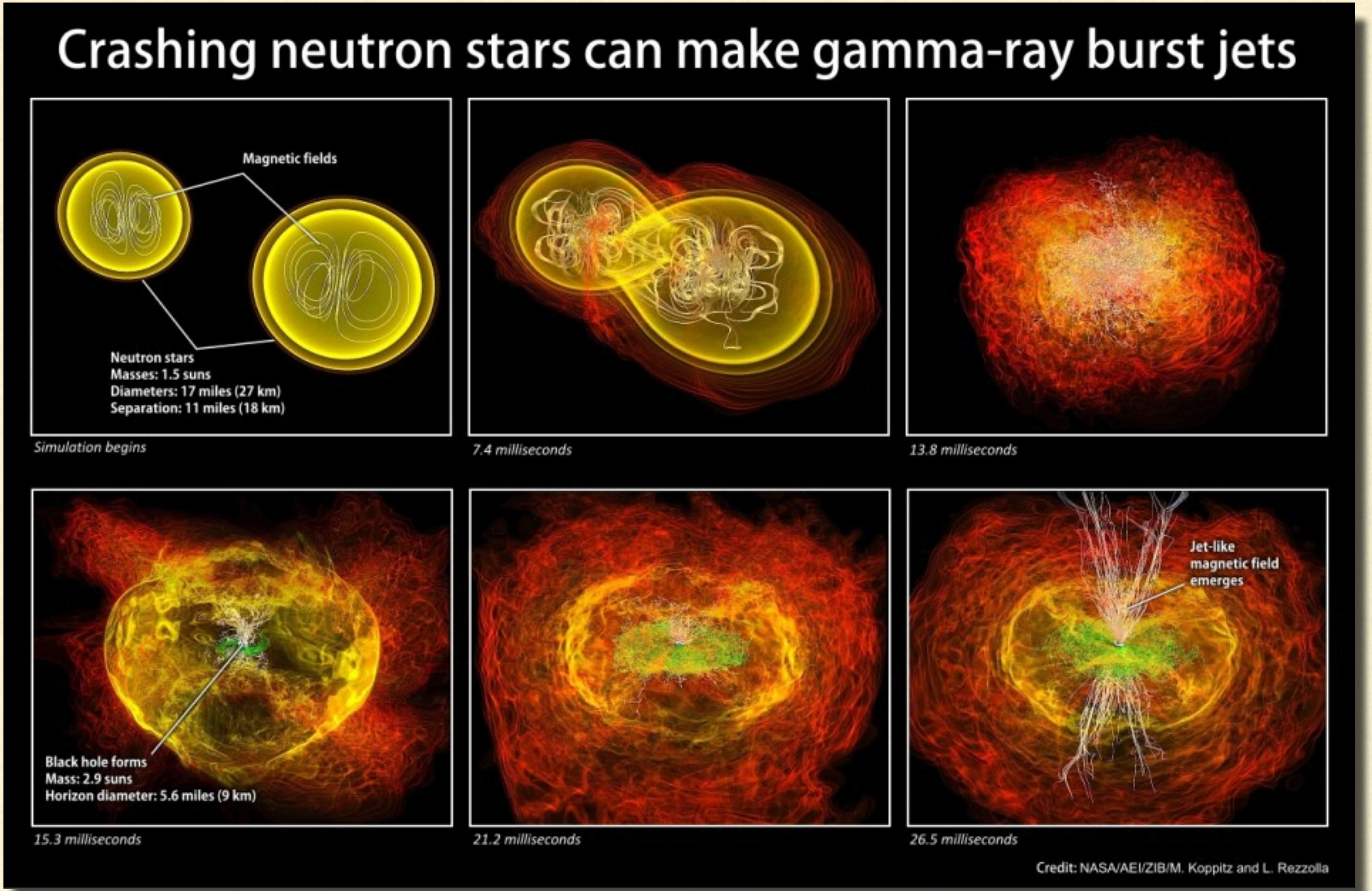
Crashing neutron stars can make gamma-ray burst jets
Magnetic fields
Neutron stars
Masses: 1.5 suns
Diameters: 17 miles (27 km)
Separation: 11 miles (18 km)
Simulation begins
7.4 milliseconds
13.8 milliseconds
Black hole forms
Mass: 2.9 suns
Horizon diameter: 5.6 miles (9 km)
15.3 milliseconds
21.2 milliseconds
Jet-like
magnetic field
emerges
26.5 milliseconds
Credit: NASA/AEI/ZIB/M. Koppitz and L. Rezzolla

Neutrino cooled accretion disks

$$p + e^- \to n + \nu_e$$
$$p + \bar{\nu}_e \to n + e^+$$
$$p + e^- + \bar{\nu}_e \to n$$
$$n + e^+ \to p + \bar{\nu}_e$$
$$n \to p + e^- + \bar{\nu}_e$$
$$n + \nu_e \to p + e^-,$$

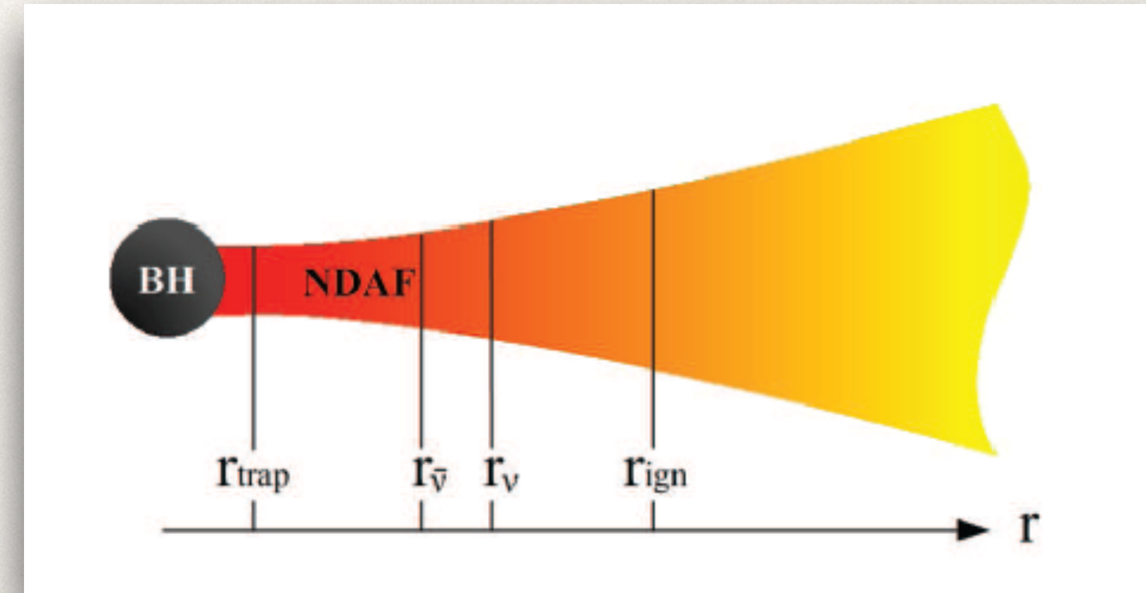

$$e^- + e^+ \to \nu_i + \bar{\nu}_i$$
$$n + n \to n + n + \nu_i + \bar{\nu}_i$$
$$\tilde{\gamma} \to \nu_e + \bar{\nu}_e.$$

$$p = p_{gas} + p_{rad} + p_e + p_\nu.$$

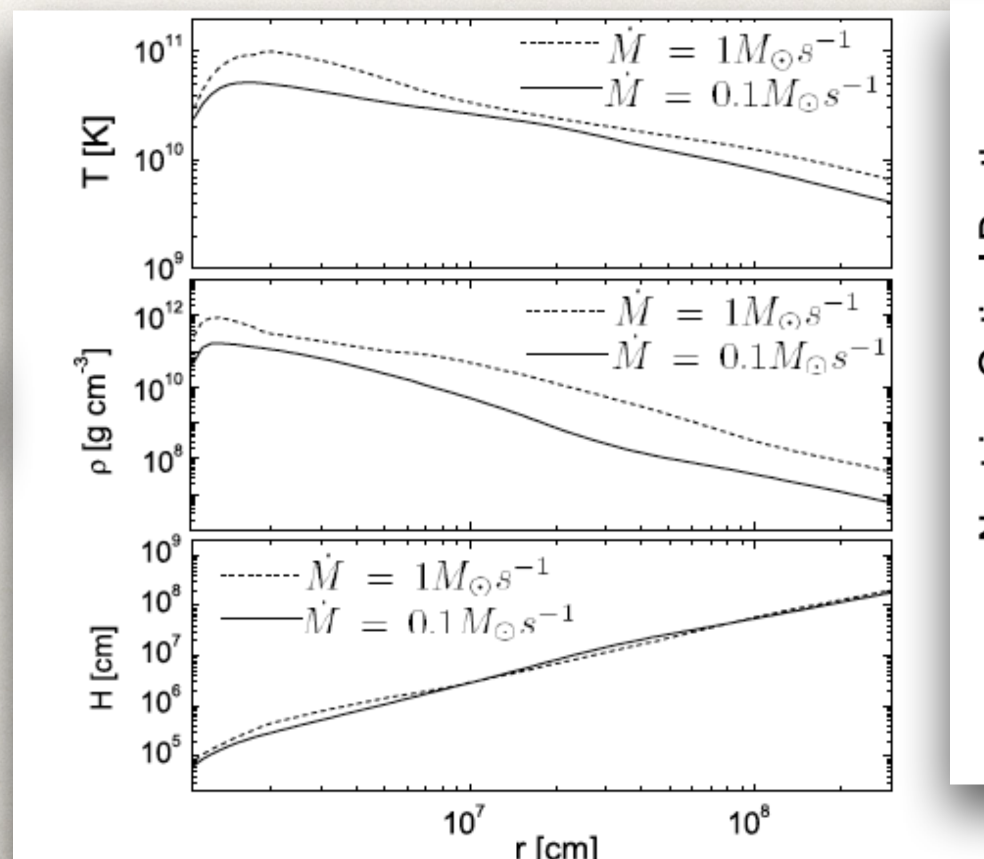

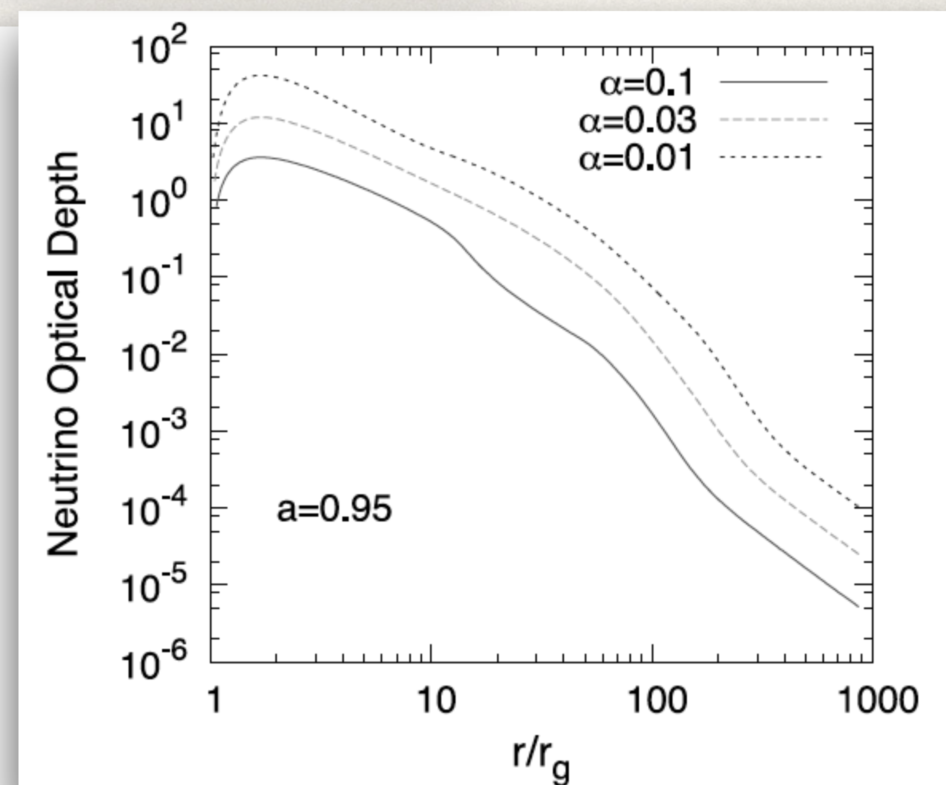

Simulations

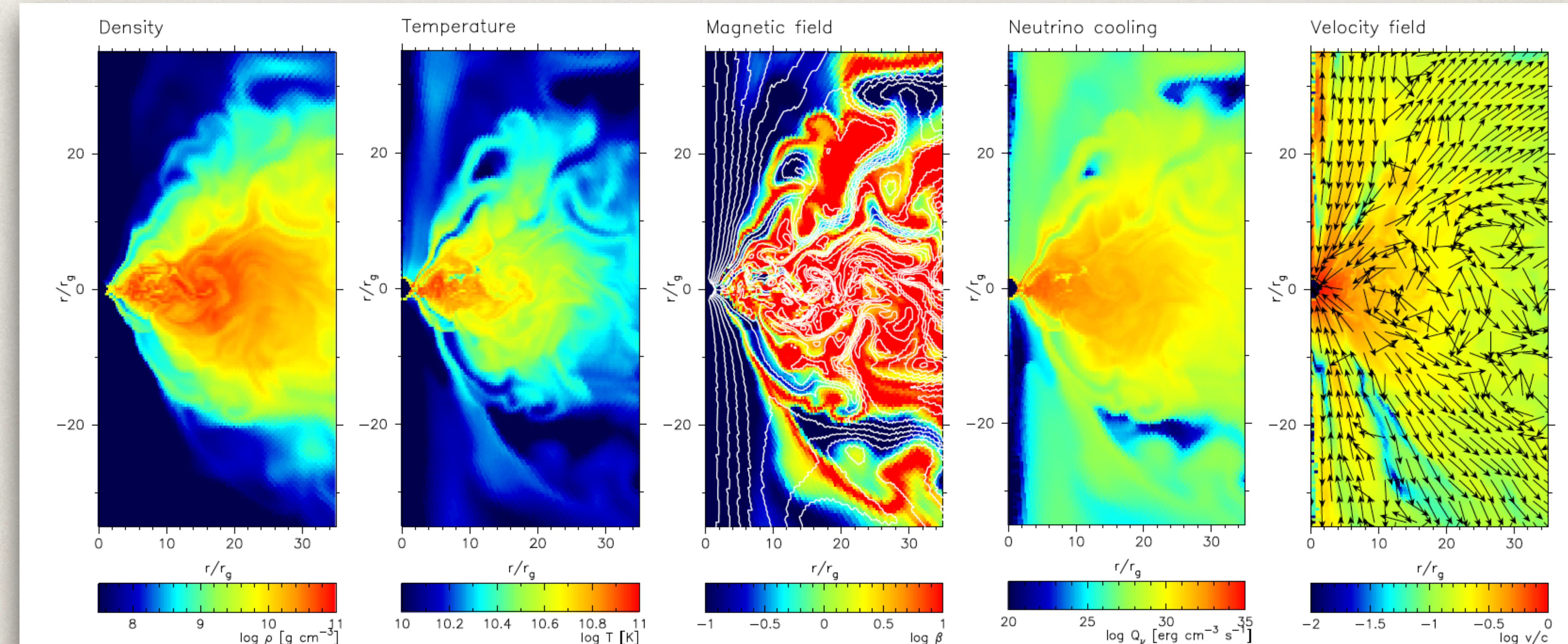

Parameters of the model: black-hole mass $M_{BH} = 3\ M_\odot$, torus mass $M_t = 0.1\ M_\odot$, and BH spin $a = 0.6$.

ß= P_{gas}/P_{mag}

Janiuk 2017

Neutrino cooled accretion disks

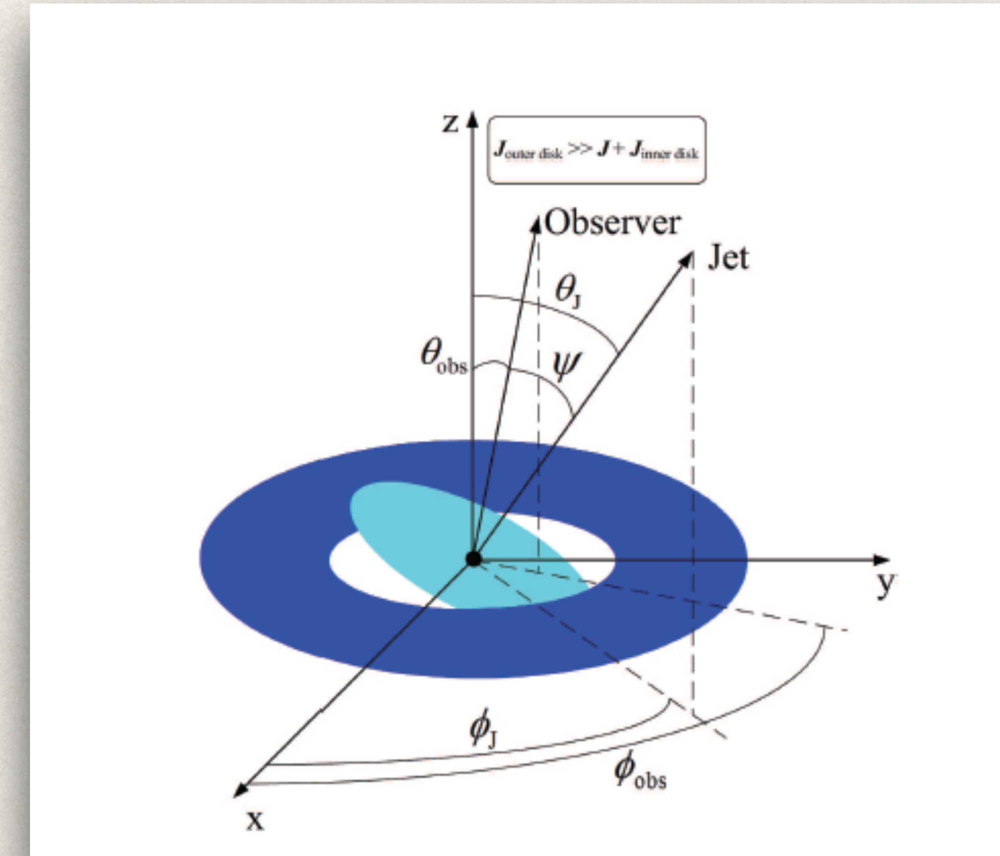

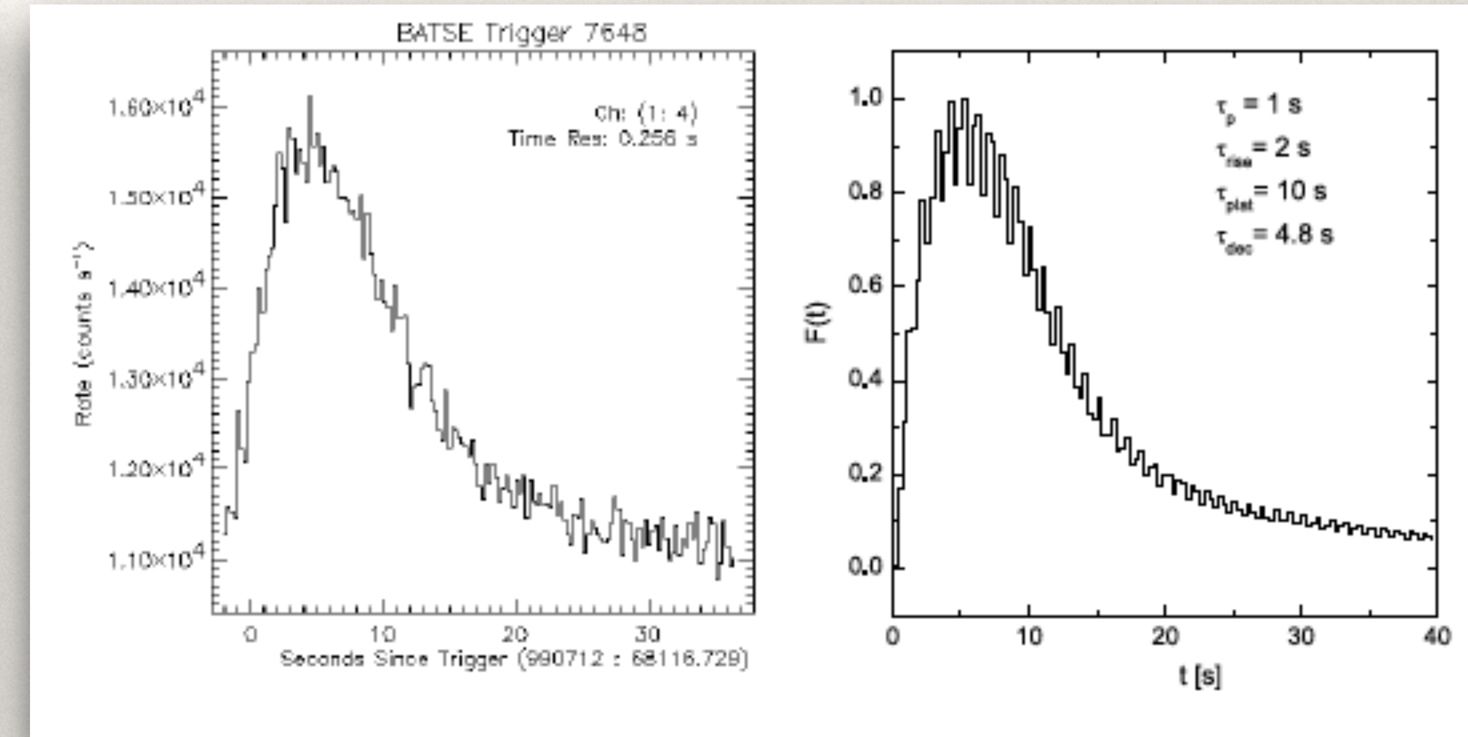

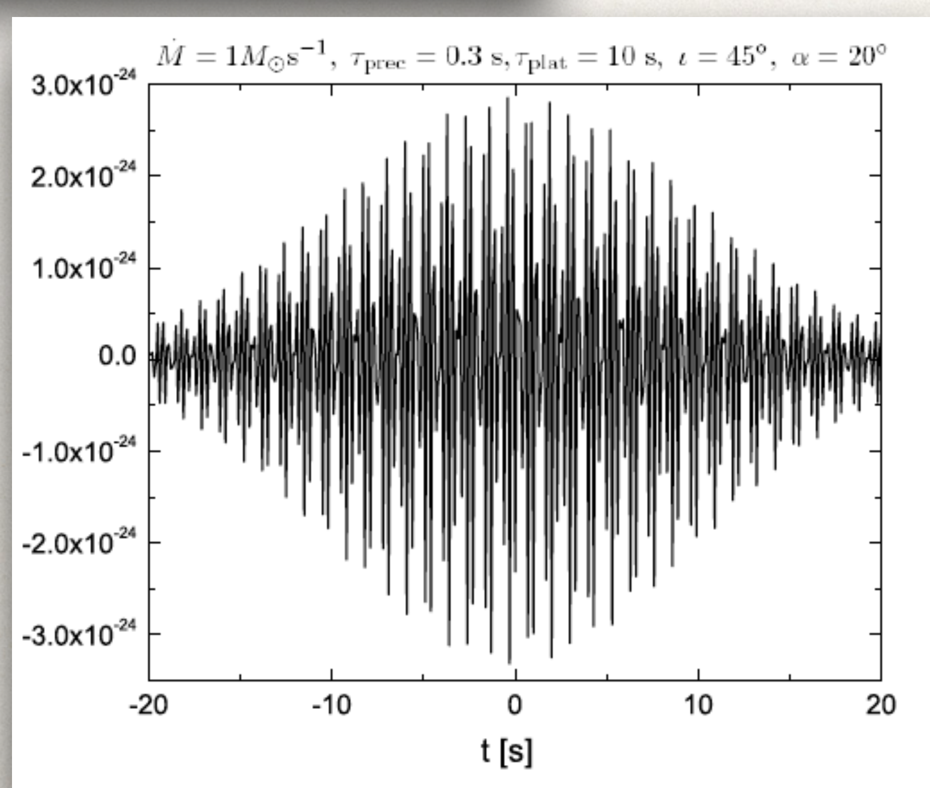

Depending on the viewing angle, these events can be detected with LIGO for d<100 Mpc (Romero et al. 2010).

Simple model

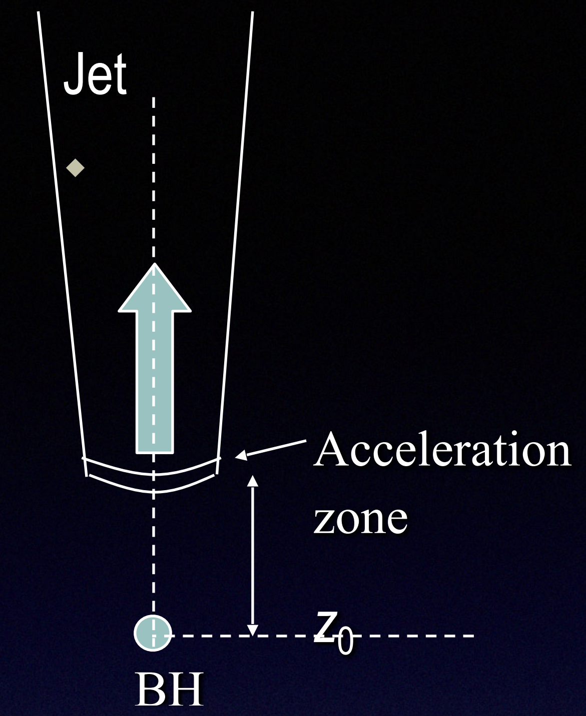

Conical jet, perpendicular to binary orbit

Mildly relativistic outflow, $\Gamma = 1.5$

Viewing angle θ=30º, moderate

Compact acceleration/emission region located where the field falls below equipartition

✓ **Content of relativistic particles**

$$L_{jet} = 0.1 L_{acc}$$

Falcke & Biermann (1995)

Körding *et al.* (2006)

$$L_{rel} = 0.1 L_{jet} \approx 2\times 10^{37}\ \mathbf{erg\ s^{-1}}$$

$$L_{rel} = L_p + L_e \quad L_p = aL_e$$

$$a = 1 - 10^3$$

✓ **Initial magnetic field**

$$B = B_o \frac{z_o}{z}$$

$$\frac{B_o^2}{8\pi} = U_{jet}^{kin}(z_o) \Rightarrow B_o \approx 10^7\, G$$

✓ Particle distributions "one-zone" approximation

$$\frac{\partial}{\partial E}\left[\frac{dE}{dt}N(E,z)\right]+\frac{N(E,z)}{T_{\rm esc}}=Q(E,z)$$

$$\Rightarrow N(E,z)\propto\begin{cases}E_p^{-\alpha}\\ E_e^{-(\alpha+1)}\end{cases}$$

$$\left.\frac{dE}{dt}\right|_{\rm acc}=\left.\frac{dE}{dt}\right|_{\rm loss}\approx\left.\frac{dE}{dt}\right|_{\rm synchr}+\left.\frac{dE}{dt}\right|_{\rm ad}$$

$$T_{\rm esc}\approx\frac{z_{\rm max}}{v_{\rm jet}}$$

$$Q_{\rm e,p}=Q^{\rm o}_{\rm e,p}\frac{E_{\rm e,p}^{-\alpha}}{z}$$

$\alpha \sim 2.2$

diffusive shock acceleration

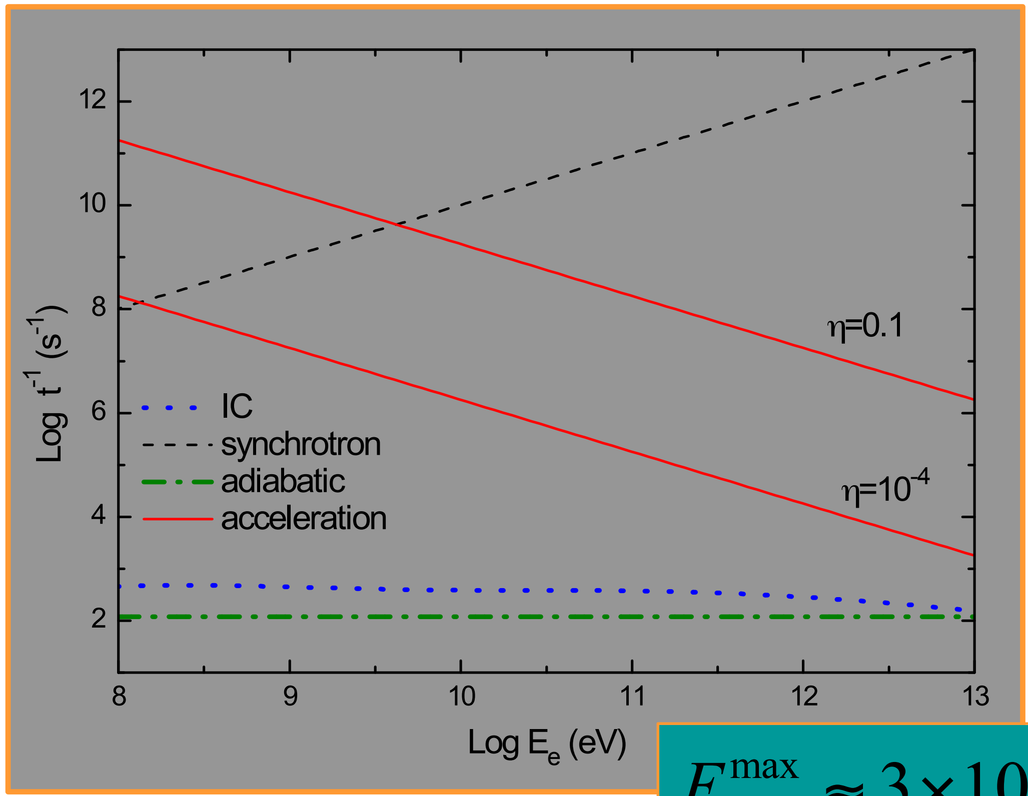

$$E_e^{\rm max}\approx 3\times10^{10}\eta^{1/2}\,\mathbf{eV}$$

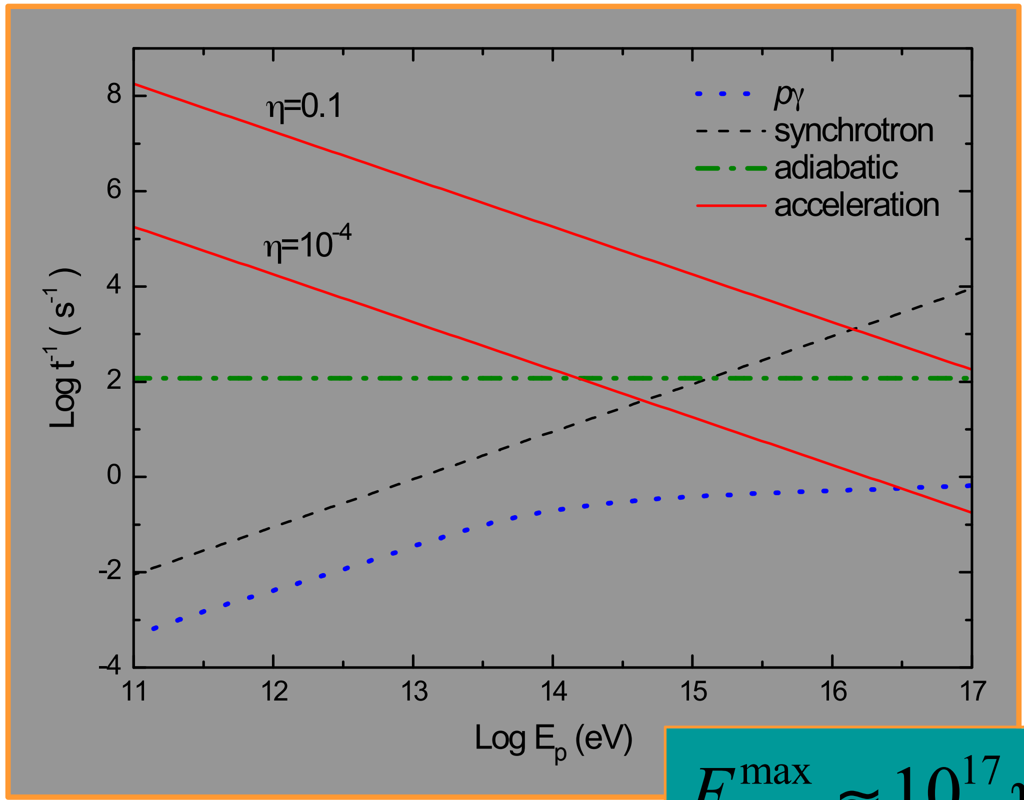

$$E_p^{\rm max}\approx 10^{17}\eta^{1/2}\,\mathbf{eV}$$

The proton microquasr jet model (Romero & Vila, A&A 485, 623 (2008), also Romero & Vila, A&A, 494, L33 (2009))

Interaction of relativistic *p* and *e*⁻ with — magnetic field / radiation fields — ***in the jet***

- Synchrotron radiation $$p,\ e^- + B \rightarrow p,\ e^- + \gamma$$
- Inverse Compton (IC) $$e^- + \gamma \rightarrow e^- + \gamma$$
- Proton-proton inelastic collisions $$p + p \rightarrow p + p + a\,\pi^0 + b(\pi^+ + \pi^-)$$
- Photohadronic interactions (*p*g) $$p + \gamma \rightarrow p + e^+ + e^-$$

$$e^\pm + B \rightarrow e^\pm + \gamma$$

$$\pi^o \rightarrow 2\gamma \qquad p + \gamma \rightarrow p + a\pi^o + b(\pi^+ + \pi^-)$$

$$\pi^{:}\ p + \gamma \rightarrow n + \pi^+ + a\pi^o + b(\pi^+ + \pi^-) \quad (\nu_\mu)$$

Lepto hadronic model for a MQ (Vila & Romero 2010)

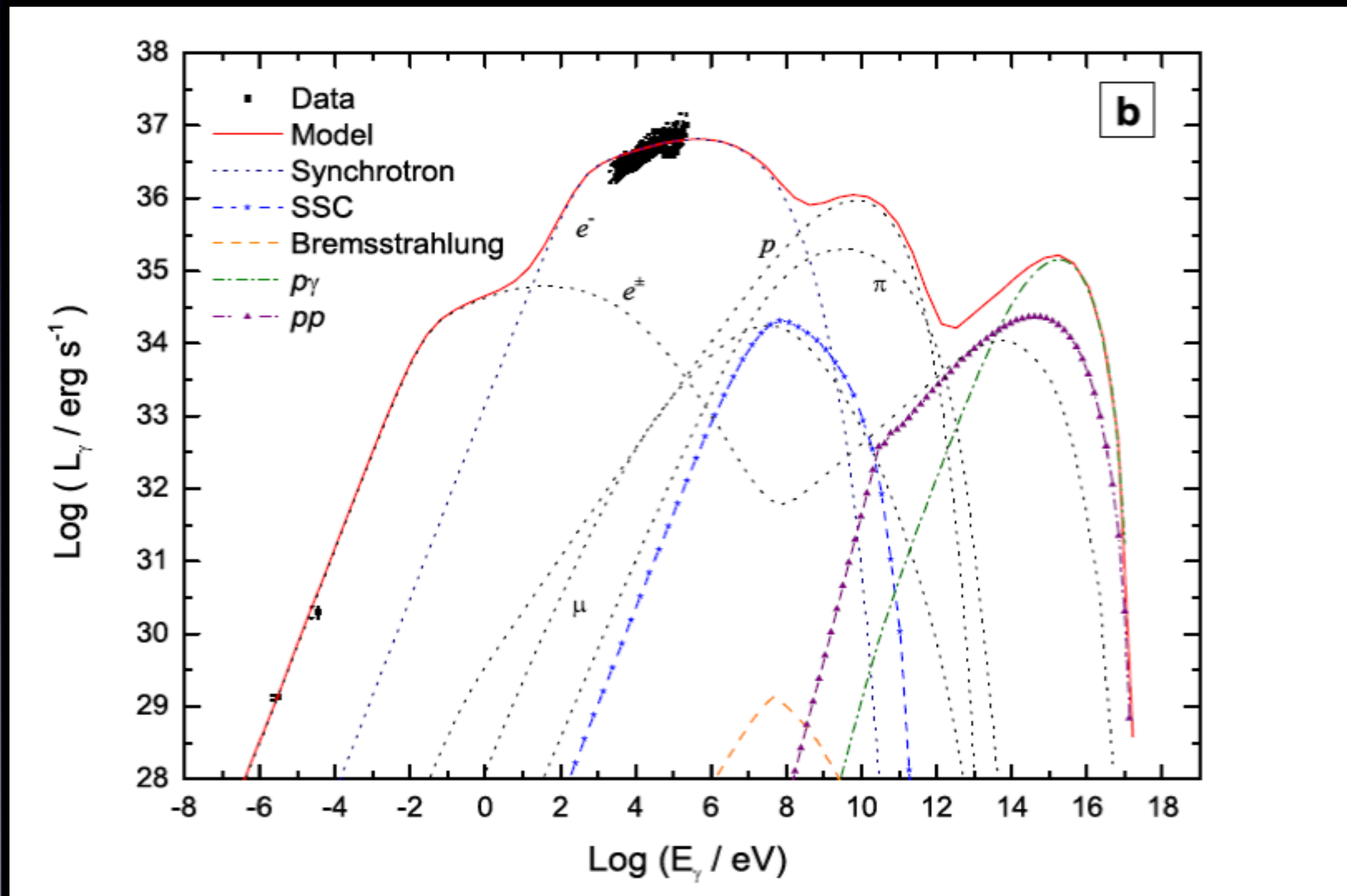

GX 339-4

Fast radio bursts

FRBs are a transient radio pulses lasting a few milliseconds. They are bright, unresolved, non-repeating, broadband flashes.

So far about 100 FRBs have been detected. Some of them repeat.

The origin of fast radio bursts is not known: they are generally thought to be extragalactic due to the anomalously high amount of pulse dispersion observed. In few cases a host galaxy was identified. Mangetars in our galaxy have been observed producing FRBs.

What are FRBs?

- First bursts: Lorimer et al. (2007)
- Reality check: Thornton et al. (2013)
- Peak flux > 0.5 Jy
- L-band (1.4 GHz)
- Highly dispersed
- Pulse widths > few ms
- Evidence for scattering
- Singular events?
- Different sky locations

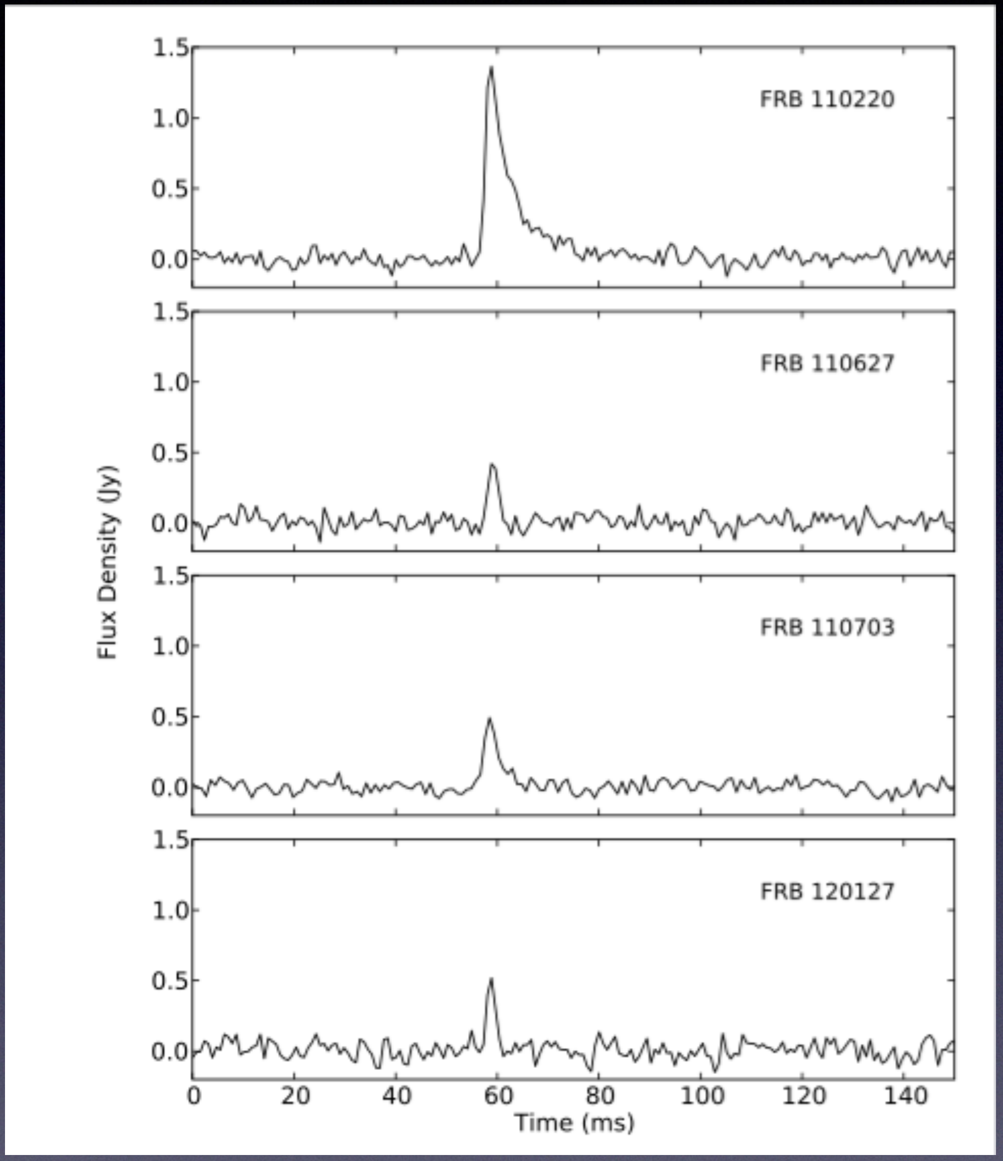

Thornton et al. (2013)

Parkes Radio Telescope

Image credit: Stephen West

Detections

Arecibo Radio Telescope

Image credit: NAIC - Arecibo Observatory, a facility of NSF

New South Wales, Australia

Multibeam Receiver (13 beams)

Discovered 9 FRBs (including the first)

First measurement of polarization

First detection in realtime

Puerto Rico, USA

Arecibo L-band Feed Array (7 beams)

Second telescope to discover an FRB

First (believable) FRB in the Galactic plane

+GBT+CHIME+LOFAR

CHIME

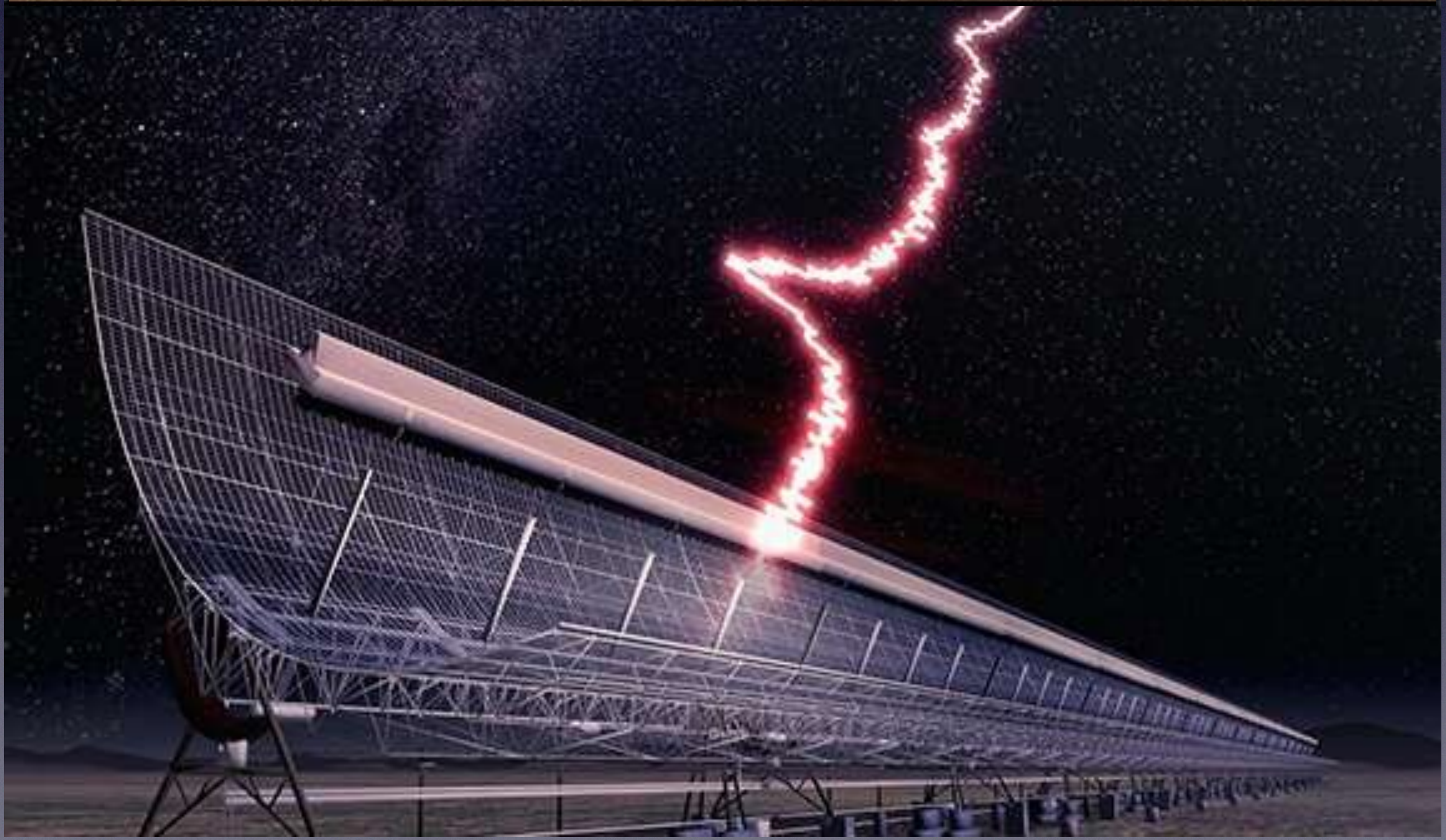

Scattering in FRB 110220

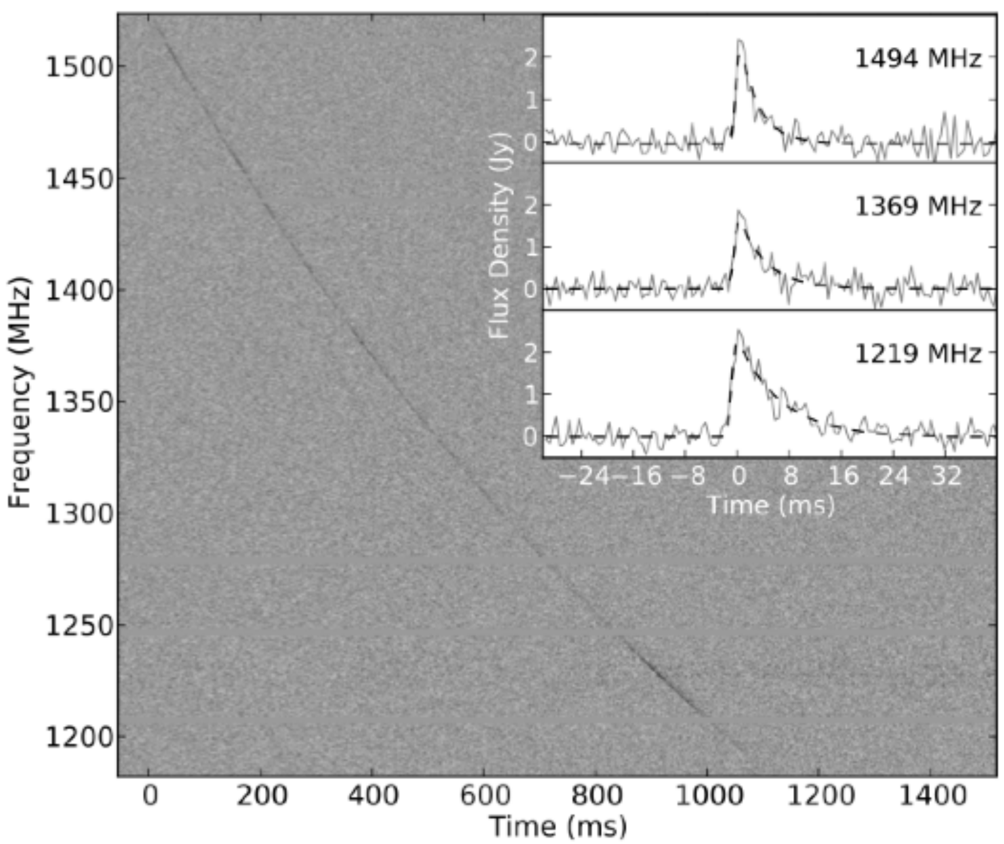

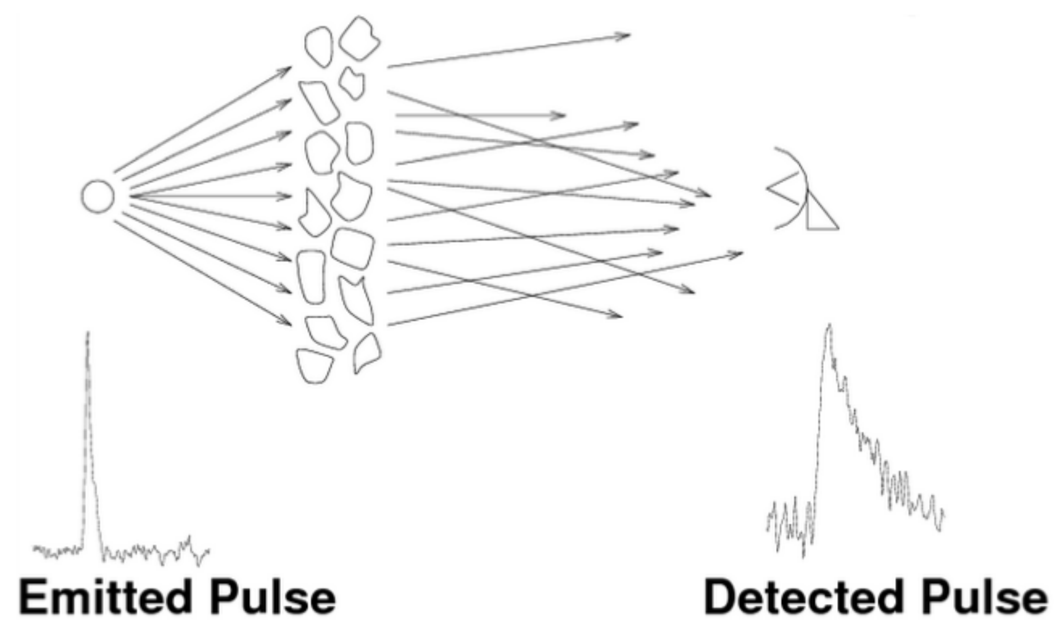

The ionized component of the ISM and the IGM, i.e. free electrons, make the group velocity of the signal frequency dependent. This results in the higher radio frequencies arriving before those emitted at the same time at lower frequencies from a source. The delay added at a frequency *v* is

$$t = k_{DM} \times \left(\frac{\mathrm{DM}}{\nu^2} \right),$$

where k_{DM} is the dispersion constant

$$k_{DM} = \frac{e^2}{2\pi m_e c} \simeq 4.149 \ \mathrm{GHz}^2 \ \mathrm{pc}^{-1} \ \mathrm{cm}^3 \ \mathrm{ms},$$

and the dispersion measure (DM) is the column density of electrons, or the number density of electrons integrated along the path traveled by the photon, d, from the source to the observer,

$$\mathrm{DM} = \int_0^d n_e \, \mathrm{d}l.$$

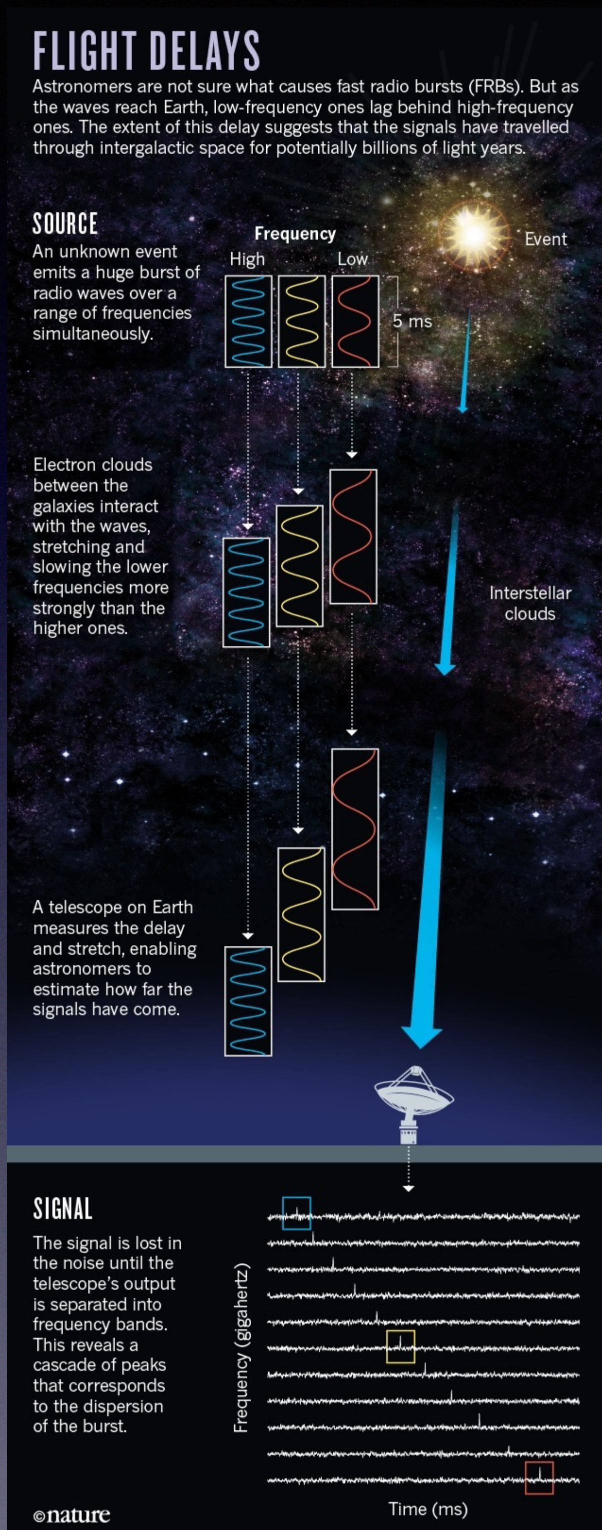

Measuring the delay in arrival times at two different frequencies allows one to obtain the signal's DM. This time delay, *t*, between high and low frequency component of a signal is (Wilson, Rohlfs, Huttemeister 2009)

$$\delta t = k_{DM} \times \mathrm{DM} \times \left(\frac{1}{\nu_l^2} - \frac{1}{\nu_h^2}\right)$$

$$\Rightarrow \mathrm{DM} = \frac{\delta t}{k_{DM}} \frac{(\nu_l \nu_h)^2}{\nu_h^2 - \nu_l^2}$$

$$\mathrm{DM} = \int_0^d n_e \, dl.$$

IGM → $\mathrm{DM} \sim 1200\, z \ \mathrm{cm}^{-3}\ \mathrm{pc}, \text{ for } z \leq 2.$

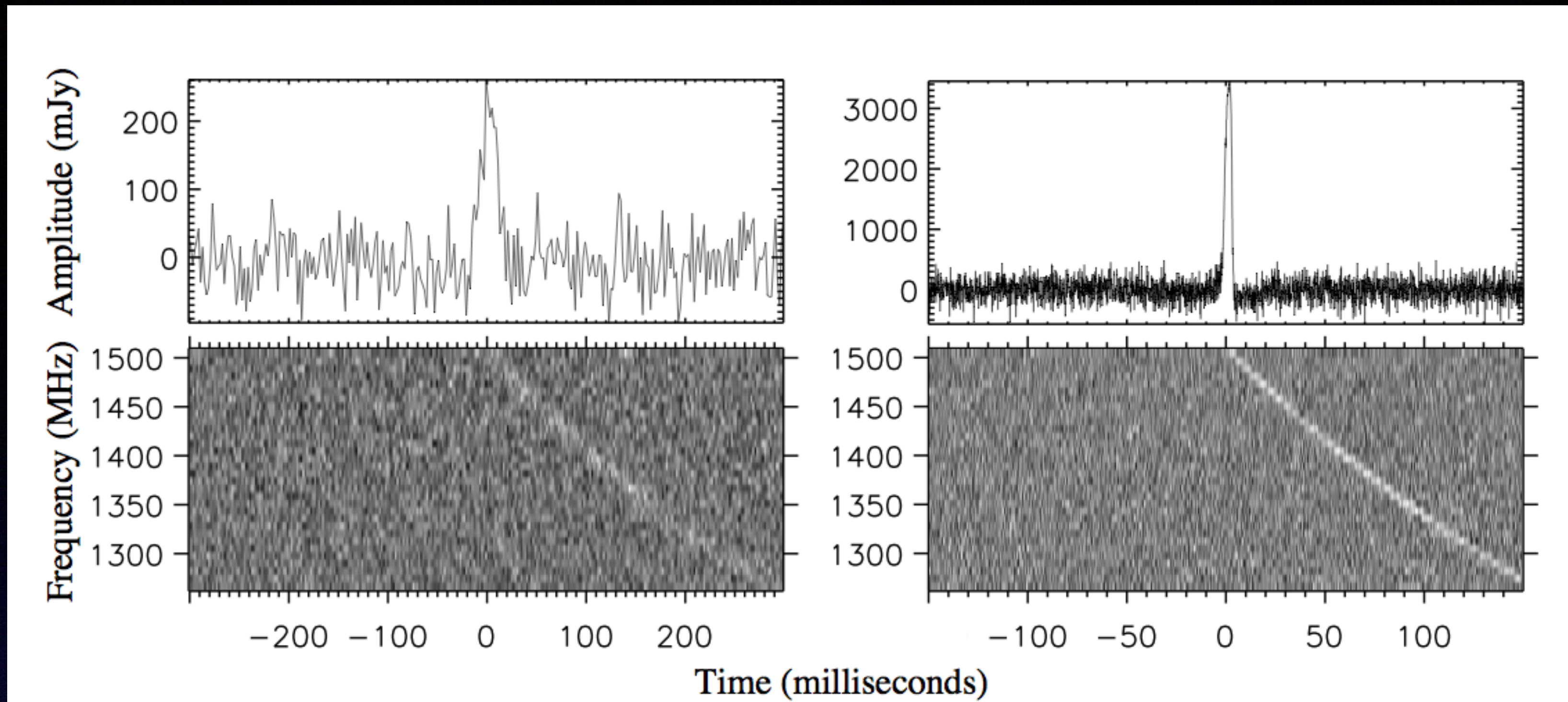
Amplitude (mJy)
200
100
0
3000
2000
1000
0
Frequency (MHz)
1500
1450
1400
1350
1300
−200 −100 0 100 200
−100 −50 0 50 100
Time (milliseconds)

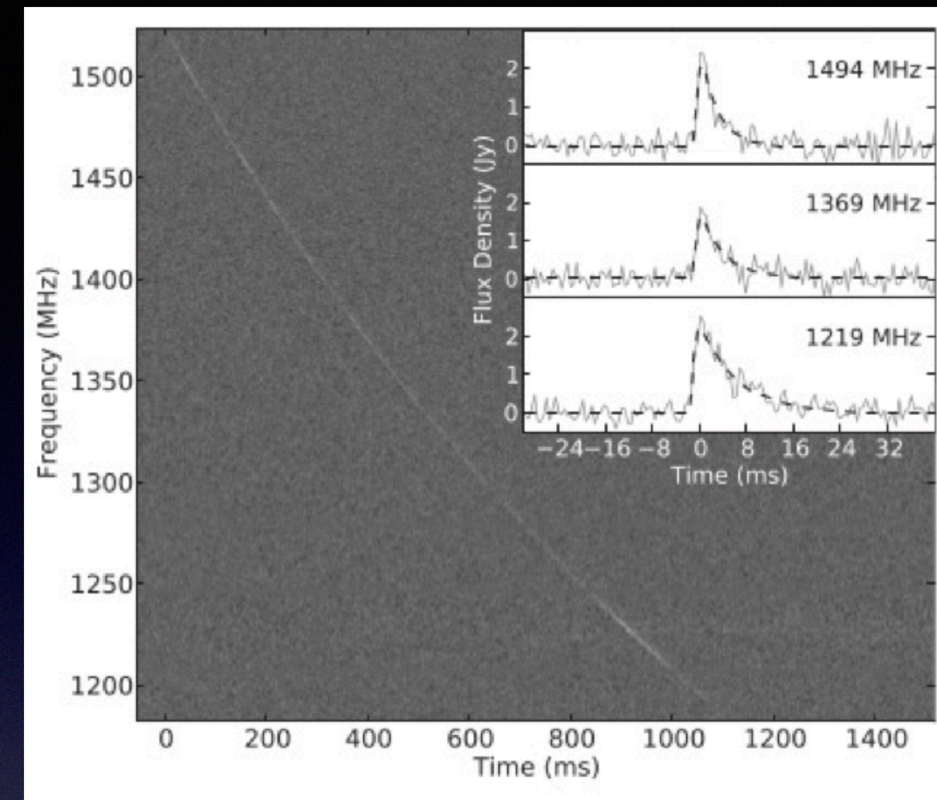
Frequency (MHz)
1500
1450
1400
1350
1300
1250
1200
0 200 400 600 800 1000 1200 1400
Time (ms)
Flux Density (Jy)
1494 MHz
1369 MHz
1219 MHz
−24 −16 −8 0 8 16 24 32
Time (ms)

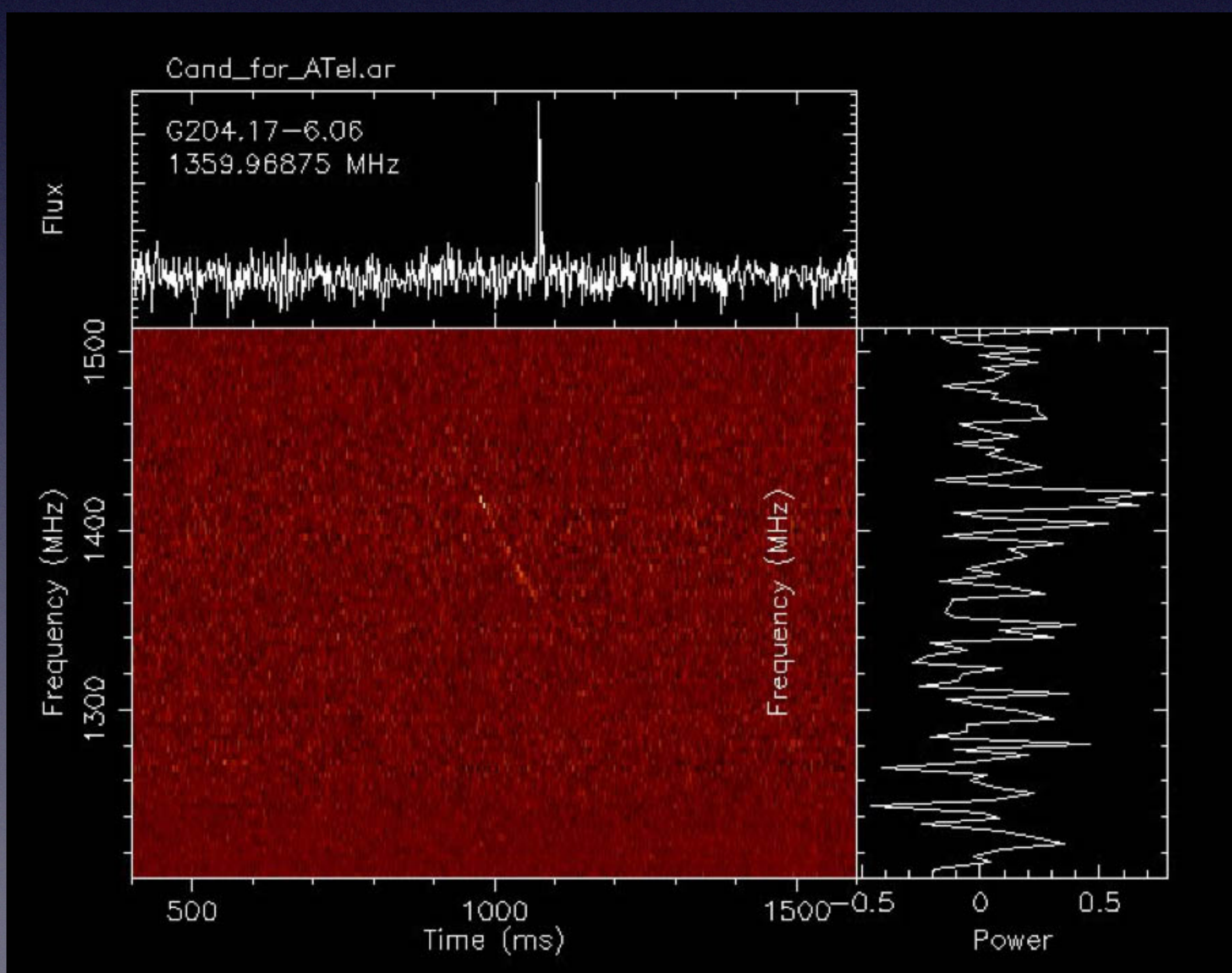
Cand_for_ATel.ar
G204.17−6.06
1359.96875 MHz
Flux
Frequency (MHz)
1500
1400
1300
500 1000 1500
Time (ms)
Frequency (MHz)
−0.5 0 0.5
Power

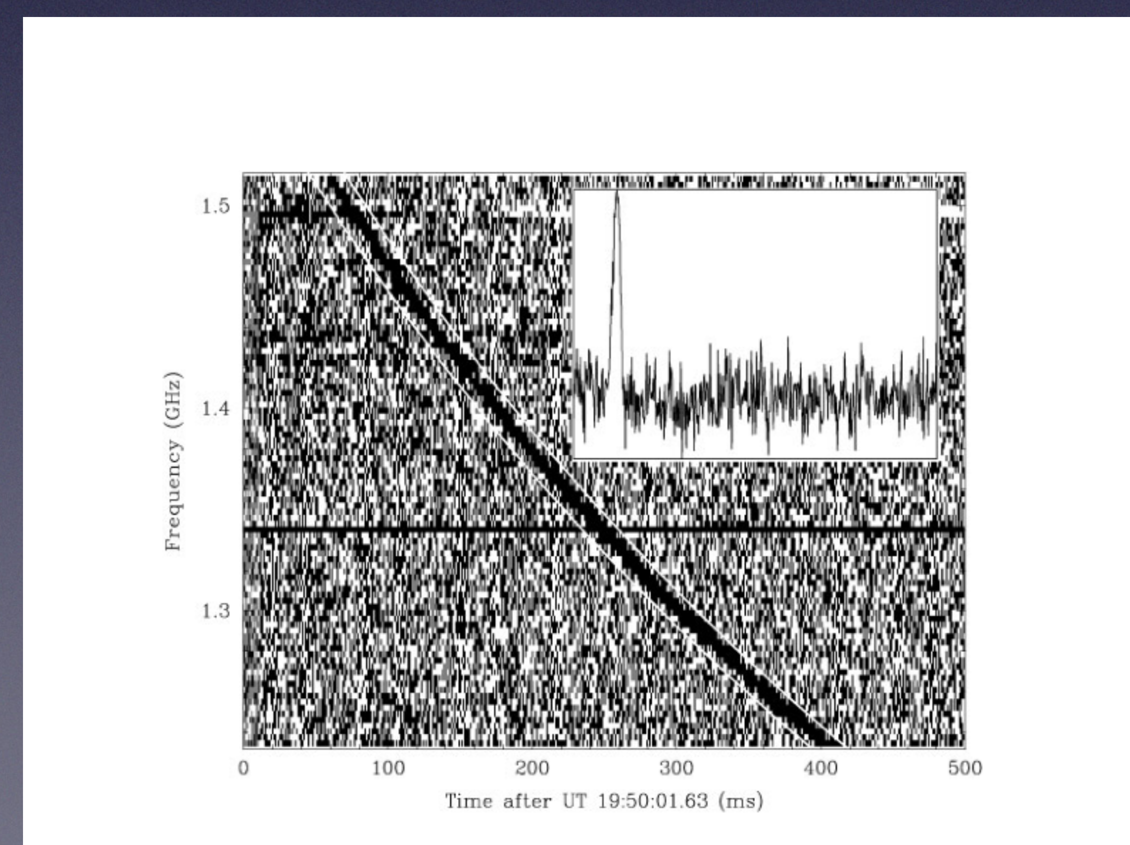
Frequency (GHz)
1.5
1.4
1.3
0 100 200 300 400 500
Time after UT 19:50:01.63 (ms)

FRBs: extraordinary probes of the distant universe

- Measure the distance → origins
- Measure the intergalactic DM
- Measure turbulence in IGM
- Probe missing baryons
- Through lensing probe dark matter
- Measure the intergalactic B-field
- Probe population at different redshifts

On 18 April 2015, FRB 150418 was detected by the ***Parkes observatory*** and within hours, several telescopes including the ***Australia Telescope Compact Array*** caught an "afterglow" of the flash, which took six days to fade (Keane et al. 2016). The ***Subaru telescope*** was used to find what was thought to be the host galaxy and determine its redshift and the implied distance to the burst.

Host galaxy for FRB 150418?

LETTER

doi:10.1038/nature17140

The host galaxy of a fast radio burst

E. F. Keane[1,2,3], S. Johnston[4], S. Bhandari[2,3], E. Barr[2], N. D. R. Bhat[3,5], M. Burgay[6], M. Caleb[2,3,7], C. Flynn[2,3], A. Jameson[2,3], M. Kramer[8,9], E. Petroff[2,3,4], A. Possenti[6], W. van Straten[2], M. Bailes[2,3], S. Burke-Spolaor[10], R. P. Eatough[8], B. W. Stappers[9], T. Totani[11], M. Honma[12,13], H. Furusawa[12], T. Hattori[14], T. Morokuma[15,16], Y. Niino[12], H. Sugai[16], T. Terai[14], N. Tominaga[16,17], S. Yamasaki[11], N. Yasuda[16], R. Allen[2], J. Cooke[2,3], J. Jencson[18], M. M. Kasliwal[18], D. L. Kaplan[19], S. J. Tingay[3,5], A. Williams[5], R. Wayth[3,5], P. Chandra[20], D. Perrodin[6], M. Berezina[8], M. Mickaliger[9] & C. Bassa[21]

z~049

In recent years, millisecond-duration radio signals originating in distant galaxies appear to have been discovered in the so-called fast radio bursts[1–9]. These signals are dispersed according to a precise physical law and this dispersion is a key observable quantity, which, in tandem with a redshift measurement, can be used for fundamental physical investigations[10,11]. Every fast radio burst has a dispersion measurement, but none before now have had a redshift measurement, because of the difficulty in pinpointing their celestial coordinates. Here we report the discovery of a fast radio burst and the identification of a fading radio transient lasting ~6 days after the event, which we use to identify the host galaxy; we measure the galaxy's redshift to be $z = 0.492 \pm 0.008$. The dispersion measure and redshift, in combination, provide a direct measurement of the cosmic density of ionized baryons in the intergalactic medium of $\Omega_{IGM} = 4.9 \pm 1.3$ per cent, in agreement with the expectation from the Wilkinson Microwave Anisotropy Probe[12], and including all of the so-called 'missing baryons'. The ~6-day radio transient is largely consistent with the radio afterglow of a short γ-ray burst[13], and its existence and timescale do not support progenitor models such as giant pulses from pulsars, and supernovae. This contrasts with the interpretation[8] of another recently discovered fast radio burst, suggesting that there are at least two classes of bursts.

Upon detection of FRB 150418 at Parkes, a network of telescopes was triggered across a wide range of wavelengths (see Methods). Beginning two hours after the FRB, observations with the Australia Telescope Compact Array (ATCA) were carried out at 5.5 GHz and 7.5 GHz, identifying two variable compact sources. One of the variable sources is consistent with a GHz-peaked-spectrum source, with a positive spectral index, as previously identified in observations at these frequencies[16]. The other variable source (right ascension, RA 07 h 16 min 34.6 s; declination, dec. −19° 00′ 40″), offset by 1.944 arcmin from the centre of the Parkes beam, was seen at 5.5 GHz at a brightness of 0.27(5) mJy per beam just 2 h after the FRB. The source was then seen to fade over subsequent epochs, settling at a brightness of ~0.09(2) mJy per beam (Fig. 2). The source is also seen at 7.5 GHz at 0.18(3) mJy per beam in the first epoch but subsequently not detected. These observations indicate a ~6-day transient with a negative spectral index; we obtain $\alpha = -1.37$ in the first epoch, for a power-law spectrum of the form $F_\nu \propto \nu^\alpha$. The subsequent quiescent level is consistent with the level expected[17] from an early-type galaxy at $z \approx 0.5$. To estimate the likelihood that this transient could occur by chance we consider the results of radio imaging surveys (see Methods). By comparing to a recent survey with the Very Large Array[18] in the 2–4 GHz band, we expect a 95% (99%) confidence upper limit of <0.001 (<0.002) such transients

Keane et al (2016)

The burst

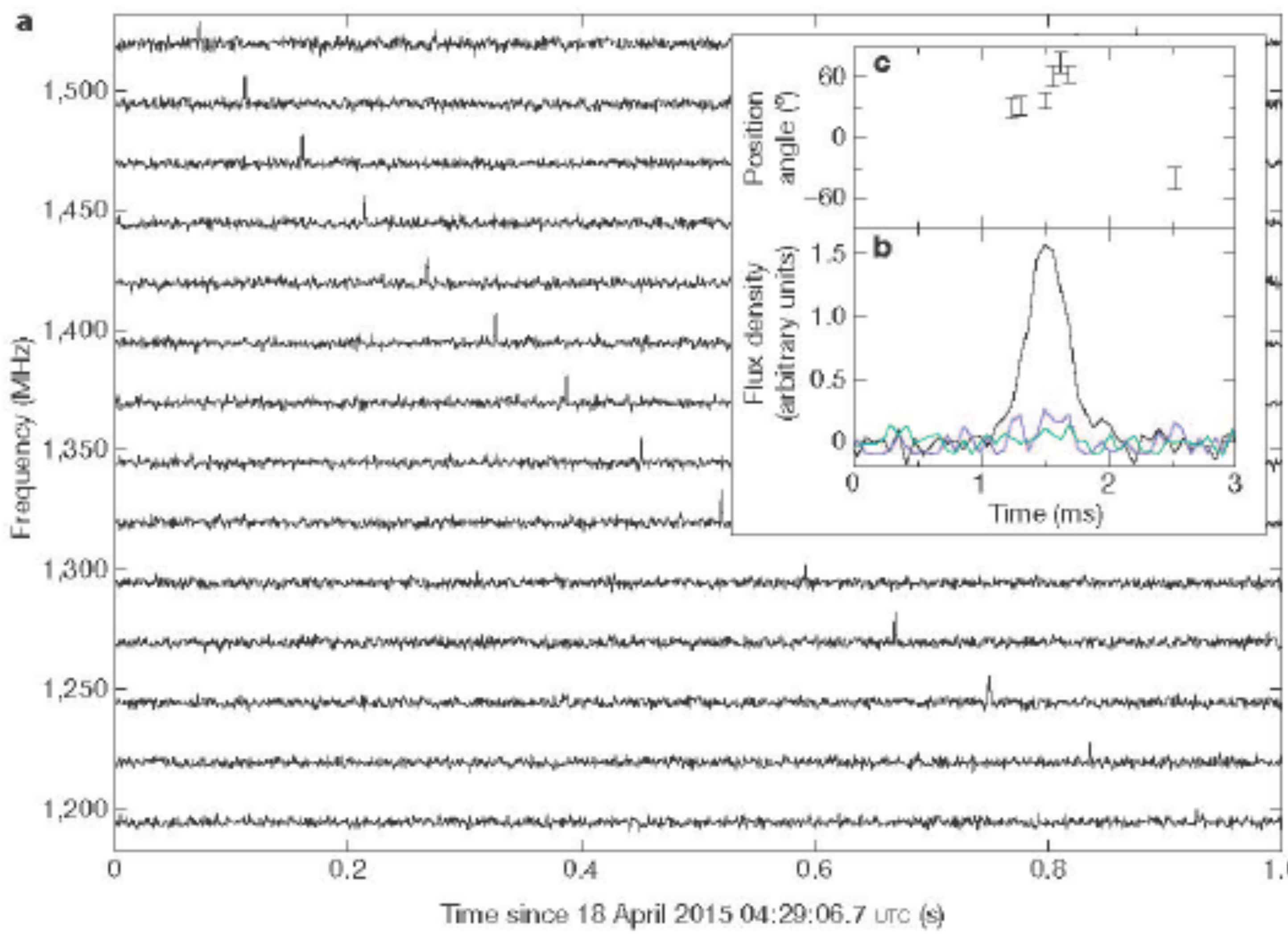
a
1,500
1,450
1,400
1,350
1,300
1,250
1,200
Frequency (MHz)
0
0.2
0.4
0.6
0.8
1.0
Time since 18 April 2015 04:29:06.7 UTC (s)
c
Position angle (°)
60
0
−60
b
Flux density (arbitrary units)
1.5
1.0
0.5
0
1
2
3
Time (ms)

FRB 150418

- DM=776 cm^{-3} pc, larger than the Galactic contribution in this direction.
- Frequency 1.382 GHz.
- Observed pulse width 0.8+/-0.3 ms. Intrinsic pulse width is unresolved.
- Radio afterglow is discovered lasting about 6 days.
- Host galaxy is identified as ***elliptical galaxy*** at z=0.492+/-0.008 with $M = 10^{11}$ solar masses.

A Repeating Fast Radio Burst

L. G. Spitler[1], P. Scholz[2], J. W. T. Hessels[3,4], S. Bogdanov[5], A. Brazier[6,7], F. Camilo[5,8], S. Chatterjee[6], J. M. Cordes[6], F. Crawford[9], J. Deneva[10], R. D. Ferdman[2], P. C. C. Freire[1], V. M. Kaspi[2], P. Lazarus[1], R. Lynch[11,12], E. C. Madsen[2], M. A. McLaughlin[12], C. Patel[2], S. M. Ransom[13], A. Seymour[14], I. H. Stairs[15,2], B. W. Stappers[16], J. van Leeuwen[3,4] & W. W. Zhu[1]

Published online by *Nature* on 2016 March 2. DOI: 10.1038/nature17168

"Here we report the detection of ten additional bursts from the direction of FRB 121102, using the 305-m Arecibo telescope. These new bursts have dispersion measures and sky positions consistent with the original burst. This unambiguously identifies FRB 121102 as repeating and demonstrates that its source survives the energetic events that cause the bursts."

$DM_{FRB}/DM_{Gal} \sim 3$,

$l = 174.89$ deg; $b = -0.23$ deg.

Two populations, at least

FRB 121102 burst morphologies and spectra

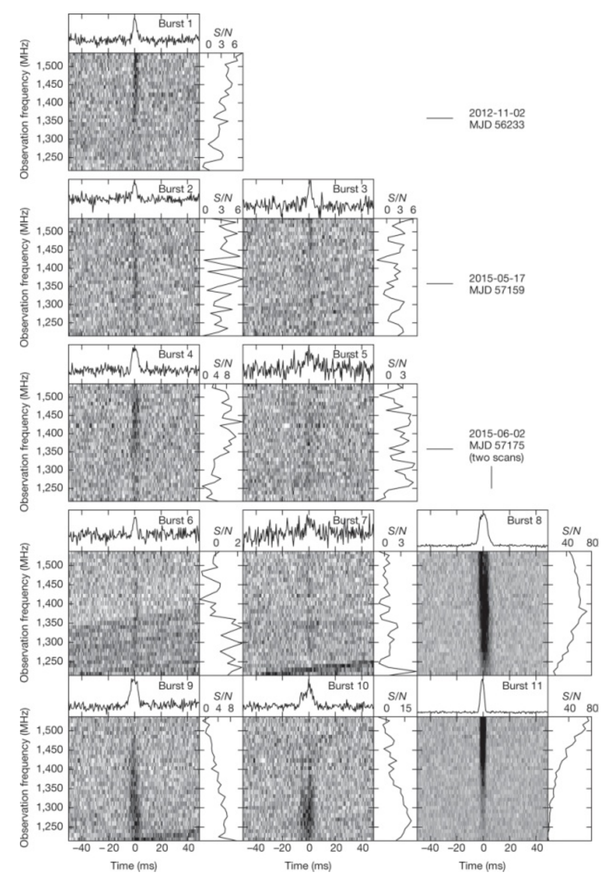

L G Spitler *et al. Nature* 1–4 (2016) doi:10.1038/nature17168

The rate of burst detections is ~3 /h

The 11 bursts have peak flux densities S1400 ≈0.02–0.3 Jy at 1.4 GHz

The other known FRBs typically have peak flux densities an order of magnitude higher, S1400 ≈0.2–2 Jy.

nature

- Emission process must be coherent

$$T_b \approx 10^{30} - 10^{38}\ \mathrm{K}$$

- Energy output is...

$$L \approx 10^{38} - 10^{40}\ \mathrm{ergs}$$

- Spectral index is not as negative as radio pulsars

What are they?

- Local: Atmospheric events? Perytons? (Kulkarni et al. 2014).
- Galactic: Magnetars.
- Extragalactic: Assorted cosmic catastrophes

Perytons: Caused by microwave ovens on Parkes site

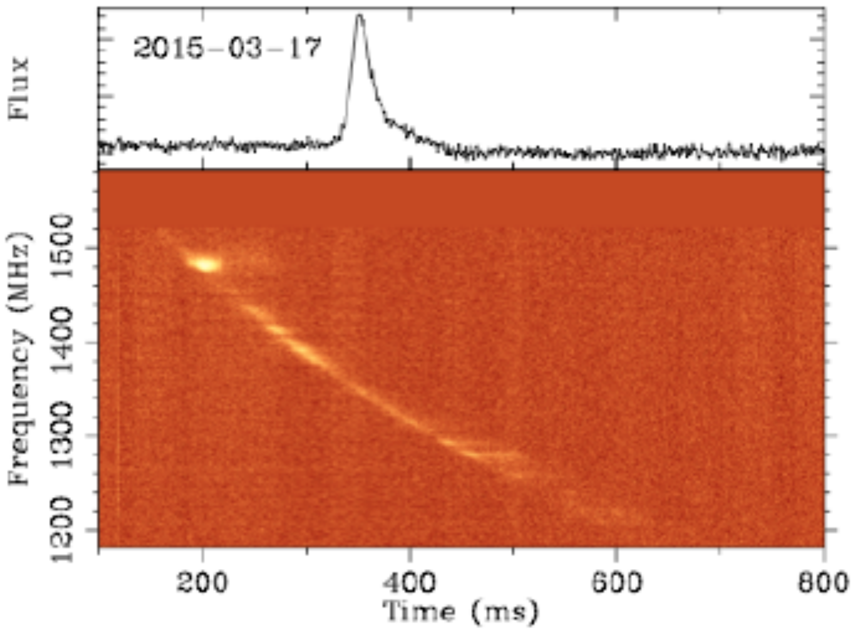

Petroff et al 2015:
astro-ph/1504.01265

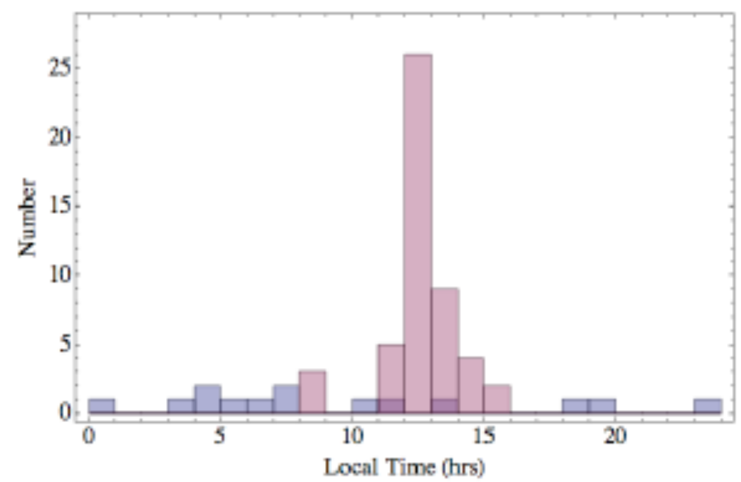

Can be generated when the microwave door is opened while microwave is still running.

The Peryton was created and described by Jorge Luis Borges in his Book of Imaginary Beings, using a supposedly long-lost medieval manuscript as a source.

Extragalactic FRBs

- Collapsing neutron stars (Falke & Rezzolla 2014)
- Discharging Kerr-Newman black holes (Liu, Romero, et al. 2016; Zhang 2016)
- Coalescing neutron stars/GRBs (Totani 2013, Zhang 2015)
- Coalescing white dwarfs (Kashiyama et al. 2013)
- Magnetar flares (Lyubarski 2014, Katz 2016)
- Giant pulses within young SNRs (Connor et al. 2015).
- Jet coherent pulses (Romero et al. 2016)
- Collision of asteroids with pulsars (Geng & Huang 2015)
- Cosmic strings...

Blitzars?

Blitzars are a hypothetical type of astronomical object in which a spinning pulsar rapidly collapses into a black hole (Falke & Rezzolla 2014).

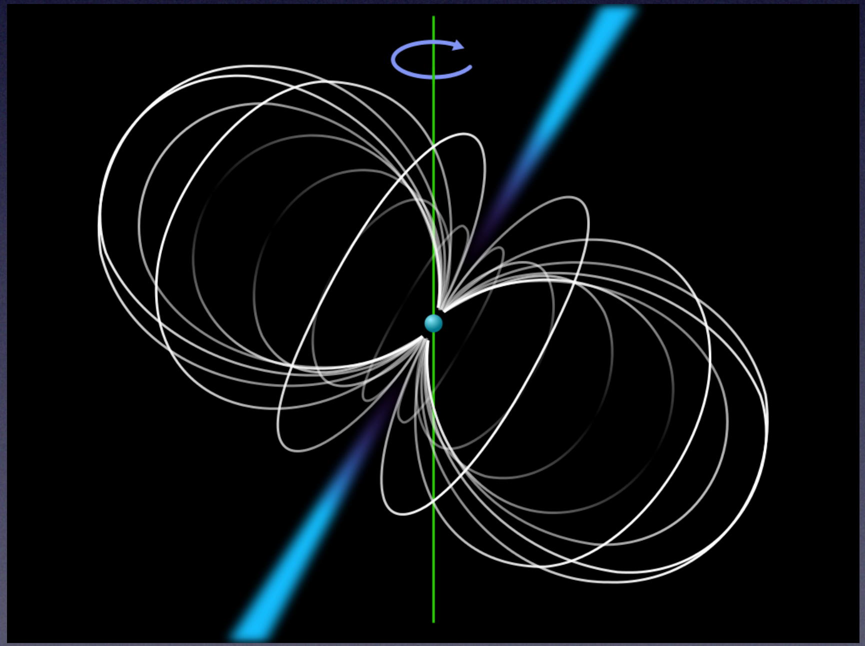

After the collapse the magnetic field violently recombines producing a coherent pulse.

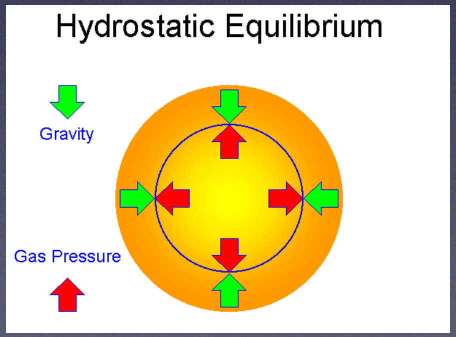

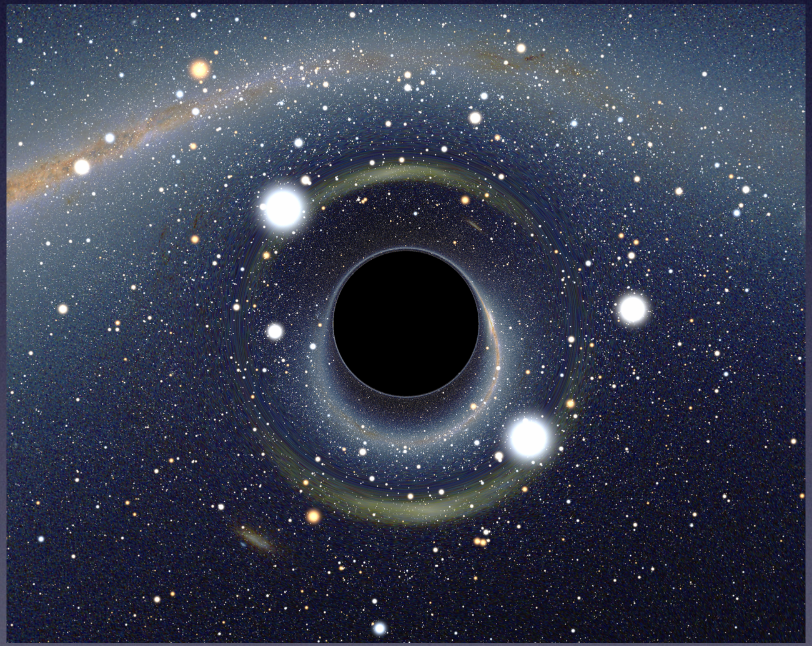

Kerr-Newman black holes?

(Liu, Romero, et al. ApJ **826**, id. 82, 2016).

For stellar-mass KNBH of MBH ~ 20 M⊙, the unstable orbit for a charged particle is calculated to be about 10^7− 10^8 cm.

$$R_{\rm mag} = c/\Omega \approx 4.8 \times 10^9 P \text{ cm.}$$

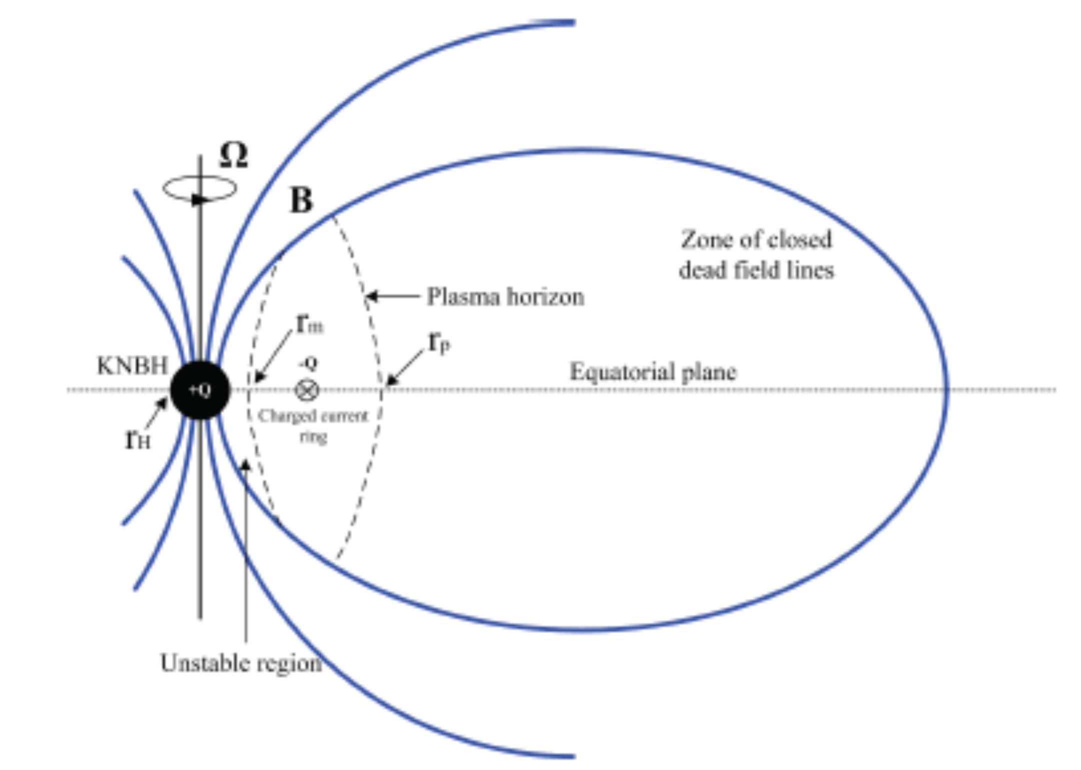

FIG. 1.— Schematic diagram of the initial state of a KNBH.

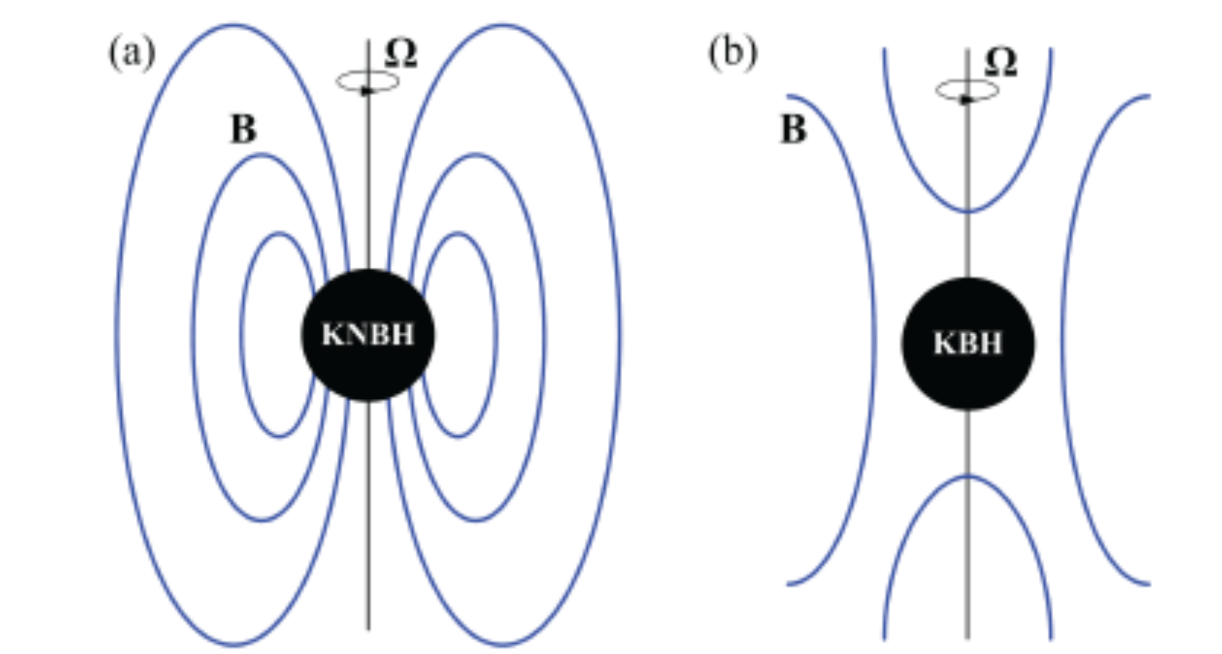

FIG. 4.— Schematic diagram of the magnetic field configuration during the discharging of a KNBH in a binary.

The charged magnetosphere is unstable

Jet-plasma interactions in GRBs and AGNs?

(Romero, et al. Phys. Rev D **93**, id. 023001, 2016).

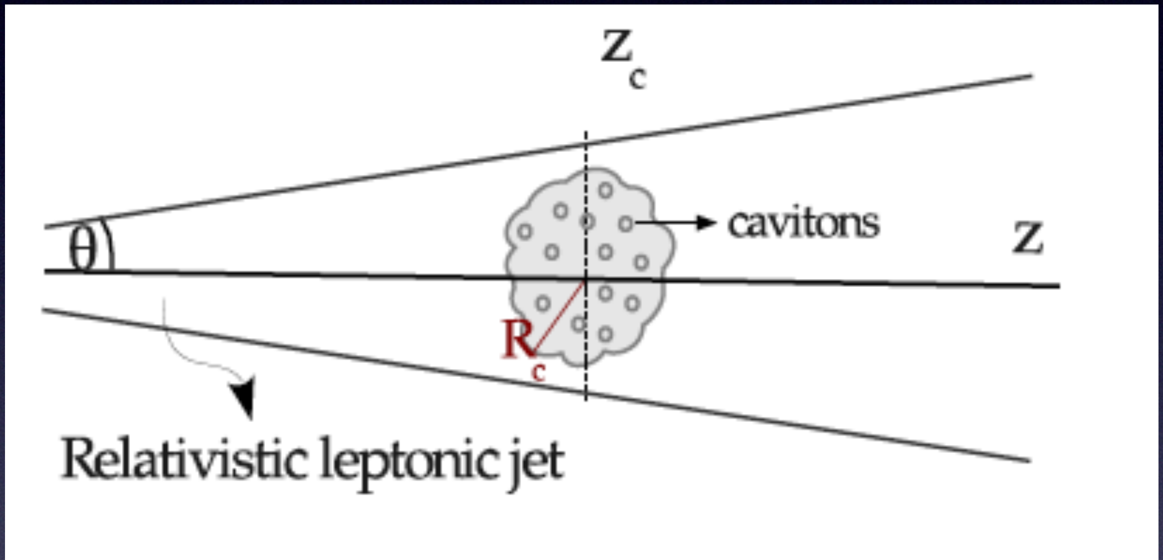

Langmuir Turbulence

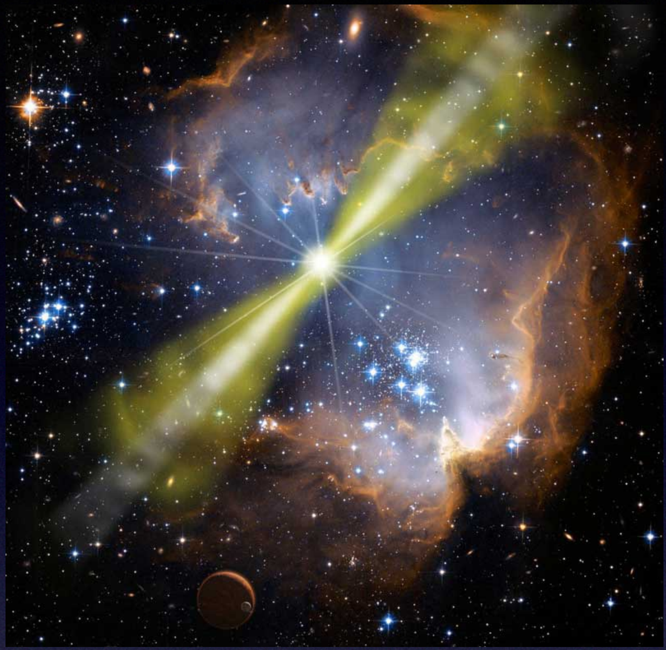

TABLE I. Main parameters of the model.

Cloud parameters	Value
n_c: density [cm^{-3}]	6×10^8
T_c: temperature [K]	10^5
R_c: radius [cm]	5×10^{13}
Jet parameters	**Value**
Γ: Lorentz factor	500
n_j: density [cm^{-3}]	6×10^6

$$t_{\rm cross} = \frac{R_c}{c\Gamma^2} \sim 6 \times 10^{-3} \left(\frac{R_c}{5 \times 10^{13}\,{\rm cm}}\right)\left(\frac{500}{\Gamma}\right)^2 \ {\rm s};$$

$$P_t \sim 1.5 \times 10^{42}\ {\rm erg\,s^{-1}} \times \left(\frac{T_c}{10^5\,{\rm K}}\right)^2 \left(\frac{f}{0.1}\right) \left(\frac{n_j}{6 \times 10^6\,{\rm cm^{-3}}}\right) \left(\frac{R_c}{5 \times 10^{13}\,{\rm cm}}\right)^3.$$

Repeaters: Magnetars

Magnetars are rapidly spinning ultra-magnetic neutron stars (they spin around their axis with a period between 3 and 12 seconds) that undergo high energy flare events which are caused by “starquakes". During these quakes rapid flares can occur and coherent radiation might be produced (Lyubarski 2014, Katz 2016).

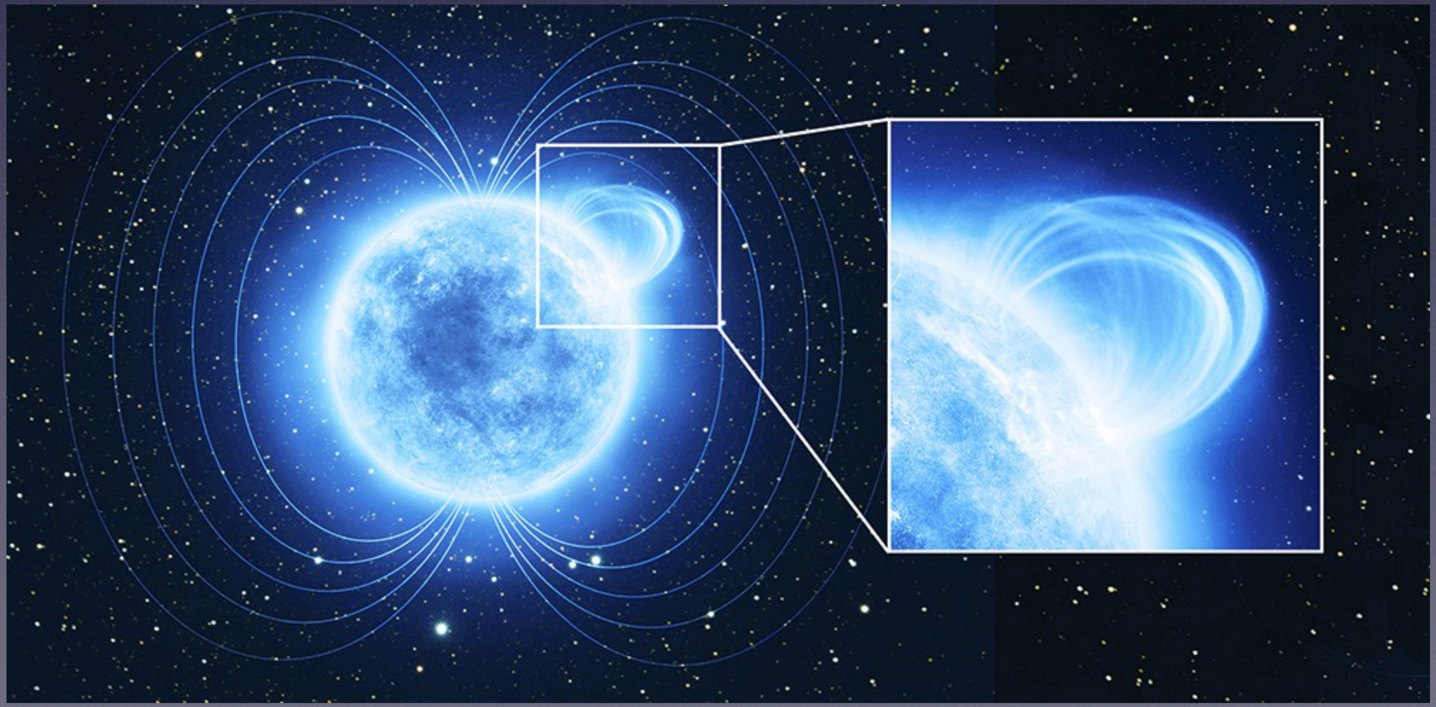

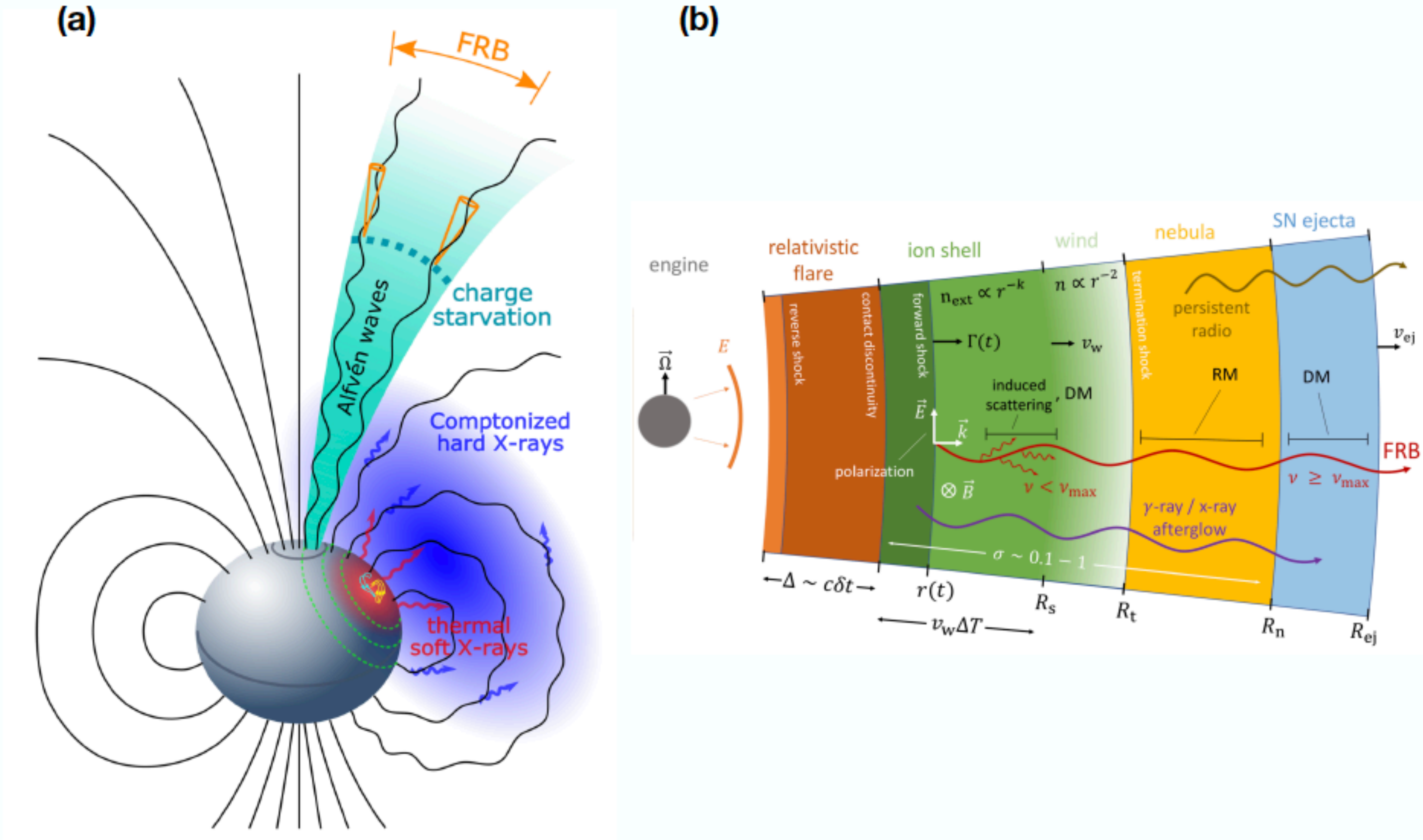
(a)
FRB
charge starvation
Alfvén waves
Comptonized hard X-rays
thermal soft X-rays
(b)
engine
relativistic flare
ion shell
wind
nebula
SN ejecta
reverse shock
contact discontinuity
forward shock
termination shock
$n_{ext} \propto r^{-k}$
$n \propto r^{-2}$
$\Gamma(t)$
v_w
v_{ej}
$\vec{\Omega}$
E
persistent radio
induced scattering, DM
RM
DM
$\vec{E}$
$\vec{k}$
polarization
$\otimes \vec{B}$
$\nu < \nu_{max}$
$\nu \geq \nu_{max}$
FRB
γ-ray / x-ray afterglow
$\sigma \sim 0.1 - 1$
$\Delta \sim c\delta t$
$r(t)$
$v_w \Delta T$
R_s
R_t
R_n
R_{ej}

	GRBs	FRBs
Are they astrophysical?	• 1967: discovery • 1973: Yes! (first paper published)	• 2007: discovery • 2013-2015: Yes! (new FRBs and microwave-oven-origin of perytons)
Are there multiple types?	• 1979: soft gamma-ray repeaters (SGRs) • 1992: long vs. short	• 2016: repeaters • 2020: do all FRBs repeat?
Where are they?	• 1979: SGRs are Galactic (or nearby) • 1997: long GRBs are cosmological • 2004: short GRBs are cosmological	• 2017: extragalactic and cosmological (FRB 121102) • 2020: Galactic (FRB 200428)
What make them?	• 1998: SGRs from magnetars • 1998: Long GRBs from massive star core collapse • 2017: Short GRBs from NS-NS mergers	• 2020: FRB 200428 from a magnetar • 2020: can other sources produce FRBs?

Bing Zhang (2020)

For more comprehensive treatments and discussions